UC Berkeley
UC Berkeley Electronic Theses and Dissertations

Title
Harnessing Covalent Chemical Probes: From Inhibition to Induced Proximity Modalities

Permalink
https://escholarship.org/uc/item/83z9h9v1

Author
Henning, Nathaniel James

Publication Date
2022

Supplemental Material
https://escholarship.org/uc/item/83z9h9v1#supplemental

Peer reviewed|Thesis/dissertation

Harnessing Covalent Chemical Probes:
From Inhibition to Induced Proximity Modalities

By

Nathaniel Henning

A dissertation submitted in partial satisfaction of the

requirements for the degree of

Doctor of Philosophy

in

Chemistry

in the

Graduate Division

of the

University of California, Berkeley

Committee in charge:

Professor Daniel K. Nomura, Chair
Associate Professor Evan Miller
Associate Professor Roberto Zoncu

Spring 2022

ABSTRACT

Harnessing Covalent Chemical Probes:
From Inhibition to Induced Proximity Modalities

By

Nathaniel J. Henning

Doctor of Philosophy in Chemistry
University of California, Berkeley
Under the Supervision of Professor Daniel K. Nomura

Covalent drugs have garnered intense interest due to the unique ways in which they can modulate protein function. Over the past decade, several covalent drugs have been approved that target EGFR, BTK, KRAS^{G12C}, and the SARS-CoV-2 M^{pro} for oncology and antiviral indications. The success of these drugs has driven scientists to design strategies to discover and characterize electrophilic molecules, including specialized screening methods and selectivity-profiling techniques. These technologies have enabled the rapid discovery of covalent chemical probes that selectively modulate protein activity to facilitate study of protein function in different biological contexts. These covalent tool compounds have frequently been further optimized to yield enzymatic inhibitors that provide clinical benefit to patients. Electrophilic compounds have also proven exceptionally useful for inducing proximity between proteins using bifunctional molecules, specifically for targeted protein degradation (TPD). Bifunctional degraders, or proteolysis targeting chimeras (PROTACs), consist of an E3 ligase recruiter linked to a ligand for a target protein. While many degraders recruit the E3s CRBN and VHL to degrade target proteins, more than 600 E3 ligases exist in human cells which could be used for this purpose. To expand the scope of TPD, I discovered a novel covalent ligand for the E3 ligase FEM1B. This ligand, EN106, can be incorporated into bifunctional PROTACs that degrade BRD4 and BCR-ABL, demonstrating that FEM1B can be used to induce degradation of target proteins. While protein degradation is often desirable, there are many cases where protein stabilization could have a therapeutic benefit instead. Here, I describe a strategy for targeted protein stabilization enabled by bifunctional deubiquitinase targeting chimeras (DUBTACs) that induce proximity between a deubiquitinase (DUB) and a target protein. Discovery of a covalent, allosteric ligand for the DUB OTUB1 led to the discovery of DUBTACs that stabilize mutant cystic fibrosis transmembrane conductance regulator (CFTR), whose degradation is central to cystic fibrosis pathology, as well as the tumor suppressor kinase Wee1. This DUBTAC platform allows the modular design of molecules that induce stabilization, unlocking proteins whose gain-of-function would be therapeutically desirable as potential drug targets. Finally, I share the discovery and optimization of covalent inhibitors of the SARS-CoV-2 main protease (M^{pro}), as part of an effort to discover pan-coronavirus antiviral compounds. This thesis describes the discovery of covalent chemical probes and how they can be harnessed to modulate protein function in ways that highlight potential opportunities for future drug discovery.

DEDICATION

To my parents and brother
who are truly the best family
one could ask for.

TABLE OF CONTENTS

ACKNOWLEDGEMENTS

I am endlessly grateful to all the amazing people I have worked with over the years. My CV contains zero papers where I am the sole first author, which means that I have been fortunate enough to work with a whole series of scientists that were as invested in my research as I was. I hope this fact says something about the way I like to do science. I am certain I have gained more from working closely with so many people than I ever could have by myself.

I'd like to thank my family, who tolerated and even supported my move to the west coast and who have always been there for me. My friends who I have made since moving to Berkeley, and old friends I've reconnected with here, have made my years here incredibly enjoyable. I don't know what I would have done during the worst of the pandemic without close friends to keep me sane. And I think my community of people here is just really incredible – couldn't ask for a better group.

Of all the people I have worked with I would like to thank Seb, who taught me the basics of my first experiments at Middlebury. I am forever in debt to Sunhee Choi for believing in me as a scientist even a I fumbled through my first projects studying amyloid beta. I am endlessly grateful to Du, who taught me a truly incredible amount of chemistry at Dana-Farber. In retrospect I have no idea how he put up with all my questions and still managed to be productive. I am so glad that Dan pushed me to come to Berkeley. I am convinced that there is no other place I could have done research I would be so proud of within the first three years of a PhD program. Dan, your encouragement and guidance has been incredibly valuable, and I cannot express how much I appreciate not just the lab resources but the vast amount of time you personally have poured into working with me on these projects. And to Lydia, I couldn't imagine a better person to work with in the lab. I appreciate so many things: your willingness to work together, to teach me, your ambition and desire for excellence, and of course your thirst for fun. Your friendship is one of the most valuable things I gained during my time at Berkeley. To all the other members of in the Nomura lab, thank you all for being so easy to work with. I know you believe me when I say I really appreciate my connection to every individual in the group. I'm so glad that I had the opportunity to work beside each one of you.

But above all, I am grateful that the people I know care deeply about their communities of friends. It's not just the individuals I mentioned who have made me appreciate my last three years, it's the fact that I feel like I have a community both at work and outside of it. So I'm looking forward to keeping that up! See you around!

LIST OF TABLES AND FIGURES

LIST OF APPENDICES

CHAPTER 1

Covalent Drugs and Discovery Strategies

This chapter is based on a manuscript submitted to *Nature Reviews Drug Discovery* and has been adapted with permission from all co-authors.

1.1 Introduction

Covalent drugs derived from natural sources have been used for centuries to treat disease.[1] Modern covalent drug discovery uses knowledge of reactive amino acid residues across the proteome to rationally design molecules that form a covalent bond with a target protein, potentially conferring both potency and selectivity.[2–4] Before optimization for *in vivo* applications, compounds that selectively bind proteins of interest to modulate their function are often referred to as chemical probes. The dramatic success of several covalent drugs over the past few decades has encouraged scientists to pour resources into the discovery of covalent chemical probes. These compounds can be used to interrogate protein function, and potentially improved to provide successful covalent drugs.

A tremendous number of innovative techniques have been invented over the past twenty years to provide a toolbox for chemical biologists interested in covalent chemical probes. These include screening approaches tailored to electrophilic molecules, chemoproteomics workflows that assess selectivity, and improvements in structure-guided compound design.[2,5,6] Most commonly, these advancements have been used to generate inhibitors of various enzymes, such as proteases and kinases. Key examples of clinically successful covalent kinase inhibitors include the BTK inhibitor ibrutinib (Abbvie) and EGFR inhibitor osimertinib (AstraZeneca), with $8.43 billion and $4.33 billion in 2020 sales, respectively.[2,7] Often, these compounds target non-conserved cysteine residues outside the active site to provide selectivity within a protein family.[1,2]

The prolonged target engagement provided by the covalent bond formation often provides a key advantage over reversible inhibitors. Using covalency to overcome high affinity for a natural substrate enables targeting proteins, such as KRAS^{G12C}, that were previously thought to be undruggable due to their lack of well-defined binding pockets. In other cases, the potency afforded by covalent engagement can provide a rapid and complete inhibition through targeting an active-site residue. SARS-CoV-2 main protease (M^{pro}) inhibitors, such as nirmatrelvir (Pfizer) and PM-2-071, described here, use this covalent mechanism of action to support their antiviral effect.[8]

Beyond inhibition, covalent chemical probes have been particularly useful for harnessing E3 ubiquitin ligases for targeted protein degradation (TPD).[9] TPD is an approach facilitated by bifunctional molecules known as proteolysis targeting chimeras (PROTACs) that induce proximity between a target protein and an E3 ligase to degrade the target protein.[10] This mechanism can have advantages over traditional inhibitors, including activity at low doses, overcoming resistance mutations, and inhibiting protein-protein interactions distal from the molecule's binding site.[11] Covalent chemical probes for a number of E3 ligases have been rapidly discovered over the last three years, enabling proof-of-concept studies demonstrating that various E3 ligases can be harnessed to induce degradation.[9] Because covalent chemical probes often bind allosteric cysteines, screening techniques often assess binding separately from enzymatic activity, and only fractional E3 ligase engagement is needed, even

unoptimized covalent chemical probes have been well-suited to use as E3 ligase recruiters for TPD.

Discovery of allosteric, non-inhibitory covalent ligands also presents an opportunity for developing other induced proximity modalities. Particularly in cases where fractional occupancy of a recruited enzyme is sufficient to induce an effect, covalent chemical probes could be quite useful as recruiters. Beyond recruiting E3 ligases to induce degradation, directing other enzymes to target proteins could modulate protein function through altering other post-translational modifications. Deubiquitinases, kinases, phosphatases, acetylases and deacetylases all come to mind as potential enzyme classes that could alter protein activity through induced proximity enabled by bifunctional molecules.[12–14] In fact, preliminary proof-of-concept studies have shown several of these mechanisms are feasible using engineered Halotag or nanobody systems or large peptidic compounds.[15] However, significant obstacles exist for clinical translation of these approaches that could be avoided by using small molecules. Covalent ligand discovery is ideally suited to identifying small molecule recruiters for these enzymes because binding reactive allosteric cysteines can preserve catalytic activity. Opening the doors of these new induced proximity modalities could enable discovery of new drugs that modulate protein function in ways that are currently impossible.

This thesis demonstrates that covalent chemical probes can be harnessed to move beyond inhibition of enzymatic activity to expand and discover induced proximity modalities. First, I review recent advances of covalent drug discovery, including the techniques that enable ligand discovery against challenging protein targets. I describe the discovery of a covalent ligand for the E3 ligase FEM1B using these approaches and show that FEM1B can be harnessed to induce protein degradation. I share the discovery of deubiquitinase targeting chimeras (DUBTACs) that induce protein stabilization, a novel induced proximity modality enabled by the discovery of the allosteric, non-inhibitory OTUB1 ligand EN523. DUBTACs provide an opportunity to stabilize proteins for therapeutic benefit, offering a modular approach to discovering molecules that induce gain-of-function. Finally, I describe the discovery of potent SARS-CoV-2 Mpro inhibitors which could provide a starting point from which to design pan-coronavirus antivirals. Together, my work demonstrates that covalent chemical probes can be used to inhibit protein function or harness it through induced proximity to modulate function of target proteins.

1.1 Background of Covalent Drugs

Covalent drugs incorporate a mildly electrophilic functional group that reacts with protein targets to confer additional affinity beyond the non-covalent interactions involved in drug binding. In the past, concerns about these reactive molecules' interference with biological assays and lack of selectivity often discouraged further investigation.[1,16] However, the number of drugs that have been discovered to act covalently after their use was already widespread indicates the potential for future successes in covalent

drug discovery efforts, and the emergence of intentionally designed covalent drugs against major disease targets over the last ten years showcases the strengths of this field.[4]

The past decade has witnessed several remarkable shifts in covalent drug discovery. Many historical covalent drugs were discovered serendipitously and bind active sites to inhibit enzymatic activity.[17] These drugs often mimic a substrate transition state that allows covalent modification of a catalytic amino acid residue. Over the past twenty years, covalently targeting non-conserved amino acids to improve selectivity has become commonplace. Covalent drugs' prolonged target engagement also provides distinct pharmacodynamic profiles and exceptional potency.[18]

These benefits of potency and selectivity have inspired medicinal chemists to explore covalent drug space despite concerns about reactivity. In many cases, compromises between these properties have produced safe and effective drugs. Examples we will discuss here include the BTK inhibitor ibrutinib (Abbvie) and EGFR inhibitor osimertinib (AstraZeneca), with $8.43 billion and $4.33 billion in 2020 sales, respectively (Fig. 1.1).[2,7] Potent inhibition through covalent modification has enabled targeting traditionally 'undruggable' proteins, such as the mutant KRAS G12C, a GTPase that has resisted decades of drug discovery efforts.[19,20] At the same time, more traditional covalent targeting of protease active sites has continued to yield valuable drugs, such as nirmatrelvir (Pfizer; Paxlovid), which inhibits the SARS-CoV-2 main protease (Mpro).[8]

While targeted covalent inhibitors are frequently discovered through structure-guided design based initially on a reversible ligand, screening libraries of electrophilic compounds to discover covalent ligands has become more common.[2,5,21] This "electrophile-first" approach is enabled by the development of chemoproteomic platforms that facilitate rapid target identification and selectivity profiling of covalent protein targets.[3,6,22–24] Combining the advances in covalent fragment screening and chemoproteomics with structural biology to empower medicinal chemistry has the potential to rapidly generate molecules that selectively bind challenging targets.

In this review we highlight historical examples of covalent drugs and the often-serendipitous discovery of their mechanisms of action. We elaborate on the major milestones in covalent drug discovery over the past decade and describe the role of covalency in these molecules' discovery and activity. Finally, we summarize the powerful techniques, with emphasis on screening strategies and selectivity profiling, that have been developed to enable covalent drug discovery.

1.3 History of Covalent Drugs

Compounds containing protein-reactive functional groups have often been avoided in medicinal chemistry and excluded from compound screening collections due to their potential for assay interference and off-target promiscuity. Many historical

examples of covalent drugs were discovered to act through covalent mechanisms after their use was already widespread. The most prominent among these is the non-steroidal antiinflammatory drug (NSAID) aspirin which has been marketed since 1899 (Fig. 1.1).[25] Aspirin's mechanism of action was unknown until 1971, when it was discovered to exert its antiinflammatory effects by acetylating Ser529 in the substrate binding channel of cyclooxygenase 1 (COX-1), preventing conversion of the substrate arachidonic acid into subsequent prostaglandins.[26]

Early covalent drugs also tend to be derived from or inspired by natural sources. β-lactam antibiotics, like Penicillin, bind to Penicillin-binding proteins (PBPs) which are involved in bacterial cell wall synthesis.[27] All PBPs contain active-site serine residues that can be acylated by penicillin, inhibiting PBP activity and leading to cell membrane rupture.[27] Another covalent antibiotic is the epoxide-containing fosfomycin, which acts by reacting with the catalytic cysteine of MurA, also disrupting peptidoglycan synthesis and inducing membrane rupture.[28–30] In a similar manner to beta-lactam antibiotics, the lactone-containing Orlistat reacts with the catalytic serine of gastric and pancreatic lipases to reduce hydrolysis of dietary fat.[31]

Proton pump inhibitors, which address gastrointestinal reflux disease, are prodrugs whose thiol-containing metabolites form disulfide bonds to inactivate their targets.[32] Omeprazole, approved by the US FDA in 1988, is an example of a proton pump inhibitor brought to market before its mechanism of action was understood to be covalent. Clopidogrel, a medication used to prevent stroke and heart attacks, is also activated by cytochrome P450 enzymes in the liver.[33] The resulting thiol-containing metabolite covalently inhibits the purinergic receptor P2Y12 on the surface of platelets to prevent clotting.

Covalent drugs have also been historically significant in cancer therapy. The pyrimidine nucleoside analog prodrugs 5-fluorouracil[34,35] and gemcitabine[36] are used to inhibit thymidylate synthase and ribonucleotide reductase I, respectively, to treat a wide range of cancers. Bortezomib, a dipeptide boronic acid which covalently binds to and inhibits the catalytic threonine residue of the 26S proteasome, was the first proteasome inhibitor approved by the FDA in 2003 to treat multiple myeloma patients.[37]

Covalent drugs have been used to treat a variety of diseases over the course of the history of medicine. However, many of these drugs were used widely before their covalent mechanisms of action were understood or discovered, and this limited researchers' ability to intentionally design covalent compounds against targets of interest
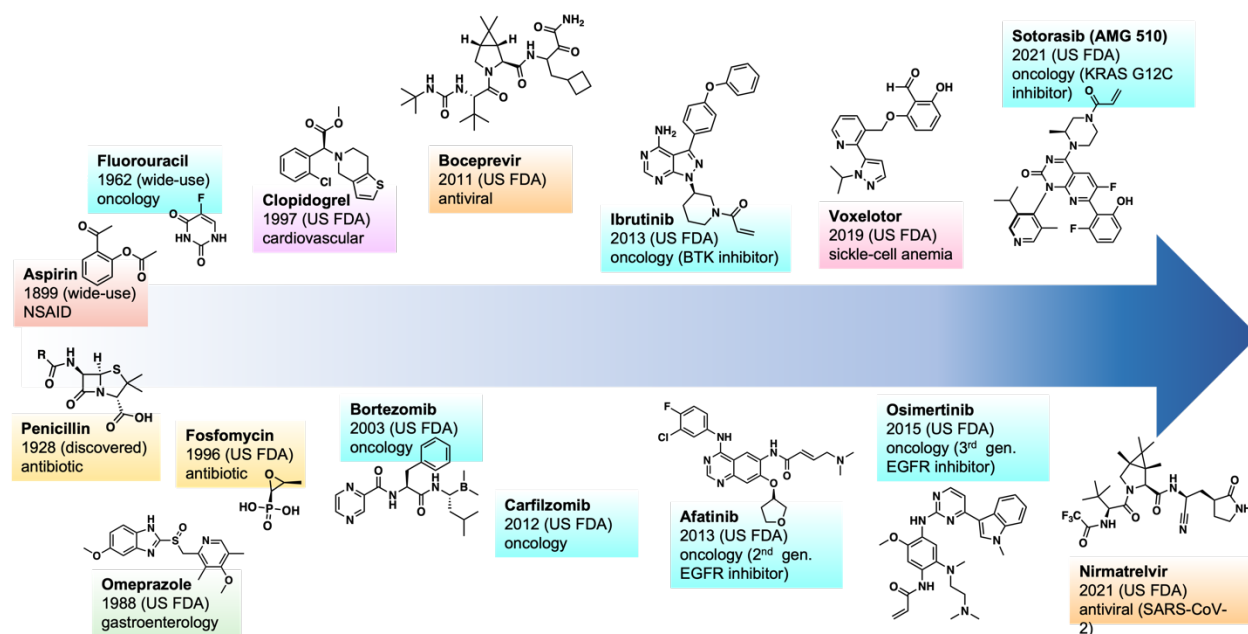
Figure 1.1. Timeline of the development of major covalent drugs.
Each covalent drug is classified to the type of disease it treat (indicated by color and label).

1.4 Targeted Covalent Inhibitors

As covalent drug discovery has improved, and issues of on-target (and off-target) toxicity have been systematically addressed, major milestones of covalent drug development have been reached. These milestones include the development of covalent EGFR inhibitors like Afatinib (approved in 2013), BTK inhibitors like Ibrutinib (approved in 2013), selective KRAS G12C inhibitors like sotorasib (approved in 2021), and the SARS-CoV-2 Mpro inhibitor nirmatrelvir (approved in 2021). These oncology and antiviral drug programs highlight the progress that covalent drug discovery has made towards developing potent and selective covalent small molecules designed to avoid toxicity issues and balance reactivity with potency and selectivity.

Covalent EGFR Inhibitors

Inhibitors of the receptor tyrosine kinase EGFR were originally developed to address EGFR's role in driving of non-small cell lung cancer (NSCLC) through its overexpression.[38] During clinical development in the early 2000s, the first approved EGFR reversible (non-covalent) inhibitors gefinitib and erlotinib were discovered to be effective against EGFR harboring somatic activating mutations, either deletions in exon 19 or the L858R point mutation which occur in 10-30% of patients with NSCLC.[38–40] Unfortunately, patients eventually still progressed in disease; in 60% of cases this was due to acquisition of the T790M "gatekeeper mutation".[41,42] The gate keeper mutation in the ATP binding site of EGFR not only reduces inhibitor binding affinity to EGFR but also increases EGFR's binding affinity to ATP.[43]
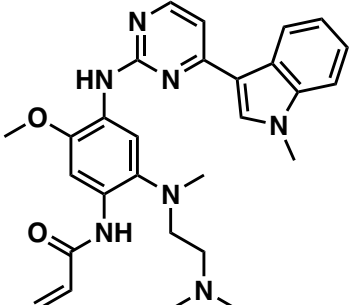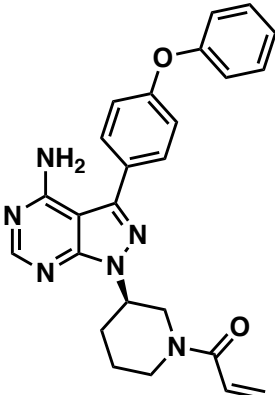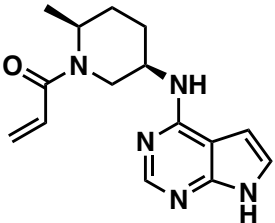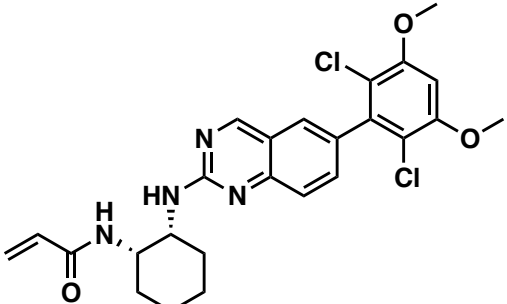
To overcome this problem, second generation covalent inhibitors were designed with acrylamide Michael acceptors to covalently engage EGFR's C797, which is located adjacent to the ATP binding site.[40] In addition to modest activity against T790M, the more durable suppression of EGFR signaling through covalent inhibition and activity against Her2 (an EGFR dimerization partner) suggested that second generation covalent EGFR inhibitors might be more efficacious than first generation reversible inhibitors like erlotinib.[40] Afatinib (Boehringer Ingelheim) was approved in 2013 as a first-line treatment for patients with metastatic NSCLC with activating mutations in EGFR.[44,45] Afatinib showed improvement over first-generation erlotinib and gefitinib, showing increased potency and prolonged target engagement due to its covalent mechanism. Despite the increased potency that covalent engagement brought against the disease target, dose-limiting toxicity likely due to wild type (wt) EGFR inhibition prevented afatinib from being as effective as platinum-based chemotherapy in treating cancers bearing the T790M gatekeeper mutation. Other second generation inhibitors include neratinib, which was approved for HER2 positive breast cancer in 2017, as it potently inhibits HER2 through covalent binding to the homologous C805 and dacomitinib (Pfizer), which was approved to treat NSCLC in 2018.[46–48]

A new third generation of covalent EGFR inhibitors followed afatinib, with the aim to selectively target for the T790M mutation over wt-EGFR (WZ-4001 (Dana-Farber),[49] Osimertinib (AstraZeneca),[50,51] and rociletinib (Clovis, CO-1686) (Table 1.1).[52] These compounds maintain the acrylamide to covalently bind C797 but exchange the quinazoline of first generation compounds for a pyrimidine to better accommodate the T790M mutation.[53] Higher affinity for T790M over wt-EGFR not only enabled efficacy in cancers with the EGFR gatekeeper mutation but also contributed to an improved safety profile and higher recommended dose than afatinib.[54] Osimertinib was granted accelerated approval by the FDA in 2015 as a second-line treatment for NSCLC and was superior to platinum-based chemotherapy in patients who had progressed during first-line EGFR TKI therapy.[55] It was then approved as a first-line treatment for metastatic NSCLC in 2018. Osimertinib does depend on C797 for covalent binding, and C797X mutations account for 15% of cases of resistance to second-line osimertinib.[56–58] Therapeutic options are limited for the resulting triple mutant L858R/T790M/C797S, though non-covalent fourth generation EGFR inhibitors (such as EAI045) have been discovered that bind reversibly to an allosteric pocket created by the displacement of the C-helix in the inactive conformation of EGFR.[59] Allosteric inhibitors could also potentially be used in combination with covalent orthosteric inhibitors such as osimertinib, though these allosteric compounds have yet to enter clinical trials.[60] In the meantime, osimertinib remains the standard of care for many types of NSCLC and demonstrates the power of covalent drugs to maintain potency despite mutations around the binding site.

The success of covalent EGFR drugs validated the approach of engaging non-catalytic, non-conserved cysteines adjacent to kinase active sites in order to boost potency and modulate pharmacodynamics. In particular, development of these drugs showed that the acrylamide electrophile was reactive enough to engage a cysteine adjacent to a compound binding site but not so reactive as to induce haptenization and

adverse immune response. Incorporating covalent binding in EGFR inhibitors also enabled selectivity among kinases by designing interactions with a non-conserved cysteine rather than active-site residues that typically interact with ATP.

Table 1.1. Highlighted Covalent Kinase Inhibitors

Drug (Company; Former compound name)	Structure	Target	Approval/Trial Status	Ref(s)
Osimertinib (Astrazeneca; AZD9291)		Mutant-selective EGFR inhibitor	FDA approved 2015 for NSCLC	50,51,54,55
Ibrutinib (Abbvie; PCI-32765)		BTK inhibitor	First FDA approval in 2013 for mantle cell lymphoma – approved for many other B cell malignancies since 2013	61–63
Ritlecitinib (Pfizer; PF-06651600)		JAK3 inhibitor	Ph III for Alopecia Areata, Ph II for many other inflammatory indications	64–66
Fisogatinib (Blueprint; BLU-554)		FGFR4 inhibitor	Ph II for hepatocellular carcinoma	67

Covalent BTK Inhibitors

Bruton's tyrosine kinase became a target of interest in chronic lymphocytic leukemia due to its critical role downstream of the B-cell receptor.[68] Activation of the B-cell receptor induces phosphorylation of BTK through Lyn and Syk kinases, and eventually activates transcription factors related to B-cell proliferation and differentiation, as well as cell migration and adhesion.[69] Additionally, BTK is mutated in X-linked agammaglobulinemia (XLA) where loss-of-function mutations result in B-cell deficiency.[70] This critical role in B-cell development indicated it was a relevant target for B-cell malignancies.

In the early 2000s, scientists at Celera Genomics used a structure-based approach to discover an acrylamide-containing inhibitor of the BTK kinase domain that could be used as a tool compound to fluorescently label BTK, and were interested in using BTK inhibitors to treat rheumatoid arthritis.[61] After acquisition by Pharmacyclics, it was discovered that the tool compound itself, later named ibrutinib, had sufficient affinity and selectivity for BTK to advance into clinical studies.[62,71] Ibruitinib (Abbvie) was approved by the FDA for the treatment of chronic lymphocytic leukemia (CLL) in 2013 following trials showing remarkable overall response rate of 70%, and progression free survival of 75% after 26 months (Table 1.1).[63,72] This was followed by a number of approvals as a second line therapy for B-cell cancers including for relapsed/refractory mantle cell lymphoma, Waldenstrom's macroglobulinemia, and chronic graft versus host disease.[73–75]

Similar to EGFR inhibitors, ibrutinib binds BTK's C481 adjacent to the ATP binding site and only a handful of kinases have a homologous cysteine.[76] Ibrutinib's rapid clearance ($t_{1/2}$ = 2-3 hours) also enables remarkable kinase selectivity: ibrutinib maintains activity against BTK due to prolonged covalent engagement while reversible off-target inhibition is minimized.[77] This combination of fast covalent engagement of BTK with rapid clearance allows for selectivity *in vivo* even despite off-targets observed in biochemical assays. Ibrutinib has a remarkable safety profile as a result, with maximum tolerated dose not reached in phase 1 studies; doses of 420 mg and 560 mg daily were recommended for CLL and MCL, respectively.[77] Despite historical concerns over potential toxicity of covalent drugs, ibrutinib demonstrates that rationally designed covalent drugs are able to achieve acceptable safety profiles and blockbuster status. In 2020 alone, Abbvie's Imbruvica revenues totaled $8.53 billion, making it the 5th highest grossing drug that year.[78] Ibrutinib's success builds on that of covalent EGFR inhibitors such as osimertinib by showing that kinase inhibitors targeting non-conserved cysteines adjacent to the ATP binding site are capable of being developed into successful drugs.

A number of other BTK kinase inhibitors have been discovered that improve on various aspects of ibrutinib. Several second-generation BTK inhibitors highlight the variety of Michael acceptors that can be used as alternatives to acrylamides for covalently binding cysteine residues. Most prominent among these is acalabrutinib (AstraZeneca), approved by the US FDA in 2019 to treat CLL, which contains a butyramide electrophile that is less reactive towards BTK C481 and GSH.[79] One crucial tool that is commonly used to assess cysteine reactivity of covalent inhibitors is a glutathione (GSH) reactivity assay, where the compound is incubated with excess GSH

and consumption of the compound is observed via LCMS.[79–81] The lower reactivity of the butyramide, in addition to other substitutions, enables acalabrutinib's superior selectivity over ibrutinib for BTK. This improved selectivity could be responsible for acalabrutinib's improved safety profile, in particular reducing cardiovascular adverse events.[82,83] Other covalent BTK inhibitors include tirabrutinib (Ono/Gilead, approved in Japan 2020) and branebrutinib (Bristol-Myers Squibb) which also contain a butyramide electrophile, while spebrutinib (Bristol-Myers Squibb) and zanubrutinib (Beigene, approved 2019 in US) and evobrutinib (Merck KGaA) contain acrylamides.[84–86] In general, these second-generation BTK inhibitors have been developed through structure-based design and each bear strong resemblance to ibrutinib.

One interesting development in designing new electrophiles for covalent drugs is the discovery that cyanoacrylamides are able to form reversible-covalent bonds with cysteine residues, and are effective in inhibiting BTK.[87–89] This covalent yet reversible interaction would ideally be able to increase potency while reducing off-target reactivity, though the cyanoacrylamide BTK inhibitor rilzabrutinib (Principia/Sanofi) was recently shown to be ineffective in treating the autoimmune disease pemphigus.[90] While BTK has been a target in inflammatory and autoimmune disease since the early 2000s, no BTK inhibitor has yet been approved for any indication in these fields.[91] This suggests that while rilzabrutinib was not successful, the tunable covalency of cyanoacrylamides may still hold value for other targets.

The discovery of ibrutinib and other covalent BTK inhibitors reemphasizes the lessons learned from covalent EGFR inhibitors. Employing structure-based design to target a non-conserved cysteine residue adjacent to the ATP binding site allowed for selective targeting of BTK. Taking advantage of the PK/PD characteristics of ibrutinib enabled by its covalent mechanism of action allowed prolonged BTK blockade while reducing off-target kinase inhibition through rapid clearance *in vivo*. Newer BTK inhibitors based on ibrutinib more finely tune the cysteine-reactivity of the electrophile and improve selectivity. Most significantly, the performance of ibrutinib in treating B-cell malignancies emphasizes that molecules once considered chemical biology tool compounds can be highly effective drugs in their own right.

Other Covalent Kinase Inhbitors

Success with covalent EGFR and BTK inhibitors has driven interest in covalent inhibitors of other kinases with non-conserved cysteines adjacent to ATP-binding sites to gain selectivity, especially within kinase families.[92,93] One example is the non-receptor tyrosine kinase JAK3, which is primarily expressed in leukocytes and whose function in cytokine signaling has led to its investigation as a target in autoimmune disease.[65] Covalent targeting of the non-conserved Cys909 of JAK3 has been used to gain selectivity over the other JAK family members by a number of covalent JAK3 inhibitors.[64,65,94–96] One of these, ritlecitinib (Pfizer, PF-06651600), has shown promising results for rheumatoid arthritis patients in a phase II clinical trial (Table 1.1).[66]

Another target of interest is the receptor tyrosine kinase FGFR4, which is implicated as a target in hepatocellular carcinoma (HCC) due to overexpression of its ligand FGF19.[67] In a very similar manner to discovery of JAK3 inhibitors, compounds have been discovered that covalently target the non-conserved Cys552 to confer

selectivity for FGFR4 over FGFR1-3, and can overcome mutations that confer resistance to first-generation FGFR inhibitors.[97] The acrylamide-containing FGFR inhibitor fisogatinib (Blueprint, BLU-554) is currently the subject of a Ph2 clinical trial (NCT04194801) (Table 1.1), while the reversible-covalent aldehyde roblitinib (Novartis, FGF401) which also reacts with Cys552 is also currently under clinical investigation (NCT02325739).[67,98]

In addition to JAK3 and FGFR4, a number of compounds have been developed to selectivity target various cyclin-dependent kinases (CDKs), including CDK7 and CDK12/13 and explore these kinases' roles in transcriptional regulation.[99,100] Overall, rational design of covalent kinase inhibitors targeting non-conserved cysteines adjacent to the ATP-binding site has become a common approach to enhance kinase inhibitor potency and selectivity.
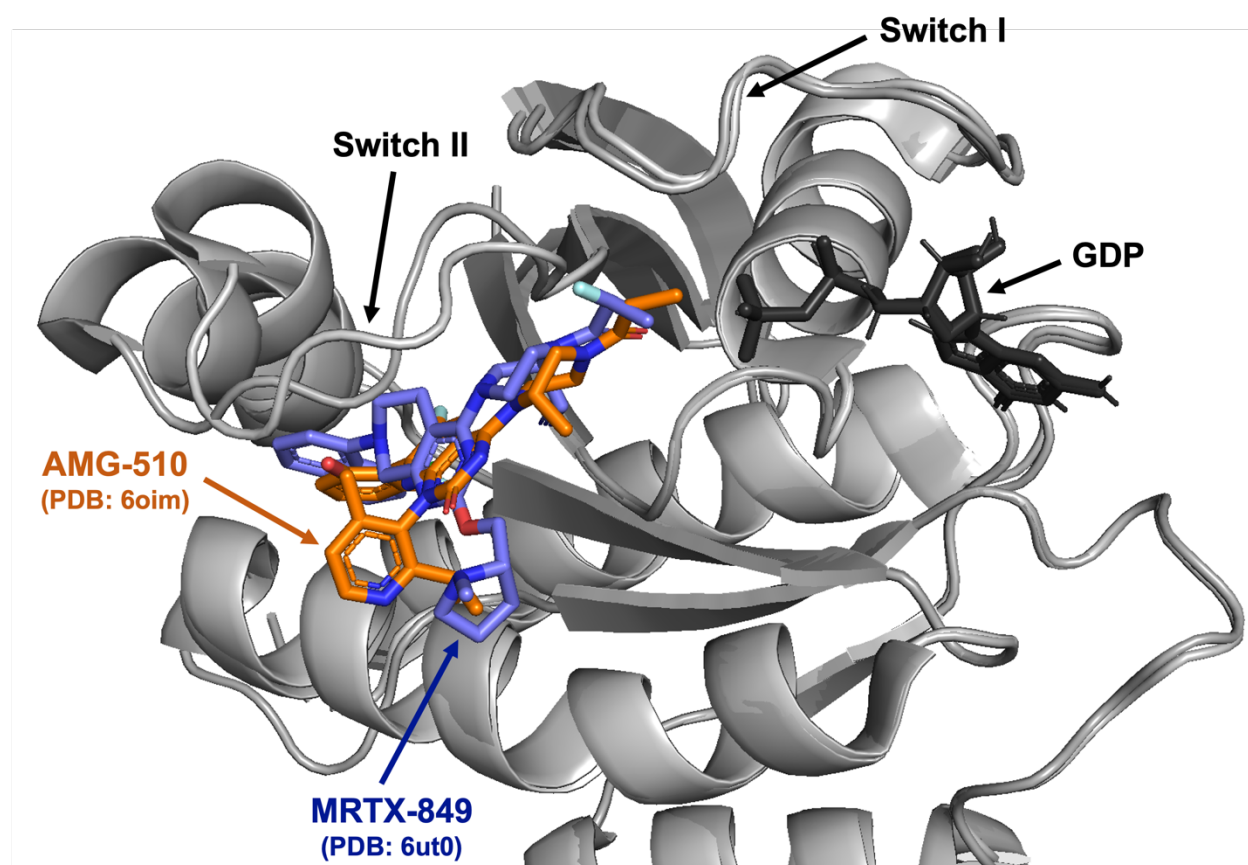
Figure 1.2. KRAS^{G12C} in complex with covalent inhibitors.
Aligned structures (PDB: 6UT0 and 6OIM) of KRAS^{G12C} co-crystalized with MRTX-849 (adagrasib) and AMG-510 (sotorasib). Inhibitors are bound to the S-IIP, adjacent to the GDP binding pocket. Switch I and II are indicated.

Covalent KRAS^{G12C} Inhibitors

One of the most exciting discovery-to-clinic stories for covalent drugs in the last ten years is the design of KRAS-G12C mutant selective covalent inhibitors. KRAS is an oncogenic GTPase that is mutated in about 25% of all cancers, most notably in

pancreatic, colorectal, and lung cancers.[101] Wild-type KRAS is carefully regulated between active GTP-bound states and inactive GDP-bound states, but mutated KRAS has a much higher affinity for the GTP-bound active conformation leading to low rates of ATP hydrolysis and elevated Ras signaling, driving tumorigenesis and clinical resistance.[102] Since the discovery of the role of KRAS in cancer nearly 30 years ago, attempts to drug it directly using traditional drug discovery methods have been unsuccessful.[19,20] KRAS does not have accessible pockets for reversible inhibitors to bind, competitive inhibitors would need to overcome picomolar binding affinities of GTP/GDP, and the development of pan-KRAS inhibitors could lead to on-target toxicity.[101,103]

In 2013, Kevan Shokat at UCSF published the first example of a selective covalent inhibitor of the mutant KRAS-G12C.[103] Developing covalent KRAS inhibitors against the G12C mutation is appealing for several reasons: 1) targeting mutant KRAS could allow for selective cytotoxicity to cancer cells, 2) the affinity enabled by covalent binding would be advantageous as KRAS lacks easily ligandable pockets, 3) 45% to 50% of KRAS mutations in NSCLC are KRAS^{G12C}, presenting a promising patient group that would directly benefit from KRAS^{G12C} inhibition, and 4) position 12 in KRAS sits closely beneath the GTP/GDP effector binding region as well as the nucleotide binding pocket, suggesting covalent KRAS^{G12C} ligands might affect KRAS function.[102]

In 2013, Ostrem et al. at UCSF used a disulfide-fragment-based screening approach called tethering, and screened a library of 480 disulfides against KRAS^{G12C} in the GDP-bound state using intact protein mass spectrometry.[103] Co-crystal structures of KRAS^{G12C} showed the tethering hits bound to the Switch-II region, and further medicinal chemistry yielded acrylamide and vinyl sulfonamide KRAS^{G12C} inhibitors active *in vitro*. Compound 12, their lead compound, induced apoptosis in KRAS^{G12C} mutant cell lines at 10 μM treatment conditions over 48 hours.[103] Compound binding to the S-IIP (switch II pocket), which was not apparent in previous structures of RAS, impairs KRAS by shifting the nucleotide affinity from favoring GTP to GDP and leads to the accumulation of KRAS in its inactive state.[104] Beyond identifying inhibitors of KRAS, the Shokat lab's breakthrough discovery of the allosteric S-IIP proved critical in understanding the mechanism of covalent inhibition of KRAS^{G12C}.

This novel mechanism for KRAS^{G12C} selective inhibition paved the way for the development of clinical covalent KRAS^{G12C} inhibitors. In 2016, Wellspring Biosciences disclosed ARS-853, a selective, covalent inhibitor of KRAS^{G12C} with *in cellulo* efficacy in the low micromolar range.[105] Patricelli et al. used a cellular LC/MS-MS-based assay to determine the degree of KRAS^{G12C} engagement in H358 cells by quantifying decreasing amounts of the Cys12–containing peptide from tryptic digests of these mutant cells upon treatment with candidate compounds. Structure-guided optimization of Ostrem et al.'s Compound 12 yielded ARS-853, which when crystalized with KRAS^{G12C}, showed significant improvements in binding of the S-IIP. ARS-853 treatment in mutant cell lines reduces active KRAS^{G12C}, inhibits downstream Ras signaling, and induces apoptosis with 1 μM treatment conditions in KRAS^{G12C} cell lines. While KRAS^{G12C} was previously thought to be constituently active, with no GTPase activity, the selective binding of ARS-853 to GDP-bound, inactive KRAS^{G12C} provided evidence that KRAS mutants indeed cycle between GTP- and GDP-bound states.

The development of improved KRAS[G12C] inhibitors continued with the publication of ARS-1620 by Wellspring. ARS-1620 was the result of an effort to overcome metabolic stability and bioavailability limitations of ARS-853 to facilitate *in vivo* studies of KRAS[G12C] inhibition.[102] ARS-1620 is based on a novel quinazoline core scaffold, designed to better occupy the S-IIP and thus rigidify a more favorable conformation for covalent reaction with the acrylamide warhead, and additionally act as a more diversifiable molecule with better drug-like properties. ARS-1620 showed efficacy in patient derived tumor xenograft studies with G12C mutations, treating at 200mg/kg. Ultimately, ARS-1620 was identified as the first example of a direct KRAS[G12C] small-molecule inhibitor that was orally bioavailable and suited for *in vivo* studies. Improved potency of this series of KRAS[G12C] inhibitors and success in *in vivo* models indicated that it might be possible to design clinically efficacious drugs.

Sotorasib (Amgen, AMG-510, Lumakras/Lumykras) was the first selective KRAS[G12C] inhibitor to enter clinical trials in 2018 (NCT03600883) and was developed by Amgen in partnership with Carmot Therapeutics (Table 1.2).[106] They screened a custom library of covalent cysteine reactive small-molecules, utilizing Carmot's Chemotype Evolution platform and structure-based design to identify sotorasib. Sotorasib was designed to occupy and exploit a previously unknown sub-pocket in the S-IIP of KRAS[G12C], interacting with H95, Y96, and Q99 (Fig. 1.2).[107] A phase II clinical trial investigating sotorasib was successfully completed in 2020, followed by FDA approval to treat adults with KRAS[G12C] -mutated locally advanced or metastatic non-small cell lung cancer (NSCLC) in May 2021.[108] Other covalent KRAS[G12C] inhibitors are quickly following sotorasib through clinical trials, including JNJ-74699157 (ARS-3248; J&J/Wellspring), which is being investigated in patients with several types of advanced solid tumors expressing KRAS[G12C] including NSCLC and colorectal cancer (NCT04006301). Mirati has also developed adagrasib (MRTX-849) with Array BioPharma by identifying tetrahydropyridopyrimidines as irreversible covalent inhibitors of KRAS[G12C] and using structure-based design approaches to optimize adagrasib, which entered clinical trials in January 2019 (NCT03785249).[109,110] Adagrasib was granted a breakthrough therapy designation by the FDA in June 2021 for use as a potential therapeutic option for patients with KRAS[G12C] NSCLC following previous systemic therapy.[111]

Designing small-molecule covalent KRAS[G12C] selective inhibitors provides an elegant solution to drugging an undruggable cancer target. This story represents a major step forward in oncology, and the process by which KRAS[G12C] inhibitors were designed can provide a map for targeting other common KRAS mutations like G12D, G13D and G13C. In the case of other diseases where a point mutation leads to the substitution of a nucleophilic amino acid, covalent inhibitors present an optimal opportunity to provide precision therapy for patients.

1.5 Covalent Protease Inhibitors

Beyond targeted covalent inhibitors that react with non-catalytic amino acids, drugs that target catalytic sites of proteases have been valuable as well. Covalent proteasome inhibitors have been approved for cancer therapy, while covalent drugs have had

significant success in targeting viral proteases, particularly the main protease (Mpro) of SARS-CoV-2.
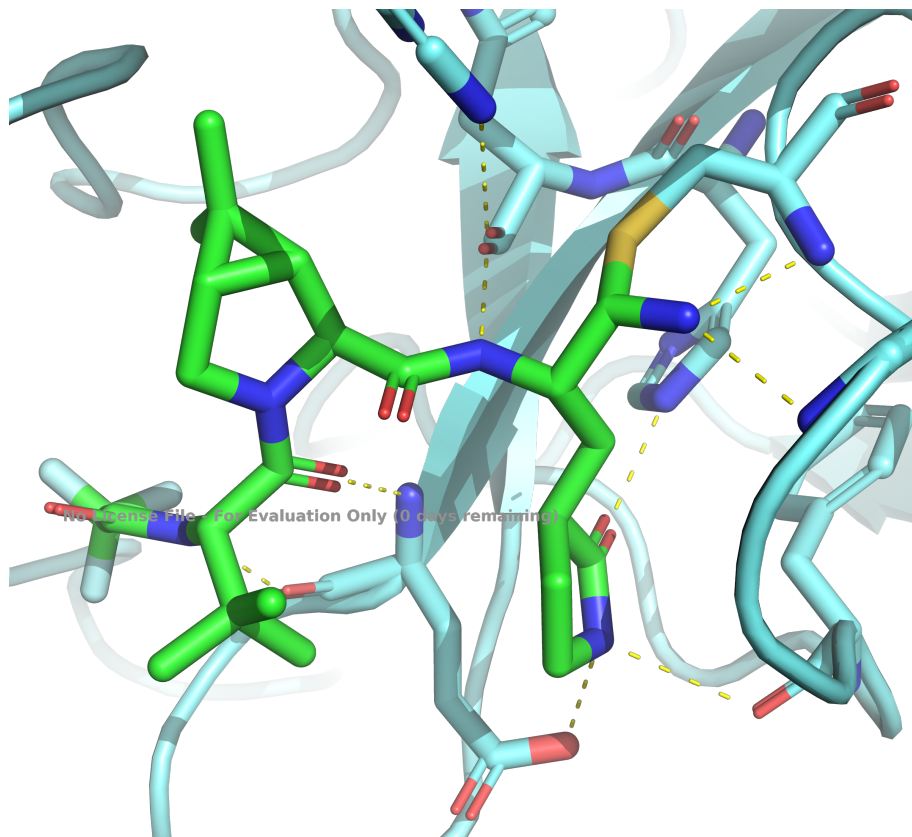
Figure 1.3. Nirmatrelvir in Complex with SARS-CoV-2 Mpro.
The nitrile of nirmatrelvir has reacted with Mpro Cys145 to form a covalent thioimidate adduct, and extensive hydrogen-bond interactions are shown throughout the pocket (PDB code 7RFW) (Owen 2021).

Covalent SARS-CoV-2 Main Protease Inhibitors

Since the beginning of the COVID-19 pandemic, over 420 million cases of COVID-19 have been reported worldwide and over 5.86 million people have died from the disease.[112] Vaccines against COVID-19 were developed at unprecedented speeds and similar research momentum is leading to the development of therapeutics that will benefit infected patients. On December 22, 2021, the FDA issued an Emergency Use Authorization (EUA) for Pfizer's Paxlovid (nirmatrelvir and ritonavir, co-packaged for oral use) to treat mild-to-moderate COVID-19 (caused by the SARS-CoV-2 coronavirus) in adults and some pediatric patients, marking the first approved oral treatment for the disease.[113] Nirmatrelvir covalently inhibits the main protease (M[pro]) of SARS-CoV-2, and ritonavir is a CYP3A inhibitor used to enhance the pharmacokinetic properties of protease inhibitors in general (Table 1.2).[16]

SARS-CoV-2 is a single-stranded RNA virus that encodes for two polyprotein precursors (pp1a and pp1ab) as well as structural and accessory proteins.[114] Viral replication depends on successful cleavage of pp1a and pp1ab by the main protease (M[pro], also referred to as 3CLpro) into functional viral proteins.[114] Additionally, viral M[pro] cleaves its substrates after Gln, which is a unique cleavage site compared with known human proteases. Therefore, M[pro] is a promising protein target for drug development against SARS-CoV-2. Because M[pro] is a cysteine protease (with a catalytic diad composed of Cys145 and His41), covalently inhibiting the catalytic cysteine should prevent viral replication.[114]

The discovery of covalent inhibitors against SARS-CoV-2 M[pro] emerged from extensive previous work towards developing protease inhibitors for SARS-CoV-1, which is the causative virus for the severe acute respiratory syndrome coronavirus 1 outbreak in 2002-2003.[114] During the 2002-2003 SARS outbreak, caused by the SARS-CoV-1 coronavirus, Anand et. al. used a crystal structure of the homologous porcine TGEV coronavirus M[pro] bound to a hexapeptidyl chloromethylketone (CMK) inhibitor as a model to provide a base for the design of potential SARS-CoV-1 M[pro] inhibitors.[115] While peptidomimetics can pose challenges due to their inherent metabolic instability, Anand et. al. argued that the significantly shared homology across all M[pro] active sites should enable the use of other viral M[pro] inhibitors as the starting point for SARS-CoV-1 specific M[pro] drugs. Rupintrivir, developed originally to target human rhinovirus (HRV) M[pro], could provide an initial scaffold for further investigation.[115]

Because the SARS-CoV-1 outbreak subsided, work into developing coronavirus M[pro] inhibitors slowed until the emergence of SARS-CoV-2 in 2019. SARS-CoV-2 M[pro] shares 96% sequence identity with SARS-CoV-1 M[pro], and there is 100% sequence overlap of the catalytic sites.[116] Renewed interest in improving on chloromethyl ketone inhibitors lead to Hoffman et. al. systematically exploring the medicinal chemistry around rupintrivir to develop potent *in vitro* SARS-CoV-2 M[pro] inhibitors (both reversible and irreversible covalent inhibitors). Rupintrivir initially showed little inhibitory activity against SARS-CoV-1 M[pro], but Hoffman et. al. were able to improve affinity enough to obtain a co-crystal structure with SARS-CoV-1 M[pro]. This enabled identification of the hydroxymethylketone PF-00835231 which demonstrated potent SARS CoV-1 M[pro] inhibition both in a FRET-based activity assay, activity in antiviral cell-based assays, good solubility, stability in plasma, and low clearance *in vivo*. The identification of PF-00835231 as a potent inhibitor of SARS-CoV-2 M[pro] spurred further pre-clinical investigation to determine if it could be used as a COVID-19 therapeutic.
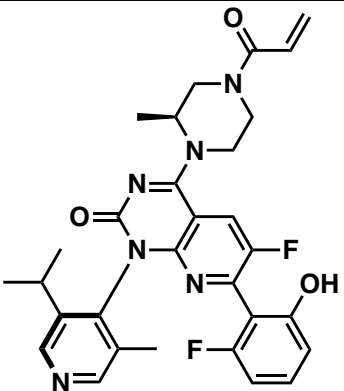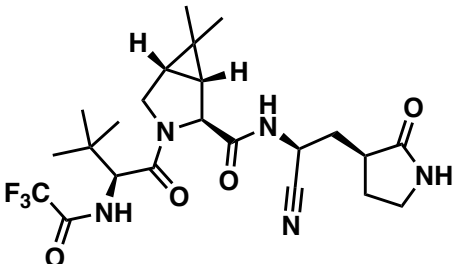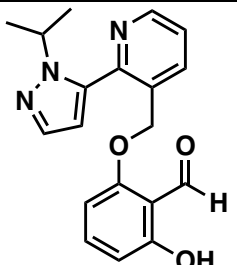
Concurrently with Hoffman et. al., Qiao et. al. designed M[pro] inhibitors based on the approved hepatitis C antivirals telaprivir and boceprevir (Table 1.2). The active site of M[pro] is composed of four sites (S1′, S1, S2, and S4), which accommodate four components of the various established inhibitors (P1′, P1, P2, and P3, respectively). Keeping P1 fixed, Qiao et. al. synthesized compounds that varied at the P2 position only based on HCV NS3/4a inhibitors boceprevir and telaprivir and varied P3 significantly across the series.[114] Activities of the compound series were measured by the standard FRET-based activity assay against recombinant SARS-CoV-2 protein, and direct binding was confirmed by differential scanning fluorimetry. MI-09 and MI-30 (both containing aldehyde warheads) were identified as the most potent hits (with IC50 values of <20 nM in the *in vitro* FRET assay). MI-09 and MI-30 inhibited SARS-CoV-2 infection

in a human angiotensin-converting enzyme 2 (hACE2) transgenic mouse model, showing these compounds could reduce lung lesions *in vivo*.

With a set of potent SARS-CoV-2 M^{pro} inhibitors in hand and established *in vitro* and *in vivo* SARS-CoV-2 assays, Owen et. al. set out to improve oral bioavailability of PF-00835231. PF-00835231 showed potent inhibitory activity in the SARS-CoV-2 FRET-based assay as well as antiviral activity (EC50 = 231 nM) in Vero E6 cells. However, improving oral bioavailability would significantly increase the potential for PF-00835231 to impact most COVID-19 patients. Owen et. al. replaced the a-hydroxymethyl ketone with a nitrile, which is capable of acting as an electrophilic warhead.[117] Nitriles are able to covalently bind particularly reactive nucleophiles, though the ease of thiol elimination from the thioimidate adduct makes nitriles more reversible than some other electrophiles such as acrylamides.[118] This compound demonstrated significant improvement in rat oral absorption, while maintaining metabolic stability, but *in vitro* and *in cellulo* antiviral activity was reduced. Hydrogen bond donors were removed by introducing a bicyclic proline derivative at P2, and the trifluoroacetamide capping group to restore potency through occupying the S3 pocket. Combining these changes yielded PF-07321332, a highly potent SARS-CoV-2 reversible covalent inhibitor that displayed potent inhibition in the FRET assay across all human coronaviruses, while no inhibitory effects were seen against human cysteine or serine proteases. *In vivo* efficacy of PF-07321332 was demonstrated in a mouse-adapted SARS-CoV-2 (SARS-CoV-2 MA10) model, and PF-07321332 additionally showed good oral bioavailability, favorable off-target selectivity, and metabolic stability in rats and monkeys. PF-07321332, named nirmatrelvir, was investigated as a monotherapy and in combination with ritonavir (a CYP3A inhibitor that enhances the PK profile of nirmatrelvir) in a randomized, double-blind, placebo-controlled, single ascending dose study in healthy adults (NCT04756531) (Fig. 1.3).[16]

Paxlovid (combination nirmatrelvir/ritonavir) was shown to be highly effective at preventing symptomatic patients' progression to severe COVID-19 in a Phase II/III clinical trial data released in November 2021.[119] The emergence of the orally bioavailable drug for COVID-19 will help to ameliorate illness for non-hospitalized patients in high-risk groups.[120] As a whole, SARS-CoV-2 M^{pro} covalent inhibitors provide a promising avenue to treat coronavirus infections either as monotherapies or in combination with other antiviral drugs. The quick adaptation of previous protease inhibitors to selectively target SARS-CoV-2 M^{pro} is an example of elegant structure-based design paired with the power of covalent drugs.

Table 1.2. Highlighted Covalent Drugs

Drug (Company; Former compound name)	Structure	Target	Approval and Indication	Ref(s)
Sotorasib (Amgen; AMG510)	(chemical structure)	KRAS^{G12C} inhibitor	FDA Approved in 2021 for NSCLC with *KRAS^{G12C}* mutation	[106–108]
Nirmatrelvir (Pfizer; PF-07321332)	(chemical structure)	SARS-CoV-2 Mpro inhibitor	FDA approved in 2021 for COVID-19	[117,119]
Voxelotor (Global Blood Therapeutics; GBT-440)	(chemical structure)	Lysine-reactive mutant hemoblobin modulator	FDA approved in 2019 for sickle cell anemia	[121–123]

Covalent HCV NS3/4a Protease Inhibitors

The NS3/4a serine protease cleaves the HCV polyprotein into multiple non-structural proteins, which are required for replication.[124] While HCV had been treated with a combination of PEGylated interferon alpha and ribavirin, modest response rates and significant adverse events prompted the discovery of NS3/4a protease inhibitors to treat HCV.[125] Based of initial observations that hexapeptide cleavage products could inhibit NS3/4a, the linear peptidomimetic inhibitors boceprevir[126,127] and telaprevir[128,129] were designed. These compounds, along with narlaprevir,[130] use a ketoamide to covalently engage the catalytic serine of NS3/4a. This covalent interaction is relatively reversible due to elimination of the serine alcohol from the protein-inhibitor adduct.[131] Boceprevir and telaprevir were effective in treating HCV and approved in 2011 after

successful trials,[132,133] though telaprevir was withdrawn in 2014 due to adverse events and boceprevir was discontinued by Merck in 2015 due to the superiority of newer direct-acting antivirals, in particular lepidasvir/sofosbuvir (Gilead) which target the HCV polymerases NS5a and NS5b.[134–136] However, the success of ketoamide NS3/4a inhibitors in improving efficacy of interferon/ribavirin therapy emphasizes the utility of the ketoamide as a serine-reactive electrophile in designing covalent antivirals.

Covalent Proteasome Inhibitors

Bortezomib, a boronic acid proteasome inhibitor, was approved in 2003 to treat multiple myeloma. To identify proteasome inhibitors with improved safety profile, a series of medicinal chemistry efforts transformed the natural product epoxomycin to carfilzomib (Proteolix/Onyx), which was approved in 2012.[137] Carfilzomib's epoxyketone is able to form a morpholino ring with the catalytic N-terminal threonine of the 20S proteasome, and this mechanism confers high selectivity because most proteases do not have N-terminal nucleophiles.[138] The mechanism of carfilzomib highlights how covalency can help drive selectivity, rather than encourage promiscuity and off-target inhibition.

1.6 The Covalent Drug Discovery Toolbox

Covalent drug discovery is enabled by a myriad of techniques that provide the means for discovery and characterization of electrophilic molecules. In particular, activity-based protein profiling (ABPP) approaches have transformed characterization of electrophilic compounds. Combining ABPP-style techniques with other advances in covalent ligand screening has enabled adoption of "electrophile-first" drug discovery efforts. This type of approach proved successful in drugging KRAS^{G12C} and has facilitated rapid discovery of E3-ligase ligands. Looking forward, the immense knowledge of reactive sites across the proteome generated through chemoproteomic experiments over the past decade will provide powerful insights into potential targets of covalent drugs.

Chemoproteomics-Enabled Covalent Ligand Discovery

One of the most important tools in covalent drug discovery is the use of chemoproteomics platforms to identify covalent compounds and their corresponding ligandable sites on target proteins directly in complex biological systems. Advances in chemoproteomics have facilitated the discovery of covalent ligands against undruggable disease targets, selectivity profiling of covalent ligands across the proteome to identify targets and off-targets of these ligands, and discovery of novel covalent E3 ligase recruiters and deubiquitinase recruiters for targeted protein degradation and stabilization platforms.
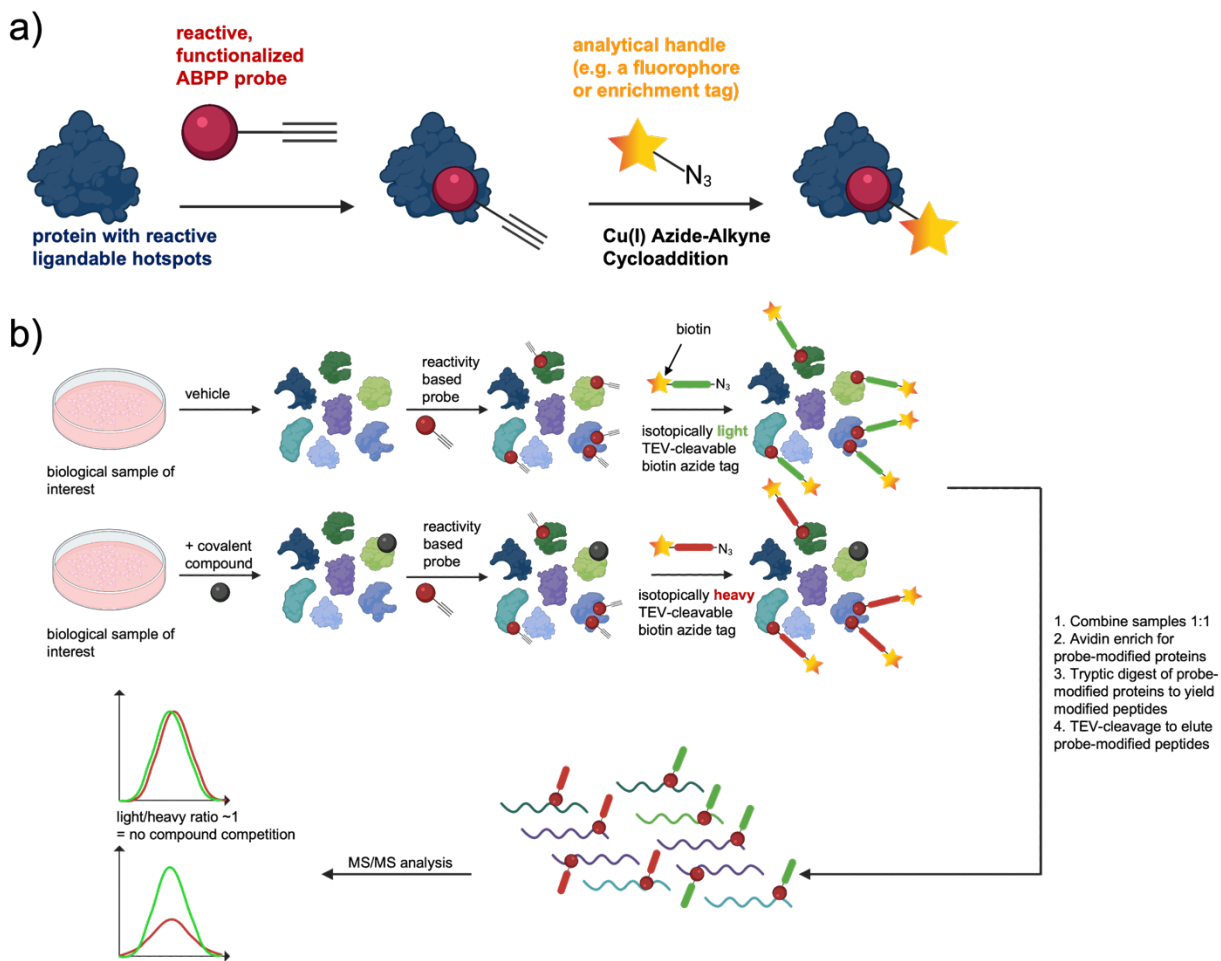
Figure 1.4. Isotopic tandem orthogonal proteoloysis–activity-based protein profiling (isoTOP-ABPP).
a) Example of a reactive probe for ABPP designed with a broadly reactive electrophilic warhead linked to an analytical handle. b) Schematic of competitive isoTOP-ABPP methodology.

Covalent Ligand Discovery Using ABPP

Activity-based protein profiling (ABPP) enables the discovery of covalently ligandable sites and corresponding ligands in complex biological samples. ABPP was initially pioneered by Cravatt and Bogyo using active-site directed chemical probes that covalently targeted catalytic residues of various enzyme classes - including hydrolases, proteases, and kinases.[139] This technique, often using gel-based assays, was employed to gain functional readouts of these active enzymes in biological contexts.[3,139,140] ABPP probes contain a warhead that covalently reacts with nucleophilic amino acids (such as cysteine) and a reporter handle to monitor probe binding such as a fluorophore, biotin, or alkyne moiety for subsequent click chemistry-enabled applications (Fig. 1.4a).[139]

Instead of focusing on active sites, more recent ABPP approaches use mass spectrometry and broadly reactive chemical probes to map allosteric reactive sites as well.[141] Weerapana et al first described the isoTOP-ABPP (isotopic tandem orthogonal proteolysis–activity-based protein profiling) approach which used an iodoacetamide (IA) probe to identify hyper-reactive cysteines across the proteome (Fig. 1.4b).[141,142] In addition to the iodoacetamide electrophile, the probe contains an alkyne which links to an azide- and biotin-containing, TEV protease-cleavable tag with either an isotopically light or heavy valine. These functionalities enable enrichment of probe modified peptides, and tandem analysis of two light/heavy samples with mass-spectrometry, controlling for run-to-run variability and allowing for quantitative comparisons between samples. Weerapana et al. discovered that cysteine hyper-reactivity predicts functionality in catalysis and at sites of PTMs.[142]

Building off this work, Backus et al used competitive isoTOP-ABPP to identify proteome-wide targets of a small covalent fragment library by competing individual acrylamides and chloroacetamides with the IA-alkyne probe.[143] This study identified >700 ligandable cysteines and provided information about the proteome-wide selectivity of each covalent fragment. Backus et al. used the covalent ligands discovered with this approach and their corresponding ligandable sites to help elucidate the role of CASP8 and CASP10 in extrinsic apoptosis in T cells, showing that this approach can rapidly identify compounds that target proteins of biological interest. Bar-Peled et al used isoTOP-ABPP to map cysteine reactivity and ligandable sites in KEAP1 mutant vs wild type KEAP1 NSCLC lines, and discovered the nuclear receptor NR0B1 has a ligandable cysteine regulated by NRF2, the substrate of KEAP1.[144] Several chloroacetamides were identified that bound NR0B1 selectively and altered the transcriptional profile and growth of NRF2-activated cells. In an impressive study, Vinogradova et al explored cysteine ligandability in activated T cells, using promiscuous acrylamide/chloroacetamide "scout-fragments" to map ligandability, and functional assays to identify elaborated electrophilic compounds that suppress T cell activity.[145] This approach identified several proteins that could be targeted covalently to impair T cell activity, including BIRC2/3, the NuRD complex, and the kinases ITK and CYTIP.

IsoTOP-ABPP can also be used to identify the protein targets of electrophilic drugs, such as the dimethyl fumarate (DMF) used to treat autoimmune disease. Though DMF has been used for decades to treat psoriasis and was approved the FDA in 2013 for multiple sclerosis, the direct covalent targets of DMF remained unclear. Separate studies have used chemoproteomic approaches to identify both protein kinase C-θ (PKCθ) and IRAK4 as targets of DMF.[146,147] In both cases, covalent engagement of a cysteine disrupted a protein-protein interaction to modulate immune cell function. Disrupting the PKCθ-CD28 interaction reduced T-cell activation, and disrupting the IRAK4-Myd88 interaction suppressed interferon-alpha production in plasmacytoid dendritic cells.[146,147]

IsoTOP-ABPP can also be used for target identification and selectivity assessment of covalently-acting small-molecules that are discovered initially from cell-based phenotypic screens (Fig. 5). Chung et al. used this approach to discover an autophagy activator which covalently targets the vacuolar proton pump ATP6V1A.[148] Using isoTOP-ABPP, hit compounds from an autophagic flux assay were shown to target ATP6V1A to induce clearance of Tar-binding protein 43 (TDP-43) aggregates

which drive amyotropic lateral sclerosis (ALS). Novel screening platforms are also often easily paired with isoTOP-ABPP target ID experiments. For example, Gruner et al developed a multiplexed *in vivo* screening platform where barcoded PDAC lines were pretreated with electrophilic compounds and injected into mice to observe compound-dependent decrease in metastatic potential.[149] IsoTOP-ABPP experiments were able to identify the lipase ABHD6 as the target of hit compounds from this screen, even though ABHD6 was not known previously to play a role in metastasis or cancer progression. Beyond identifying the lipase ABHD6 as critical for metastatic fitness, this approach allowed screening in a biological context more relevant to the disease state through adaptation of covalent ligand screening to a multiplexed *in vivo* phenotypic assay. In an example of targeting a traditionally undruggable protein with a covalent molecule, Boike and Cioffi et. al. used ABPP paired with phenotypic covalent ligand screening to identify a covalent MYC ligand EN4.[150] EN4 targets Cys171 within a predicted intrinsically disordered region of MYC, and showed selectivity on a proteome-wide scale profiling >1,500 cysteines using competitive isoTOP-ABPP.

Recent adaptations of isoTOP-ABPP have been developed to increase the coverage of cysteines across the proteome and increase throughput. Yan et al. used sample preparation steps (SP3) including off-line fractionation and a FAIMS source, which allows for additional separation before MS detection, to identify more than 30,000 reactive cysteines across a panel of tumor cell lines.[151] Kuljanin et. al. designed a tandem mass tag (TMT)-based streamlined cysteine activity-based protein profiling (SLC-ABPP) methodology to dramatically increase sample throughput, profiling an electrophilic fragment library at a depth of >8,000 reactive cysteine sites at 18 min per compound.[152]

ABPP-Enabled Induced Proximity: Targeted Protein Degradation and Beyond

ABPP-based chemoproteomics facilitates the expansion of targeted protein degradation approaches and the development of new therapeutic modalities by enabling the discovery of covalent recruiters against classically undruggable protein classes such as E3 ubiquitin ligases and deubiquitinases (DUBs).[3,153–160] Although most bifunctional degrader molecules (also known as proteolysis-targeting chimeras, or PROTACs) recruit the E3 ligases CRBN or VHL to degrade target proteins, there are over 600 E3 ligases with varying substrate scopes. Since 2019, covalent recruiters have been used to validate a large portion of the E3 ligases that have been harnessed for targeted protein degradation, including the E3s RNF114, RNF4, DCAF16, DCAF11, KEAP1, and most recently FEM1B.[153–159] In 2019, Spradlin et al used isoTOP-ABPP to identify RNF114 as the target of the enone-containing natural product nimbolide, which was used to make bifunctional degraders of BRD4 and BRC-ABL.[153] Simultaneously, Zhang et al used "scout fragments" to construct bifunctional molecules that degraded FKBP12 and BRD4, and identified the DCAF16 as the covalent target responsible for degradation.[156] These discoveries led to the variety of covalent E3 recruiters now available, which have been reviewed elsewhere.[9] Based on analyses of chemoproteomic datasets assessing cysteine reactivity, 97% of E3 ligases possess reactive cysteines, suggesting that covalent approaches to harness more E3 ligases could continue to be successful.[9]

ABPP has also enabled the development of new induced proximity-based therapeutic modalities beyond targeted protein degradation. Henning and Boike et. al. recently developed a targeted protein stabilization platform, termed Deubiquitinase Targeting Chimeras (DUBTACs).[160] By assessing aggregate chemoproteomic data describing proteome-wide cysteine reactivity, the authors to identified a reactive allosteric cysteine C23 in the DUB OTUB1. An ABPP-based screen against pure OTUB1 yielded a covalent, allosteric OTUB1 ligand that binds C23, EN523, which was used to design heterobifunctional DUBTACs linking OTUB1 to protein-targeting ligands. The authors demonstrated proof-of-concept of the DUBTAC platform with stabilization of mutant CFTR, whose ubiquitination and degradation drives cystic fibrosis, and the tumor suppressor WEE1 kinase for potential therapeutic in cystic fibrosis and cancer, respectively.[160] Overall, these studies have showcased how ABPP and covalent ligand discovery approaches have been used to expand the scope of TPD and develop new therapeutic modalities for drug discovery.

Covalent Library Screening Platforms beyond ABPP

While ABPP-based screening approaches are valuable in discovering covalent ligands, limited throughput has encouraged alternative screening methods. These often involve MS-based detection, uniquely possible in covalent ligand screening, which offers additional information about binding stoichiometry (Fig. 1.5). Other phenotypic or computational approaches have also been used, which are then paired with MS-based validation, ABPP-based experiments to inform selectivity, and structural biology to enable medicinal chemistry. The growth of commercial libraries of electrophilic fragment-like compounds contribute to the rise of these "electrophile-first" discovery strategies.
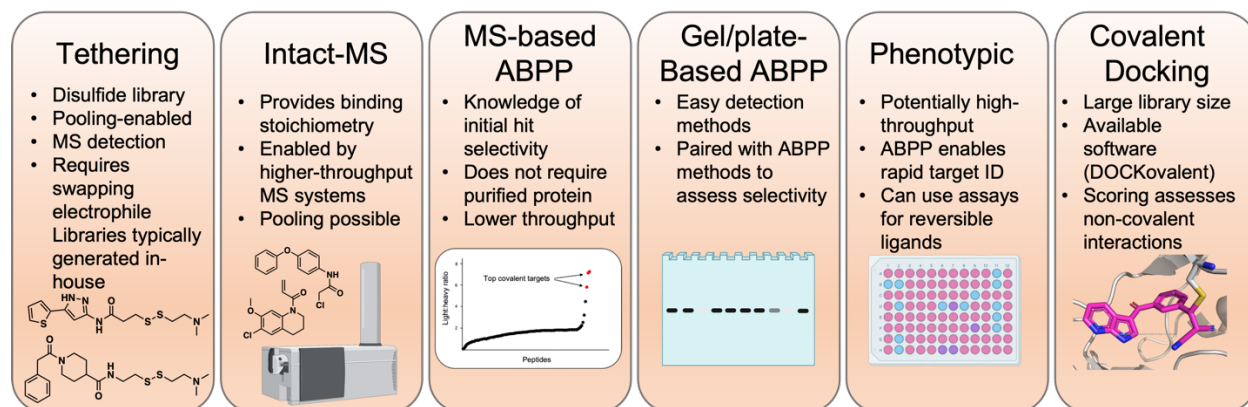

Figure 1.5. Screening methods for covalent drug discovery.
For each strategy, unique features and advantages are highlighted.

MS-enabled Covalent Ligand Screening

Originally, MS-based compound screening grew out of "tethering," a technique employed since 2000 that uses libraries of compounds linked to disulfides to identify fragments that bind cysteine-adjacent pockets.[161,162] Molecules that bind undergo disulfide exchange with the cysteine (which could be endogenous or engineered) to form an adduct with the protein, and pooled screening with MS detection can identify the bound compound. Binding fragments can be combined or grown in a fragment-based approach to identify high-affinity ligands. This strategy was originally designed to identify reversible ligands for challenging targets, but covalent binding can be designed back in by replacing the disulfide with an electrophile such as an acrylamide, as in the case of the covalent KRAS[G12C] inhibitors first discovered at UCSF.[103] This approach has often been employed to discover compounds that modulate protein-protein interactions,[163,164] and one recent study employed a similar tethering strategy using aldehydes to form imines with lysine residues.[165]

Over the past decade covalent ligand discovery has shifted towards screening more drug-like electrophilic fragments, in particular enabled by the commercial availability of acrylamide-focused libraries.[5] In 2014, Kathman et al. appended an acrylate functionality to 100 fragments to identify non-peptidic inhibitors of papain protease.[166] Electrophilic fragments were pooled, and screening through ESI-MS was able to identify hit compounds out of pooled experiments. Use of a similar library of acrylates enabled discovery of covalent inhibitors for the HECT E3 ligase Nedd4-1.[167] Co-crystal structures were critical to understanding the mechanism of these compounds, which prevent association of ubiquitin with the E3 ligase and thus induce a switch from a processive to distributive mechanism. In another example, acrylate-based inhibitors of the RBR E3 HOIP were also discovered using MS-based screening, highlighting how covalent fragment screening approaches can be useful for protein classes which have been challenging to develop ligands against, such as E3 ligases.[168]

More recently, Resnick et al. reported screening a commercial library of 993 acrylamides and chloroacetamides using intact-MS to identify ligands of the deubiquitinase OTUB2 and the pyrophosphatase NUDT7.[169] As is often the case, the authors used co-crystal structures with OTUB2 and NUDT7 in complex with the hit compounds to inform fragment growing to increase potency. Because generally weak interactions of hit compounds in covalent fragment screens necessitates medicinal chemistry optimization, the pairing of MS-based screening and structure-guided FBDD is particularly helpful.

The same compound collection used by Resnick et al. was also used to screen against the peptidyl-proline *cis-trans* isomerase Pin1, which is overexpressed or activated in a number of tumor types but has been challenging to target selectively.[170] The resulting chloroacetamide Sulfopin was shown to be selective for Pin1 using a CITe-Id chemoproteomics experiment, phenocopied Pin1 knockdown effects in cell lines, and was effective in regressing neuroblastoma growth in mice. This suggests that though chloroacetamides have liabilities, including rapid metabolism, they can be valuable tool compounds with which to assess target relevance in a variety of disease models.

One particularly powerful example of covalent ligand screening is the discovery of initial compounds in the series that led to the first approved KRAS G12C inhibitor, sotorasib (Amgen). A library of 3300 acrylamides was screened in three assays, a thiol

reactivity assay, a RAF-coupled nucleotide exchange assay, and an intact MS assay.[171] Combined with crystallographic data that revealed un-occupied sub-pockets, this effort provided the basis for rapid discovery of novel KRASG12C inhibitors, discussed above.

Covalent DNA Encoded Libraries

DNA-encoded libraries present an alternative screening approach that takes advantage of massive library size. Unlike MS or ABPP approaches there is no specialized advantage of covalency in enabling DEL screening, but the throughput of DELs allows screening of much larger covalent libraries through a similar workflow of immobilization, enrichment, amplification, and sequencing. First reports of electrophilic protein-nucleic acid encoded libraries described targeting protease active sites,[172] but in over the past 5 years cysteine-targeted DNA or PNA-encoded libraries have identified covalent ligands for JNK1, MEK2 and Her2.[173,174] A covalent ligand of MAP2K6 was also identified serendipitously through screening a DEL against a DNA-encoded protein library.[175] More recently, covalent DELs of larger size (~100,000,000 members) have been developed and used to identify acrylamide- and epoxide-based BTK inhibitors with novel scaffolds.[176] This expansion of library size and commercial availability represents an excited development, and DELs containing electrophilic molecules may become more widespread in covalent ligand discovery.

Covalent Docking

A small but growing set of studies have used computational methods to screen electrophilic compounds. Development of the DOCKovalent method by London et al. in 2014 allowed for the discovery of boronic acid Amp-C beta-lactamase and cyanoacrylamide inhibitors of JAK3.[177] Since then, the same method has been used to identify novel covalent inhibitors of the kinase MKK7,[178] as well as compounds that bind KRAS[G12C] to destabilize the protein and accelerate nucleic acid exchange.[179] We see these developments as exciting and expect to see continual improvement and adoption of computational screening methods for covalent compounds.

Measuring the Potency of Covalent Drugs

While IC50s values are often used to measure potency of covalent inhibitors, the kinact/Ki parameter has been preferred as a more accurate measure because it describes the efficiency of covalent bond formation.[180,181] Kinact/Ki can be obtained through a number of methods, including TR-FRET assays using competitive fluorescent probes.[182] In part to ease the burden of measuring this kinetic parameter, a handful of models have been formulated that relate time-dependent IC50 values to kinact/Ki.[183,184] Scientists working on a covalent JAK3 inhibitor program at Pfizer, however, suggested that fixed-time point IC50 values can serve as a valuable surrogate for kinact/Ki.[65] When using IC50 as a surrogate extra care should be taken to ensure covalent engagement (such as measuring off-rates), but with an appropriate choice of time-point IC50 values can be a useful tool to rapidly assess potency for covalent inhibitors. Regardless,

determination of kinact/Ki provides the most complete information to medicinal chemists about binding affinity and kinetics of covalent target engagement.

1.7 Lysine-directed Covalent Ligands

Cysteine's low abundance enables selectivity but limits opportunities for covalently targeting specific proteins of interest. This has driven scientists to look towards discovering lysine-targeted covalent molecules. Especially due to the lower nucleophilicity relative to cysteine under physiological conditions, efficient lysine-targeting covalent ligand discovery requires identification of unusually reactive lysines. isoTOP-ABPP experiments using several lysine-directed probes have proven especially powerful to profile lysine reactivity across the proteome.[185,186] Through isoTOP-ABPP experiments, Hacker et al. identified >9,000 ligandable lysines and showed alongside Ward et al. that more elaborated pentafluorophenol- or NHS ester-containing compounds could selectively label specific proteins of interest.[185,186] Building on these experiments, Abbasov et al. assembled a library of ~180 electrophiles and used isoTOP-ABPP experiments to assess the selectivity of different chemotypes and identify lysines ligandable with small molecules.[187] Their study yielded more broadly reactive electrophiles, such as dicarboxaldehydes, that could be used for further lysine profiling experiments, but also identified less reactive electrophiles including N-acyl-N-alkyl sulfonamides which had been previously used as tools for bioconjugation in cells.[187,188]

Voxelotor is a lysine-targeted covalent drug, used to treat sickle-cell anemia, whose discovery was dependent upon knowledge of heightened side-chain reactivity (Table 1.2). Sickle cell anemia is caused by a single mutation on the beta-hemoglobin chain that induces polymerization of mutant hemoglobin (HbS) under hypoxic conditions.[123] Previously, an aldehyde containing natural product and several synthetic aldehyde analogs were found to prevent polymerization through increasing HbS affinity for oxygen.[121] These aldehydes bind in a reversible covalent manner, forming a Schiff-base with the a-Hb chain's N-terminal valine.[121] Almost 50 years ago, this N-terminal amine was discovered to have a particularly low pKa of 6.9, indicating that it is primarily unprotonated under physiological conditions, and as a result more nucleophilic.[189] Based off earlier aldehydes, Voxelotor (Global Blood Therapeutics) was discovered through a structure-guided effort to discover compounds that increase HbS oxygen affinity, and was designed to bind the HbS tetramer in a 1:1 stoichiometry unlike the 2:1 ratio of initial structures.[121,122] With a remarkable RBC/plasma ratio of ~150 that likely reduces off-target effects, Voxelotor was approved in the US in 2019 with a recommended dose of 1.5 grams daily, an unusually high dose for a covalent drug.[123,190] Voxelotor's success compounds with ibruitinib's to show that covalent drugs can be dosed at high concentrations given favorable ADME properties. Furthermore, Voxelotor's discovery shows the power of identifying unusually reactive amino acid residues such as the a-Hb N-terminus.

Most other lysine-targeted ligands have been designed using structure-based methods from an existing ligand, often through rationally placing an electrophilic sulfonyl fluoride, fluorosulfate, or vinyl sulfone in an appropriate orientation to react with an epsilon-amino group of a lysine adjacent to an established binding site. These have

included a kinetic transthyretin stabilizer,[191] an isoform selective PI3Kdelta inhibitor,[192] and inhibitors of CDK2[193] and Hsp90.[194] A sulfonyl fluoride-bearing promiscuous kinase inhibitor targeting a conserved lysine in the ATP-binding site was also used as a probe to profile kinase inhibitor selectivity in live cells.[195] Sulfonyl fluoride-based probes are not completely selective for lysine, however. In the case of the mRNA decapping scavenger enzyme DcpS, a sulfonyl fluoride-based tool compound was used to competitively determine intracellular target engagement through covalent targeting of tyrosine.[176] A recent preprint profiled the amino-acid reactivity preference of 54 different electrophiles using chemical proteomics, which will prove to be a great resource for covalent ligand discovery.[197] Combining comprehensive electrophile profiling, lysine-directed chemoproteomics, and structure-guided approaches will allow scientists to leverage the abundance of lysine adjacent to ligand binding sites to enhance covalent drug discovery.

1.8 Covalent Drug Discovery Today

Over the last decade, impressive advancements in covalent drug discovery have led to promising drugs including EGFR inhibitors (osimertinib), BTK inhibitors (ibrutinib), KRAS-G12C mutant specific inhibitors (sotorasib), and Mpro inhibitors to treat patients infected with SARS-CoV-2. These major milestones in drug development showcase the evolution of covalent drug discovery from a serendipitous effort to a field with a well-established roadmap for success. The technologies that enable this success include covalent screening platforms, chemoproteomics discovery platforms including selectivity profiling, and structure-guided drug design.

Covalent drug discovery overcomes obstacles in traditional drug discovery, making possible the design of small-molecule ligands against many traditionally "undruggable" disease targets. I expect covalent drug discovery to continue to shift towards "electrophile first" approaches because of the power of chemoproteomic techniques to identify potential ligandable sites that cannot originally be identified with reversible ligands. Successful discovery of inhibitors of KRAS^{G12C}, one of oncology's most notoriously challenging drug targets, suggest that electrophile-centric covalent ligand discovery strategies are here to stay.

1.9 Acknowledgements

CHAPTER 2

Discovery of a Covalent FEM1B Recruiter for Targeted Protein Degradation Applications

This chapter is based on an article published in *The Journal of the American Chemical Society* entitled "Discovery of a Covalent FEM1B Recruiter for Targeted Protein Degradation Applications" and has been adapted with permission from all co-authors.[159]

2.1 Targeted Protein Degradation

Targeted protein degradation (TPD) is an approach often facilitated by bifunctional molecules known as proteolysis targeting chimeras (PROTACs) that induce proximity between a target protein and an E3 ligase to degrade the target protein.[10] These bifunctional compounds were inspired by a similar class of compounds called molecular glue degraders. The discovery in that the multiple myeloma drug lenalidomide works through inducing proximity between the E3 ligase Cereblon (CRBN) and transcription factors IKZF1/3 demonstrated that protein degradation is a viable therapeutic strategy. Knowledge of the CRBN-based molecular glues was combined with work previously done with PROTACs designed to recruit the Von-Hippel Lindau protein (VHL) E3 ligase to yield an explosive interest in the field in the mid-2010s.

Degraders have advantages over traditional inhibitors due to the "event-driven" mechanism. The catalytic action of the compounds enables including activity at low concentration and potential to overcome resistance mutations. Protein degradation side-steps certain compensating efforts such as increased target expression, and can prevent protein-protein interactions distal from the molecule's binding site.[11] However, one bottleneck with TPD platforms is the relatively small number of E3 ligase recruiters that are available, despite the >600 E3 ligases that exist in human cells. In fact, most efficient degraders recruit CRBN or VHL, but E3 ligases may have different potential substrate scopes, requiring use of other E3s to degrade a particular target of interest.[9,153] Furthermore, pairing a target with an E3 ligase that is not widely expressed could present opportunities for tissue-selective degradation.

2.2 Covalent recruiters as a part of TPD

Indications that chemoproteomics-enabled covalent ligand discovery platforms could be used to discover novel covalent E3 ligase recruiters for proteolysis-targeting chimera (PROTAC) applications were initially revealed by Backus et al., who demonstrated the ligandability of E3 ligases with cysteine-reactive covalent ligands.[6] This discovery enabled the development of bifunctional molecules containing electrophiles that react with the E3 ligases DCAF16, RNF4, and RNF114, allowing them to be recruited to model proteins and trigger their degradation.[153,155,156]

Since these initial proof-of-concept studies, similar strategies have been used to discover and apply additional covalent ligands that recruit RNF114 and DCAF11 as protein degradation triggers.[154,157] Overall, this previous work has highlighted the utility of covalent PROTACs that irreversibly bind the E3 ligase and has showcased how chemoproteomic approaches and cysteine-targeting ligands can be used to expand the arsenal of E3 ligase recruiters for TPD applications.

The reactivity of cysteine residues in cells is maintained by specific signaling pathways that are often centered on E3 ligases and maintain the cellular redox state. Under optimal redox balance, the CUL3 E3 ligase Kelch-like ECH associated protein

(KEAP1) sequesters the nuclear transcription factor NRF2 in the cytosol to induce its ubiquitylation and proteasome-mediated degradation. Under conditions of oxidative stress, redox-sensing cysteines on KEAP1 become oxidized to prevent KEAP1-mediated ubiquitylation and degradation of NRF2, subsequently allowing NRF2 accumulation and antioxidant gene expression.

2.3 Discovery of EN106

To identify a covalent FEM1B recruiter, we screened a library of 566 cysteine-reactive covalent ligands in a competitive fluorescence polarization assay using a TAMRA-conjugated FNIP1$^{562-591}$ degron and recombinant mouse FEM1B (Figure 2.1a,b, Table S2.1). Through this screen, we identified the chloroacetamide EN106 that inhibited FEM1B-FNIP1 degron fluorescence polarization with a 50% inhibitory concentration (IC50) of 2.2 μM (Figure 2.1c,d). From the initial screen, EN106 showed the most significant inhibition of FEM1B interactions with the FNIP1 degron (Figure 2.1b). EN106 showed competition against labeling of FEM1B with a cysteine-reactive rhodamine-conjugated iodoacetamide (IA-rhodamine) probe by gel-based activity-based protein profiling (ABPP), confirming a direct interaction of EN106 with a cysteine on FEM1B (Figure 2.1e).

Analysis of EN106 reactivity with recombinant FEM1B by liquid-chromatography-tandem mass spectrometry (LC-MS/MS) analysis of FEM1B tryptic digests revealed an EN106 adduct only on C186, the site that was previously shown to be critical for FEM1B substrate recognition (Figure 2.1f).[198,199] We also demonstrated that a nonreactive version of EN106, NJH-2-082, does not inhibit FEM1B interactions with the FNIP1 degron, confirming the importance of the covalent interactions of the cysteine-reactive warhead with C186 (Figure S2.1).
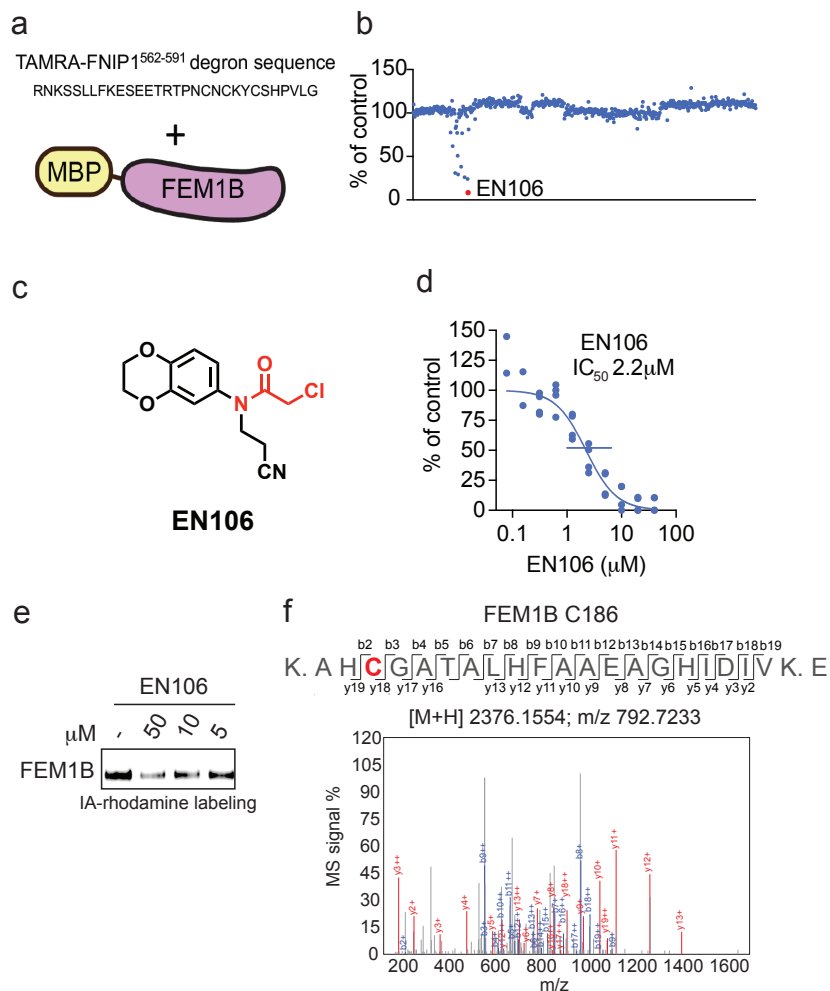
Figure 2.1. Discovering a FEM1B recruiter.
(a, b) Screening a cysteine-reactive covalent ligand library in a fluorescence polarization assay with TAMRA-conjugated FNIP1562−591 degron with recombinant MBP-tagged FEM1B (a). FEM1B was preincubated with DMSO vehicle or covalent ligand (50 µM) for 1 h prior to addition of the TAMRA-conjugated degron (b). Data are in Table S1. (c) Structure of EN106 with covalent chloroacetamide handle in red. (d) Dose− response of EN106 inhibition of FEM1B and TAMRA-conjugated FNIP1 interaction assessed by fluorescence polarization expressed as percent fluorescence polarization compared to DMSO control. (e) Gel-based ABPP of EN106. 50 nM pure FEM1B protein was pretreated with DMSO or EN106 for 30 min at room temperature prior to addition of IA-rhodamine (500 nM, 30 min) at room temperature, after which protein was resolved on SDS/PAGE and visualized by in-gel fluorescence. (f) Site of modification of EN106 on FEM1B. FEM1B was labeled with EN106 (50 µM) for 30 min, and FEM1B tryptic digests were analyzed by LC-MS/MS for the EN106 adduct. Data in (b) show average from n = 2/group. Data in (d) show individual data replicates from n = 2−4/group. Data in (e) show representative gel from n = 3/group.

To confirm that EN106 engaged FEM1B in cells, we synthesized NJH-2-030, an alkyne-functionalized derivative of EN106 (Figure 2.2a). To maintain engagement of C186, the alkyne was positioned distal to the chloroacetamide by exchanging the benzodioxan for a dihydro[1,4]benzoxazine scaffold. The starting benzoxazine was Boc-

protected to give 1 before reduction of the nitro group to provide aniline 2. Alkylation of 2 with acrylonitrile provided the propionitrile-substituted compound, which was acylated to obtain the chloroacetamide 3. Boc deprotection and acylation with hex-5-ynoyl chloride provided alkyne probe NJH-2-030 (Figure 2.2a).

NJH-2-030 maintained inhibitory activity against FEM1B recognition of the FNIP1 degron with an IC50 of 0.67 µM (Figure 2.2b). The improved potency with the amide substituent may indicate additional favorable contacts within the FEM1B substrate recognition domain. The NJH-2-030 probe showed FEM1B engagement in HEK293T cells, as demonstrated by FEM1B enrichment from NJH-2-030 treatment in cells by subsequent appendage of biotin-azide by copper-catalyzed azide−alkyne cycloaddition (CuAAC) in cell lysates, avidin pull-down, and blotting for FEM1B in HEK293T cells compared to vehicle-treated controls (Figure 2.2c). An unrelated target GAPDH was not enriched by NJH-2-030 treatment and pull-down (Figure 2.2c).
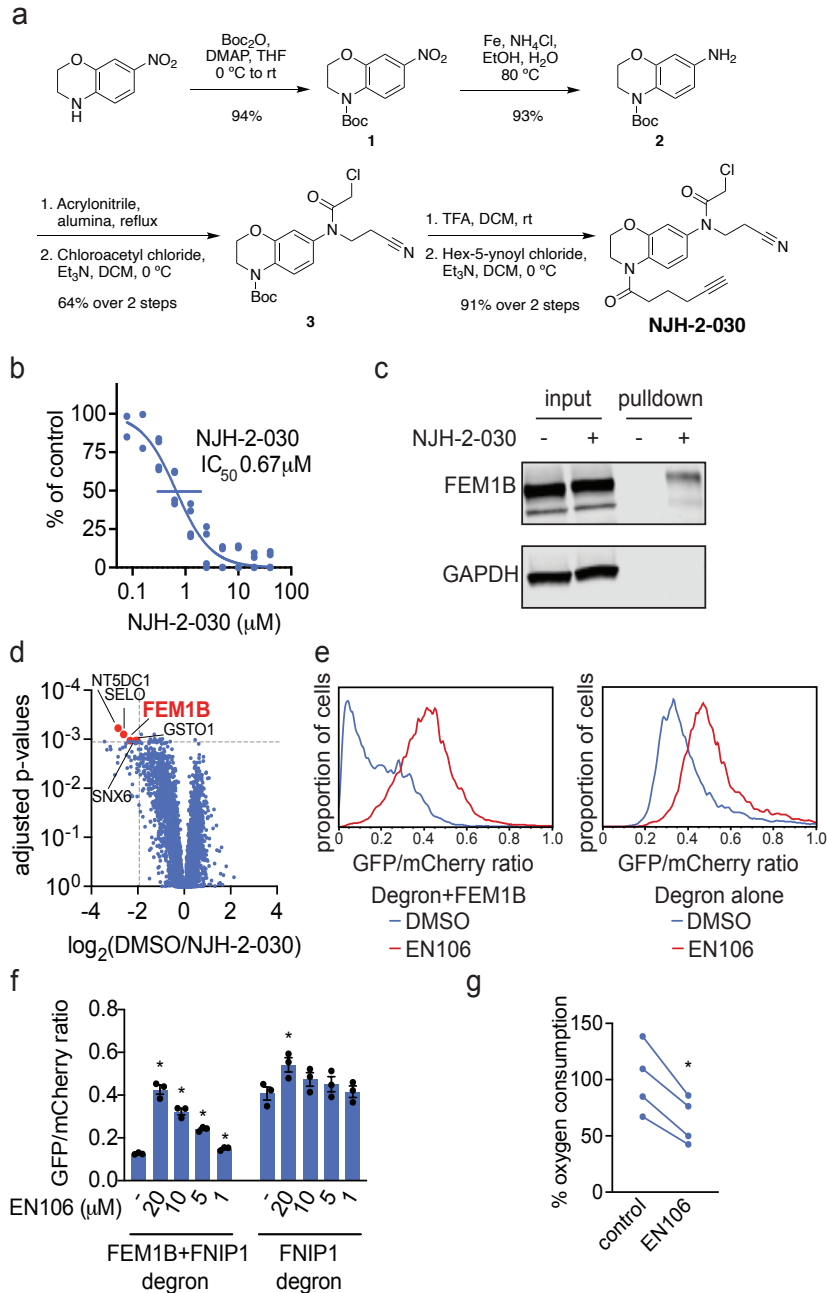
Figure 2.2. Characterization of EN106 binding with FEM1B.
(a) Synthesis of NJH-2-030. (b) Dose−response of NJH-2-030 inhibition of FEM1B and TAMRA-conjugated FNIP1 interaction assessed by fluorescence polarization. (c, d) NJH-2-030 engagement of FEM1B in cells. HEK293T cells were treated with DMSO or NJH-2-030 (10 μM) for 4 h. Cell lysates were subjected to CuAAC with biotin picolyl azide, and probe-modified proteins were avidin-enriched, eluted, and analyzed by SDS/PAGE and Western blotting for FEM1B or loading control GAPDH (c) or analyzed by TMT-based quantitative proteomic profiling (d). Data are from n = 3/group. Proteins annotated and highlighted in red showed >2-fold enrichment with probe over DMSO with adjusted p-values = 0.001 or p-values < 0.001. (e, f) Flow cytometry analysis of GFP-FNIP1 degron levels compared to mCherry levels with EN106 treatment in HEK293T cells for 12 h with either basal levels of FEM1B or transient FEM1B overexpression. Representative flow cytometry traces of DMSO and EN106 (20 μM) treatment groups shown in (e) and quantified data

shown in (f). (g) EN106 inhibits oxygen consumption in HEK293T cells. HEK293T cells were treated with DMSO vehicle or EN106 (10 μM) for 16 h, after which mitochondrial oxygen consumption was read out with MitoXpress Xtra reagent. Shown in (b), (f), and (g) are individual biological replicate values and/or average ± sem for n = 2−4/group. Significance in (f) and (g) is expressed as *p < 0.05 compared to vehicle-treated controls in each group in (f) or compared to each paired control in (g).

To assess the proteome-wide cysteine reactivity of EN106, we also performed a competitive isotopic tandem orthogonal proteolysis-ABPP (isoTOP-ABPP) study to quantitatively assess proteome-wide cysteine reactivity of EN106 in cells (Figure S2.2; Table S2.2). While we did not capture FEM1B in our chemoproteomics experiment, we only observed two targets of EN106 in cells -- C63 of HNRNPA3 and C127 of PRDX3 -- across 1465 quantified cysteines (Figure S2.2). Neither of these off-targets of EN106 were E3 ligases.

Given that we did not detect C186 of FEM1B in isoTOP-ABPP experiments, we also used our NJH-2-030 probe in situ in HEK293T cells to perform pull-down quantitative proteomic experiments to further confirm target engagement and proteome-wide selectivity of this close EN106 derivative (Figure 2.2d; Table S2.3). FEM1B was one of the most significantly enriched targets by the NJH-2-030 probe compared to DMSO controls with four additional off-targets detected -- GSTO1, SNX6, SELO, and NT5DC1 -- of which none of these proteins were E3 ligases (Figure 2.2d; Table S2.3). These data collectively showed that EN106 or its derivatives functionally engaged FEM1B in cells without detectable off-target effects on other endogenous degradation pathway components.

To further demonstrate that EN106 disrupted substrate recognition by FEM1B in cells, we monitored the degradation of GFP linked to an FNIP1 degron compared to IRES-driven expression of mCherry from the same plasmid in HEK293T cells by flow cytometry. EN106 treatment significantly stabilized FNIP1 degron-GFP levels, compared to vehicle-treated controls in a dose-responsive manner in FEM1B-overexpressing cells (Figure 2.2e,f). EN106 increased FNIP1 reporter levels in cells lacking exogenously expressed FEM1B to a similar extent as previously observed upon deletion of FEM1B,[198] indicating that this compound can target the endogenous E3 ligase (Figure 2.2e,f).

EN106 did not affect the pomalidomide-induced degradation of an unrelated E4F1 degron by the E3 ligase Cereblon (Figure S3). These findings thus indicate that EN106 not only engages but also inhibits CUL2^{FEM1B}-dependent ubiquitylation. Stabilization of the mitochondrial pool of FNIP1 impairs mitochondrial activity, as being read out by the oxygen consumption rate.[198–200] In line with engaging endogenous FEM1B and stabilizing FNIP1, we showed that EN106 significantly reduced cellular mitochondrial oxygen consumption in HEK293T cells (Figure 2.2g).

2.4 Discovery of FEM1B-based BRD4 degraders

To demonstrate that EN106 could be used as a covalent FEM1B recruiter in TPD applications, we next synthesized a series of FEM1B-based BET bromodomain degraders by linking EN106 to the BET bromodomain inhibitor JQ1, which targets BRD4 as well as other BET family proteins via six different linkers (Figure 2.3a, Figure S2.5). Maintaining the core benzoxazine of the alkyne probe NJH-2-030, we first attached an acetate spacer to provide methyl ester 4. The nitro group was reduced, and the resulting aniline 5 monoalkylated with acrylonitrile and acylated to provide the chloroacetamide intermediate 6. The methyl ester was hydrolyzed under mild basic conditions and coupled to amines 7a−7f, JQ1 derivatives with different linker attachments, to provide the bifunctional degraders NJH-2-088, NJH-1-106, NJH-2-090, NJH-2-091, NJH-2-092, and NJH-2-093 (scheme for NJH-1-106 shown in Figure 3a; Figure S4).

These compounds all degraded BRD4 in HEK293T cells to varying extent, with NJH-1-106 showing the best degradation potency with a DC50 of 250 nM and 94% maximal degradation of BRD4 (Figure 3b,c, Figure S2.4). NJH-1-106 maintained inhibitory activity against FEM1B recognition of the FNIP1 degron with an IC50 of 1.5 μM (Figure 2.3d). This BRD4 degradation was time-dependent with significant degradation observed by 4 h of treatment with NJH-1-106 (Figure 2.3e,f). NJH-1-106 also degraded BRD4 in cancer cell lines including the 231MFP breast cancer and HAP1 leukemia cancer cell lines (Figure S2.5a,b).
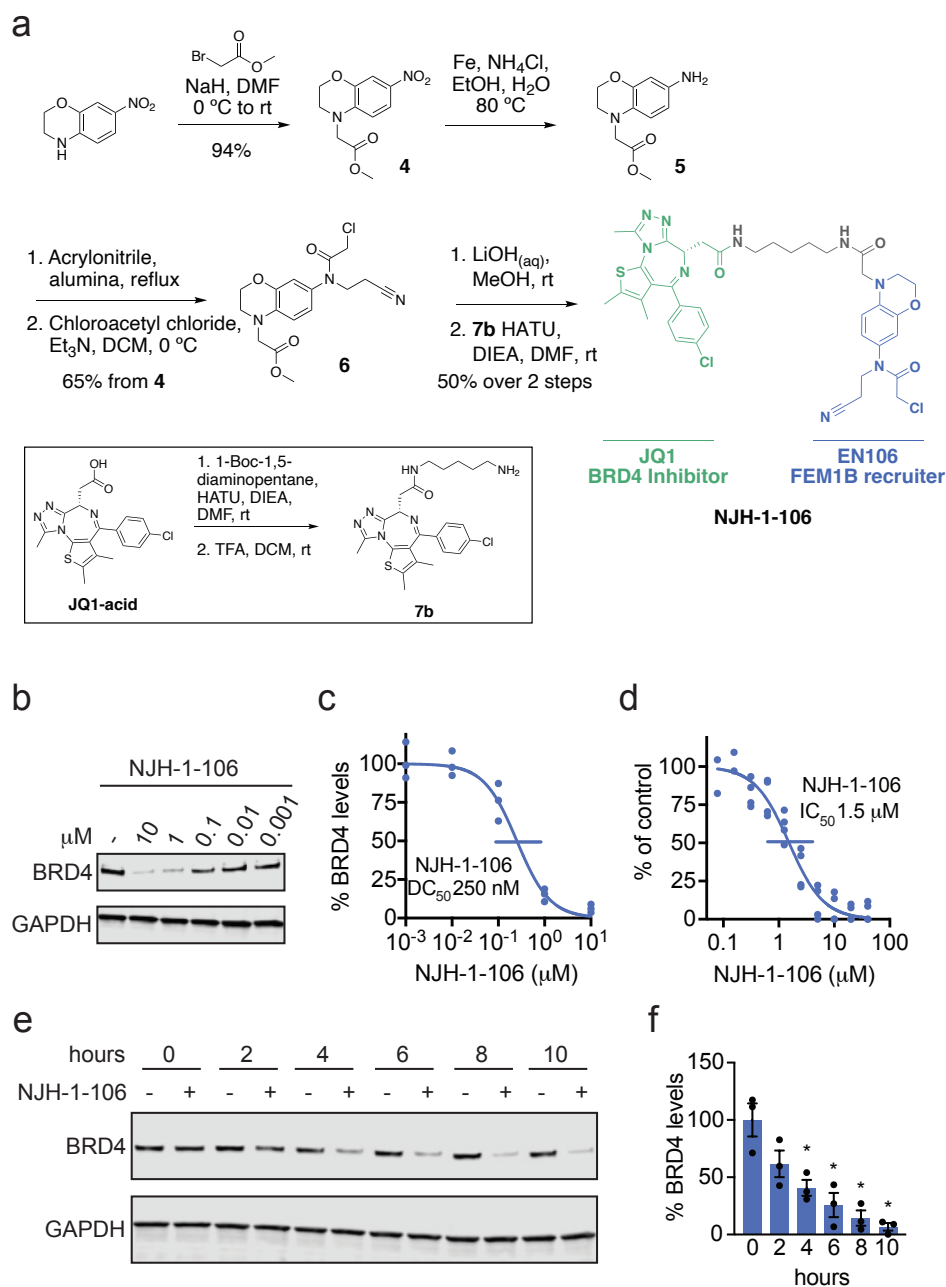
Figure 2.3. A FEM1B-based BRD4 degrader.
(a) Synthesis of FEM1Bbased BRD4 degrader NJH-1-106 linking EN106 to JQ1. (b) Degradation of BRD4 by NJH-1-106. NJH-1-106 was treated in HEK293T cells for 8 h, and BRD4 and loading control GAPDH levels were detected by Western blotting. (c) Quantification of BRD4 degradation from experiment in (b) and 50% degradation concentration value (DC50). Individual biological replicate values shown in (b) from n = 2−4/group. Gel shown in (b) is representative of n = 3/group, which are shown in (c). (d) Dose−response of NJH- 1-106 inhibition of FEM1B and TAMRA-conjugated FNIP1 interaction assessed by fluorescence polarization expressed as percent fluorescence polarization compared to DMSO vehicle-treated control. (e) Time course of BRD4 degradation with NJH-1-106 treatment. HEK293T cells were treated with DMSO vehicle or NJH-1-106 (10 μM) for 0, 2, 4, 6, 8, and 10 h, and BRD4 and loading control GAPDH levels were detected by Western blotting. Gel shown is representative of n = 3/group. (f) Quantification of BRD4

degradation shown in bar graph as average ± sem with individual biological replicate points shown from experiment designed in (e). Data shown in (c), (d), and (f) are averages with sem in (f) and individual biological replicate values from n = 2−4/group.

Consistent with the necessity of the covalent warhead, the nonreactive version of NJH-1-106, NJH-2-105, did not inhibit FEM1B interactions with the FNIP1 degron and did not degrade BRD4 (Figure S2.6a−d). Loss of BRD4 was attenuated by proteasome and NEDDylation inhibitors, consistent with a proteasome- and Cullin E3 ligase-dependent mechanism of BRD4 degradation (Figure 2.4a,b). FEM1B levels remained unaltered by NJH-1-106 treatment in HEK293T cells (Figure 2.4a,b). BRD4 degradation was also attenuated by pretreatment of cells with EN106 or JQ1, showing the necessity of the ternary complex and both ends of the molecule to degrade BRD4 (Figure 2.4c). In addition, BRD4 degradation was attenuated in FEM1B knockout (KO) cells compared to wild-type (WT) cells, further demonstrating FEM1B-dependent degradation of BRD4 (Figure 2.4d). The incomplete rescue we observe in FEM1B KO cells could be due to residual wildtype cells in the FEM1B KO population or due to other potential off-target E3 ligases.

Global proteomic profiling in HEK293T cells treated with NJH-1-106 also showed selective degradation of BRD4 among 4446 quantified proteins with only the largely uncharacterized PNMAL1 as an apparent off-target (Figure 2.4e; Table S2.4). PNMAL1, however, was a likely false positive of our proteomic analysis (Figure S2.7). While JQ1 is a pan BET bromodomain inhibitor, we only observed degradation of BRD4, but not BRD2 or BRD3 (Table S2.4). However, we cannot rule out that these other bromodomains could be degraded under longer treatments. The observed smaller fold change for BRD4 compared to the Western blot data likely reflects the well-known fold change suppression in TMT-based quantitative proteomics.[15]

2.5 FEM1B-based BCR-ABL/c-ABL degraders

We further demonstrated that this FEM1B recruiter can be used to degrade additional targets beyond BRD4. An FEM1B-based kinase degrader linking EN106 to dasatinib, an inhibitor of BCR-ABL and c-ABL among other kinases, exhibited degradation of BCR-ABL in K562 leukemia cancer cells (Figure 4f,g). Of the two compounds synthesized, NJH-2-142 was the more potent BCR-ABL degrader, with NJH-2-143 showing minimal activity, if any (Figure S8a,b). NJH-2-142's activity was compared to treatment of dasatinib and EN106 alone, neither of which affected BCR-ABL or c-ABL levels alone (Figure S8a,b). Together, these results document that covalent modification of a cysteine residue in the CUL2 adaptor FEM1B can lead to the development of specific E3 ligase recruiters for targeted protein degradation.
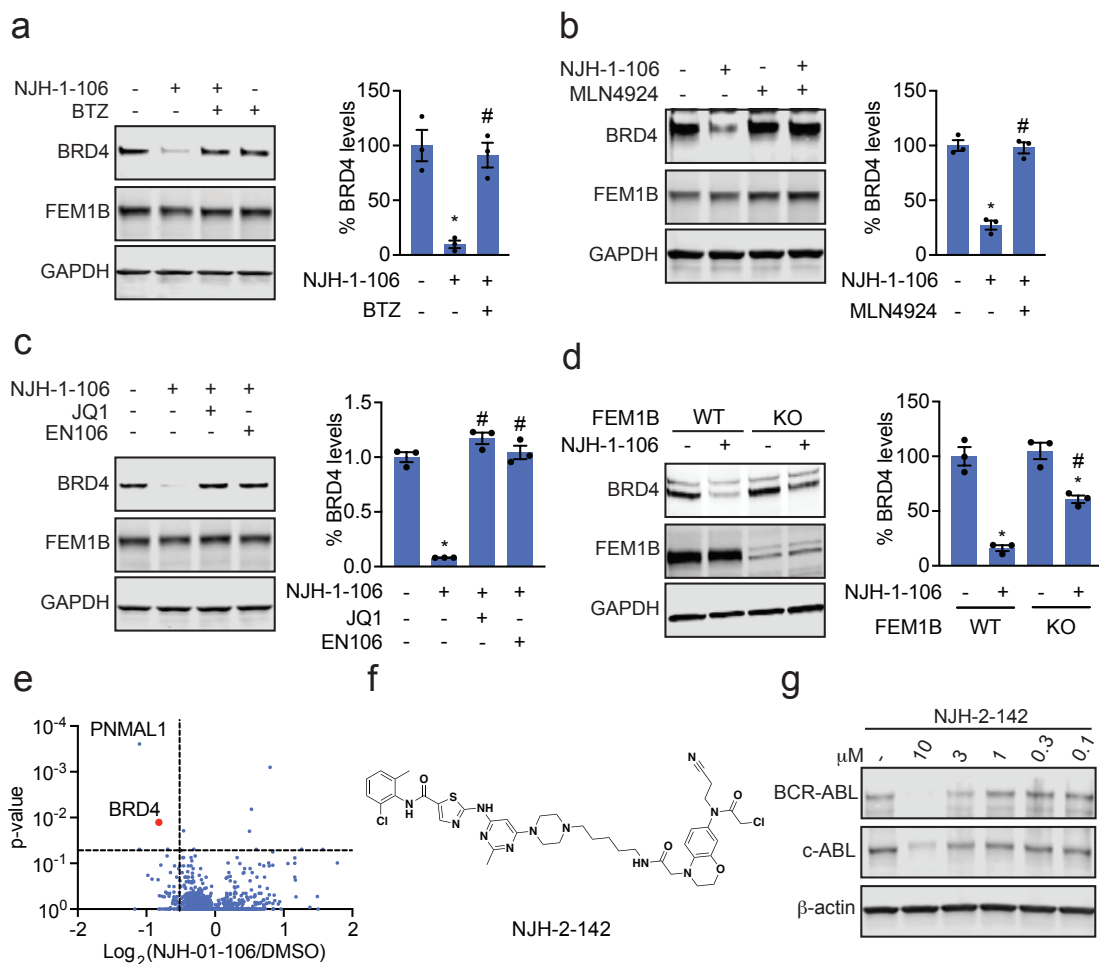
Figure 2.4. Characterization of FEM1B-based degraders.
(a, b) Proteasome and NEDDylation dependence of NJH-1-106-mediated degradation of BRD4. HEK293T cells were pretreated with DMSO vehicle, proteasome inhibitor bortezomib (BTZ) (1 μM), or NEDDylation inhibitor MLN4924 (0.2 μM) for 2 h prior to treatment with DMSO vehicle, NJH-1-106 (10 μM), or MZ1 (1 μM) for 8 h. (c) Attenuation of BRD4 degradation by EN106 and JQ1. HEK293T cells were pretreated with DMSO vehicle, EN106 (50 μM), or JQ1 (50 μM) for 2 h prior to treatment with DMSO vehicle or NJH-1-106 (10 μM) for 8 h. (d) BRD4 degradation by NJH-1-106 in FEM1B wild-type (WT) and knockout (KO) HEK293T cells. Cells were treated with DMSO vehicle or NJH-1-106 (1 μM) for 8 h. (e) Proteomic profiling of NJH-1-106 treatment in HEK293T cells. HEK293T cells were treated with DMSO vehicle or NJH-1-106 (1 μM) for 12 h. Protein level changes in cell lysate were quantitatively assessed by TMT-based proteomic profiling. (f) Structure of FEM1B-based BCR-ABL/c-ABL degraders linking EN106 to dasatinib. (g) K562 cells were treated with DMSO vehicle or NJH-2-142 at the designated concentrations for 24 h. Gels shown in (a)−(e) and (g) are from n = 3/group. Gels shown in (a)−(d) and (g) are representative gels from n = 3/group. Individual replicate and average ± sem values for (a)−(d) are shown in bar graphs. Significance is shown as *p < 0.05 compared to vehicle-treated groups, and #p < 0.05 compared to NJH-1-106-treated groups in (a)−(c) and the NJH-1-106-treated WT group in (d).

2.6 FEM1B in the TPD space

In this study, we discovered the covalent recruiter EN106 against FEM1B, the E3 ligase controlling the reductive stress response, which can be used for TPD applications. While zinc has been discovered to be a molecular glue that brings together FEM1B with its endogenous substrate FNIP1,[14] EN106 represents the first synthetic small-molecule ligand against FEM1B. While EN106 is an early hit tool compound with low micromolar potency against FEM1B with a metabolically unstable chloroacetamide warhead and requires further medicinal chemistry efforts to improve potency, selectivity, and drug-like properties, we demonstrate that EN106 targets a cysteine residue in FEM1B that is essential for substrate recognition. We show that EN106 can be used as a FEM1B recruiter in bifunctional degraders to recruit potential neosubstrates to the physiological target recognition site of FEM1B, likely placing them in an optimal manner for ubiquitylation through CUL2-RBX1.

Surprisingly, we observed BRD4 degradation with all of the FEM1B-based BRD4 PROTACs regardless of linker length, although there were preferences for optimal Dmax and DC50s. These data could potentially suggest that positive cooperativity is less crucial with a covalent FEM1B degrader as long as protein clashes are avoided.

Future studies will be needed to determine whether EN106 or its derivatives can act as molecular glue degraders to recruit potential neosubstrates for FEM1B-dependent ubiquitylation and degradation. More broadly, it will also be of future interest to determine whether cell-state-specific degraders can be developed. Additionally, determining whether EN106 and more potent derivatives can be used therapeutically to inhibit CUL2^{FEM1B} and disrupt reductive stress signaling through stabilization on FNIP1 in certain cancer settings would be of future interest. Overall, our study underscores the utility of covalent ligand screening in expanding the scope of E3 ligase recruiters for TPD applications.

2.7 Acknowledgements

CHAPTER 3

Deubiquitinase-targeting Chimeras for Targeted Protein Stabilization

3.1 Targeted Protein Stabilization

Engaging the mostly undruggable proteome to uncover new disease therapies not only requires technological innovations that facilitate rapid discovery of ligandable hotspots across the proteome but also demands new therapeutic modalities that alter protein function through novel mechanisms.[3,201] While targeted protein degradation (TPD) tackles the undruggable proteome by targeting specific proteins for ubiquitination and proteasomal degradation, not all proteins can be degraded through the proteasome for therapeutic benefit.[10,202,203] New approaches for TPD have also arisen that exploit endosomal and lysosomal degradation pathways with lysosome-targeting chimeras or autophagy with autophagy-targeting chimeras.[204,205]

Beyond degradation, a host of other induced proximity modalities represent possible avenues for modulating protein function. In a similar way that E3s affect target protein activity through ubiquitination, other enzymes that affect post-translational modification (PTM) status could be co-opted to modulate the activity of a target protein. These include deubiquitinases, kinases, phosphatases, and (de)acetylases. Proof of concept has already been shown for several of these mechanisms by using engineered HaloTag or fused nanobody systems, or with large peptidic ligands.[12–14,206]

While highly valuable for validation of an induced proximity modality as a feasible way to modulate protein function, these engineered strategies present a host of problems for *in vivo* applications and clinical translation. Ideally, drug-like small molecules similar to molecular glue degraders and PROTACs could be used to induce proximity and alter PTM. One particularly interesting mechanism is targeted protein stabilization (TPS) through deubiquitination. This could unlock targeting proteins whose gain-of-function would be therapeutically beneficial. No small molecules exist that induce deubiquitination and subsequent stabilization of proteins.[13,206]

Active ubiquitination and degradation of proteins is the root cause of number of diseases, including many tumor suppressors in cancer (for example, TP53, CDKN1A, CDN1C and BAX), and mutated and misfolded proteins, such as ΔF508-CFTR in cystic fibrosis or glucokinase in pancreatic cells in maturity-onset diabetes of the young type 2. In these cases, a targeted protein stabilization (TPS) therapeutic strategy, rather than degradation, would be beneficial.[207–210]

Analogous to TPD, we hypothesized that TPS could be enabled by the discovery of a small molecule deubiquitinase (DUB) recruiter that could be linked to a protein-targeting ligand to form a chimeric molecule, which would induce the deubiquitination and stabilization of target proteins. We call this heterobifunctional stabilizer a deubiquitinase targeting chimera, or DUBTAC (Fig. 3.1a). In this study, we report the discovery of a covalent recruiter for the K48-ubiquitin chain-specific DUB OTUB1, which when linked to a protein-targeting ligand stabilizes an actively degraded target protein to demonstrate proof of concept for the DUBTAC platform.

Figure 3.1. The DUBTAC platform.
a, DUBTACs are heterobifunctional molecules consisting of a protein-targeting ligand linked to a DUB recruiter via a linker. DUBTACs are ideally used for stabilizing the levels of actively ubiquitinated proteins that are degraded by the proteasome. When treated in cells, a DUBTAC will induce the proximity of a DUB with a target protein to remove polyubiquitin chains to prevent the protein from undergoing proteasome-mediated degradation, thereby stabilizing and elevating the level of the actively degraded protein; Ub, ubiquitin. b, Of 65 DUBs mined in our research group's aggregate chemoproteomic datasets of cysteine-reactive probe labeling with IA-alkyne in various complex proteomes, we identified probe-modified cysteines across 100% of the 65 DUBs. This is shown in the first pie chart. Among the 65 DUBs that showed probe-modified cysteines, 40 of these DUBs showed >10 aggregate spectral counts across our chemoproteomic datasets. Twenty-four, or 60%, of the 40 DUBs showed labeling of the DUB catalytic or active-site cysteines. c, Mining the DUB data, we identified 10 DUBs wherein there was one probe-modified cysteine that represented >50% of the total aggregate spectral counts for probe-modified cysteine peptides for the particular DUB. Seven of the 10 DUBs do not target a known catalytic cysteine, whereas three do target the catalytic cysteine (abbreviated by 'cat'); USP, ubiquitin-specific proteases; UCH, ubiquitin C-terminal hydrolases; OTU, ovarian tumor proteases. d, Analysis of aggregate chemoproteomic data for OTUB1 IA-alkyne labeling showing that C23 is the dominant site labeled by IA-alkyne compared to the catalytic (cat) C91. Chemoproteomic data analysis of DUBs across aggregated datasets can be found in Supplementary Table 1.

3.2 Identifying allosteric sites within DUBs

To enable the DUBTAC platform, our first goal was to identify a small-molecule recruiter that targeted an allosteric site on a DUB without inhibiting DUB function, as the recruitment of a functional DUB would be required to deubiquitinate and stabilize the target protein. While many DUBs possess well-defined active sites bearing a catalytic and highly nucleophilic cysteine, there have not yet been systematic evaluations of allosteric, non-catalytic and ligandable sites on DUBs that could be pharmacologically targeted to develop a DUB recruiter.

Chemoproteomic platforms, such as activity-based protein profiling (ABPP), have proven to be powerful approaches to map proteome-wide covalently ligandable sites. ABPP utilizes reactivity-based amino acid-specific chemical probes to profile reactive, functional and potentially ligandable sites directly in complex biological systems.[3,142] When used in a competitive manner, pretreatment with libraries of covalent small-molecule ligands can be used to screen for competition of probe binding to recombinant protein or complex proteomes to enable covalent ligand discovery against potential ligandable sites revealed by the reactivity-based probe.[143] Previous studies have shown that isotopic tandem orthogonal proteolysis-ABPP (isoTOP-ABPP) platforms for mapping sites of labeling with reactivity-based probes using quantitative proteomic approaches can identify hyperreactive, functional and ligandable cysteines.[142,143]

To identify DUB candidates that possess potential ligandable allosteric cysteines, we analyzed our research group's aggregate chemoproteomic data of proteome-wide sites modified by reactivity-based probes collected since the start of our laboratory. Specifically, we mined our collective chemoproteomic data of cysteine-reactive alkyne-functionalized iodoacetamide (IA-alkyne) probe labeling sites from 455 isoTOP-ABPP experiments in human cell line proteomes for total aggregate spectral counts identified for each probe-modified site across the DUB family. We postulated that probe-modified cysteines within DUBs that showed the highest spectral counts aggregated over all chemoproteomic datasets compared to those sites within the same DUB that showed lower spectral counts may represent more reactive and potentially more ligandable cysteines. Caveats to this premise include cysteines that might be located in regions within a protein sequence that do not yield suitable tryptic peptides with respect to ionization and compatibility with MS-based sequencing and labeling of surface-exposed cysteines that may not be part of binding pockets. However, we conjectured that the aggregate chemoproteomics data would still yield candidate allosteric ligandable sites within DUBs that could be prioritized for covalent ligand screening.

We initially mined our aggregate chemoproteomic data for 66 members of the cysteine protease family of DUBs, including ubiquitin-specific proteases, ubiquitin C-terminal hydrolases, Machado–Josephin domain proteases and ovarian tumor proteases (OTU), as they encompass the majority of DUB superfamilies. Interestingly, we found probe-modified cysteines across all of these DUB enzymes (Fig. 3.1b and Supplementary Table 3.1). Consistent with our aggregate chemoproteomic data of

probe-modified sites being enriched in functional sites within DUBs, among the 40 DUBs that showed a total of >10 aggregate spectral counts of probe-modified peptides, 24 (60%) showed labeling of the DUB catalytic cysteine (Fig. 3.1b).

We next prioritized this list of 40 DUBs to identify suitable candidates for TPS. We prioritized DUBs where the dominant probe-modified cysteine was (1) located at an allosteric site and not the catalytic cysteine such that we could target the identified cysteine with a covalent ligand while retaining the catalytic activity of the DUB; (2) in a dominantly identified probe-labeled peptide compared to other probe-modified sites within the same DUB, which could indicate a high degree of reactivity and potential covalent ligandability of the identified allosteric cysteine compared to the catalytic site and (3) frequently identified in chemoproteomics datasets, which would indicate the general accessibility of the cysteine in complex proteomes.

We found 10 DUBs where one probe-modified cysteine represented >50% of the spectral counts of all modified cysteines for the particular protein, of which 7 of these DUBs showed primary sites of probe modification that did not correspond to the catalytic cysteine (Fig. 3.1c). Of these 10 DUBs, OTUB1 C23 was captured with >1,000 total aggregate spectral counts compared to <500 aggregate spectral counts for the other DUBs (Supplementary Fig. 3.1a). In our aggregated chemoproteomic data, the tryptic peptide encompassing OTUB1 C23 was the dominant peptide labeled by IA-alkyne, with >1,500 total spectral counts compared to 15 spectral counts for the peptide encompassing the catalytic C91 and 115 spectral counts for C212 (Fig. 3.1d).

3.3 Discovering a covalent recruiter against OTUB1

We performed a gel-based ABPP screen in which we screened 702 cysteine-reactive covalent ligands against labeling of pure OTUB1 protein with a rhodamine-functionalized cysteine-reactive iodoacetamide (IA-rhodamine) probe (Fig. 3.2a, Supplementary Fig. 3.1b and Supplementary Table 3.2). Through this screen, we identified the acrylamide EN523 (1) as a top hit (Fig. 3.2b). We confirmed that EN523 dose-responsively displaced IA-rhodamine labeling of OTUB1 without causing any protein aggregation or precipitation (Fig. 3.2c). We next performed liquid chromatography–tandem MS analysis (LC–MS/MS) of tryptic peptides from EN523 bound to OTUB1 and showed that EN523 selectively targets C23, with no detectable modification of the catalytic C91 (Fig. 3.2d).
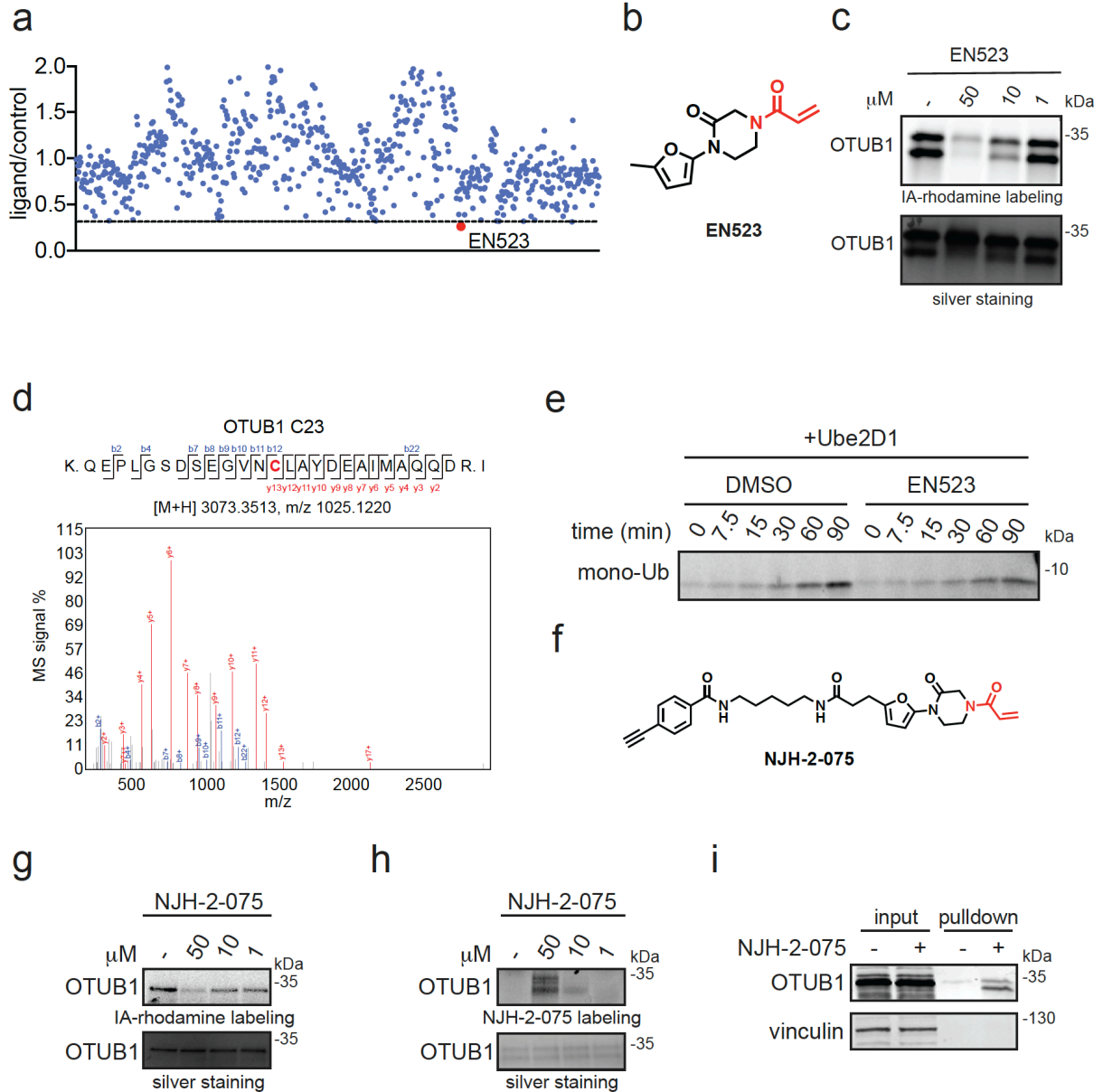
Figure 3.2. Discovery of covalent ligands that target OTUB1.

a, Covalent ligand screen of a cysteine-reactive library competed against IA-rhodamine labeling of recombinant OTUB1 to identify binders to OTUB1 by gel-based ABPP. Vehicle DMSO or cysteine-reactive covalent ligands (50 µM) were preincubated with OTUB1 for 30 min at room temperature before IA-rhodamine labeling (500 nM for 30 min at room temperature). OTUB1 was then separated by SDS–PAGE, and in-gel fluorescence was assessed and quantified. Gel-based ABPP data and quantification of in-gel fluorescence are shown in Supplementary Fig. 3.1b and Supplementary Table 3.2. EN523 annotated in red was the top hit that showed the greatest inhibition of OTUB1 IA-rhodamine labeling. b, Structure of EN523, with cysteine-reactive acrylamide highlighted in red. c, Gel-based ABPP confirmation showing dose-responsive inhibition of IA-rhodamine binding of OTUB1. Vehicle DMSO or EN523 were preincubated with recombinant OTUB1 for 30 min at 37 °C before IA-rhodamine labeling (500 nM for 30 min at room temperature). OTUB1 was then separated by SDS–PAGE, and in-gel fluorescence was assessed. The silver staining demonstrates protein loading. Shown is a representative gel of n = 3 biologically independent samples per group. d, LC–

MS/MS data showing an EN523-modified adduct on C23 of OTUB1. OTUB1 (10 µg) recombinant protein was incubated with EN523 (50 µM) for 30 min, after which the protein was precipitated and digested with trypsin, and tryptic digests were analyzed by LC–MS/MS to identify modified sites. e, OTUB1 DUB activity monitored by cleavage of K48 diubiquitin. Recombinant OTUB1 was preincubated with DMSO or EN523 (50 µM) for 1 h. After preincubation, OTUB1 was added to a mixture of diubiquitin and UBE2D1. The appearance of monoubiquitin (mono-Ub) was monitored by western blotting. f, Structure of the alkyne-functionalized EN523 probe NJH- 2-075. g, Gel-based ABPP of NJH-2-075. Vehicle DMSO or NJH-2-075 were preincubated with OTUB1 for 30 min at 37 °C before IA-rhodamine labeling (500 nM for 30 min at room temperature). OTUB1 was then separated by SDS–PAGE, and in-gel fluorescence was assessed. Also shown is silver staining demonstrating protein loading. h, NJH-2-075 labeling of recombinant OTUB1. OTUB1 (0.5 µg) was labeled with DMSO or NJH-2-075 for 1.5 h at 37 °C, after which rhodamine-azide was appended by CuAAC, OTUB1 was separated by SDS–PAGE and in-gel fluorescence was assessed. Also shown is silver staining demonstrating protein loading. i, NJH-2-075 engagement of OTUB1 in HEK293T cells. HEK293T cells were treated with DMSO vehicle or NJH-2- 075 (50 µM) for 2 h, after which cell lysates were subjected to CuAAC with biotin picolyl azide, and NJH-2-075-labeled proteins were subjected to avidin pulldown, elution, separation by SDS–PAGE and blotting for OTUB1 and vinculin. Both input lysate and pulldown levels are shown. Gels or blots shown in c, e and g–i are representative of n = 3 biologically independent samples per group. Raw gels and blots can be found in the source data.

Following these data, we performed an in vitro reconstituted OTUB1 deubiquitination activity assay monitoring monoubiquitin release from diubiquitin and demonstrated that EN523 does not inhibit OTUB1 deubiquitination activity (Fig. 3.2e).[211] These studies were performed in the presence of OTUB1-stimulating ubiquitin-conjugating enzyme E2 D1 (UBE2D1), an E2 ubiquitin ligase that engages in a complex with OTUB1 to stimulate OTUB1 activity.[212–214]

We next used NMR analysis to further characterize EN523 binding to OTUB1. A 13C-heteronuclear multiple quantum coherence (HMQC) spectrum of OTUB1 revealed the presence of a homogenous and mostly folded protein with well-dispersed {U}-2H,1H/13C-methyl-Ile/Leu/Val/Ala (ILVA) methyl group resonances (Supplementary Fig. 3.2a). EN523 treatment of OTUB1 led to subtle but significant chemical shift perturbations (Supplementary Fig. 3.2b). As we did not assign any peaks in the OTUB1 spectrum, we could not determine the exact binding site of the small molecule. However, almost all affected resonances had stronger intensities than the average signal strengths and had chemical shifts that are close to the random coil values of the respective amino acids. These observations suggest that the amino acids giving rise to these resonances are located in unfolded sections of the protein (in agreement with our PONDR data), predicting that C23 (the site of EN523 binding) belongs to an intrinsically disordered region of the protein.[215]

Next, we investigated if the covalent binding of EN523 to C23 prevented the interaction of OTUB1 with the ubiquitin-loaded and free forms of UBE2D2. As the latter protein activates OTUB1 DUB activity, we wanted to confirm that EN523 did not interfere with this protein– protein interaction. We mixed OTUB1 with ubiquitinylated or free UBE2D2 and compared the chemical shifts of OTUB1 residues in the presence and

absence of EN523. Binding of either form of the conjugating enzyme to OTUB1 induced strong peak perturbations (Supplementary Fig. 3.2c,d). These shift differences were almost identical for samples with and without EN523. The only differences we detected were shift changes for peaks that are affected by compound binding. These results indicated that EN523 did not interfere with binding of UBE2D2 to OTUB1.

We also explored structure–activity relationships (SARs) of our OTUB1 recruiter (**2–12**). Consistent with the necessity of the reactive acrylamide warhead for interacting with C23 of OTUB1, a non-reactive acetamide version of EN523, NJH-2-080 (**2**), showed loss in binding against OTUB1 (Supplementary Fig. 3.3). Replacing the methylfuran substituent with a benzoimidazolone, benzothiophene, benzofuran, phenyloxazole or imidazopyridine, but not methylimidazole, still retained potency against OTUB1 (Supplementary Fig. 3.3). We also explored preliminary SARs of the piperazinone core as well. Dimethyl and methylpiperazinone substitutions with a tert-butyl propionate extension from the furan still maintained potency against OTUB1. We also found that the (R)-methylpiperazinone derivative was more potent than the (S)-methylpiperazinone derivative of EN523, indicating that we may be able to achieve stereochemically specific interactions with OTUB1 (Supplementary Fig. 3.3). These data also demonstrated that extension off the furan may present an optimal exit vector for synthesis of DUBTACs. Overall, while the SAR showed room for flexibility within the EN523 core scaffold, we did not identify significantly more potent OTUB1 ligands, and thus we chose to further pursue EN523 as our OTUB1 recruiter for follow-up studies.

An alkyne-functionalized probe of EN523 (NJH-2-075 (**13**)) was then synthesized with the goal of assessing whether this ligand engaged OTUB1 in cells (Fig. 3.2f). NJH-2-075 retained binding to OTUB1 in vitro, as shown by (1) gel-based ABPP demonstrating competition of NJH-2-075 against IA-rhodamine labeling of recombinant OTUB1 and (**2**) direct labeling of recombinant OTUB1 by NJH-2-075 visualized by copper-catalyzed azide-alkyne cycloaddition (CuAAC) of azide-functionalized rhodamine to NJH-2-075-labeled OTUB1 (monitored by in-gel fluorescence; Fig. 3.2g,h). We demonstrated NJH-2-075 engagement of OTUB1 in cells by enrichment of endogenous OTUB1, but not that of an unrelated protein vinculin, through NJH-2-075 compared to vehicle treatment in HEK293T cells (Fig. 3.2i). Collectively, these data highlighted EN523 as a promising covalent OTUB1 ligand that targeted a non-catalytic and allosteric C23 on OTUB1 without inhibiting OTUB1 deubiquitination activity and engaged OTUB1 in cells.

3.4 Proof of concept with del-F508 CFTR DUBTACs

To demonstrate the feasibility of using EN523 as an OTUB1-recruiting module of a heterobifunctional DUBTAC, we identified the mutant ΔF508-CFTR chloride channel as a proof-of-concept case where protein stabilization would be therapeutically desirable. ΔF508, a frameshift mutation caused by deletion at codon 508 in exon 10 of CFTR, resulting in the absence of a phenylalanine residue, is the most common mutation that induces the cystic fibrosis phenotype.[216] This mutation causes the protein

to become conformationally unstable, leading to K48 polyubitiquination and degradation before trafficking from the endoplasmic reticulum to the cell surface.[210,216] Previous studies have demonstrated the feasibility of stabilizing mutant CFTR not only by genetic and pharmacological inhibition of the cognate E3 ligase RNF5 but also through targeted recruitment of DUBs using a genetically encoded and engineered DUB targeted to CFTR using a CFTR-targeting nanobody.[12,217,218]

Importantly for our work, suitable CFTR-targeting small-molecule ligands exist. Lumacaftor, a drug for cystic fibrosis developed by Vertex Pharmaceuticals, acts as a chemical chaperone for ΔF508-CFTR and corrects its misfolding, leading to increased trafficking of ΔF508-CFTR to the cell membrane and partial restoration of protein function.[219] Despite lumacaftor's chaperoning activity, the vast majority of ΔF508-CFTR is still actively ubiquitinated and degraded, making the potential of a synergistic effect via DUBTAC-induced deubiquitination a therapeutically attractive option.

With this in mind, we synthesized DUBTACs linking the OTUB1 recruiter EN523 to the CFTR chaperone lumacaftor with two different C3 or C5 alkyl linkers, NJH-2-056 (**14**) and NJH-2-057 (**15**) (Fig. 3.3a,b). We confirmed that these two DUBTACs still engaged recombinant OTUB1 in vitro by gel-based ABPP (Fig. 3.3c,d). We used CFBE41o-4.7 human bronchial epithelial cells expressing ΔF508-CFTR, a human cystic fibrosis bronchial epithelial cell line, as a model system to test our DUBTACs. We first showed that EN523 did not alter OTUB1 protein levels in these cells (Supplementary Fig. 3.4a). We also demonstrated that the alkyne-functionalized EN523 probe NJH-2-075 still engaged OTUB1 in this cell line (Supplementary Fig. 3.4b).
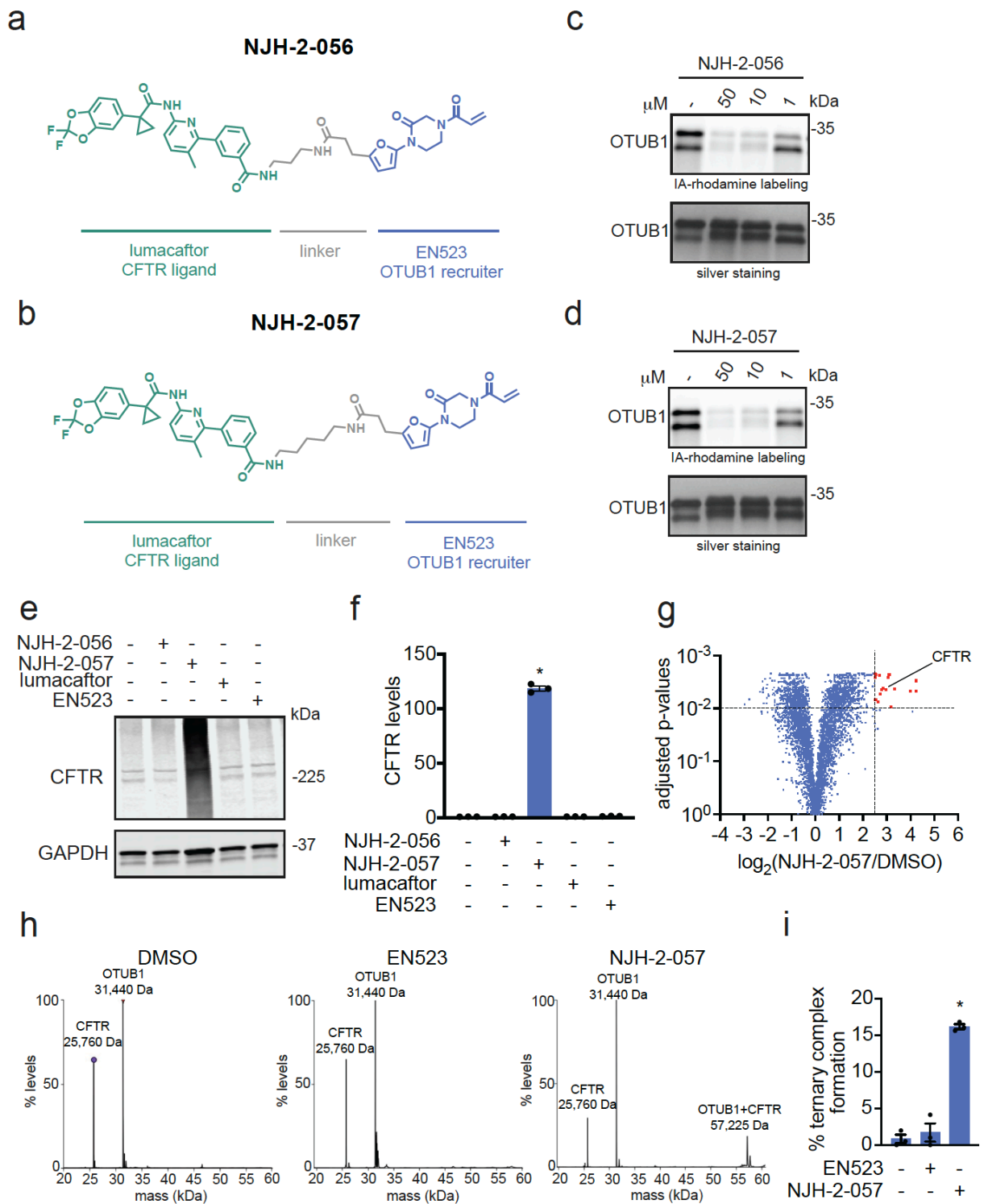
Figure 3.3. DUBTAC against mutant CFTR.
a,b, Structures of NJH-2-056 (a) and NJH-2-057 (b); these DUBTACs against mutant CFTR protein are formed by linking the CFTR ligand lumacaftor to the OTUB1 recruiter EN523 through C3 and C5 alkyl linkers, respectively. c,d, Gel-based ABPP analysis of NJH-2- 056 (c) and NJH-2-057 (d) against OTUB1. Vehicle DMSO or DUBTACs were preincubated with recombinant OTUB1 for 30

min at 37 °C before addition of IA-rhodamine (100 nM) for 30 min at room temperature. OTUB1 was run on SDS–PAGE, and in-gel fluorescence was assessed. Protein loading was assessed by silver staining. e, Effect of DUBTACs on mutant CFTR levels. CFBE41o-4.7 cells expressing ΔF508-CFTR were treated with vehicle DMSO, NJH-2-056 (10 μM), NJH-2-057 (10 μM), lumacaftor (10 μM) or EN523 (10 μM) for 24 h, and mutant CFTR and loading control GAPDH levels were assessed by western blotting. f, Quantification of the experiment described in e. g, Tandem mass tags (TMT)-based quantitative proteomic profiling of NJH-2-057 treatment. CFBE41o-4.7 cells expressing ΔF508-CFTR were treated with vehicle DMSO or NJH-2-057 (10 μM) for 24 h. Data shown are from n = 3 biologically independent samples per group. Full data for this experiment can be found in Supplementary Table 3. h, Native MS analysis of DUBTAC-mediated ternary complex formation. OTUB1 (2 μM) and the CFTR nucleotide-binding domain (2 μM) were incubated with DMSO vehicle, EN523 (50 μM) or NJH-2-057 (50 μM) in 150 mM ammonium acetate with MgCl2 (100 μM) and ATP (100 μM). Representative mass spectra from n = 3 biologically independent samples per group are shown. i, Percentage of ternary complex formation assessed by measuring the CFTR–OTUB1 complex formed in the experiment described in h. Gels shown in c, d and e are representative of n = 3 biologically independent samples per group. Data in f and i show individual biological replicate values and average ± s.e.m. from n = 3 biologically independent samples per group. Statistical significance was calculated with unpaired two-tailed Student's t-tests in f and i compared to vehicle-treated controls and is expressed as *P < 0.05. Raw gels and blots, bar graph data and exact P values can be found in the source data.

The DUBTACs were then tested in these cells alongside lumacaftor or EN523 treatment alone. Treatment with NJH-2-056, lumacaftor or EN523 did not alter mutant CFTR levels; however, we observed a robust and significant increase in CFTR protein levels with NJH-2-057 treatment (Fig. 3.3e,f). This stabilization was dose responsive and time dependent (Supplementary Fig. 3.5). We further confirmed that the stabilized protein was CFTR using three additional commercially available CFTR antibodies (Supplementary Fig. 3.6) and showed that the DUBTAC-stabilized CFTR band was attenuated following CFTR knockdown (Supplementary Fig. 3.7).

We also explored the dependence of CFTR stabilization on linker length and composition (**14–20**) (Supplementary Fig. 3.8). DUBTACs bearing C5 and C6 alkyl linkers, but not C3 and C4 alkyl linkers, stabilized CFTR. Interestingly, none of the DUBTACs bearing PEG linkers were able to stabilize CFTR (Supplementary Fig. 3.8). We also made eight additional CFTR DUBTACs bearing more rigid heterocycle-containing linkers (**21–28**) to determine whether these compounds that may be less flexible and potentially more drug-like may perform better in stabilizing mutant CFTR (Supplementary Fig. 3.9). Interestingly, nearly all these DUBTACs increased CFTR levels, with substantially improved response from GL-03 (**23**) (bearing a fused azepine-pyrrolidine linker) compared to NJH-2-075 (Supplementary Fig. 3.9).

Consistent with the necessity of the cysteine-reactive warhead in binding to OTUB1, we also demonstrated that a non-reactive propionamide version of NJH-2-057, NJH-2-106 (**29**), was incapable of stabilizing CFTR (Supplementary Fig. 3.10). The alkyne probe NJH-2-075, which contains an identical linker to NJH-2-057 but exchanges

an ethynylphenyl group for lumacaftor, also did not induce CFTR stabilization (Supplementary Fig. 3.10).

The CFTR smear that we observed in the blot with NJH- 2-057 treatment is consistent with previous studies investigating CFTR and in line with our observations with the proteasome inhibitor bortezomib that would maximally stabilize actively ubiquitinated and degraded mutant CFTR protein (Supplementary Fig. 3.11). This smear likely represents a combination of differential glycosylation states, other forms of ubiquitination on CFTR that may not be removed by OTUB1 (for example, K63 ubiquitin chains) and previously observed anomalous migration of CFTR on SDS–PAGE due to the presence of SDS-resistant ternary structures within the protein.[216,220,221] Based on the molecular weight of the darkest part of the CFTR blot >225 kDa, we conjectured that we are stabilizing the fully mature glycosylated form of mutant CFTR (Fig. 3.3e).

To further validate our western blot data for CFTR stabilization and to assess the proteome-wide activity of NJH-2-057, we performed a TMT-based quantitative proteomic analysis of NJH-2-057-treated CFBE41o-4.7 cells expressing ΔF508-CFTR. Satisfyingly, the proteomic analysis showed CFTR among the most robustly stabilized proteins (ratio of 7.8 comparing NJH-2-057 to vehicle treatment; Fig. 3.3g and Supplementary Table 3.3). While there were additional proteins with significant changes in abundance levels, we only observed 21 proteins that were significantly stabilized by greater than fivefold with an adjusted P value of <0.01 compared to vehicle-treated controls out of 4,552 total quantified proteins (Fig. 3.3g and Supplementary Table 3.3). These observed changes in protein abundance levels by the DUBTAC appear to be DUBTAC-specific changes because these changes were not detected with EN523 or lumacaftor treatment alone (Supplementary Fig. 3.2 and Supplementary Table 3.3) and may represent compensatory changes occurring from elevations in CFTR levels in cells or could represent changes resulting from off-targets of the DUBTAC.

Interestingly, among proteins elevated along with CFTR were several protein chaperones, including heat shock 70-kDa protein 6, DnaJ heat shock protein family Hsp40 member B1, heat shock 50-kDa protein 1A and DNAJ homolog subfamily B member 4. These changes could reflect potential compensatory on-target upregulation of protein chaperones in response to highly elevated levels of a relatively unstable mutant CFTR. Nonetheless, we did not observe widespread alterations in protein levels with DUBTAC treatment, suggesting that we were not substantially disrupting global protein turnover.

Having identified NJH-2-057 as a DUBTAC that was capable of stabilizing mutant CFTR in cells, we next sought to confirm the formation of a ternary complex between CFTR, NJH-2-057 and OTUB1 in vitro using recombinant protein and native MS-based approaches (Fig. 3.3h,i). While the highest intensity signals corresponded to unmodified OTUB1 and the ΔF508-harboring CFTR nucleotide-binding domain used in this experiment, potentially indicating low levels of target engagement under these experimental conditions, we observed significant CFTR–OTUB1 complex formation with NJH-2-057 treatment but not with DMSO vehicle or EN523 treatment (Fig. 3h,i). The

predominantly observed mass for this complex corresponded to OTUB1 and CFTR but not the combined masses of OTUB1, CFTR and NJH-2-057. This may be because the NJH-2-057 adduct on OTUB1 may be unstable to electrospray ionization and desolvation energy conditions required to observe the protein complex, as we were also not able to observe the NJH-2-057 mass adduct on OTUB1. However, minor peaks indicated the presence of adducts consistent with either full NJH- 2-057 or either MS-induced fragments or breakdown products (Supplementary Fig. 3.3). Nonetheless, given that this OTUB1–CFTR complex was only observed with DUBTAC treatment but not with DMSO or EN523 treatment, our data strongly suggest that the DUBTAC enables ternary complex formation.

To further confirm that the robust stabilization in mutant CFTR levels conferred by NJH-2-057 was due to the proposed on-target activity, we demonstrated that stabilization of CFTR was attenuated by pretreatment with either lumacaftor or EN523, indicating that stabilization by the DUBTAC was due to targets engaged by both lumacaftor and EN523 (Fig. 3.4a,b). These data also indicate the necessity for ternary complex formation to stabilize CFTR levels. To further verify that the CFTR stabilization was dependent on OTUB1, OTUB1 knockdown significantly attenuated mutant CFTR stabilization by NJH-2-057 (Fig. 3.4c,d).
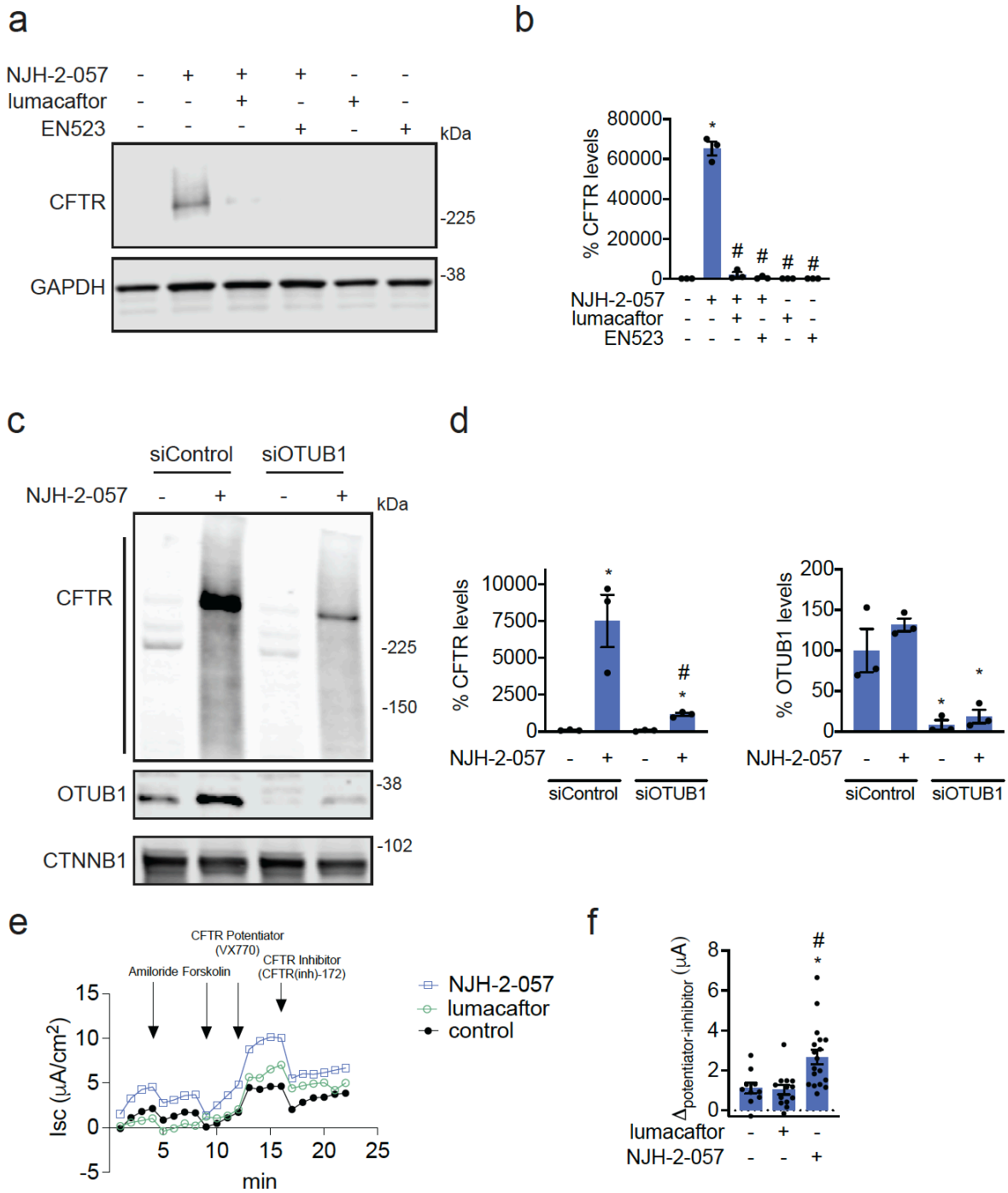
Figure 3.4. Characterizing the mechanism of the CFTR DUBTAC NJH-2-057.
a, Effect of lumacaftor or EN523 preincubation on NJH-2-057 DUBTAC-mediated stabilization of mutant CFTR levels. CFBE41o-4.7 cells expressing ΔF508-CFTR were pretreated with vehicle DMSO, lumacaftor (100 μM) or EN523 (100 μM) for 1 h before treatment with NJH-2-057 (10 μM) for 24 h. Mutant CFTR and loading control GAPDH levels were assessed by western blotting. b, Quantification of the experiment described in a. c, Effect of OTUB1 knockdown on NJH-2-057 DUBTAC-mediated mutant CFTR stabilization. CFBE41o-4.7 cells expressing ΔF508-CFTR were transiently transfected with non-targeting short interfering RNA (siRNA; siControl) or siOTUB1

oligonucleotides for 48 h before treatment of cells with vehicle DMSO or NJH-2-057 (10 µM) for 16 h. Mutant CFTR, OTUB1 and loading control GAPDH levels were assessed by western blotting. d, Levels of mutant CFTR and OTUB1 from the experiment described in c. e, Transepithelial conductance in primary human cystic fibrosis donor bronchial epithelial cells bearing the ΔF508-CFTR mutation. Cells were treated with DMSO vehicle, NJH-2-057 (10 µM) or lumacaftor (10 µM) 24 h before the TECC24 assay in which cells received four additional sequential treatments with a sodium channel inhibitor amiloride (10 µM), a cAMP activator forskolin (20 µM), a CFTR potentiator VX770 (0.5 µM) and a CFTR inhibitor CFTR(inh)-172 (30 µM). Shown are the average values from conductance from a single donor. Experiments were conducted in primary cells from two donors. f, Changes in current between potentiator VX770 (ivacaftor) treatment and the CFTR inhibitor treatment in the experiment described in e in two primary human cystic fibrosis donor bronchial epithelial cells bearing the ΔF508-CFTR mutation. Individual replicate data are shown in the bar graph from n = 10 biologically independent samples in the DMSO vehicle-treated group, n = 13 biologically independent samples in the lumacaftor-treated group and n = 18 biologically independent samples in the NJH-2-057-treated group. Gels shown in a and c are representative of n = 3 biologically independent samples per group. Data in b and d show individual biological replicate values and average ± s.e.m. from n = 3 biologically independent samples per group. Statistical significance was calculated with unpaired two-tailed Student's t-tests in b, d and f and is expressed as *P < 0.05 compared to vehicle-treated control in b and f and compared to vehicle-treated siControl in d. Statistical significance is expressed as #P< 0.05 compared to the NJH-2-057-treated group in b and compared to the NJH-2-057-treated siControl group for CFTR levels in d. Raw gels and blots, bar graph and line plot data and exact P values can be found in the source data

We next performed a competitive isoTOP-ABPP study to assess the overall proteome-wide selectivity and cysteine reactivity of NJH-2-057 treatment in CFBE41o-4.7 cells expressing ΔF508-CFTR (Supplementary Fig. 3.4 and Supplementary Table 3.4). Of 1,270 IA-alkyne probe-modified peptides quantified in two of three biological replicates, there were only five targets that showed isotopically light-to-heavy or control-to-NJH-2-057 treatment probe-modified peptide ratios of >4 with an adjusted P value of <0.05: VDAC2 C76, TUBB1 C201, RLF C744, VDAC2 C47 and VDAC3 C66 (Supplementary Fig. 3.4 and Supplementary Table 3.4). Yang et al. previously showed that Nedd4 could ubiquitinate VDAC2 and VDAC3, and overexpression of Nedd4 significantly increased K48-linked ubiquitination of VDAC2 and VDAC3.[222] However, none of these targets would be expected to directly influence the activity of our DUBTAC. OTUB1 C23 was captured in our isoTOP-ABPP experiment but only showed a ratio of 1.6, which would correspond to ~60% target occupancy (Supplementary Table 3.3).

This likely indicates that the observed CFTR stabilization by NJH-2-057 is occurring through relatively low levels of OTUB1 occupancy in cells, which would also be in line with our in vitro labeling and native MS data. The activity of heterobifunctional molecules has also been reported previously in studies using covalent E3 ligase recruiters for targeted protein degradation applications showing that relatively minimal target occupancy of E3 ligases can still lead to robust degradation of target proteins due to the catalytic mechanism of action of the E3 ligases.[153,155–157] We conjectured that a similar catalytic effect in a DUBTAC also leads to robust stabilization of the target protein with partial OTUB1 occupancy.

Having shown stabilization of CFTR protein levels with our DUBTAC, we next sought to determine whether our DUBTAC-mediated increase in CFTR protein levels led to improved cell surface CFTR function (Fig. 3.4e,f). We measured transepithelial conductance in primary human cystic fibrosis donor bronchial epithelial cells bearing the ΔF508-CFTR mutation. These cells were pretreated with vehicle, lumacaftor or NJH-2-057 for 24 h before sequential treatments with a sodium channel inhibitor amiloride, a cAMP activator forskolin and a CFTR potentiator VX770 (ivacaftor) to fully activate CFTR function in cells. After chloride channel conductance was potentiated with VX770, the cells were treated with a CFTR inhibitor, CFTR(inh)-172, to show CFTR dependence of any increases observed in transepithelial conductance. The difference in conductance between potentiator VX770 and CFTR inhibitor treatment were quantified under the three different treatment conditions (vehicle, lumacaftor or DUBTAC treatment) to ascertain the effects that our DUBTAC had on CFTR-mediated conductance compared to lumacaftor or vehicle treatment (Fig. 3.4e,f). Our studies showed that treatment of these primary cells with NJH-2-057 led to significant improvement in CFTR-dependent transepithelial conductance compared to lumacaftor or vehicle treatment, indicating that our CFTR DUBTAC elevated not only CFTR protein levels but also functional CFTR at the cell surface, leading to improved CFTR function (Fig. 3.4e,f).

3.5 Using DUBTACs to stabilize Wee1

Using DUBTACs to stabilize WEE1. We next sought to show a second example of TPS with DUBTACs against another actively degraded target for which a well-validated ligand had been reported in the literature. We selected WEE1, a tumor suppressor kinase in non-malignant eukaryotic somatic cells that phosphorylates the cyclin-dependent kinase (CDK1)–cyclin B1 complex to inhibit cell cycle progression during S and G2 phases of mitosis and whose activity must be downregulated for mitotic progression to occur.[223,224] One mechanism through which WEE1 activity is suppressed is via ubiquitin-mediated proteasomal degradation.[224,225] Clinical WEE1 inhibitors, such as AZD1775, have been developed to be given in combination with DNA-damaging chemotherapy agents for inducing premature mitosis to exert anticancer effects, and WEE1 PROTACs using AZD1775 have also been developed to selectively degrade WEE1 in cancer cells.[226]

We first confirmed previously reported results that treatment of HEP3B hepatoma cancer cell lines with a proteasome inhibitor bortezomib stabilized WEE1 levels, confirming that WEE1 was regulated by ubiquitin-mediated proteasomal degradation in this cell line (Fig. 3.5a).[225] We next synthesized four DUBTACs linking AZD1775 to our OTUB1 recruiter EN523 through no linker (LEB-03-153) (**30**), a C3 alkyl linker (LEB-03-144) (**31**), a C5 alkyl linker (LEB-03-145) (**32**) or a PEG linker (LEB-03-146) (**33**) (Fig. 3.5b). LEB-03-144 and LEB-03-146 with the C3 alkyl linker and the PEG linker, respectively, showed significant WEE1 stabilization in HEP3B cells comparable to WEE1 levels observed with bortezomib treatment, whereas EN523 or AZD1775

treatment alone had no impact on WEE1 levels (Fig. 3.5c,d). While the therapeutic relevance of a WEE1 DUBTAC using a WEE1 inhibitor remains to be seen, these data show additional mechanistic proof of concept for TPS using DUBTACs.
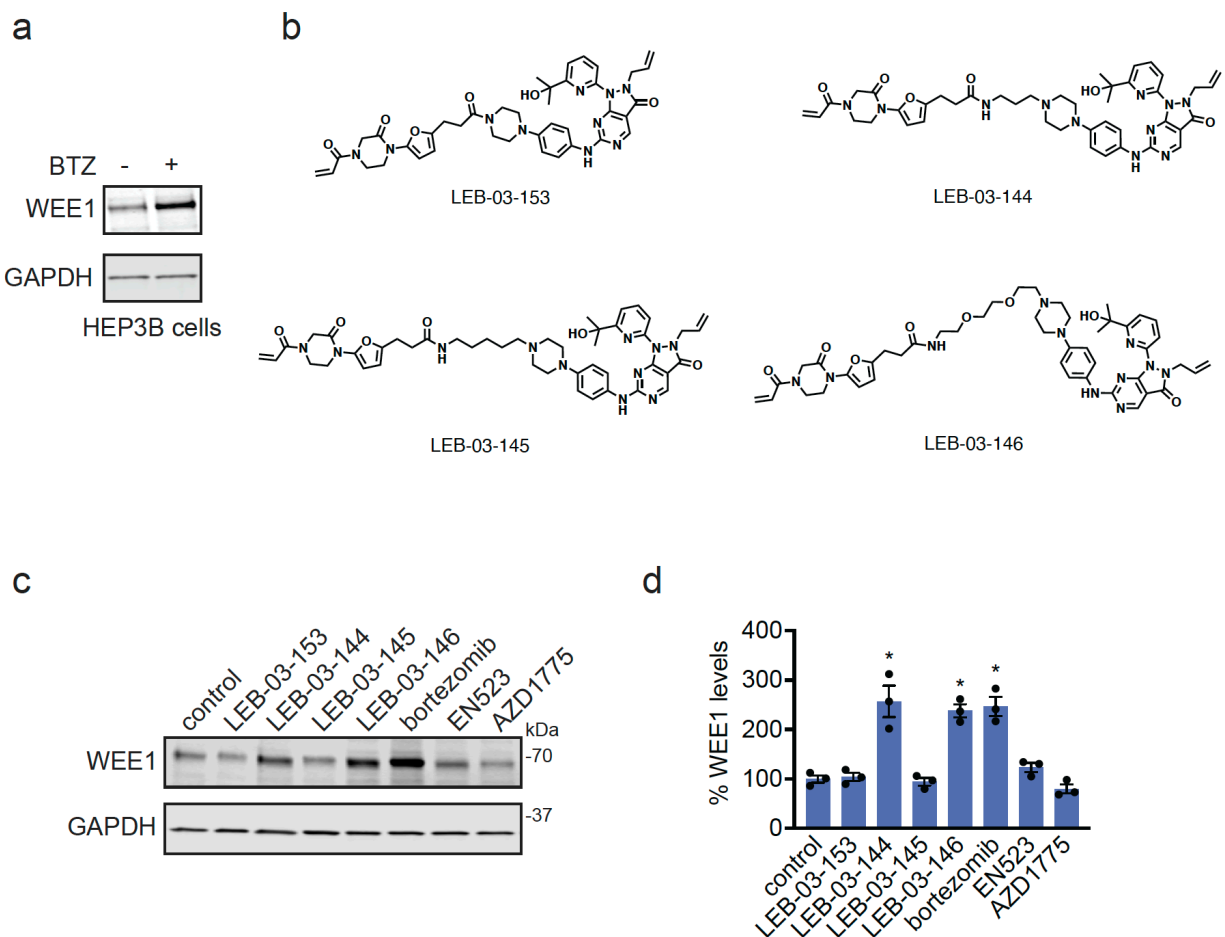

Figure 3.5. WEE1 DUBTAC.
a, HEP3B cells were treated with DMSO vehicle or bortezomib (1 µM) for 24 h. WEE1 and loading control GAPDH levels were assessed by western blotting. b, Structures of four WEE1 DUBTACs linking AZD1775 to the OTUB1 recruiter EN523 through four different linkers. c, HEP3B cells were treated with DMSO vehicle, the four DUBTACs, bortezomib, EN523 or AZD1775 at 1 µM for 24 h. WEE1 and loading control GAPDH levels were assessed by western blotting. d, Quantitation of the data shown in c. Blots shown in a and b are representative blots from n = 3 biologically independent samples per group. Data in bar graphs show individual biological replicate values and average ± s.e.m. from n = 3 biologically independent samples per group. Raw blots, bar graphs and exact P values can be found in the source data.

3.6 DUBTAC and TPS Outlook

In this study, we discovered a covalent small-molecule recruiter EN523 for the K48-ubiquitin chain-specific DUB OTUB1. We demonstrated that this recruiter can be incorporated into fully synthetic heterobifunctional DUBTACs by linking a DUB recruiter to protein-targeting ligands to enable TPS of actively degraded target proteins in cells. We showed two successful examples of TPS with ΔF508-CFTR and WEE1. For ΔF508-CFTR, we also demonstrated that we not only heightened the levels of the mutant protein but also improved cell surface chloride channel conductance of CFTR with our DUBTAC in combination with the potentiator ivacaftor compared to lumacaftor and ivacaftor treatments.

While we showed early validation of the DUBTAC platform here, there are many avenues for future exploration. These include further optimization of DUB recruiters against OTUB1 to improve their potency and proteome-wide selectivity as well as the discovery of new recruiters against other candidate DUBs. Much like with PROTACs, we observe significant dependency on linker length and composition for stabilizing target proteins with DUBTACs. Further exploration of this linker dependence with DUBTACs will be necessary for improving potency and kinetics of stabilization and bioavailability.

In addition, elucidating the mechanism, structural underpinnings and kinetics in the formation of the ternary complex formed between the target protein and DUB and understanding how the target protein is deubiquitinated by the DUBTAC will be important. Using more advanced methods beyond native MS to monitor ternary complex formation, including AlphaLISA and time-resolved fluorescence resonance energy transfer, will be useful to achieve these goals.[227]

Given our initial proof of concept for CFTR and WEE1 stabilization with a DUBTAC, there are many promising areas that could benefit from targeted deubiquitination of actively ubiquitinated and degraded proteins to provide therapeutic benefit. Targets that could benefit from a DUBTAC that already possess protein-targeting ligands include stabilizing BAX levels in the mitochondria to induce apoptosis, stabilizing STING for immunooncology applications or stabilizing glucokinase in pancreatic cells for maturity-onset diabetes of the young type 2.[228–231] Other targets that would benefit from a DUBTAC would be various tumor suppressors that are actively ubiquitinated and degraded to maintain cancer cell proliferation.[232]

There are also many other genetic disorders beyond cystic fibrosis where mutations can lead to protein destabilization and ubiquitin-mediated degradation that can also be stabilized by DUBTACs for therapeutic benefit. These include glucocerebrosidase mutations in Gaucher's disease or Parkinson's disease and phenylalanine hydroxylase and fumarylacetoacetate hydroxylase mutations in phenylketonuria.[233,234] These disorders could directly benefit from TPS via DUBTACs. In

diseases caused by haploinsufficiency where loss of one copy of a gene leads to disease pathology, DUBTACs could potentially slow down the turnover rate of the protein to increase the levels of the protein to alleviate the disease.[235]

Overall, this study puts forth the discovery of DUB recruiters and shows proof of concept for the DUBTAC platform for TPS via induced proximity of a DUB with a target protein. In addition, our study underscores the utility of using chemoproteomics-enabled covalent ligand discovery platforms to facilitate development of unique induced proximity-based therapeutic modalities beyond TPD.

Materials and Methods, Supplementary Figures and Tables, and Chemical Synthesis information for Chapter 2 can be found in Appendix A.

3.7 Acknowledgments

CHAPTER 4

Discovery of a Potent Covalent Main Protease Inhibitor Against SARS-COV-2

While covalent drugs over the past twenty years have shifted towards targeting non-conserved cysteines to gain selectivity and potency, covalent protease inhibitors targeting proteases have continued to be discovered. These include proteasome inhibitors bortezomib and carfilzomib, as well as hepatitis C virus (HCV) NS3/4a inhibitors boceprevir and telaprevir. The most recent addition to this repertoire of covalent protease inhibitors is nirmatrelvir, the SARS-CoV-2 main protease (M[pro]) inhibitor marketed as Paxlovid (Pfizer) for the treatment of symptomatic COVID-19. Nirmatrelvir was the result of an intense effort at Pfizer based off original work on M[pro] inhibitors following the SARS outbreak in 2002-2003. In this chapter, I describe work undertaken during the beginning of the COVID-19 pandemic in 2020 to discover covalent M[pro] inhibitors, where optimization of compounds discovered by gel-based ABPP screening yielded highly potent M[pro] inhibitors.

4.1 SARS-CoV-2 M[pro]

While vaccines are now being deployed for the current SARS-CoV-2 pandemic, we need more effective antiviral therapeutics that can effectively combat this COVID-19 pandemic and future coronavirus outbreaks that will inevitably occur. Furthermore, the appearance of dangerous variants of SARS-CoV-2 and the dependence of vaccines on the mutation-prone Spike protein renders the power of vaccination less secure in the future. This makes a potential pan-coronavirus antiviral drug that will be effective against variants of the SARS-CoV-2 virus as well as any future coronaviruses highly valuable.
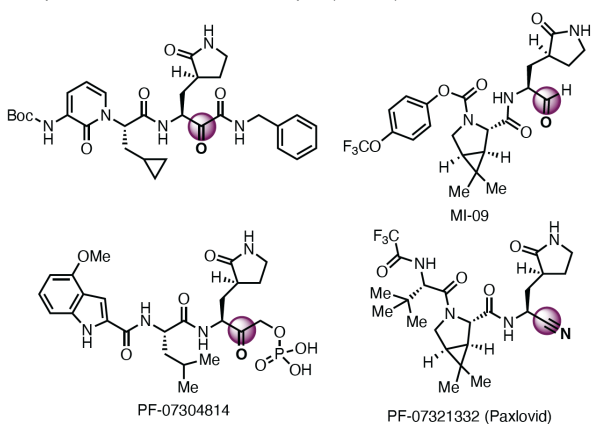
All coronaviruses have several highly conserved genes that can be exploited to develop an antiviral therapy that could be effective against not only SARS-CoV-2, but also past and future coronaviruses.[8] Among the various genes and proteins encoded by coronaviruses, one particularly "druggable" or relatively easy-to-drug target is the coronavirus Main Protease (M[pro]) also known as 3C-like protease, an enzyme that is involved in cleaving a long peptide translated by the viral genome into its individual protein components that are then assembled into the virus to enable viral replication in the cell.[8] The replicase gene of SARS-CoV-2 encodes two overlapping polyproteins—pp1a and pp1ab—that are required for viral replication and transcription [1]. M[pro] is responsible for most proteolytic processing events to release the functional polypeptides with at least 11 proteolytic cleavage events starting with the autolytic cleavage of M[pro] itself from pp1a and pp1ab.[236]

Inhibiting M[pro] with a small-molecule antiviral could effectively stop the ability of the virus to replicate, providing immediate and complete therapeutic benefit.[117,119,120] Unlike the viral Spike protein that currently all vaccines and antibody therapeutics target, which is highly prone to mutations that give rise to resistant variants, M[pro] protein sequence is highly conserved across all former coronaviruses indicating that making a potent and effective M[pro] inhibitor for one coronavirus would result in an efficacious drug for all future coronaviruses. Because M[pro] is a critical protein necessary for coronavirus replication, mutations in the core active site domain of this protein would likely impair its
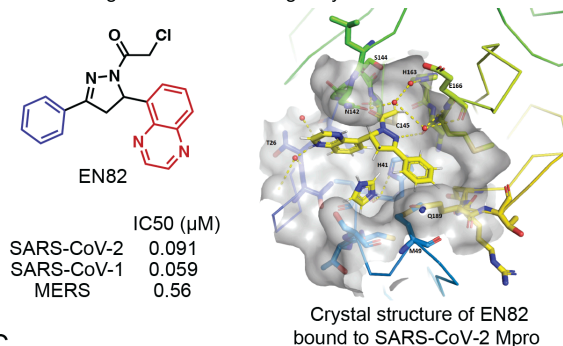
61

catalytic activity and the ability of the virus to replicate, and thus M[pro] inhibitor antivirals would be unlikely to run into resistance through viral mutations.

There has been considerable effort over the past two years by many academic and industrial labs to discover M[pro] inhibitors (Fig. 4.1A).[237,238] For example, Pfizer has now developed an effective orally bioavailable covalently-acting peptide-based M[pro] inhibitor Paxlovid that been given emergency use authorization by the United States Food and Drug Administration (Fig. 4.1A).[117,239] However, these inhibitors may not be effective against M[pro] enzymes from future variants of SARS-CoV-2 or other future coronaviruses.

A Peptidomimetic SARS-CoV-2 Mpro (3CL[pro]) covalent inhibitors

MI-09

PF-07304814

PF-07321332 (Paxlovid)

B Promising Initial Hit Containing a Pyrazoline Core

EN82

	IC50 (μM)
SARS-CoV-2	0.091
SARS-CoV-1	0.059
MERS	0.56

Crystal structure of EN82 bound to SARS-CoV-2 Mpro

C

(R)-EN82

(S)-EN82

(R)-EN82 IC50 0.53 μM

(S)-EN82 IC50 2.7 μM

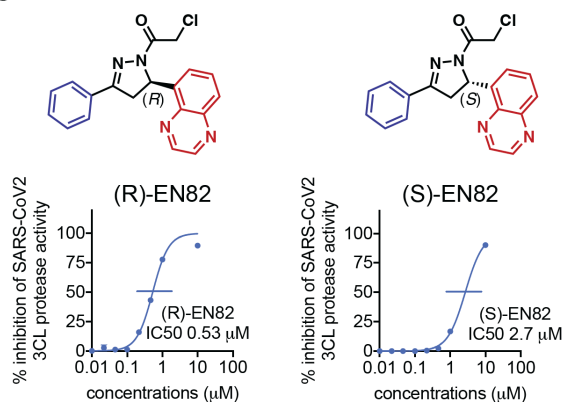% inhibition of SARS-CoV2 3CL protease activity

concentrations (μM)

Figure 4.1. Discovery of pyrazoline-based SARS-CoV-2 main protease inhibitors.
(A) Examples of peptidic SARS-CoV-2 M^pro inhibitors. (B) Structure of our top hit EN82 and potency of EN82 against SARS-CoV-2, SARS-CoV-1, and MERS-CoV M^pro. IC50s are derived from a rhodamine-based M^pro substrate peptide activity assay. On the left is a crystal structure of EN82 covalently bound to the catalytic C145 in the SARS-CoV-2 M^pro active site. (C) Potency of (R)- and (S)-EN82 against SARS-CoV-2 M^pro. IC50s were derived from averages of 3 biological replicates/group.

Thus, there is still significant room for discovering additional M^pro inhibitor scaffolds that may be tractable for drug discovery and development efforts. M^pro is a cysteine protease that bears a catalytic cysteine (C145 for SARS-CoV-2 M^pro) that coordinates it catalytic protease activity[1]. As such, chemoproteomic platforms and cysteine-reactive covalent ligand discovery approaches are particularly attractive for developing potent, selective, non-peptidic, more drug-like, and covalently-acting M^pro inhibitors that irreversibly interact with the M^pro catalytic cysteine.

4.2 Identification of EN82

To rapidly identify cysteine-reactive inhibitors against SARS-CoV-2 M^pro, we screened a library of 582 acrylamides and chloroacetamides in a gel-based activity-based protein profiling (ABPP) screen, in which we competed these cysteine-reactive covalent ligands against the binding of a cysteine-reactive rhodamine-functionalized iodoacetamide probe (IA-rhodamine) using previously described gel-based ABPP approaches [11,12] (Fig. S4.1-S4.2).[154,155] The most promising hits clustered together on pyrazoline-based chloroacetamide ligands EN71, EN82, EN216, and EN223 that demonstrated dose-responsive inhibition of M^pro IA-rhodamine labeling (Fig. S4.3A).

We subsequently tested these four compounds in a FRET-based activity assay employing an M^pro peptide substrate to identify compounds that inhibited M^pro activity (Fig. S4.3B). The most promising hit to arise from this screen was a pyrazoline EN82 which displayed encouraging potency against the SARS-CoV-2 M^pro with a 50 % inhibitory concentration (IC50) value of 0.16 µM compared to 0.52-4.8 µM for EN216, EN71, and EN223 (Fig. S4.3B). The FRET-based peptide probe required significant concentrations of M^pro protein (115 nM) to obtain reliable M^pro activity readouts, and would thus hinder our ability to detect more potent inhibitors with IC50 values <100 nM.

For subsequent M^pro activity assays, we switched over to a rhodamine-based M^pro substrate activity assay which required significantly less protein. Using this rhodamine-based assay, EN82 showed potent IC50 values against SARS-CoV-2 (0.091 µM), SARS-CoV-1 (0.059 µM) and MERS (0.56 µM) (Fig. 4.1B). We next performed chemoproteomic profiling of EN82 cysteine-reactivity in HEK293T cell lysate to assess whether this compound demonstrated some degree of selectivity or whether this compound was non-specific (Fig. 4.2).
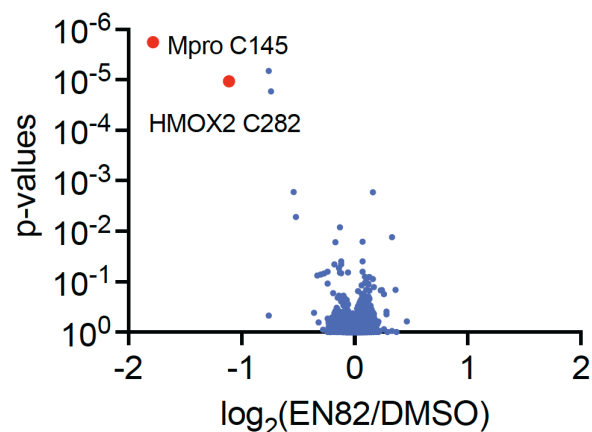
Figure 4.2. Proteome-wide cysteine-reactivity of EN82 in HEK293T cell lysate.
Cell lysate was treated with DMSO or EN82 (50 µM), followed by labeling of proteomes with alkyne-functionalized iodoacetamide probe and subsequent MS-ABPP method. Shown in blue are >2-fold ratios with p<0.05 showing 41 potential off-targets of EN82 out of 7281 distinct cysteine sites quantified.

Using mass spectrometry-based activity-based protein profiling (MS-ABPP), in which HEK293T cell lysates spiked with pure M^{pro} protein were pre-treated with vehicle or EN82 (50 µM), and subsequently labeled with an alkyne-functionalized cysteine-reactive iodoacetamide probe for subsequent quantitative chemoproteomic analysis of EN82 competed cysteine sites, we observed M^{pro} C145 as the primary target of EN82 with 1 additional off-target HMOX2 C282 out of >1000 distinct quantified probe-modified cysteines.

Thus, as an initial hit compound, EN82 showed a high degree of proteome-wide selectivity with only one potential off-target (Fig. 4.2). EN82 was a racemic mixture of two compounds. Upon enantioselective synthesis of each isomer, (R)-EN82 (0.53 µM) proved more active than (S)-EN82 (2.7 µM), consistent with a crystal structure obtained of (R)-EN82 bound to the catalytic cysteine C145 of SARS-CoV-2 M^{pro} (Fig. 4.1B). With EN82 as an encouraging starting point, structure-activity relationship (SAR) studies around the central pyrazoline core were conducted to optimize for potency.

4.3 Optimization to PM-2-071

We next devised an expedient synthesis of 3,5-disubstituted pyrazolines starting with an aldol condensation between commercially available aldehyde and acetophenone precursors to form the corresponding chalcone, followed by hydrazine condensation to access the unprotected pyrazoline core, and subsequent N-acylation to yield the final pyrazoline chloroacetamide in three steps (Fig. 4.3A). A number of nitrogen-containing heterocycles were introduced at the pyrazoline C5-carbon (Ar1) in an attempt to

improve potency. Differentially substituted quinoxalines, quinolines, indoles, azaindoles, benzotriazoles and pyridines were tested at this position, but no significant breakthrough was achieved (Fig. 4.3B). Several of these derivatives showed comparable potency to EN82, suggesting there is some flexibility for C5-pyrazoline substituent.
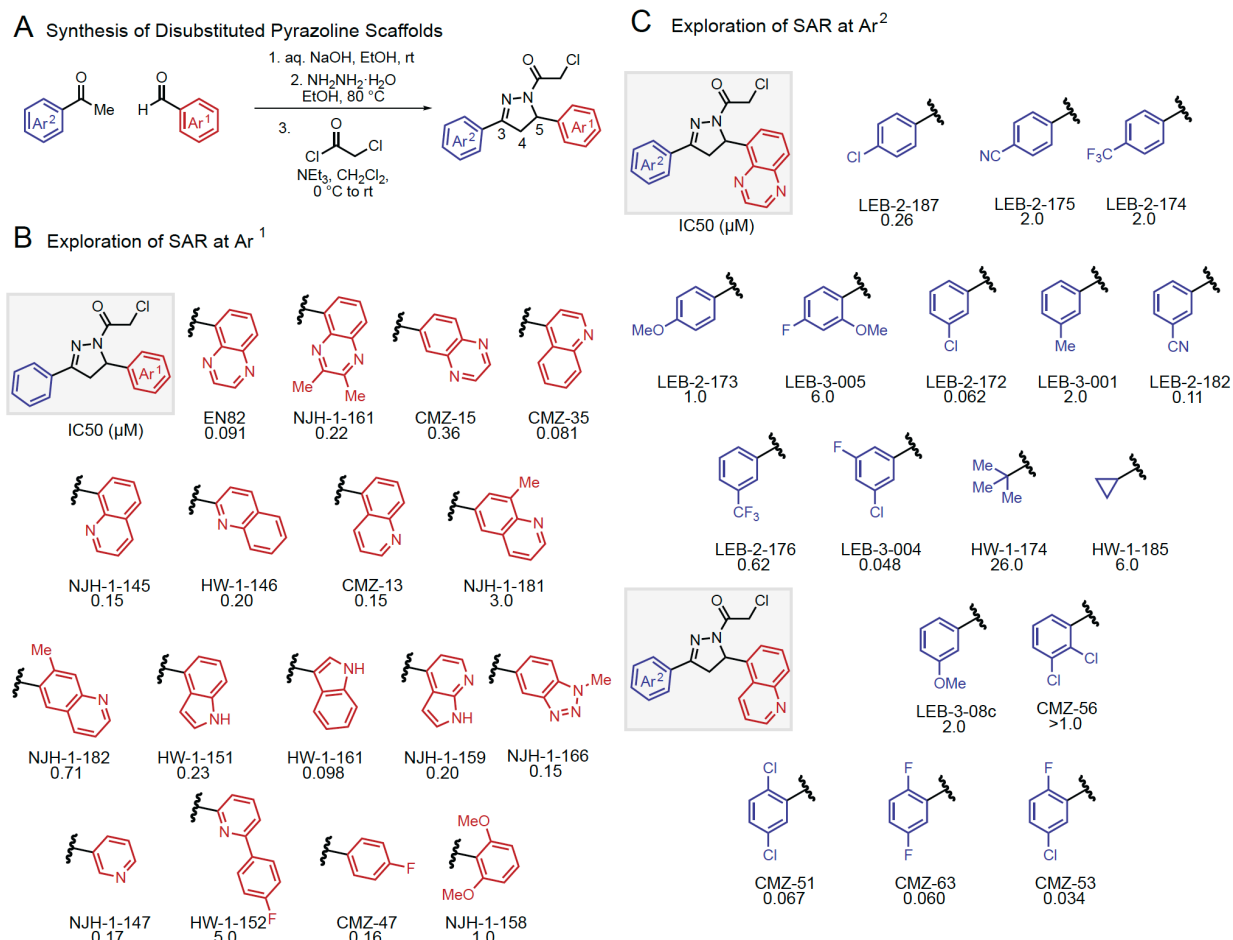

Figure 4.3. Exploration of 3,5-disubstituted pyrazoline SAR.
(A) Synthesis of disubstituted pyrazoline scaffolds. (B) Exploration of SAR at Ar1. (C) Exploration of SAR at Ar2. IC50 values determined by rhodamine-based substrate activity assay for SARS-CoV-2 Mpro from n=3 biological replicates.

SAR at the pyrazoline C3-carbon (Ar2) was explored next (Fig. 4.3C). Inhibitors with larger 4-substituted arenes (LEB-2-187, LEB-2-175, LEB-2-174, LEB-2-173) showed decreased potency compared to smaller 3-substituted arenes (LEB-2-172, LEB-3-001, LEB-2-182, LEB-2-176, and LEB-3-004). This was consistent with the relatively shallow pocket in which the C3-arene is located in the EN82-bound Mpro crystal structure (Fig. 4.1B). Simple aliphatic tert-butyl and cyclopropyl substituents (HW-1-174, HW-1-185) at this position exhibited a significant loss of activity.

Exploration of SAR was also examined using a 5-quinolinyl bearing pyrazoline scaffold (Fig. 4.3C, bottom), given that this scaffold displayed better overall solubility relative to the 5-quinoxalinyl derivatives. A consistent trend was observed with smaller 3- and 2-substituted arenes at the C3 position showing better activity. Ultimately, a 5-chloro-2-fluorophenyl C3-substituent (CMZ-53) proved optimal and provided a nearly three-fold improvement in potency compared to EN82.

We next explored the possibility of adding a substituent at the C4 position of the pyrazoline core. Examination of the crystal structure of EN82 bound to the SARS-CoV-2 M^{pro} revealed a small pocket occupied by an imidazole that should be accessible with cis-trisubstituted pyrazolines (Fig. 4.1B). Consistent with this premise, the trisubstituted cis-pyrazoline PM-2-020B showed improved potency compared to EN82 and its disubstituted analog EN23 (Fig. 4.4B). In contrast, trans-pyrazoline PM-2-020A showed an approximate 30-fold lower potency compared to cis-PM-02-020B, highlighting the profound impact of relative stereochemistry on the activity of these trisubstituted pyrazolines.
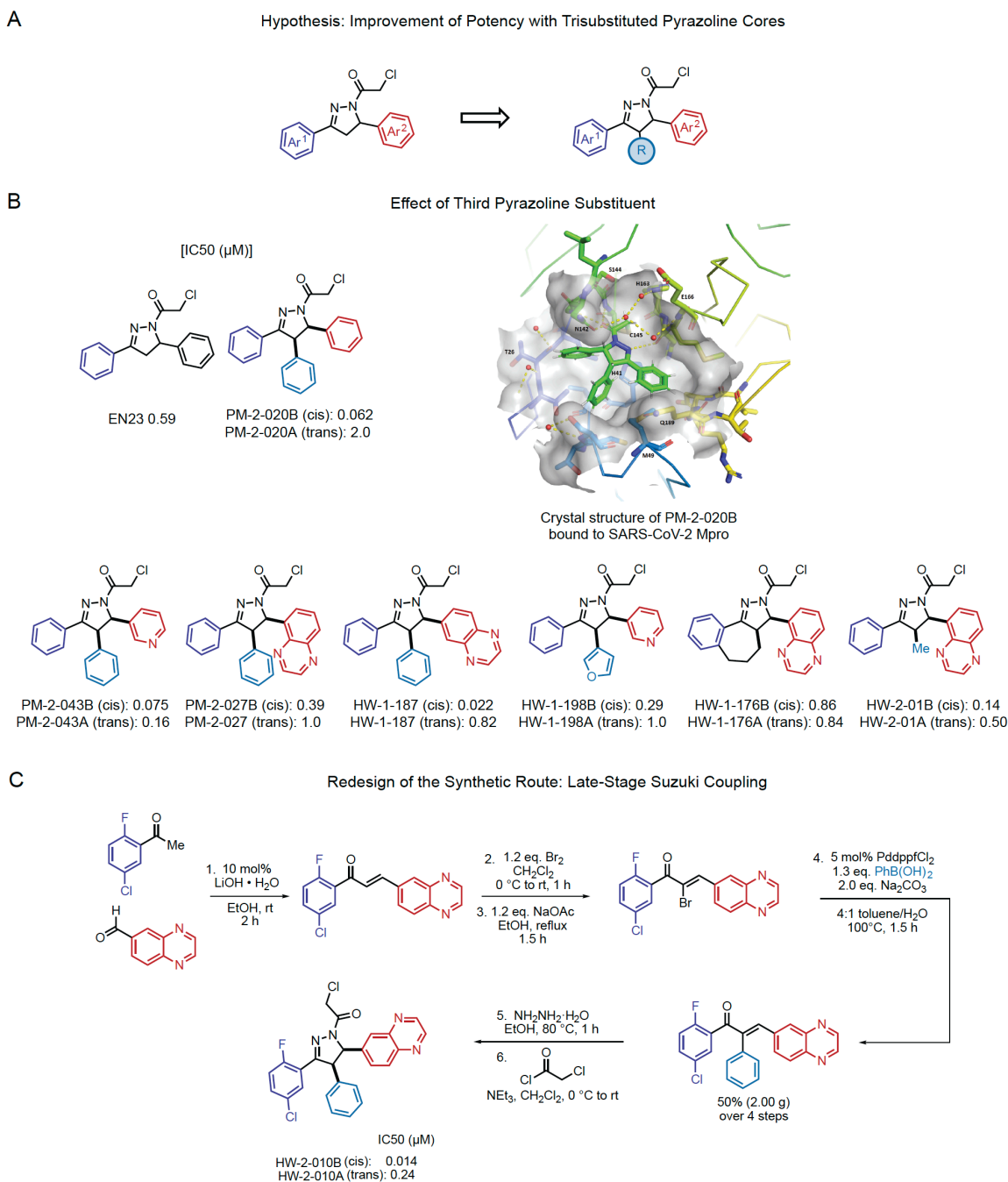
Figure 4.4. Exploration of trisubstituted pyrazoline inhibitors.
(A) We hypothesized that potency would be improved through trisubstitution of the pyrazoline core.
(B) Effect of third pyrazoline substituent on inhibitory potency of compounds against SARS-CoV-2 M^{pro}. Shown is the crystal structure of PM-2-20B covalently bound to the catalytic C145 of the SARS-CoV-2 Mpro active site. IC50 values determined by rhodamine-based substrate activity assay for SARS-CoV-2 M^{pro} from n=3 biological replicates. (C) Redesign of the synthetic late-stage Suzuki coupling to yield HW-2-010B and HW-2-010A. Potencies against SARS-CoV-2 M^{pro} are shown from n=3 biological replicates.

A crystal structure of PM-2-020B bound to the SARS-CoV-2 M^{pro} was obtained which corroborated the initial hypothesis, with the C4-phenyl group nestled in the previously empty sub-pocket. Trisubstituted analogs with C5-heterocycles were next tested while holding the C4-phenyl group constant. A smaller 3-pyridyl C5-substituent (cis-PM-2-043B) was slightly less potent, while a 5-quinoxalinyl substituent (cis-PM-2-027B) proved even less potent, perhaps due to unfavorable steric clash between the C4/C5 aryl substituents. Consistent with this hypothesis, a smaller isomeric 6-quinoxalinyl derivative (cis-HW-1-187B) proved to be our most potent inhibitor yet (IC50 = 0.022 µM). Other heteroaryl and alkyl C4-substituents were also tested but showed no significant improvement (HW-1-198B, HW-1-176B, HW-2-01B).

A revised modular synthetic route was next designed for each pyrazoline substituent to originate from different building blocks. Ideally, the C4-substituent could be installed at a later stage via cross-coupling to avoid having to be introduced in the first aldol condensation step from 2-arylacetophenone derivatives which are not readily available. Initial aldol condensation, followed by mono-bromination and Suzuki coupling led to a tri-arylated chalcone intermediate, which then led to the final pyrazoline core via hydrazine condensation and acylation (Fig. 3C). With this route, the optimal 5-chloro-2-fluorophenyl C3-substituent could be installed, leading to our most potent 0.014 µM chloroacetamide inhibitor (HW-2-010B).

Along with exploring the SAR around the pyrazoline core, concurrent efforts were aimed at identifying an alternative cysteine reactive warhead given chloroacetamides could potentially present metabolic stability issues (Fig. 4.5). A vinylsulfonamide was ultimately identified as a more promising alternative warhead,[4,240] culminating in the synthesis of PM-2-071B, a 0.091 µM inhibitor (Fig. 4.5, Fig. 4.6). Chiral SFC separation of PM-2-071B revealed that the (S,S)-enantiomer is most potent (0.035 µM), contrasting what is observed in the chloroacetamide series where the (R)-enantiomer of EN82 is most active (Fig. 4.6). This suggests a different binding mode may be at play with vinylsulfonamides relative to chloroacetamides. Other vinylsulfonamide derivatives were also tested; a modest improvement in potency was obtained with a 3-methoxy C4-substituent (PM-2-167B) while loss in potency was observed with a larger 3-benzyl substituent.
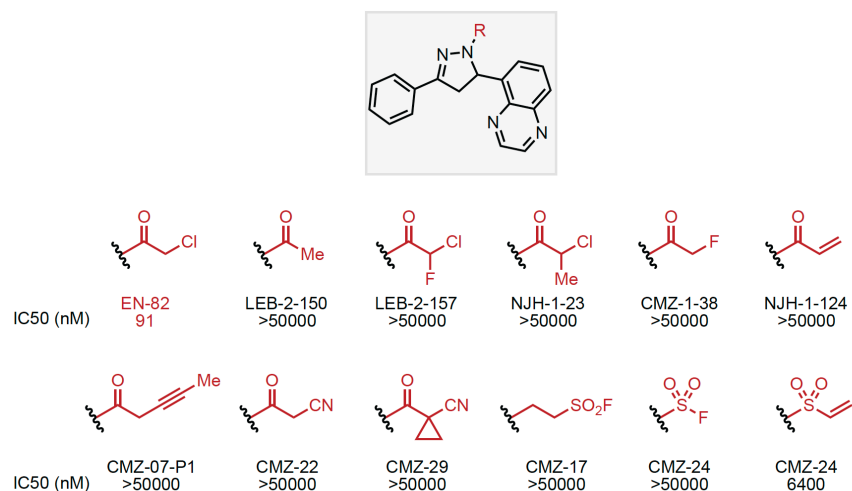
Figure 4.5. Exploration of Cysteine Reactive Warheads.
IC50 values determined by rhodamine-based substrate activity assay for SARS-CoV-2 M^{pro} from n=3 biological replicates.
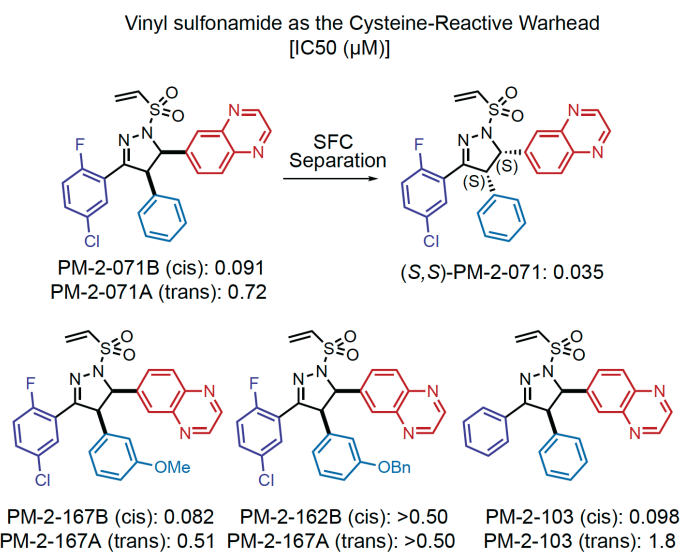

Figure 4.6. Trisubstituted pyrazoline inhibitors with a vinyl sulfonamide warhead.
IC50 values determined by rhodamine-based substrate activity assay for SARS-CoV-2 M^{pro} from n=3 biological replicates.

We also tested several of the di- and tri-substituted compounds, including PM-2-071, from our study against a panel of M^{pro} enzymes from other former coronaviruses, including SARS-CoV-2, SARS-CoV-1, HCoV-HKU1, HCoV-229E, MERS-CoV, PorCoV-HKU15, HCoV-NL63, avian infectious bronchitis virus (IBV), and HCoV-OC43. For these assays, we used an even more sensitive M^{pro} activity assay using an Agilent RapidFire-based substrate peptide activity assay that requires even less M^{pro} protein compared to the rhodamine-based activity assays to comparatively assess potencies of

some of our best covalent ligands. In these assays, we show that most of the compounds tested inhibit M^pro from these other coronaviruses with IC50 values in the nanomolar range (Fig. S4.1, Fig. 4.7). Most notably, we demonstrate that PM-2-071 shows IC50s <2 nM across SARS-CoV-2, HCoV-HKU1, and HCoV-OC43, and IC50s <1 µM for SARS-CoV-1, HCoV-NL63, IBV, and HCoV-229E M^pro enzymes (Fig. 7). Thus, this chemical scaffold may represent a promising starting point for further optimization of pan-coronavirus M^pro inhibitors.
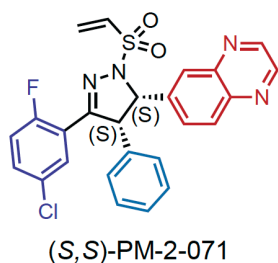
(S,S)-PM-2-071

	IC50 (µM)
SARS-CoV-2	<0.0025
SARS-CoV-1	0.0117
HCoV-NL63	0.091
IBV	0.22
HCoV-HKU1	<0.0025
HCoV-OC43	<0.0025
HCoV-229E	0.012

Figure 4.7. Profiling *(S,S)*-PM-2-071 M^pro inhibition across coronaviruses.
IC50 values determined by MS-based substrate activity assay for SARS-CoV-2 M^pro.

4.4 The Future of M^pro inhibitors

In conclusion, in this study, we have discovered some of the most potent SARS-CoV-2 M^pro inhibitors based on pyrazoline-based chloroacetamides and vinyl sulfonamides. We further demonstrate that many of the inhibitors developed here also show exceptional potency against M^pro from previous coronaviruses, indicating the potential to develop a pan-coronavirus M^pro inhibitor. Exploration of SAR at the pyrazoline core revealed the importance of relative stereochemistry at the C4 and C5 carbons. We note that unfortunately our optimized inhibitors such as (S,S)-PM-2-071A appeared to have issues with solubility, metabolic stability, and cell permeability. We did not observe antiviral activity in cells with these series of compounds against SARS-CoV-2. As such, further medicinal chemistry optimization is required to optimize these potent inhibitors for their drug-like properties to promote antiviral efficacy. Nonetheless, we believe that this general scaffold and the exploration of cysteine-reactive warheads here represents a good foundational starting point for the development of more advanced non-peptidic and more drug-like pan-coronavirus M^pro inhibitors in the future.

4.5 Acknowledgments

CONCLUDING REMARKS

Focused screening of cysteine-reactive electrophilic compounds has enabled the discovery of chemical probes that either act as enzymatic inhibitors or act through induced proximity mechanisms. For example, SARS-CoV-2 M^{pro} inhibitors such as PM-2-071 use the prolonged target engagement afforded by their covalent mechanism of action to induce effective protease inhibition. Though many other recently discovered covalent drugs target non-catalytic cysteines, covalent target engagement is broadly used to increase potency of inhibition. Covalency can be used as a strategy whether natural substrate affinity is particularly high, as with KRAS, or when particularly complete inhibition is needed for efficacy, as with SARS-CoV-2 M^{pro}.

Aside from additional potency, covalent chemical probes have successfully been used to induce proximity between proteins. The discovery that FEM1B can be recruited with covalent ligands adds a new E3 ligase to the repertoire of E3s that can be harnessed for targeted protein degradation. While many targets have been effectively degraded by CRBN-based degraders, using new E3 ligases represents opportunities to improve the specificity of degradation both across the proteome and between different tissue types and cell states. While CRBN and VHL recruiters have been optimized over the last decade, covalent drug discovery approaches have facilitated extremely rapid discovery of new E3 ligase recruiters. Even though these compounds face challenges for *in vivo* use, the proof-of-concept enables further discovery efforts. Now, more E3 ligases can be harnessed for TPD with covalent recruiters than reversible ones.

This extensive work on covalent E3 ligase recruiters, including advancements in covalent fragment ligand screening and chemical proteomics, paved the way for the discovery of DUBTACs that induce targeted protein stabilization. Analysis of DUB covalent ligandability based on previously gathered chemoproteomic data made it possible to identify a reactive allosteric cysteine on OTUB1. Covalent ligand screening techniques that measure binding regardless of enzymatic function allowed the discovery of a non-inhibitory OTUB1 ligand. This discovery of a suitable DUB ligand represented a key obstacle to overcome prior to synthesis and discovery of any DUBTACs, and the suite of covalent ligand discovery techniques proved particularly useful in approaching this challenge.

Discovery of DUBTACs represents a significant leap forward for induced-proximity modalities, unlocking protein stabilization as a potential therapeutic strategy. Such a modular approach to protein stabilization is particularly powerful because of the challenges associated with discovering small molecule activators of protein function. DUBTACs can be used to systematically convert non-functional binders, which are easier to identify, to stabilizing bifunctional molecules. While there are limitations to current DUBTAC applications, such as the requirement that target protein abundance is regulated through K48-linked ubiquitination, further iterations of the DUBTAC platform could harness different DUBs to various effects. DUBs that cleave K63 chains or monoubiquitin could be recruited to influence cellular localization of selected target proteins for instance. In short, DUBTACs provide many possible opportunities to modulate protein function and highlight the contribution of covalent ligands in enabling discovery of new induced proximity modalities.

Why have covalent ligands been so successful in recruiting E3 ligases for degradation, and now DUBs for stabilization? As noted above, covalent screening strategies often interrogate binding regardless of enzyme functionality.[3] For induced proximity mechanisms where directing protein function is the goal, identifying ligands that target allosteric cysteines represents a powerful approach, as exemplified with DUBTACs. Beyond the requirement for non-inhibitory ligands and the ease of discovering low-affinity ligands in covalent library screens, there are key features of these induced proximity modalities that covalent chemical probes can take advantage of – in particular the sufficiency of partial engagement and the importance of ternary complex lifetime.

The critical concept behind these induced proximity mechanisms is the idea of event-driven pharmacology.[11] The complex consisting of both proteins and the compound must only exist for as long as it takes for one protein (e.g. the E3) to exert its activity (ubiquitination) upon the other. This has been noted as a rationale for degradation providing certain advantages over inhibition, specifically the catalytic activity of the degrader that enables full degradation at low concentrations and doses.[10] This means that the E3 recruiter does not need to achieve full engagement of the E3. As opposed to enzymatic inhibitors, where >90% of the protein may need to be bound to see an effect, engagement of a small fraction of the E3 would still enable target degradation.

This means that reversible degraders with very low cell permeability can still be capable of inducing robust target degradation. On the other hand, permeable but weak covalent ligands can similarly lead to robust degradation. Unoptimized, low-affinity covalent chemical probes may not be effective at showing phenotypic effects in cell-based or in vivo assays. For example, even though the Shokat lab's original KRAS[G12C] inhibitors showed binding in MS-based assays, they were not effective in cell models of KRAS[G12C]-driven cancer without further optimization undertaken by Araxes Pharma.[102,103] However, unoptimized covalent E3 recruiters, that likely only partially engage their protein targets at relevant concentrations, have been employed successfully time over time to induce full degradation of targets such as BRD4, FKBP12, and the androgen receptor.[154,156,157,159] Requirement of only partial engagement could also explain why even though EN523 only partially labels OTUB1, as observed by MS based experiments, EN523-based DUBTACs can still recruit OTUB1 to induce deubiquitination of target proteins.[160]

Unique kinetic considerations of induced proximity modalities could also play into the hands of covalent ligands. Because bifunctional molecules must hold a ternary complex together long enough for the enzyme to act upon the target (e.g. ubiquitination), rapid dissociation from either protein could yield an ineffective compound.[241] The formation of a covalent adduct with the E3 or DUB changes the relevant complex from an Enzyme:Compound:Target ternary complex to an Enzyme–Compound:Target binary complex. Covalently engaging the E3 ligase or DUB prevents an opportunity for the complex to dissociate, potentially increasing lifetime of the

relevant complex. One potential implication of this is that binding cooperativity could be less relevant for covalent degrader activity versus reversible degraders. FEM1B-based BRD4 degraders show remarkably wide SAR within the linker, as do previously published DCAF16-based FKBP12 degraders.[156,159] This suggests that if the linker allows for the correct geometry and the target ligand is sufficiently potent, the target can be degraded, albeit with lower efficiency. Together with ease of finding low-affinity hits, these key features of induced proximity modalities seem to lend an advantage to covalent molecules.

The utility of covalent chemical probes for induced proximity modalities has become clear at the same time as several high-profile covalent drugs have achieved great success. The kinase inhibitors ibrutinib and osimertinib, as well as KRAS[G12C] inhibitor sotorasib and SARS-CoV-2 M[pro] inhibitor nirmatrelvir, have demonstrated that rationally designed covalent drugs can be safe and effective. These successes have encouraged remarkable advancements in strategies for discovering covalent chemical probes, including a shift from adding electrophilic groups onto potent reversible ligands to "electrophile-first" approaches that optimize molecules around a core covalent warhead. New techniques for covalent ligand discovery can be paired with induced proximity modalities to rapidly discover chemical probes and explore therapeutic approaches. In the same way that DUBTACs could be employed to stabilize protein targets that are otherwise undruggable due to the challenge of finding activating ligands, future induced proximity mechanisms will exploit other post translational modifications to modulate function of traditionally undruggable proteins. This powerful combination of covalent ligand discovery platforms and novel therapeutic modalities indicates a bright future ahead for covalent chemical probes and drug discovery.

REFERENCES

1.   Singh, J., Petter, R. C., Baillie, T. A. & Whitty, A. The resurgence of covalent drugs. *Nat Rev Drug Discov* **10**, 307–317 (2011).

2.   Lonsdale, R. & Ward, R. A. Structure-based design of targeted covalent inhibitors. *Chem. Soc. Rev.* **47**, 3816–3830 (2018).

3.   Spradlin, J. N., Zhang, E. & Nomura, D. K. Reimagining Druggability Using Chemoproteomic Platforms. *Acc. Chem. Res.* **54**, 1801–1813 (2021).

4.   Sutanto, F., Konstantinidou, M. & Dömling, A. Covalent inhibitors: a rational approach to drug discovery. *RSC Med. Chem.* **11**, 876–884 (2020).

5.   Lu, W. *et al.* Fragment-based covalent ligand discovery. *RSC Chem. Biol.* **2**, 354–367 (2021).

6.   Moellering, R. E. & Cravatt, B. F. How Chemoproteomics Can Enable Drug Discovery and Development. *Chemistry & Biology* **19**, 11–22 (2012).

7.   Sagonowsky, E. The top 20 drugs by worldwide sales in 2020. *Fierce Pharma* https://www.fiercepharma.com/special-report/top-20-drugs-by-2020-sales (2021).

8.   Vandyck, K. & Deval, J. Considerations for the discovery and development of 3-chymotrypsin-like cysteine protease inhibitors targeting SARS-CoV-2 infection. *Current Opinion in Virology* **49**, 36–40 (2021).

9.   Belcher, B. P., Ward, C. C. & Nomura, D. K. Ligandability of E3 Ligases for Targeted Protein Degradation Applications. *Biochemistry* acs.biochem.1c00464 (2021) doi:10.1021/acs.biochem.1c00464.

10.   Burslem, G. M. & Crews, C. M. Proteolysis-Targeting Chimeras as Therapeutics and Tools for Biological Discovery. *Cell* **181**, 102–114 (2020).

11.   Lai, A. C. & Crews, C. M. Induced protein degradation: an emerging drug discovery paradigm. *Nat Rev Drug Discov* **16**, 101–114 (2017).

12.   Kanner, S. A., Shuja, Z., Choudhury, P., Jain, A. & Colecraft, H. M. Targeted deubiquitination rescues distinct trafficking-deficient ion channelopathies. *Nat Methods* **17**, 1245–1253 (2020).

13.   Siriwardena, S. U. *et al.* Phosphorylation-Inducing Chimeric Small Molecules. *J. Am. Chem. Soc.* **142**, 14052–14057 (2020).

14.   Wang, W. W. *et al.* Targeted Protein Acetylation in Cells Using Heterobifunctional Molecules. *J. Am. Chem. Soc.* **143**, 16700–16708 (2021).

15.   Ng, C. S. C. & Banik, S. M. Recent advances in induced proximity modalities. *Current Opinion in Chemical Biology* **67**, 102107 (2022).

16.   Ghosh, A. K., Samanta, I., Mondal, A. & Liu, W. R. Covalent Inhibition in Drug Discovery. *ChemMedChem* **14**, 889–906 (2019).

17.   De Cesco, S., Kurian, J., Dufresne, C., Mittermaier, A. K. & Moitessier, N. Covalent inhibitors design and discovery. *European Journal of Medicinal Chemistry* **138**, 96–114 (2017).

18.   Zhang, T., Hatcher, J. M., Teng, M., Gray, N. S. & Kostic, M. Recent Advances in Selective and Irreversible Covalent Ligand Development and Validation. *Cell Chemical Biology* **26**, 1486–1500 (2019).

19.   Moore, A. R., Rosenberg, S. C., McCormick, F. & Malek, S. RAS-targeted therapies: is the undruggable drugged? *Nat Rev Drug Discov* **19**, 533–552 (2020).

20.   Huang, L., Guo, Z., Wang, F. & Fu, L. KRAS mutation: from undruggable to druggable in cancer. *Sig Transduct Target Ther* **6**, 386 (2021).

21.   Lagoutte, R., Patouret, R. & Winssinger, N. Covalent inhibitors: an opportunity for rational target selectivity. *Current Opinion in Chemical Biology* **39**, 54–63 (2017).

22.   Roberts, A. M., Ward, C. C. & Nomura, D. K. Activity-based protein profiling for mapping and pharmacologically interrogating proteome-wide ligandable hotspots. *Current Opinion in Biotechnology* **43**, 25–33 (2017).

23.   Drewes, G. & Knapp, S. Chemoproteomics and Chemical Probes for Target Discovery. *Trends in Biotechnology* **36**, 1275–1286 (2018).

24.   Maurais, A. J. & Weerapana, E. Reactive-cysteine profiling for drug discovery. *Current Opinion in Chemical Biology* **50**, 29–36 (2019).

25.   Chandrasekharan, N. & Simmons, D. L. The cyclooxygenases. *Genome Biology* **5**, (2004).

26.   Vane, J. R. Inhibition of Prostaglandin Synthesis as a Mechanism of Action forAspirin-like Drugs. *Nature* **231**, 232–235 (1971).

27.   Nicola, G., Tomberg, J., Pratt, R. F., Nicholas, R. A. & Davies, C. Crystal Structures of Covalent Complexes of β-Lactam Antibiotics with *Escherichia coli* Penicillin-Binding Protein 5: Toward an Understanding of Antibiotic Specificity. *Biochemistry* **49**, 8094–8104 (2010).

28.   Dijkmans, A. C. *et al.* Fosfomycin: Pharmacological, Clinical and Future Perspectives. *Antibiotics* **6**, 24 (2017).

29.   Hendlin, D. *et al.* Phosphonomycin, a New Antibiotic Produced by Strains of *Streptomyces*. *Science* **166**, 122–123 (1969).

30.   Kahan, F. M., Kahan, J. S., Cassidy, P. J. & Kropp, H. The Mechanism of Action of Fosfomycin (Phosphonomycin). *Ann NY Acad Sci* **235**, 364–386 (1974).

31.   Heck, A. M., Yanovski, J. A. & Calis, K. A. Orlistat, a New Lipase Inhibitor for the Management of Obesity. *Pharmacotherapy* **20**, 270–279 (2000).

32.   Olbe, L., Carlsson, E. & Lindberg, P. A proton-pump inhibitor expedition: the case histories of omeprazole and esomeprazole. *Nat Rev Drug Discov* **2**, 132–139 (2003).

33.   Savi, P. *et al.* Identification and Biological Activity of the Active Metabolite of Clopidogrel. *Thromb Haemost* **84**, 891–896 (2000).

34.	Thomas, D. & Zalcberg, J. 5-FLUOROURACIL: A PHARMACOLOGICAL PARADIGM IN THE USE OF CYTOTOXICS. *Clin Exp Pharmacol Physiol* **25**, 887–895 (1998).

35.	Danenberg, P. V., Langenbach, R. J. & Heidelberger, C. Structures of Reversible and Irreversible Complexes of Thymidylate Synthetase and Fluorinated Pyrimidine Nucleotidest. 8.

36.	Xu, H., Faber, C., Uchiki, T., Racca, J. & Dealwis, C. Structures of eukaryotic ribonucleotide reductase I define gemcitabine diphosphate binding and subunit assembly. *Proceedings of the National Academy of Sciences* **103**, 4028–4033 (2006).

37.	Curran, M. P. & McKeage, K. Bortezomib: A Review of its Use in Patients with Multiple Myeloma. *Drugs* **69**, 859–888 (2009).

38.	Lynch, T. J., Okimoto, R. A., Supko, J. G. & Settleman, J. Activating Mutations in the Epidermal Growth Factor Receptor Underlying Responsiveness of Non–Small-Cell Lung Cancer to Gefitinib. *The New England Journal of Medicine* 11 (2004).

39.	Paez, J. G. *et al. EGFR* Mutations in Lung Cancer: Correlation with Clinical Response to Gefitinib Therapy. *Science* **304**, 1497–1500 (2004).

40.	Ou, S.-H. I. Second-generation irreversible epidermal growth factor receptor (EGFR) tyrosine kinase inhibitors (TKIs): A better mousetrap? A review of the clinical evidence. *Critical Reviews in Oncology/Hematology* **83**, 407–421 (2012).

41.	Yu, H. A. *et al.* Analysis of Tumor Specimens at the Time of Acquired Resistance to EGFR-TKI Therapy in 155 Patients with *EGFR* -Mutant Lung Cancers. *Clin Cancer Res* **19**, 2240–2247 (2013).

42.	Recondo, G., Facchinetti, F., Olaussen, K. A., Besse, B. & Friboulet, L. Making the first move in EGFR-driven or ALK-driven NSCLC: first-generation or next-generation TKI? *Nat Rev Clin Oncol* **15**, 694–708 (2018).

43.	Yun, C.-H. *et al.* The T790M mutation in EGFR kinase causes drug resistance by increasing the affinity for ATP. *Proceedings of the National Academy of Sciences* **105**, 2070–2075 (2008).

44.	Soria, J.-C. *et al.* Afatinib versus erlotinib as second-line treatment of patients with advanced squamous cell carcinoma of the lung (LUX-Lung 8): an open-label randomised controlled phase 3 trial. *The Lancet Oncology* **16**, 897–907 (2015).

45.	Yu, H. A. & Pao, W. Afatinib—new therapy option for EGFR-mutant lung cancer. *Nat Rev Clin Oncol* **10**, 551–552 (2013).

46.	Tsou, H.-R. *et al.* Optimization of 6,7-Disubstituted-4-(arylamino)quinoline-3-carbonitriles as Orally Active, Irreversible Inhibitors of Human Epidermal Growth Factor Receptor-2 Kinase Activity. *J. Med. Chem.* **48**, 1107–1131 (2005).

47.	Deeks, E. D. Neratinib: First Global Approval. *Drugs* **77**, 1695–1704 (2017).

48.	Shirley, M. Dacomitinib: First Global Approval. *Drugs* **78**, 1947–1953 (2018).

49.   Zhou, W. *et al.* Novel mutant-selective EGFR kinase inhibitors against EGFR T790M. *Nature* **462**, 1070–1074 (2009).

50.   Cross, D. A. E. *et al.* AZD9291, an Irreversible EGFR TKI, Overcomes T790M-Mediated Resistance to EGFR Inhibitors in Lung Cancer. *Cancer Discovery* **4**, 1046–1061 (2014).

51.   Finlay, M. R. V. *et al.* Discovery of a Potent and Selective EGFR Inhibitor (AZD9291) of Both Sensitizing and T790M Resistance Mutations That Spares the Wild Type Form of the Receptor. *J. Med. Chem.* **57**, 8249–8267 (2014).

52.   Walter, A. O. *et al.* Discovery of a Mutant-Selective Covalent Inhibitor of EGFR that Overcomes T790M-Mediated Resistance in NSCLC. *Cancer Discovery* **3**, 1404–1415 (2013).

53.   Butterworth, S., Cross, D. A. E., Finlay, M. R. V., Ward, R. A. & Waring, M. J. The structure-guided discovery of osimertinib: the first U.S. FDA approved mutant selective inhibitor of EGFR T790M. *Med. Chem. Commun.* **8**, 820–822 (2017).

54.   Jänne, P. A. *et al.* AZD9291 in EGFR Inhibitor–Resistant Non–Small-Cell Lung Cancer. *N Engl J Med* **372**, 1689–1699 (2015).

55.   Mok, T. S. *et al.* Osimertinib or Platinum–Pemetrexed in EGFR T790M–Positive Lung Cancer. *n engl j med* 12 (2016).

56.   Passaro, A., Jänne, P. A., Mok, T. & Peters, S. Overcoming therapy resistance in EGFR-mutant lung cancer. *Nat Cancer* **2**, 377–391 (2021).

57.   Leonetti, A. *et al.* Resistance mechanisms to osimertinib in EGFR-mutated non-small cell lung cancer. *Br J Cancer* **121**, 725–737 (2019).

58.   Thress, K. S. *et al.* Acquired EGFR C797S mutation mediates resistance to AZD9291 in non–small cell lung cancer harboring EGFR T790M. *Nat Med* **21**, 560–562 (2015).

59.   Jia, Y. *et al.* Overcoming EGFR(T790M) and EGFR(C797S) resistance with mutant-selective allosteric inhibitors. *Nature* **534**, 129–132 (2016).

60.   To, C. *et al.* Single and Dual Targeting of Mutant EGFR with an Allosteric Inhibitor. *Cancer Discov* **9**, 926–943 (2019).

61.   Pan, Z. *et al.* Discovery of Selective Irreversible Inhibitors for Bruton's Tyrosine Kinase. *ChemMedChem* **2**, 58–61 (2007).

62.   Honigberg, L. A. *et al.* The Bruton tyrosine kinase inhibitor PCI-32765 blocks B-cell activation and is efficacious in models of autoimmune disease and B-cell malignancy. *Proceedings of the National Academy of Sciences* **107**, 13075–13080 (2010).

63.   Byrd, J. C. *et al.* Targeting BTK with Ibrutinib in Relapsed Chronic Lymphocytic Leukemia. *N Engl J Med* **369**, 32–42 (2013).

64.   Telliez, J.-B. *et al.* Discovery of a JAK3-Selective Inhibitor: Functional Differentiation of JAK3-Selective Inhibition over pan-JAK or JAK1-Selective Inhibition. *ACS Chem. Biol.* **11**, 3442–3451 (2016).

65.   Thorarensen, A. *et al.* Design of a Janus Kinase 3 (JAK3) Specific Inhibitor 1-((2 *S* ,5 *R*)-5-((7 *H* -Pyrrolo[2,3- *d*]pyrimidin-4-yl)amino)-2-methylpiperidin-1-yl)prop-2-en-1-one (PF-06651600) Allowing for the Interrogation of JAK3 Signaling in Humans. *J. Med. Chem.* **60**, 1971–1993 (2017).

66.   Robinson, M. F. *et al.* Efficacy and Safety of PF-06651600 (Ritlecitinib), a Novel JAK3/TEC Inhibitor, in Patients With Moderate-to-Severe Rheumatoid Arthritis and an Inadequate Response to Methotrexate. *Arthritis Rheumatol* **72**, 1621–1631 (2020).

67.   Kim, R. D. *et al.* First-in-Human Phase I Study of Fisogatinib (BLU-554) Validates Aberrant FGF19 Signaling as a Driver Event in Hepatocellular Carcinoma. *Cancer Discov* **9**, 1696–1707 (2019).

68.   Pal Singh, S., Dammeijer, F. & Hendriks, R. W. Role of Bruton's tyrosine kinase in B cells and malignancies. *Mol Cancer* **17**, 57 (2018).

69.   Burger, J. A. & Buggy, J. J. Bruton tyrosine kinase inhibitor ibrutinib (PCI-32765). *Leukemia & Lymphoma* **54**, 2385–2391 (2013).

70.   Brooimans, R. A. *et al.* Identification of novel Bruton's tyrosine kinase mutations in 10 unrelated subjects with X linked agammaglobulinaemia. *Journal of Medical Genetics* **34**, 484–488 (1997).

71.   Herman, S. E. M. *et al.* Bruton tyrosine kinase represents a promising therapeutic target for treatment of chronic lymphocytic leukemia and is effectively targeted by PCI-32765. *Blood* **117**, 6287–6296 (2011).

72.   Byrd, J. C. *et al.* Ibrutinib Treatment for First-Line and Relapsed/Refractory Chronic Lymphocytic Leukemia: Final Analysis of the Pivotal Phase Ib/II PCYC-1102 Study. *Clin Cancer Res* **26**, 3918–3927 (2020).

73.   Wang, M. L. *et al.* Targeting BTK with Ibrutinib in Relapsed or Refractory Mantle-Cell Lymphoma. *N Engl J Med* **369**, 507–516 (2013).

74.   Treon, S. P. *et al.* Ibrutinib in Previously Treated Waldenström's Macroglobulinemia. *N Engl J Med* **372**, 1430–1440 (2015).

75.   Miklos, D. *et al.* Ibrutinib for chronic graft-versus-host disease after failure of prior therapy. *Blood* **130**, 2243–2250 (2017).

76.   Davids, M. S. & Brown, J. R. Ibrutinib: a first in class covalent inhibitor of Bruton's tyrosine kinase. *Future Oncology* **10**, 957–967 (2014).

77.   Advani, R. H. *et al.* Bruton Tyrosine Kinase Inhibitor Ibrutinib (PCI-32765) Has Significant Activity in Patients With Relapsed/Refractory B-Cell Malignancies. *JCO* **31**, 88–94 (2013).

78.   Imbruvica. *FiercePharma* https://www.fiercepharma.com/special-report/top-20-drugs-by-2020-sales-imbruvica.

79.   Barf, T. *et al.* Acalabrutinib (ACP-196): A Covalent Bruton Tyrosine Kinase Inhibitor with a Differentiated Selectivity and In Vivo Potency Profile. *J Pharmacol Exp Ther* **363**, 240–252 (2017).

80.   Flanagan, M. E. *et al.* Chemical and Computational Methods for the Characterization of Covalent Reactive Groups for the Prospective Design of Irreversible Inhibitors. *J. Med. Chem.* **57**, 10072–10079 (2014).

81.   Ward, R. A. *et al.* Structure- and Reactivity-Based Development of Covalent Inhibitors of the Activating and Gatekeeper Mutant Forms of the Epidermal Growth Factor Receptor (EGFR). *J. Med. Chem.* **56**, 7025–7048 (2013).

82.   Byrd, J. C. *et al.* Acalabrutinib (ACP-196) in Relapsed Chronic Lymphocytic Leukemia. *N Engl J Med* **374**, 323–332 (2016).

83.   Byrd, J. C. *et al.* Acalabrutinib Versus Ibrutinib in Previously Treated Chronic Lymphocytic Leukemia: Results of the First Randomized Phase III Trial. *JCO* **39**, 3441–3452 (2021).

84.   Narita, Y. *et al.* Phase I/II study of tirabrutinib, a second-generation Bruton's tyrosine kinase inhibitor, in relapsed/refractory primary central nervous system lymphoma. *Neuro-Oncology* **23**, 122–133 (2021).

85.   Guo, Y. *et al.* Discovery of Zanubrutinib (BGB-3111), a Novel, Potent, and Selective Covalent Inhibitor of Bruton's Tyrosine Kinase. *J. Med. Chem.* **62**, 7923–7940 (2019).

86.   Caldwell, R. D. *et al.* Discovery of Evobrutinib: An Oral, Potent, and Highly Selective, Covalent Bruton's Tyrosine Kinase (BTK) Inhibitor for the Treatment of Immunological Diseases. *J. Med. Chem.* **62**, 7643–7655 (2019).

87.   Serafimova, I. M. *et al.* Reversible targeting of noncatalytic cysteines with chemically tuned electrophiles. *Nat Chem Biol* **8**, 471–476 (2012).

88.   Miller, R. M., Paavilainen, V. O., Krishnan, S., Serafimova, I. M. & Taunton, J. Electrophilic Fragment-Based Design of Reversible Covalent Kinase Inhibitors. *J. Am. Chem. Soc.* **135**, 5298–5301 (2013).

89.   Bradshaw, J. M. *et al.* Prolonged and tunable residence time using reversible covalent kinase inhibitors. *Nat Chem Biol* **11**, 525–531 (2015).

90.   Sanofi: Press Releases, Thursday, September 9, 2021. *https://www.sanofi.com/en/media-room/press-releases/2021/2021-09-09-07-00-00-2293920* https://www.sanofi.com/media-room/press-releases/2021/2021-09-09 07-00-00 2293920.

91.   Zhang, D., Gong, H. & Meng, F. Recent Advances in BTK Inhibitors for the Treatment of Inflammatory and Autoimmune Diseases. *Molecules* **26**, 4907 (2021).

92.   Zhao, Z. & Bourne, P. E. Progress with covalent small-molecule kinase inhibitors. *Drug Discovery Today* **23**, 727–735 (2018).

93.   Liu, Q. *et al.* Developing Irreversible Inhibitors of the Protein Kinase Cysteinome. *Chemistry & Biology* **20**, 146–159 (2013).

94.   Goedken, E. R. *et al.* Tricyclic Covalent Inhibitors Selectively Target Jak3 through an Active Site Thiol. *Journal of Biological Chemistry* **290**, 4573–4589 (2015).

95.   Tan, L. *et al.* Development of Selective Covalent Janus Kinase 3 Inhibitors. *J. Med. Chem.* **58**, 6589–6606 (2015).

96.   Kempson, J. *et al.* Discovery of highly potent, selective, covalent inhibitors of JAK3. *Bioorganic & Medicinal Chemistry Letters* **27**, 4622–4625 (2017).

97.   Tan, L. *et al.* Development of covalent inhibitors that can overcome resistance to first-generation FGFR kinase inhibitors. *Proc Natl Acad Sci USA* **111**, E4869–E4877 (2014).

98.   Weiss, A. *et al.* FGF401, A First-In-Class Highly Selective and Potent FGFR4 Inhibitor for the Treatment of FGF19-Driven Hepatocellular Cancer. *Mol Cancer Ther* **18**, 2194–2206 (2019).

99.   Kwiatkowski, N. *et al.* Targeting transcription regulation in cancer with a covalent CDK7 inhibitor. *Nature* **511**, 616–620 (2014).

100.   Zhang, T. *et al.* Covalent targeting of remote cysteine residues to develop CDK12 and CDK13 inhibitors. *Nat Chem Biol* **12**, 876–884 (2016).

101.   Goebel, L., Müller, M. P., Goody, R. S. & Rauh, D. KRasG12C inhibitors in clinical trials: a short historical perspective. *RSC Med. Chem.* **11**, 760–770 (2020).

102.   Janes, M. R. *et al.* Targeting KRAS Mutant Cancers with a Covalent G12C-Specific Inhibitor. *Cell* **172**, 578-589.e17 (2018).

103.   Ostrem, J. M., Peters, U., Sos, M. L., Wells, J. A. & Shokat, K. M. K-Ras(G12C) inhibitors allosterically control GTP affinity and effector interactions. *Nature* **503**, 548–551 (2013).

104.   Lito, P., Solomon, M., Li, L.-S., Hansen, R. & Rosen, N. Allele-specific inhibitors inactivate mutant KRAS G12C by a trapping mechanism. *Science* **351**, 604–608 (2016).

105.   Patricelli, M. P. *et al.* Selective Inhibition of Oncogenic KRAS Output with Small Molecules Targeting the Inactive State. *Cancer Discov* **6**, 316–329 (2016).

106.   Canon, J. *et al.* The clinical KRAS(G12C) inhibitor AMG 510 drives anti-tumour immunity. *Nature* **575**, 217–223 (2019).

107.   Lanman, B. A. *et al.* Discovery of a Covalent Inhibitor of KRAS [G12C] (AMG 510) for the Treatment of Solid Tumors. *J. Med. Chem.* **63**, 52–65 (2020).

108.   Skoulidis, F. *et al.* Sotorasib for Lung Cancers with *KRAS* p.G12C Mutation. *N Engl J Med* **384**, 2371–2381 (2021).

109.   Fell, J. B. *et al.* Identification of the Clinical Development Candidate **MRTX849** , a Covalent KRAS [G12C] Inhibitor for the Treatment of Cancer. *J. Med. Chem.* **63**, 6679–6693 (2020).

110.   Hallin, J. *et al.* The KRAS [G12C] Inhibitor MRTX849 Provides Insight toward Therapeutic Susceptibility of KRAS-Mutant Cancers in Mouse Models and Patients. *Cancer Discov* **10**, 54–71 (2020).

111.   Mirati Therapeutics. Mirati Therapeutics' Adagrasib Receives Breakthrough Therapy Designation from U.S. Food and Drug Administration for Patients with Advanced Non-Small Cell Lung Cancer Harboring the KRAS G12C Mutation. https://www.prnewswire.com/news-

releases/mirati-therapeutics-adagrasib-receives-breakthrough-therapy-designation-from-us-food-and-drug-administration-for-patients-with-advanced-non-small-cell-lung-cancer-harboring-the-kras-g12c-mutation-301319824.html.

112.   COVID-19 Data Explorer. *Our World in Data* https://ourworldindata.org/coronavirus-data-explorer.

113.   Commissioner, O. of the. Coronavirus (COVID-19) Update: FDA Authorizes First Oral Antiviral for Treatment of COVID-19. *FDA* https://www.fda.gov/news-events/press-announcements/coronavirus-covid-19-update-fda-authorizes-first-oral-antiviral-treatment-covid-19 (2021).

114.   Qiao, J. *et al.* SARS-CoV-2 M [pro] inhibitors with antiviral activity in a transgenic mouse model. *Science* **371**, 1374–1378 (2021).

115.   Anand, K., Ziebuhr, J., Wadhwani, P., Mesters, J. R. & Hilgenfeld, R. Coronavirus Main Proteinase (3CLpro) Structure: Basis for Design of Anti-SARS Drugs. **300**, 6 (2003).

116.   Hoffman, R. L. *et al.* Discovery of Ketone-Based Covalent Inhibitors of Coronavirus 3CL Proteases for the Potential Therapeutic Treatment of COVID-19. *J. Med. Chem.* **63**, 12725–12747 (2020).

117.   Owen, D. R. *et al.* An oral SARS-CoV-2 Mpro inhibitor clinical candidate for the treatment of COVID-19. *Science* eabl4784 (2021) doi:10.1126/science.abl4784.

118.   Bandyopadhyay, A. & Gao, J. Targeting biomolecules with reversible covalent chemistry. *Current Opinion in Chemical Biology* **34**, 110–116 (2016).

119.   Hammond, J. *et al.* Oral Nirmatrelvir for High-Risk, Nonhospitalized Adults with Covid-19. *N Engl J Med* NEJMoa2118542 (2022) doi:10.1056/NEJMoa2118542.

120.   Mahase, E. Covid-19: Pfizer's paxlovid is 89% effective in patients at risk of serious illness, company reports. *BMJ* n2713 (2021) doi:10.1136/bmj.n2713.

121.   Metcalf, B. *et al.* Discovery of GBT440, an Orally Bioavailable R-State Stabilizer of Sickle Cell Hemoglobin. *ACS Med. Chem. Lett.* **8**, 321–326 (2017).

122.   Oksenberg, D. *et al.* GBT 440 increases haemoglobin oxygen affinity, reduces sickling and prolongs RBC half-life in a murine model of sickle cell disease. *Br J Haematol* **175**, 141–153 (2016).

123.   Vichinsky, E. *et al.* A Phase 3 Randomized Trial of Voxelotor in Sickle Cell Disease. *N Engl J Med* **381**, 509–519 (2019).

124.   de Leuw, P. & Stephan, C. Protease inhibitor therapy for hepatitis C virus-infection. *Expert Opinion on Pharmacotherapy* **19**, 577–587 (2018).

125.   Hézode, C. *et al.* Telaprevir and Peginterferon with or without Ribavirin for Chronic HCV Infection. *The New England Journal of Medicine* 12 (2009).

126.   Venkatraman, S. *et al.* Discovery of (1 *R* ,5 *S*)- *N* -[3-Amino-1-(cyclobutylmethyl)-2,3-dioxopropyl]- 3-[2(*S*)-[[[(1,1-dimethylethyl)amino]carbonyl]amino]-3,3-dimethyl-1-oxobutyl]- 6,6-

dimethyl-3-azabicyclo[3.1.0]hexan-2(*S*)-carboxamide (SCH 503034), a Selective, Potent, Orally Bioavailable Hepatitis C Virus NS3 Protease Inhibitor: A Potential Therapeutic Agent for the Treatment of Hepatitis C Infection. *J. Med. Chem.* **49**, 6074–6086 (2006).

127.	Venkatraman, S. Discovery of boceprevir, a direct-acting NS3/4A protease inhibitor for treatment of chronic hepatitis C infections. *Trends in Pharmacological Sciences* **33**, 289–294 (2012).

128.	Lin, C., Kwong, A. & Perni, R. Discovery and Development of VX-950, a Novel, Covalent, and Reversible Inhibitor of Hepatitis C Virus NS3.4A Serine Protease. *IDDT* **6**, 3–16 (2006).

129.	Kwong, A. D., Kauffman, R. S., Hurter, P. & Mueller, P. Discovery and development of telaprevir: an NS3-4A protease inhibitor for treating genotype 1 chronic hepatitis C virus. *Nat Biotechnol* **29**, 993–1003 (2011).

130.	Arasappan, A. *et al.* Discovery of Narlaprevir (SCH 900518): A Potent, Second Generation HCV NS3 Serine Protease Inhibitor. *ACS Med. Chem. Lett.* **1**, 64–69 (2010).

131.	McCauley, J. A. & Rudd, M. T. Hepatitis C virus NS3/4a protease inhibitors. *Current Opinion in Pharmacology* **30**, 84–92 (2016).

132.	Kwo, P. Y. *et al.* Efficacy of boceprevir, an NS3 protease inhibitor, in combination with peginterferon alfa-2b and ribavirin in treatment-naive patients with genotype 1 hepatitis C infection (SPRINT-1): an open-label, randomised, multicentre phase 2 trial. *The Lancet* **376**, 705–716 (2010).

133.	Sherman, K. E. *et al.* Response-Guided Telaprevir Combination Treatment for Hepatitis C Virus Infection. *N Engl J Med* **365**, 1014–1024 (2011).

134.	Ramsay, I. D., Lestner, J. M. & Barker, C. I. S. Antiviral drugs. in *Side Effects of Drugs Annual* vol. 35 503–550 (Elsevier, 2014).

135.	Merck & Co., Inc. Merck Voluntarily Discontinuing VICTRELIS. (2015).

136.	Lawitz, E. *et al.* Sofosbuvir and ledipasvir fixed-dose combination with and without ribavirin in treatment-naive and previously treated patients with genotype 1 hepatitis C virus infection (LONESTAR): an open-label, randomised, phase 2 trial. *The Lancet* **383**, 515–523 (2014).

137.	Kim, K. B. & Crews, C. M. From epoxomicin to carfilzomib: chemistry, biology, and medical outcomes. *Nat. Prod. Rep.* **30**, 600 (2013).

138.	Groll, M., Kim, K. B., Kairies, N., Huber, R. & Crews, C. M. Crystal Structure of Epoxomicin:20S Proteasome Reveals a Molecular Basis for Selectivity of α',β'-Epoxyketone Proteasome Inhibitors. *J. Am. Chem. Soc.* **122**, 1237–1238 (2000).

139.	Cravatt, B. F., Wright, A. T. & Kozarich, J. W. Activity-Based Protein Profiling: From Enzyme Chemistry to Proteomic Chemistry. *Annu. Rev. Biochem.* **77**, 383–414 (2008).

140.	Liu, Y., Patricelli, M. P. & Cravatt, B. F. Activity-based protein profiling: The serine hydrolases. *Proceedings of the National Academy of Sciences* **96**, 14694–14699 (1999).

141.   Weerapana, E., Speers, A. E. & Cravatt, B. F. Tandem orthogonal proteolysis-activity-based protein profiling (TOP-ABPP)—a general method for mapping sites of probe modification in proteomes. *Nat Protoc* **2**, 1414–1425 (2007).

142.   Weerapana, E. *et al.* Quantitative reactivity profiling predicts functional cysteines in proteomes. *Nature* **468**, 790–795 (2010).

143.   Backus, K. M. *et al.* Proteome-wide covalent ligand discovery in native biological systems. *Nature* **534**, 570–574 (2016).

144.   Bar-Peled, L. *et al.* Chemical Proteomics Identifies Druggable Vulnerabilities in a Genetically Defined Cancer. *Cell* **171**, 696-709.e23 (2017).

145.   Vinogradova, E. V. *et al.* An Activity-Guided Map of Electrophile-Cysteine Interactions in Primary Human T Cells. *Cell* **182**, 1009-1026.e29 (2020).

146.   Blewett, M. M. *et al.* Chemical proteomic map of dimethyl fumarate–sensitive cysteines in primary human T cells. *Sci. Signal.* **9**, (2016).

147.   Zaro, B. W. *et al.* Dimethyl Fumarate Disrupts Human Innate Immune Signaling by Targeting the IRAK4–MyD88 Complex. *J.I.* **202**, 2737–2746 (2019).

148.   Chung, C. Y.-S. *et al.* Covalent targeting of the vacuolar H+-ATPase activates autophagy via mTORC1 inhibition. *Nat Chem Biol* **15**, 776–785 (2019).

149.   Grüner, B. M. *et al.* An in vivo multiplexed small-molecule screening platform. *Nat Methods* **13**, 883–889 (2016).

150.   Boike, L. *et al.* Discovery of a Functional Covalent Ligand Targeting an Intrinsically Disordered Cysteine within MYC. *Cell Chemical Biology* S2451945620303421 (2020) doi:10.1016/j.chembiol.2020.09.001.

151.   Yan, T. *et al.* SP3-FAIMS Chemoproteomics for High-Coverage Profiling of the Human Cysteinome. *ChemBioChem* **22**, 1841–1851 (2021).

152.   Kuljanin, M. *et al.* Reimagining high-throughput profiling of reactive cysteines for cell-based screening of large electrophile libraries. *Nat Biotechnol* **39**, 630–641 (2021).

153.   Spradlin, J. N. *et al.* Harnessing the anti-cancer natural product nimbolide for targeted protein degradation. *Nat Chem Biol* **15**, 747–755 (2019).

154.   Luo, M. *et al.* Chemoproteomics-enabled discovery of covalent RNF114-based degraders that mimic natural product function. *Cell Chemical Biology* **28**, 559-566.e15 (2021).

155.   Ward, C. C. *et al.* Covalent Ligand Screening Uncovers a RNF4 E3 Ligase Recruiter for Targeted Protein Degradation Applications. *ACS Chem. Biol.* **14**, 2430–2440 (2019).

156.   Zhang, X., Crowley, V. M., Wucherpfennig, T. G., Dix, M. M. & Cravatt, B. F. Electrophilic PROTACs that degrade nuclear proteins by engaging DCAF16. *Nat Chem Biol* **15**, 737–746 (2019).

157.   Zhang, X. *et al.* DCAF11 Supports Targeted Protein Degradation by Electrophilic Proteolysis-Targeting Chimeras. *J. Am. Chem. Soc.* **143**, 5141–5149 (2021).

158.   Tong, B. *et al.* Bardoxolone conjugation enables targeted protein degradation of BRD4. *Sci Rep* **10**, 15543 (2020).

159.   Henning, N. J. *et al.* Discovery of a Covalent FEM1B Recruiter for Targeted Protein Degradation Applications. *J. Am. Chem. Soc.* jacs.1c03980 (2022) doi:10.1021/jacs.1c03980.

160.   Henning, N. J. *et al.* Deubiquitinase-targeting chimeras for targeted protein stabilization. *Nat Chem Biol* (2022) doi:10.1038/s41589-022-00971-2.

161.   Erlanson, D. A. *et al.* Site-directed ligand discovery. *Proceedings of the National Academy of Sciences* **97**, 9367–9372 (2000).

162.   Erlanson, D. A., Wells, J. A. & Braisted, A. C. Tethering: Fragment-Based Drug Discovery. *Annu. Rev. Biophys. Biomol. Struct.* **33**, 199–223 (2004).

163.   Arkin, M. R. *et al.* Binding of small molecules to an adaptive protein-protein interface. *Proceedings of the National Academy of Sciences* **100**, 1603–1608 (2003).

164.   Keedy, D. A. *et al.* An expanded allosteric network in PTP1B by multitemperature crystallography, fragment screening, and covalent tethering. *eLife* **7**, e36307 (2018).

165.   Wolter, M. *et al.* Fragment-Based Stabilizers of Protein–Protein Interactions through Imine-Based Tethering. *Angew. Chem. Int. Ed.* **59**, 21520–21524 (2020).

166.   Kathman, S. G., Xu, Z. & Statsyuk, A. V. A Fragment-Based Method to Discover Irreversible Covalent Inhibitors of Cysteine Proteases. *J. Med. Chem.* **57**, 4969–4974 (2014).

167.   Kathman, S. G. *et al.* A Small Molecule That Switches a Ubiquitin Ligase From a Processive to a Distributive Enzymatic Mechanism. *J. Am. Chem. Soc.* **137**, 12442–12445 (2015).

168.   Johansson, H. *et al.* Fragment-Based Covalent Ligand Screening Enables Rapid Discovery of Inhibitors for the RBR E3 Ubiquitin Ligase HOIP. *J. Am. Chem. Soc.* **141**, 2703–2712 (2019).

169.   Resnick, E. *et al.* Rapid Covalent-Probe Discovery by Electrophile-Fragment Screening. *J. Am. Chem. Soc.* **141**, 8951–8968 (2019).

170.   Dubiella, C. *et al.* Sulfopin is a covalent inhibitor of Pin1 that blocks Myc-driven tumors in vivo. *Nat Chem Biol* **17**, 954–963 (2021).

171.   Shin, Y. *et al.* Discovery of *N* -(1-Acryloylazetidin-3-yl)-2-(1 *H* -indol-1-yl)acetamides as Covalent Inhibitors of KRAS [G12C]. *ACS Med. Chem. Lett.* **10**, 1302–1308 (2019).

172.   Debaene, F., Da Silva, J. A., Pianowski, Z., Duran, F. J. & Winssinger, N. Expanding the scope of PNA-encoded libraries: divergent synthesis of libraries targeting cysteine, serine and metallo-proteases as well as tyrosine phosphatases. *Tetrahedron* **63**, 6577–6586 (2007).

173.   Zimmermann, G. *et al.* A Specific and Covalent JNK-1 Ligand Selected from an Encoded Self-Assembling Chemical Library. *Chem. Eur. J.* **23**, 8152–8155 (2017).

174.   Zambaldo, C., Daguer, J.-P., Saarbach, J., Barluenga, S. & Winssinger, N. Screening for covalent inhibitors using DNA-display of small molecule libraries functionalized with cysteine reactive moieties. *Med. Chem. Commun.* **7**, 1340–1351 (2016).

175.   Chan, A. I., McGregor, L. M., Jain, T. & Liu, D. R. Discovery of a Covalent Kinase Inhibitor from a DNA-Encoded Small-Molecule Library × Protein Library Selection. *J. Am. Chem. Soc.* **139**, 10192–10195 (2017).

176.   Guilinger, J. P. *et al.* Novel irreversible covalent BTK inhibitors discovered using DNA-encoded chemistry. *Bioorganic & Medicinal Chemistry* **42**, 116223 (2021).

177.   London, N. *et al.* Covalent docking of large libraries for the discovery of chemical probes. *Nat Chem Biol* **10**, 1066–1072 (2014).

178.   Shraga, A. *et al.* Covalent Docking Identifies a Potent and Selective MKK7 Inhibitor. *Cell Chemical Biology* **26**, 98-108.e5 (2019).

179.   Nnadi, C. I. *et al.* Novel K-Ras G12C Switch-II Covalent Binders Destabilize Ras and Accelerate Nucleotide Exchange. *J. Chem. Inf. Model.* **58**, 464–471 (2018).

180.   Strelow, J. M. A Perspective on the Kinetics of Covalent and Irreversible Inhibition. *SLAS DISCOVERY: Advancing the Science of Drug Discovery* **22**, 3–20 (2017).

181.   McWhirter, C. Kinetic mechanisms of covalent inhibition. in *Annual Reports in Medicinal Chemistry* vol. 56 1–31 (Elsevier, 2021).

182.   Schnute, M. E. *et al.* Aminopyrazole Carboxamide Bruton's Tyrosine Kinase Inhibitors. Irreversible to Reversible Covalent Reactive Group Tuning. *ACS Med. Chem. Lett.* **10**, 80–85 (2019).

183.   Maurer, T. S., Tabrizi-Fard, M. A. & Fung, H. Impact of mechanism-based enzyme inactivation on inhibitor potency: Implications for rational drug discovery. *J. Pharm. Sci.* **89**, 1404–1414 (2000).

184.   Krippendorff, B.-F., Neuhaus, R., Lienau, P., Reichel, A. & Huisinga, W. Mechanism-Based Inhibition: Deriving K_I and k_{inact} Directly from Time-Dependent IC_{50} Values. *J Biomol Screen* **14**, 913–923 (2009).

185.   Hacker, S. M. *et al.* Global profiling of lysine reactivity and ligandability in the human proteome. *Nature Chem* **9**, 1181–1190 (2017).

186.   Ward, C. C., Kleinman, J. I. & Nomura, D. K. NHS-Esters As Versatile Reactivity-Based Probes for Mapping Proteome-Wide Ligandable Hotspots. *ACS Chem. Biol.* **12**, 1478–1483 (2017).

187.   Abbasov, M. E. *et al.* A proteome-wide atlas of lysine-reactive chemistry. *Nat. Chem.* **13**, 1081–1092 (2021).

188.   Tamura, T. *et al.* Rapid labelling and covalent inhibition of intracellular native proteins using ligand-directed N-acyl-N-alkyl sulfonamide. *Nat Commun* **9**, 1870 (2018).

189.   Garner, M. H., Bogardt, R. A. & Gurd, F. R. Determination of the pK values for the alpha-amino groups of human hemoglobin. *Journal of Biological Chemistry* **250**, 4398–4404 (1975).

190.   Blair, H. A. Voxelotor: First Approval. *Drugs* **80**, 209–215 (2020).

191.	Grimster, N. P. *et al.* Aromatic Sulfonyl Fluorides Covalently Kinetically Stabilize Transthyretin to Prevent Amyloidogenesis while Affording a Fluorescent Conjugate. *J. Am. Chem. Soc.* **135**, 5656–5668 (2013).

192.	Dalton, S. E. *et al.* Selectively Targeting the Kinome-Conserved Lysine of PI3Kδ as a General Approach to Covalent Kinase Inhibition. *J. Am. Chem. Soc.* **140**, 932–939 (2018).

193.	Anscombe, E. *et al.* Identification and Characterization of an Irreversible Inhibitor of CDK2. *Chemistry & Biology* **22**, 1159–1164 (2015).

194.	Cuesta, A., Wan, X., Burlingame, A. L. & Taunton, J. Ligand Conformational Bias Drives Enantioselective Modification of a Surface-Exposed Lysine on Hsp90. *J. Am. Chem. Soc.* **142**, 3392–3400 (2020).

195.	Zhao, Q. *et al.* Broad-Spectrum Kinase Profiling in Live Cells with Lysine-Targeted Sulfonyl Fluoride Probes. *J. Am. Chem. Soc.* **139**, 680–685 (2017).

196.	Hett, E. C. *et al.* Rational Targeting of Active-Site Tyrosine Residues Using Sulfonyl Fluoride Probes. *ACS Chem. Biol.* **10**, 1094–1098 (2015).

197.	Zanon, P. R. A. *et al.* Profiling the proteome-wide selectivity of diverse electrophiles. 10.

198.	Manford, A. G. *et al.* A Cellular Mechanism to Detect and Alleviate Reductive Stress. *Cell* **183**, 46-61.e21 (2020).

199.	Manford, A. G. *et al.* Structural basis and regulation of the reductive stress response. *Cell* **184**, 5375-5390.e16 (2021).

200.	Bellezza, I., Giambanco, I., Minelli, A. & Donato, R. Nrf2-Keap1 signaling in oxidative and reductive stress. *Biochimica et Biophysica Acta (BBA) - Molecular Cell Research* **1865**, 721–733 (2018).

201.	Dixon, S. J. & Stockwell, B. R. Identifying druggable disease-modifying gene products. *Current Opinion in Chemical Biology* **13**, 549–555 (2009).

202.	Nalawansha, D. A. & Crews, C. M. PROTACs: An Emerging Therapeutic Modality in Precision Medicine. *Cell Chemical Biology* **27**, 998–1014 (2020).

203.	Schapira, M., Calabrese, M. F., Bullock, A. N. & Crews, C. M. Targeted protein degradation: expanding the toolbox. *Nat Rev Drug Discov* **18**, 949–963 (2019).

204.	Banik, S. M. *et al.* Lysosome-targeting chimaeras for degradation of extracellular proteins. *Nature* **584**, 291–297 (2020).

205.	Takahashi, D. *et al.* AUTACs: Cargo-Specific Degraders Using Selective Autophagy. *Molecular Cell* **76**, 797-810.e10 (2019).

206.	Yamazoe, S. *et al.* Heterobifunctional Molecules Induce Dephosphorylation of Kinases–A Proof of Concept Study. *J. Med. Chem.* **63**, 2807–2813 (2020).

207.	Sabapathy, K. & Lane, D. P. Therapeutic targeting of p53: all mutants are equal, but some mutants are more equal than others. *Nat Rev Clin Oncol* **15**, 13–30 (2018).

208.   Li, B. & Dou, Q. P. Bax degradation by the ubiquitin/proteasome-dependent pathway: Involvement in tumor survival and progression. *Proceedings of the National Academy of Sciences* **97**, 3850–3855 (2000).

209.   Abbas, T. & Dutta, A. p21 in cancer: intricate networks and multiple activities. *Nat Rev Cancer* **9**, 400–414 (2009).

210.   Ward, C. L., Omura, S. & Kopito, R. R. Degradation of CFTR by the Ubiquitin-Proteasome Pathway. *Cell* **83**, 121–127 (1995).

211.   Wiener, R. *et al.* E2 ubiquitin-conjugating enzymes regulate the deubiquitinating activity of OTUB1. *Nat Struct Mol Biol* **20**, 1033–1039 (2013).

212.   Nakada, S. *et al.* Non-canonical inhibition of DNA damage-dependent ubiquitination by OTUB1. *Nature* **466**, 941–946 (2010).

213.   Que, L. T., Morrow, M. E. & Wolberger, C. Comparison of Cross-Regulation by Different OTUB1:E2 Complexes. *Biochemistry* **59**, 921–932 (2020).

214.   Wiener, R., Zhang, X., Wang, T. & Wolberger, C. The mechanism of OTUB1-mediated inhibition of ubiquitination. *Nature* **483**, 618–622 (2012).

215.   Dunker, A. K. *et al.* Intrinsically disordered protein. *Journal of Molecular Graphics and Modelling* **19**, 26–59 (2001).

216.   Riordan, J. R. CFTR Function and Prospects for Therapy. *Annu. Rev. Biochem.* **77**, 701–726 (2008).

217.   Tomati, V. *et al.* Genetic Inhibition Of The Ubiquitin Ligase Rnf5 Attenuates Phenotypes Associated To F508del Cystic Fibrosis Mutation. *Sci Rep* **5**, 12138 (2015).

218.   Sondo, E. *et al.* Pharmacological Inhibition of the Ubiquitin Ligase RNF5 Rescues F508del-CFTR in Cystic Fibrosis Airway Epithelia. *Cell Chemical Biology* **25**, 891-905.e8 (2018).

219.   Lopes-Pacheco, M. CFTR Modulators: The Changing Face of Cystic Fibrosis in the Era of Precision Medicine. *Front. Pharmacol.* **10**, 1662 (2020).

220.   Rath, A., Glibowicka, M., Nadeau, V. G., Chen, G. & Deber, C. M. Detergent binding explains anomalous SDS-PAGE migration of membrane proteins. *PNAS* **106**, 1760–1765 (2009).

221.   French, M. E., Koehler, C. F. & Hunter, T. Emerging functions of branched ubiquitin chains. *Cell Discov* **7**, 6 (2021).

222.   Yang, Y. *et al.* Nedd4 ubiquitylates VDAC2/3 to suppress erastin-induced ferroptosis in melanoma. *Nat Commun* **11**, 433 (2020).

223.   Ghelli Luserna di Rorà, A., Cerchione, C., Martinelli, G. & Simonetti, G. A WEE1 family business: regulation of mitosis, cancer progression, and therapeutic target. *J Hematol Oncol* **13**, 126 (2020).

224.   Smith, A., Simanski, S., Fallahi, M. & Ayad, N. G. Redundant Ubiquitin Ligase Activities Regulate Wee1 Degradation and Mitotic Entry. *Cell Cycle* **6**, 2795–2799 (2007).

225. Hashimoto, O. *et al.* Inhibition of proteasome-dependent degradation of Wee1 in G2-arrested Hep3B cells by TGFβ1. *Mol. Carcinog.* **36**, 171–182 (2003).

226. Li, Z. *et al.* Development and Characterization of a Wee1 Kinase Degrader. *Cell Chemical Biology* **27**, 57-65.e9 (2020).

227. Casement, R., Bond, A., Craigon, C. & Ciulli, A. Mechanistic and Structural Features of PROTAC Ternary Complexes. in *Targeted Protein Degradation: Methods and Protocols* (eds. Cacace, A. M., Hickey, C. M. & Békés, M.) 79–113 (Springer US, 2021). doi:10.1007/978-1-0716-1665-9_5.

228. Gavathiotis, E., Reyna, D. E., Bellairs, J. A., Leshchiner, E. S. & Walensky, L. D. Direct and selective small-molecule activation of proapoptotic BAX. *Nat Chem Biol* **8**, 639–645 (2012).

229. Pryde, D. C. *et al.* The discovery of potent small molecule activators of human STING. *European Journal of Medicinal Chemistry* **209**, 112869 (2021).

230. Zorn, J. A. & Wells, J. A. Turning enzymes ON with small molecules. *Nat Chem Biol* **6**, 179–188 (2010).

231. Ramanjulu, J. M. *et al.* Design of amidobenzimidazole STING receptor agonists with systemic activity. *Nature* **564**, 439–443 (2018).

232. Chen, L., Liu, S. & Tao, Y. Regulating tumor suppressor genes: post-translational modifications. *Sig Transduct Target Ther* **5**, 90 (2020).

233. Riboldi, G. M. & Di Fonzo, A. B. GBA, Gaucher Disease, and Parkinson's Disease: From Genetic to Clinic to New Therapeutic Approaches. *Cells* **8**, 364 (2019).

234. Sarodaya, N., Suresh, B., Kim, K.-S. & Ramakrishna, S. Protein Degradation and the Pathologic Basis of Phenylketonuria and Hereditary Tyrosinemia. *IJMS* **21**, 4996 (2020).

235. Bartha, I., di Iulio, J., Venter, J. C. & Telenti, A. Human gene essentiality. *Nat Rev Genet* **19**, 51–62 (2018).

236. Jin, Z. *et al.* Structure of Mpro from SARS-CoV-2 and discovery of its inhibitors. *Nature* **582**, 289–293 (2020).

237. von Delft, F. *et al.* A white-knuckle ride of open COVID drug discovery. *Nature* **594**, 330–332 (2021).

238. Zaidman, D. *et al.* An automatic pipeline for the design of irreversible derivatives identifies a potent SARS-CoV-2 Mpro inhibitor. *Cell Chemical Biology* **28**, 1795-1806.e5 (2021).

239. How Pfizer scientists transformed an old drug lead into a COVID-19 antiviral. *Chemical & Engineering News* https://cen.acs.org/pharmaceuticals/drug-discovery/How-Pfizer-scientists-transformed-an-old-drug-lead-into-a-COVID-19-antiviral/100/i3.

240. Ettari, R. *et al.* Development of Novel Peptidomimetics Containing a Vinyl Sulfone Moiety as Proteasome Inhibitors. *ChemMedChem* **6**, 1228–1237 (2011).

241.   Gadd, M. S. *et al.* Structural basis of PROTAC cooperative recognition for selective protein degradation. *Nat Chem Biol* **13**, 514–521 (2017).

242.   Jessani, N., Niessen, S., Mueller, B. M. & Cravatt, B. F. Breast Cancer Cell Lines Grown In Vivo: What Goes in Isn't Always the Same as What Comes Out. *Cell Cycle* **4**, 252–254 (2005).

APPENDICES

Appendix A – Supplementary Information for Chapter 2

A.1 Supplementary Table Legends
A.2 Supplementary Figures
A.3 Materials and Methods
A.4 Chemical Synthesis and Characterization

A.1 Supplementary Table Legends

Table S2.1. Cysteine-reactive covalent ligand screening against FEM1B.
Tab 1 shows the compound name, Enamine catalog number, molecular weight, and structures of the compounds screened. Tab 2 shows data from screening a cysteine-reactive covalent ligand library in a fluorescence polarization assay with TAMRA-conjugated FNIP1562-591 degron with recombinant MBP-tagged FEM1B. FEM1B was pre-incubated with DMSO vehicle or covalent ligand (50 µM) for 30 min prior to addition of the TAMRA-conjugated degron.

Table S2.2. IsoTOP-ABPP analysis of EN106 in HEK293T cells.
HEK293T cells were treated with DMSO vehicle or EN106 (10 µM) for 90 min. Cell lysates were subsequently labeled with IA-alkyne (200 µM) for 1 h and taken through the isoTOP-ABPP method. Data shown in Tab 1 are all probe-modified peptides detected. Data shown in Tab 2 are probe-modified peptides that were observed in at least 2 out of the 3 biological replicates.

Table S2.3. Pulldown proteomic studies with alkyne-functionalized EN106 probe NJH-2-030.
HEK293T cells were treated with DMSO vehicle or NJH-2-030 (10 µM) for 4 h. Cell lysates were subjected to CuAAC with biotin picolyl azide after which probe-modified proteins were avidin-enriched, eluted, and analyzed for TMT-based quantitative proteomic profiling. Data are from n=3 biological replicates/group.

Table S2.4. Proteomic profiling of NJH-1-106 treatment in HEK293T cells.
HEK293T cells were treated with DMSO vehicle or NJH-1-106 (10 µM) for 12 h. Protein level changes in cell lysate were quantitatively assessed by TMT-based proteomic profiling. The first tab shows all identified proteins across three biologically independent replicates/group. The second tab shows quantified proteins with at least 2 unique peptides.

A.2 Supplementary Figures
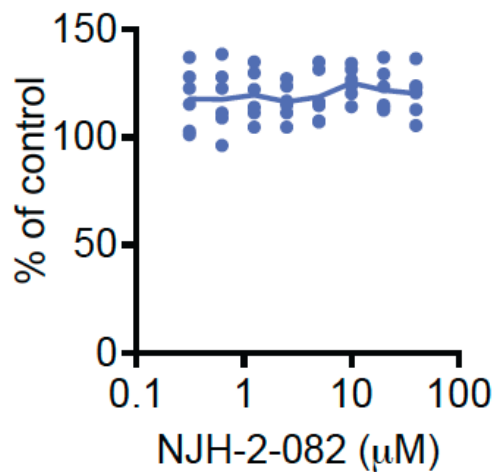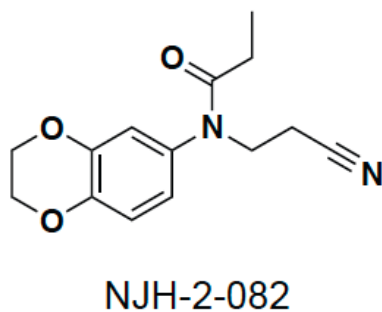
Figure S2.1. Non-reactive EN106 analog NJH-2-082 does not inhibit FEM1B/FNIP1 degron interactions.
Structure of non-reactive EN106 analog NJH-2-082 shown on the left. On the right is a dose-response of NJH-2-082 effects on FEM1B and TAMRA-conjugated FNIP1 interaction assessed by fluorescence polarization expressed as percent fluorescence polarization compared to DMSO vehicle-treated control. Data shown are average values with individual biological replicate data shown. Data are from n=6 biologically independent samples/group.
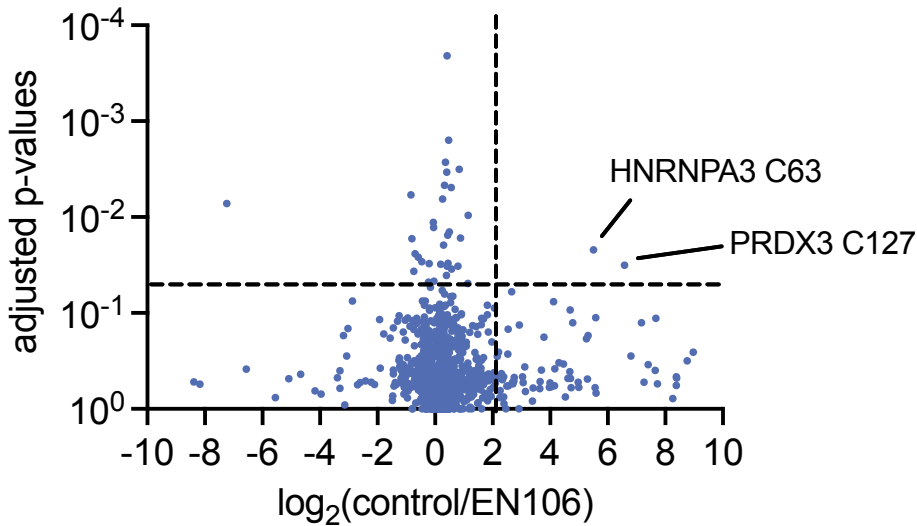
Figure S2.2. isoTOP-ABPP analysis of EN106 in HEK293T cells.
HEK293T cells were treated with DMSO vehicle or EN106 (10 µM) for 90 min. Cell lysates were subsequently labeled with IA-alkyne (200 µM) for 1 h and taken through the isoTOP-ABPP method. Shown in red are targets that showed ratios >2 for control/treated with false-discovery rate corrected p-values <0.05. Data shown are for individual probe-modified peptide quantified ratios that were present in at least 2 out of 3 biologically independent replicates/group.
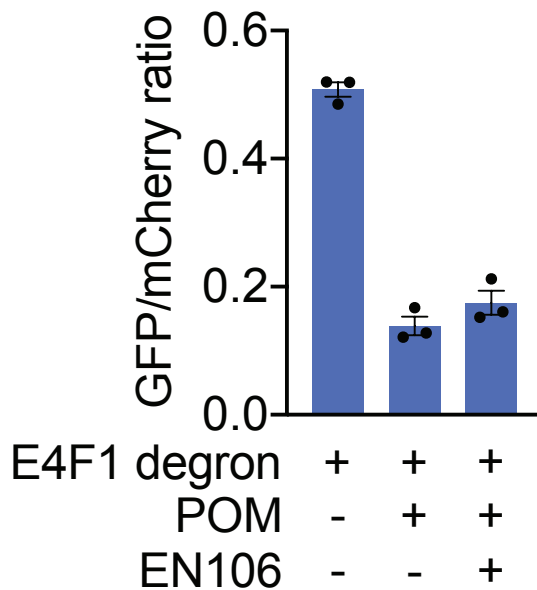
Figure S2.3. Exploration of potential CRBN dependence of EN106 effect.

Flow cytometry analysis of E4F1-GFP degron levels compared to mCherry levels with DMSO vehicle, pomalidomide (10µM, 4h), or pomalidomide (10µM, 4h) and EN106 (10µM, 12h) treatment in HEK293T cells.

JQ1
BRD4 inhibitor

EN106
FEM1B Recruiter
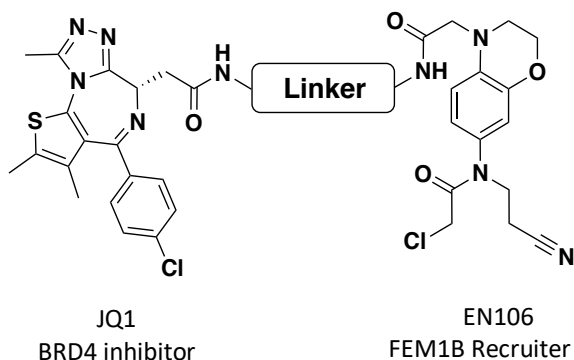
Compound	Linker	DC_{50} (µM)	D_{max} (%)
NJH-2-088		0.81	71
NJH-01-106		0.25	94
NJH-2-090		0.82	81
NJH-2-091		1.1	85
NJH-2-092		3.6	60
NJH-2-093		1.6	80

Figure S2.4. Structure activity relationships of FEM1B-based BRD4 degraders.
HEK293T cells were treated with DMSO vehicle or degraders for 8 h in dose-response experiments and BRD4 and loading control GAPDH levels were detected by Western blotting. Gels were quantified and the concentration for which we observed 50 % degradation of BRD4 (DC50) values and maximum percent degradation of BRD4 (Dmax) were calculated. Data are derived from n=3 biological replicates/group.
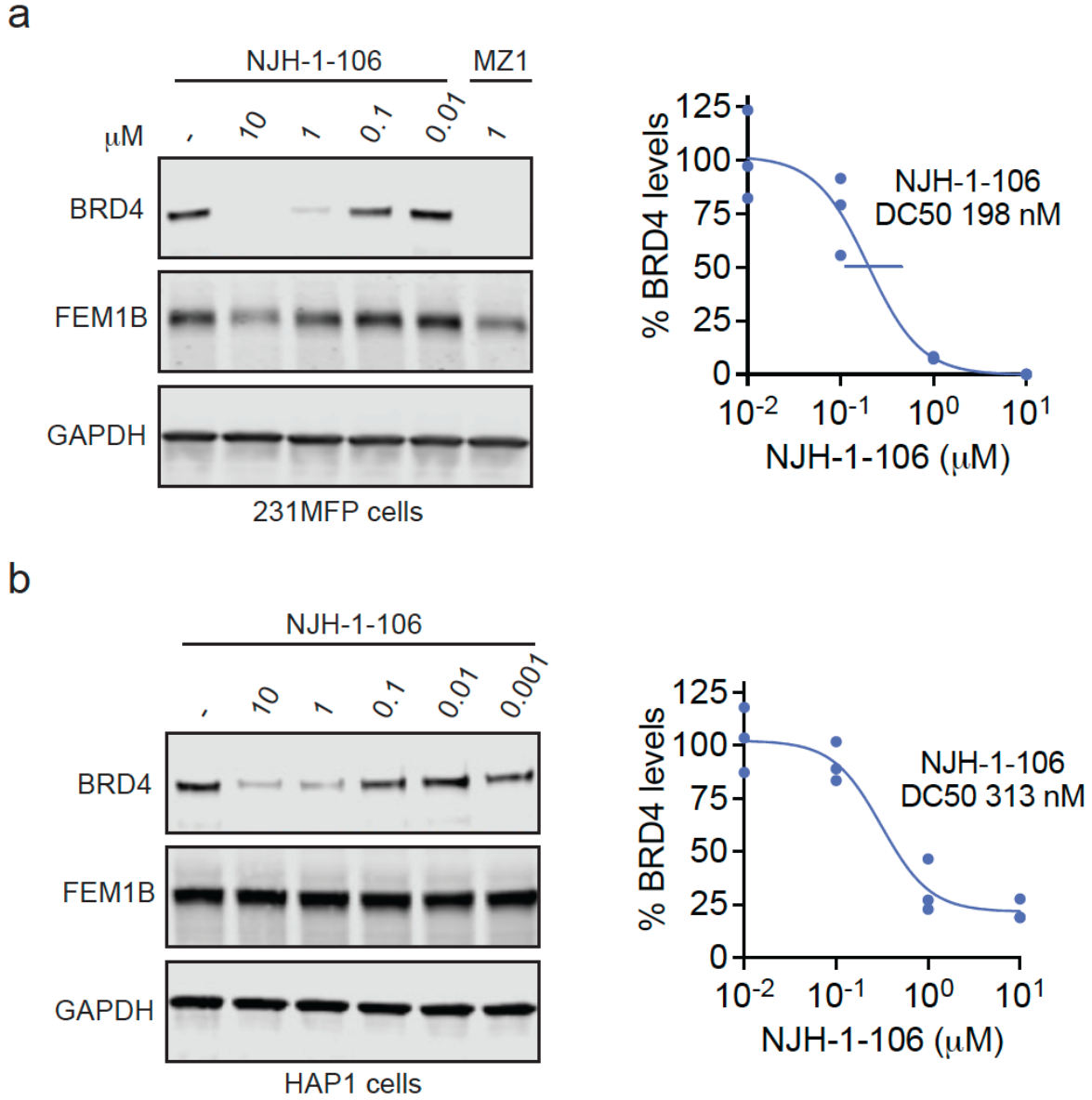
Figure S2.5. NJH-1-106 degradation of BRD4 in 231MFP breast cancer and HAP1 leukemia cell lines.

(a, b) 231MFP (a) and HAP1 (b) cells were treated with DMSO vehicle or NJH-1-106 for 8h and BRD4, FEM1B, and loading control GAPDH levels were detected by Western blotting. Gels shown are representative of n=3 biologically independent replicates/group. BRD4 levels were quantified by densitometry and normalized to GAPDH and average   sem and individual biological replicate data points are shown in the dose-response curves with DC50 values annotated.

a

NJH-2-105

b

c

| NJH-1-106 | - | + | - |
| NJH-2-105 | - | - | + |

BRD4

GAPDH

d
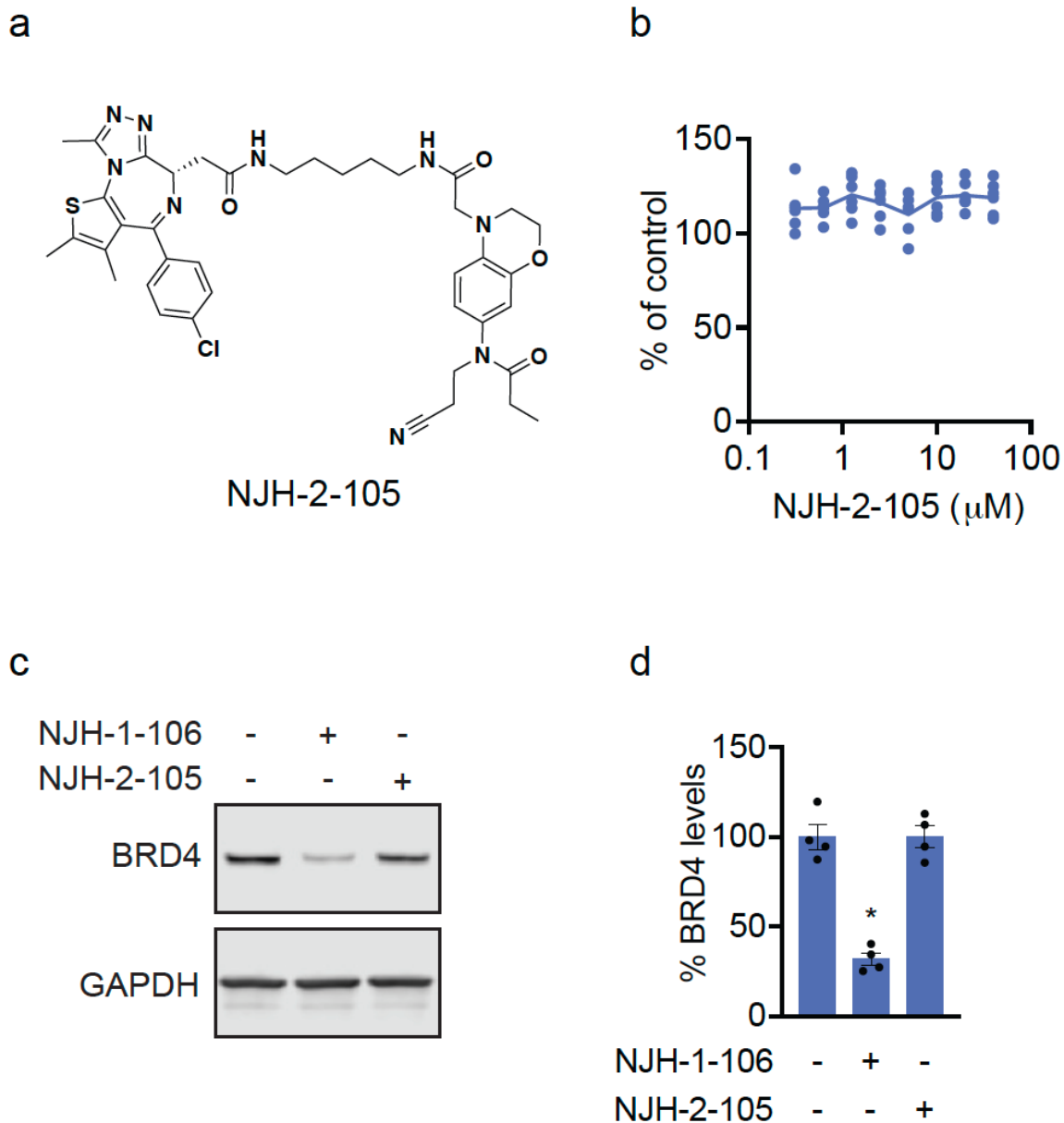
| NJH-1-106 | - | + | - |
| NJH-2-105 | - | - | + |

Figure S2.6. Negative control non-reactive PROTAC does not interfere with FEM1B/FNIP1 interations and does not degrade BRD4.
(a) Structure of NJH-2-105, a non-reactive version of active BRD4 degrader NJH-1-106. (b) Dose-response of NJH-2-105 effects on FEM1B and TAMRA-conjugated FNIP1 interaction assessed by fluorescence polarization expressed as percent fluorescence polarization compared to DMSO vehicle-treated control. (c) HEK293T cells were treated with DMSO vehicle, 10 μM NJH-1-106, or 10 μM NJH-2-105 and BRD4 and GAPDH levels were detected by western blotting. (d) Quantification of BRD4 abundance in (c) shown in bar graph as average ± sem with individual biological replicate points shown. Significance expressed as *p<0.05 compared to DMSO treatment.
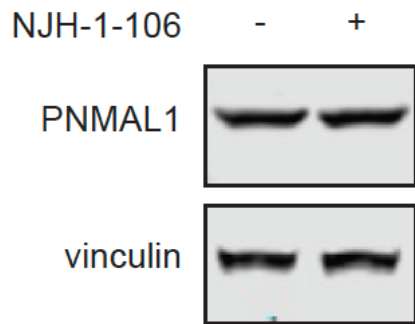
Figure S2.7. PNMAL1 levels with NJH-1-106 treatment in HEK293T cells.
HEK293T cells were treated with NJH-1-106 (10 µM) for 8 h. PNMAL1 and loading control vinculin levels were assessed by Western blotting. Shown is a representative gel of n=3 biological replicates/group.

a
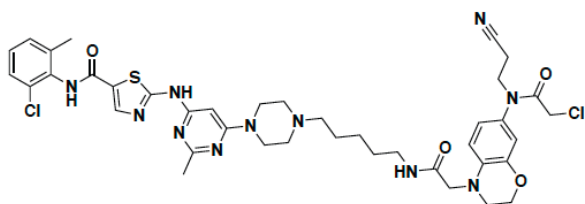
NJH-2-142
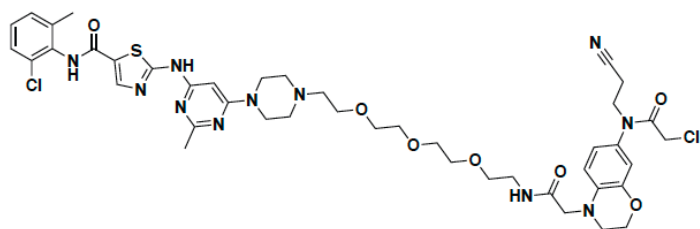
NJH-2-143

b

NJH-2-142	-	+	-	-	-	-
NJH-2-143	-	-	+	-	-	-
dasatinib	-	-	-	+	-	+
EN106	-	-	-	-	+	+

BCR-ABL

c-ABL

β-actin
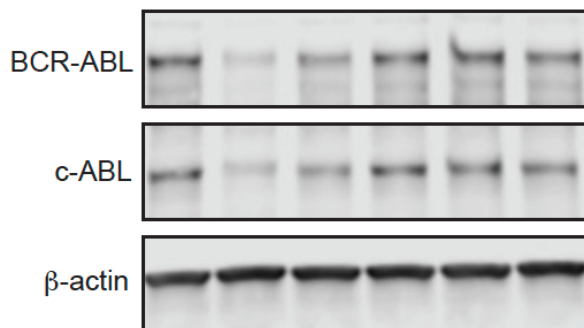
Figure S2.8. FEM1B-based BCR-ABL/c-ABL degraders.
(a) Structures of two FEM1B-based BCR-ABL/c-ABL degraders linking EN106 to dasatinib. (b) K562 cells were treated with DMSO vehicle, degraders (10 µM), dasatinib (10 µM), and/or EN106 (10 µM) for 24 h. Shown are representative gels from n=3 biological replicates/group.

A.3 Materials and Methods

Materials
Cysteine-reactive covalent ligand libraries were purchased from Enamine. Cysteine-reactive covalent ligand libraries are stored as 50 mM DMSO stock solutions and arrayed into single-use plates for screening. Compound integrity of our stock solutions have been confirmed through spot-checking, and degraded compounds have been replaced with repurchased material, Primary antibodies used were: BRD4 (Cell Signaling Technologies (CST) #13440), GAPDH (ProteinTech 60004-1-Ig), FEM1B (ProteinTech 19544-1-AP), beta-Actin (CST 8H10D10 #3700), c-Abl (CST #2862).

Fluorescence polarization assay
Fluorescence polarization assays were performed with purified mouse MBP-FEM1B 1, TAMRA-labeled FNIP1 peptide (5,6-TAMRA-RNKSSLLFKESEETRTPNCNCKYCSHPVLG, Koch Institute/MIT Biopolymers lab). For the screen, 0.5 µL of 2.5 mM compounds were spotted into 384 well non-binding plates (Greiner, 781900). 12.5 µL of 250 nM MBP-FEM1B in binding buffer (40 mM HEPES 7.5, 150 mM NaCl, 0.2 % NP40 substitute, and 100 µM TCEP (Tris(2-carboxyethyl)phosphine hydrochloride)) was added to each well and incubated for 1 hour at room temperature. After the incubation, 12.5 µL of 100 nM FNIP1 peptide diluted in binding buffer was added bringing the final concentration to 50 nM for the peptide and 125 nM for MBP-FEM1B. After 1 hour of incubation plates were measured on a Perkin Elmer 2104 Envision plate reader. Data was calculated from mP values $(1000*(S-G*P)/(S+G*P)$, S = 595s channel 2 and P = 595p channel 1, G=1.1) subtracted from peptide only plate. Dose response assays were performed as above, but with 250 nM MBP-FEM1B treated with indicated concentrations of compound (relative to the final reaction volume) or DMSO in separate tubes for 1 hour at room temperature. 12.5 µl of treated MBP-FEM1B (125 nM final) was then added to 12.5 µl of peptide (10 nM final) and incubated with gentle rocking for 30 minutes before measuring fluorescence polarization.

Gel-Based ABPP
Recombinant MBP-FEM1B1-377 (0.1µg/sample) was pre-treated with either DMSO vehicle or EN106 or at 37℃ for 30 min in 25 µL of PBS, and subsequently treated with of IA-Rhodamine (concentrations designated in figure legends) (Setareh Biotech) at room temperature for 1 h. The reaction was stopped by addition of 4×reducing Laemmli SDS sample loading buffer (Alfa Aesar). After boiling at 95℃ for 5 min, the samples were separated on precast 4−20% Criterion TGX gels (Bio-Rad). Probe-labeled proteins were analyzed by in-gel fluorescence using a ChemiDoc MP (Bio-Rad).

Cell Culture
HEK293T, K562, and HAP1 cells were obtained from the UC Berkeley Cell Culture Facility and cultured in DMEM (Gibco) containing 10% (v/v) fetal bovine serum (FBS) and maintained at 37 °C with 5% CO2. 231MFP cells were obtained from Benjamin

Cravatt and were generated from explanted tumor xenografts of MDA-MB-231 cells as previously described.[242] The FEM1B knockout HEK293T cell line was generated as described by Manford et al.[198]

Oxygen consumption measurements

HEK293T cells were plated into two black 96 well clear bottom plates at 100,000 cells per well in 200 µl of DMEM 10% Fetal Bovine Serum. 8 hours after plating cells were treated as indicated for *16* hours. After the 16 hours, the media was changed 3 x with fresh media leaving a final volume 90 µl. The cells were equilibrated back to 37°C for 15min, after which 10 µl of prewarmed MitoXpress Xtra reagent (MX-200-4, Agilent) was added to each well. Prewarmed mineral oil was quickly layered on top of all analysis wells and the plate was measured over time using Perkin Elmer 2104 Envision plate reader at 37°C using time-resolved fluorescence measurement. 5-6 wells for each condition were analyzed (occasional wells with negative slopes were omitted) and the average rate (RFU/hour) was normalized to the cell count of three wells from the second 96 well plate.

NJH-2-030 Pulldown and Blotting for FEM1B or for TMT-based Quantitative Proteomics

HEK293T cells were treated with DMSO or 10 µM NJH-2-030 in situ for 8h. Cells were harvested, lysed via sonication and normalized to 2.0 mg/mL. Following normalization, 100 µL of each lysate sample was removed for Western blot analysis of input, and 500 µL of each lysate sample was incubated for 1 h at room temperature with 10 µL of 5 mM biotin picolyl azide (in water) (Sigma Aldrich 900912), 10 µL of 50 mM TCEP (in water), 30 µL of TBTA ligand (0.9 mg/mL in DMSO:t-butanol = 1:4), and 10 µL of 50 mM Copper (II) Sulfate (12.5 mg/mL in water). Proteins were precipitated, washed 3 x 1 mL with cold MeOH, resolubilized in 1 mL of 1.2% SDS/PBS (w/v), heated for 5 min at 90 °C, and centrifuged to remove any insoluble components. 1 mL of each resolubilized sample was then transferred to 15 mL conical tubes containing 5 mL PBS with 85 µL streptavidin resin (Thermo Scientific 53114) to give a final SDS concentration of 0.2%. Samples were incubated with the streptavidin beads at 4 °C overnight on a rotator. The following day the samples were warmed to room temperature and washed with 0.2% SDS, then transferred to spin columns and further washed 3 x with 500 µL PBS and 3 x with 500 µL water to remove non-probe-labeled proteins. The washed beads were resuspended in 100 µL PBS, transferred to 1.5 mL eppendorf low-adhesion tubes, combined with 30 µL Laemmli Sample Buffer (4 x) and heated to 95 °C for Western blotting detection or were processed for TMT-based quantitative proteomic profiling using methods described later.

Flow Cytometry Analysis of GFP-FNIP1 degron/mCherry

HEK293T cells/well were seeded into 6 well plates. The next day the cells were transfected with 0.1 µg of pCS2-GFP-FNIP1562-591-IRES-mCherry or 0.1 µg of pCS2-E4F123432-GFP-IRES-mCherry, with 0.075 µg pCS2-3xFLAG-FEM1B as indicated. Empty pCS2 was added to 2 µg total DNA for each transfection in 300 µl Opti-MEM (Thermo Fisher, 31985-070) with 12 µg polyethyleneimine (PEI, Polysciences 23966-1).

Each well was transfected with 65 μl of the transfection mix. 12 hours post-transfection, indicated concentrations of EN106 or DMSO was added. After 12 hours of EN106 treatment, cells were trypsinized, spun down, resuspended in DMEM + 10% FBS and analyzed on Fortessa X20. Data was processed using FlowJo and all quantifications are the median GFP/mCherry ratios. For the pomalidomide treated cells, 10 μM pomalidomide (MedChemExpress, HY-10984) was added for 4 hours before analyzing.

Cell Lysis Protocol
Pelleted cells were lysed with RIPA lysis buffer (50mM Tris-HCl, 165mM NaCl, 12mM sodium deoxycholate, 1% Triton X-100, 0.01% SDS), protein concentration normalized using a BCA assay (Thermo).

Western Blot Protocol
Proteins were resolved by SDS–PAGE (4–20% TGX gels, Bio-Rad Laboratories, Inc.) and transferred to nitrocellulose membranes using the Trans-Blot Turbo transfer system (Bio-Rad). Membranes were blocked with 5% BSA in Tris-buffered saline containing Tween 20 (TBST) solution for 1 h at room temperature, washed in TBST and probed with primary antibody diluted in diluent, as recommended by the various manufacturers, overnight at 4 °C. Primary antibodies used were: BRD4 (Cell Signaling Technologies #13440), GAPDH (ProteinTech 60004-1-Ig), FEM1B (ProteinTech 19544-1-AP). Following washes with TBST, the blots were incubated in the dark with secondary antibodies purchased from Li-Cor Biosciences and used at 1:10,000 dilution in 5% BSA in TBST at room temperature for 1 h. Blots were visualized using an Odyssey Li-Cor scanner after additional washes. Protein intensity was quantified using ImageJ software.

IsoTOP-ABPP Chemoproteomic Experiments
Cells were lysed by probe sonication in PBS and protein concentrations were measured by BCA assay. Cells were treated for 4 h with either DMSO vehicle or EN106 (from 1,000x DMSO stock) before cell collection and lysis. Proteomes were subsequently labeled with IA-alkyne labeling (100 μM) for 1 h at room temperature. CuAAC was used by sequential addition of tris(2-carboxyethyl)phosphine (1 mM, Strem, 15-7400), tris[(1-benzyl-1H-1,2,3-triazol-4-yl)methyl]amine (34 μM, Sigma, 678937), copper(II) sulfate (1 mM, Sigma, 451657) and biotin-linker-azide—the linker functionalized with a tobacco etch virus (TEV) protease recognition sequence as well as an isotopically light or heavy valine for treatment of control or treated proteome, respectively. After CuAAC, proteomes were precipitated by centrifugation at 6,500g, washed in ice-cold methanol, combined in a 1:1 control:treated ratio, washed again, then denatured and resolubilized by heating in 1.2% SDS–PBS to 80 °C for 5 min. Insoluble components were precipitated by centrifugation at 6,500g and soluble proteome was diluted in 5 ml 0.2% SDS–PBS. Labeled proteins were bound to streptavidin-agarose beads (170 μl resuspended beads per sample, Thermo Fisher, 20349) while rotating overnight at 4 °C. Bead-linked proteins were enriched by washing three times each in PBS and water, then resuspended in 6 M urea/PBS, and reduced in TCEP (1 mM, Strem, 15-7400), alkylated with iodoacetamide (18 mM, Sigma), before being washed and resuspended in 2 M urea/PBS and trypsinized overnight with 0.5 μg /μL sequencing grade trypsin (Promega, V5111). Tryptic peptides were eluted off. Beads were washed three times

each in PBS and water, washed in TEV buffer solution (water, TEV buffer, 100 µM dithiothreitol) and resuspended in buffer with Ac-TEV protease (Invitrogen, 12575-015) and incubated overnight. Peptides were diluted in water and acidified with formic acid (1.2 M, Fisher, A117-50) and prepared for analysis.

IsoTOP-ABPP Mass Spectrometry Analysis

Peptides from all chemoproteomic experiments were pressure-loaded onto a 250 µm inner diameter fused silica capillary tubing packed with 4 cm of Aqua C18 reverse-phase resin (Phenomenex, 04A-4299), which was previously equilibrated on an Agilent 600 series high-performance liquid chromatograph using the gradient from 100% buffer A to 100% buffer B over 10 min, followed by a 5 min wash with 100% buffer B and a 5 min wash with 100% buffer A. The samples were then attached using a MicroTee PEEK 360 µm fitting (Thermo Fisher Scientific p-888) to a 13 cm laser pulled column packed with 10 cm Aqua C18 reverse-phase resin and 3 cm of strong-cation exchange resin for isoTOP-ABPP studies. Samples were analyzed using an Q Exactive Plus mass spectrometer (Thermo Fisher Scientific) using a five-step Multidimensional Protein Identification Technology (MudPIT) program, using 0, 25, 50, 80 and 100% salt bumps of 500 mM aqueous ammonium acetate and using a gradient of 5–55% buffer B in buffer A (buffer A: 95:5 water:acetonitrile, 0.1% formic acid; buffer B 80:20 acetonitrile:water, 0.1% formic acid). Data were collected in data-dependent acquisition mode with dynamic exclusion enabled (60 s). One full mass spectrometry (MS1) scan (400–1,800 mass-to-charge ratio (m/z)) was followed by 15 MS2 scans of the nth most abundant ions. Heated capillary temperature was set to 200 °C and the nanospray voltage was set to 2.75 kV.

Data were extracted in the form of MS1 and MS2 files using Raw Extractor v.1.9.9.2 (Scripps Research Institute) and searched against the Uniprot human database using ProLuCID search methodology in IP2 v.3 (Integrated Proteomics Applications, Inc.)6. Cysteine residues were searched with a static modification for carboxyaminomethylation (+57.02146) and up to two differential modifications for methionine oxidation and either the light or heavy TEV tags (+464.28596 or +470.29977, respectively). Peptides were required to be fully tryptic peptides and to contain the TEV modification. ProLUCID data were filtered through DTASelect to achieve a peptide false-positive rate below 5%. Only those probe-modified peptides that were evident across two out of three biological replicates were interpreted for their isotopic light to heavy ratios. For those probe-modified peptides that showed ratios greater than two, we only interpreted those targets that were present across all three biological replicates, were statistically significant and showed good quality MS1 peak shapes across all biological replicates. Light versus heavy isotopic probe-modified peptide ratios are calculated by taking the mean of the ratios of each replicate paired light versus heavy precursor abundance for all peptide-spectral matches associated with a peptide. The paired abundances were also used to calculate a paired sample t-test P value in an effort to estimate constancy in paired abundances and significance in change between treatment and control. P values were corrected using the Benjamini–Hochberg method.

Quantitative TMT Proteomics Analysis

Quantitative TMT-based proteomic analysis was performed as previously described 4. Acquired MS data was processed using Proteome Discoverer v. 2.2.0.388 software (Thermo) utilizing Mascot v 2.5.1 search engine (Matrix Science, London, UK) together with Percolator validation node for peptide-spectral match filtering 7. Data was searched against Uniprot protein database (canonical human and mouse sequences, EBI, Cambridge, UK) supplemented with sequences of common contaminants. Peptide search tolerances were set to 10 ppm for precursors, and 0.8 Da for fragments. Trypsin cleavage specificity (cleavage at K, R except if followed by P) allowed for up to 2 missed cleavages. Carbamidomethylation of cysteine was set as a fixed modification, methionine oxidation, and TMT-modification of N-termini and lysine residues were set as variable modifications. Data validation of peptide and protein identifications was done at the level of the complete dataset consisting of combined Mascot search results for all individual samples per experiment via the Percolator validation node in Proteome Discoverer. Reporter ion ratio calculations were performed using summed abundances with most confident centroid selected from 20 ppm window. Only peptide-to-spectrum matches that are unique assignments to a given identified protein within the total dataset are considered for protein quantitation. High confidence protein identifications were reported using a Percolator estimated <1% false discovery rate (FDR) cut-off. Differential abundance significance was estimated using a background-based ANOVA with Benjamini-Hochberg correction to determine adjusted p-values.

A.4 Chemical Synthesis and Characterization

Starting materials, reagents and solvents were purchased from commercial suppliers and were used without further purification unless otherwise noted. All reactions were monitored by TLC (TLC Silica gel 60 F_{254}, Sepulco Millipore Sigma). Reaction products were purified by flash column chromatography using a Biotage Isolera with Biotage Sfar® or Silicycle normal-phase silica flash columns (5 g, 10 g, 25 g, or 40 g). 1H NMR and 13C NMR spectra were recorded on a 400 MHz Bruker Avance I spectrometer or a 600 MHz Bruker Avance III spectrometer equipped with a 5 mm 1H/BB Prodigy cryo-probe. Chemical shifts are reported in parts per million (ppm, δ) downfield from tetramethylsilane (TMS). Coupling constants (J) are reported in Hz. Spin multiplicities are described as br (broad), s (singlet), d (doublet), t (triplet), q (quartet) and m (multiplet).

General Procedure A: A carboxylic acid (e.g. JQ1-COOH) was dissolved in DMF (0.2 M) followed by mono-Boc diamine linker (1.2 Eq) and DIEA (5.0 Eq.). HATU (2.0 Eq) was added and the reaction mixture was stirred for 1h. The reaction was diluted with water and extracted with EtOAc three times. Combined organic extracts were washed with brine and dried over sodium sulfate, then concentrated and purified by silica gel chromatography (0-6% MeOH/DCM) to provide the Boc-protected compounds. This intermediate was dissolved in DCM and TFA was added (1:1 DCM:TFA), and the solution was stirred for 2 hours at rt. The volatiles were evaporated, and DCM was added and re-evaporated three times, to provide the amine as a TFA salt without further purification.

General Procedure B: A Methyl ester (**6** or **8**) (2.0 Eq, 15 mg, 0.043 mmol) was dissolved in in MeOH (600 μL) and treated with aqueous LiOH (400 μL, 0.5M, 0.2 mmol) at rt for 1h. The mixture diluted with DCM (5 mL) and acidified with aqueous HCl (400 μL, 1M) and the mixture extracted with DCM. Combined organic extracts were dried over Na_2SO_4, concentrated, and the crude residue dissolved in DMF (0.5 mL). An amine, compounds **7a-f** (1.0 Eq., 0.026 mmol), was added followed by DIEA (5.0 Eq, 0.13 mmol) and HATU (2.0 Eq., 0.052 mmol). The reaction was stirred at rt for no more than 5 minutes, before water was added and the mixture was extracted with EtOAc three times. The short reaction time was critical to avoid forming an adduct due to 3H-[1,2,3]triazolo[4,5-b]pyridin-3-ol displacing the chloroacetamide chloride. Combined organic extracts were washed with brine, dried over sodium sulfate, concentrated, and purified by silica gel chromatography to provide the bifunctional molecule.

General Procedure C: Amine (1.0) and alkyl bromide (1.2 Eq.) were dissolved in DMF (~0.1 M amine) and TEA (3.0 Eq) was added. The solutions were stirred at rt for two days. Water was added, and the mixture extracted three times with 4:1 $CHCl_3$:IPA. Organic extracts were combined, washed with brine, dried over sodium sulfate, and concentrated. The crude residue was purified by silica get chromatoraphy (0-8% MeOH/DCM) to provide the Boc-protected intermediate. This was dissolved in DCM (~1 M) and an equal volume of TFA was added, then the solution was stirred for 2 hours at

rt. The volatiles were evaporated, and DCM was added and re-evaporated three times, to provide the dasatinib-linked amine as a TFA salt without further purification.

1
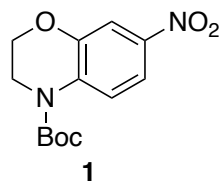
tert-butyl 7-nitro-2,3-dihydro-4H-benzo[b][1,4]oxazine-4-carboxylate (1): 7-nitro-3,4-dihydro-2H-benzo[b][1,4]oxazine (1.0 g, 5.55 mmol) was dissolved in THF (20 mL) and DMAP (67 mg, 0.55 mmol) was added at 0 ºC followed by Boc$_2$O (1.45 g, 6.66 mmol). The ice bath was removed after 5 minutes and the mixture stirred overnight at room temperature. The reaction was basified with 15 mL 1M NaOH, stirred for 2 hours, concentrated, and the aqueous mixture extracted with EtOAc. Organic extracts were combined and washed with 1M HCl, brine, dried over Na$_2$SO$_4$, and concentrated to provide **1** as an orange solid (1.46 g, 5.21 mmol, 94%). **LC/MS** [M+H]$^+$ *m/z* calc. 281.11, found 281.1. **1H NMR** (300 MHz, CDCl3) δ 8.11 (d, J = 9.1 Hz, 1H), 7.81 (s, 2H), 4.35 (s, 2H), 3.96 (s, 2H), 1.61 (s, 9H).


2
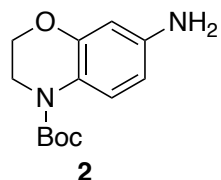
tert-butyl 7-amino-2,3-dihydro-4H-benzo[b][1,4]oxazine-4-carboxylate (**2**): Nitrobenzoxazine **1** (1.46g, 5.21mmol) was dissolved in EtOH (20 mL) and water (5 mL) before NH$_4$Cl (1.78 g, 33.3 mmol) was added. The mixture was heated to 60 ºC, Fe powder (932 mg, 16.7 mmol) was added, and the mixture heated at 80 ºC for 13 hours. The reaction was filtered through Celite, and celite washed with EtOAc. Water was added to the filtrate and the mixture extracted with EtOAc. Combined organic extracts were washed with brine, dried over Na$_2$SO$_4$, and concentrated to provide the aniline **2** as an orange oil (1.21 g, 4.82 mmol, 93%). **LC/MS** [M+H]$^+$ *m/z* calc. 251.1, found 251.1. **1H NMR** (300 MHz, CDCl3) δ 7.54 (s, 1H), 6.33 – 6.21 (m, 2H), 4.24 (s, 2H), 3.85 (s, 2H), 3.58 (s, 2H), 1.56 (s, 9H).


3
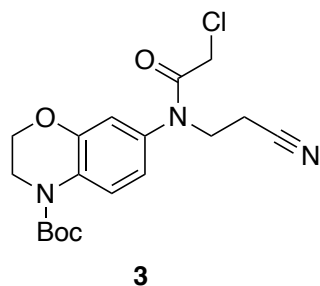
tert-butyl 7-(2-chloro-N-(2-cyanoethyl)acetamido)-2,3-dihydro-4H-benzo[b][1,4]oxazine-4-carboxylate (**3**): Aniline **2** (1.41 g, 5.66 mmol) was dissolved in acrylonitrile (20 mL). Alumina (1.13 g, 11.1 mmol) was added and the mixture refluxed for 48 hours, before being diluted with EtOAc and filtered through Celite to remove alumina. The filtrate was concentrated to provide the alkylated aniline intermediate (1.82 g) as an orange oil, which was as a mixture of double and single alkylation. LCMS [M+H]$^+$ calc 304.2, found 304.2. One sixth of this crude intermediate, (304 mg, ~1.0 mmol) was dissolved in DCM (6 mL), the solution cooled to 0 ºC, and TEA (556 µL, 4 mmol) was added followed by chloroacetyl chloride (202 µL, 2.5 mmol). The solution was stirred at 0 ºC for 5 minutes and allowed to warm to rt over 1 hour. Aqueous NaHCO$_3$ was added, the mixture partitioned, the aqueous layer extracted with DCM. Combined organic extracts were dried over Na$_2$SO$_4$, concentrated and purified by silica gel chromatography to obtain chloroacetamide **3** (244 mg, 0.64 mmol, 68% over two steps) as an orange solid. **LC/MS** [M+H]$^+$ *m/z* calc. 380.1, found 308.1. **1H NMR** (400 MHz, CDCl3) δ 8.01 (s, 1H), 6.87 – 6.79 (m, 2H), 4.35 – 4.28 (m, 2H), 4.06 – 3.89 (m, 6H), 2.75 (t, J = 6.8 Hz, 2H), 1.60 (s, 9H).
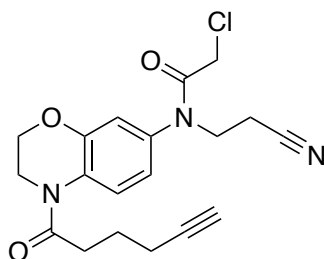
NJH-2-030

2-chloro-N-(2-cyanoethyl)-N-(4-(hex-5-ynoyl)-3,4-dihydro-2H-benzo[b][1,4]oxazin-7-yl)acetamide (**NJH-2-030**): Oxalyl chloride (150 µL of 2.0 M solution in DCM, 0.3 mmol) was added to solution of 5-hexynoic acid (17 µL, 0.15 mmol) and 1 drop of DMF in 1 mL in DCM at room temperature. The solution was stirred for 30 minutes before being concentrated to give crude hex-5-ynoyl chloride as a pink foam. Meanwhile, benzoxazine **3** (20 mg, 0.052 mmol) was dissolved in DCM (400 µL) and TFA (400 µL) was added. The solution turned light purple and after stirring 5 min at rt the mixture was concentrated under vacuum, and the resulting aniline was redissolved in DCM (0.5 mL). At 0C, TEA (109 µL, 0.78 mmol) was added to the solution followed by the crude hex-5-ynoyl chloride dissolved in DCM (1 mL). The reaction was stirred for 5 minutes at 0 ºC, water was added, the mixture partitioned and the aqueous layer extracted with DCM. Combined organic extracts were dried over Na$_2$SO$_4$, concentrated, and purified by silica gel chromatography to obtain **NJH-2-030** (17 mg, 0.047 mmol, 91%). **HRMS** [M+H]$^+$ *m/z* calc. 374.1193, found 374.1247. **1H NMR** (400 MHz, DMSO) δ 7.94 (s, 1H), 7.03 (d, J = 2.5 Hz, 1H), 6.93 (d, J = 8.7 Hz, 1H), 4.30 (t, J = 4.5 Hz, 2H), 4.07 (s, 2H), 3.94 – 3.82 (m, 4H), 2.80 (s, 1H), 2.75 – 2.64 (m, 4H), 2.27 – 2.19 (m, 2H), 1.76 (p, J = 7.2 Hz, 2H). **13C NMR** (151 MHz, CDCl3) δ 170.93, 166.76, 147.68, 127.10, 125.66, 119.46, 117.48, 116.71, 83.31, 69.48, 60.39, 46.18, 41.62, 32.78, 23.77, 21.05, 17.76, 16.38, 14.20.
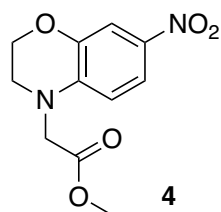
methyl 2-(7-nitro-2,3-dihydro-4H-benzo[b][1,4]oxazin-4-yl)acetate (**4**): 7-nitro-3,4-dihydro-2H-benzo[b][1,4]oxazine (1.0 g, 5.55 mmol) was dissolved in DMF (20 mL) and cooled to 0 ºC. NaH (233 mg, 5.83 mmol, 60% in mineral oil) was then added to the solution portionwise, and allowed to stir at 0 ºC for 30 minutes before methyl bromoacetate (650 µL, 4.43 mmol) was added dropwise. The solution was then allowed to warm to room temperature and stirred for 2 hours, before it was again cooled to 0 ºC and diluted with water (80 mL). The resulting suspension was filtered to obtain **4** (1.32 g, 5.23 mmol, 94%) as a bright yellow powder. **LC/MS** [M+H]$^+$ *m/z* calc 253.07, found 253.2. **1H NMR** (300 MHz, CDCl3) δ 7.83 (d, J = 9.2 Hz, 1H), 7.75 (s, 1H), 6.50 (d, J = 8.8 Hz, 1H), 4.34 (s, 2H), 4.17 (d, J = 1.9 Hz, 2H), 3.81 (s, 3H), 3.62 (s, 2H).
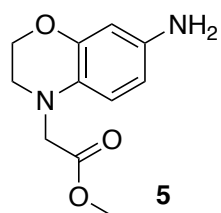
methyl 2-(7-amino-2,3-dihydro-4H-benzo[b][1,4]oxazin-4-yl)acetate (**5**): Nitrobenzoxazine **4** (1.32 g, 5.23 mmol) was dissolved in EtOH (30 mL) and water (8 mL) before NH$_4$Cl (1.68 g, 31.4 mmol) was added. The mixture was heated to 60 ºC, Fe powder (876 mg, 15.7 mmol) was added, and the mixture heated at 80 ºC for 17 hours. The reaction mixture was filtered through Celite, and the celite pad washed with EtOAc. Water was added to the filtrate and the mixture extracted with EtOAc. Combined organic extracts were washed with brine, dried over Na$_2$SO$_4$, and concentrated to provide **5** (270 mg, 1.0 mmol, 102%) as a brown oil without further purification. **LC/MS** [M+H]$^+$ *m/z* calc 223.1, found 223.1. **1H NMR** (300 MHz, DMSO) δ 6.30 (d, J = 8.3 Hz, 1H), 6.09 – 6.03 (m, 2H), 4.49 (d, J = 15.6 Hz, 2H), 4.15 (s, 2H), 4.05 (d, J = 10.8 Hz, 2H), 3.63 (d, J = 2.0 Hz, 3H), 3.37 (s, 2H).
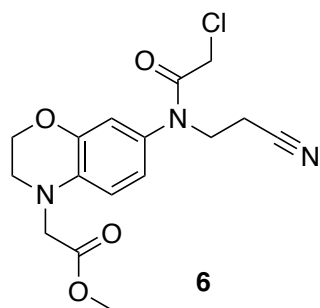
methyl 2-(7-(2-chloro-N-(2-cyanoethyl)acetamido)-2,3-dihydro-4H-benzo[b][1,4]oxazin-4-yl)acetate (**6**): Aniline **5** (974 mg, 4.20 mmol) was dissolved in acrylonitrile (15 mL) and basic alumina (857 mg, 8.40 mmol) was added and the mixture stirred at 80 ºC for 36 hours. The reaction mixture was then diluted with EtOAc and filtered through Celite. Water was added to the filtrate, the mixture partitioned, and the aqueous layer extracted with EtOAc. Combined organic extracts were washed with brine, dried over Na$_2$SO$_4$, concentrated, and the crude residue purified by silica gel chromatography to obtain a mixture of double and single alkylated aniline (886 mg) as an amber oil. LC/MS [M+H]$^+$ *m/z* calc 276.13, found 276.1. One fourth of this intermediate (215 mg, ~0.78 mmol) was dissolved in DCM (4 mL). The solution was cooled to 0C and TEA (326 µL, 2.34 mmol) was added, followed by chloroacetyl chloride (92 µL, 1.17 mmol). After 15 minutes at 0 ºC, the reaction mixture was concentrated and the crude residue purified by silica gel chromatography to obtain chloroacetamide **6** (229 mg, 0.65 mmol, 62% over two steps) as amber oil. **LCMS** [M+H]$^+$ *m/z* calc 352.1, found 352.1. **1H NMR** (400 MHz, DMSO) δ 6.82 – 6.72 (m, 2H), 6.62 (dd, J = 8.5, 2.1 Hz, 1H), 4.29 – 4.18 (m, 4H), 4.08 – 3.98 (m, 3H), 3.80 (t, J = 6.7 Hz, 2H), 3.66 (d, J = 2.2 Hz, 3H), 3.44 (s, 2H), 2.68 (t, J = 6.7 Hz, 2H).

7a
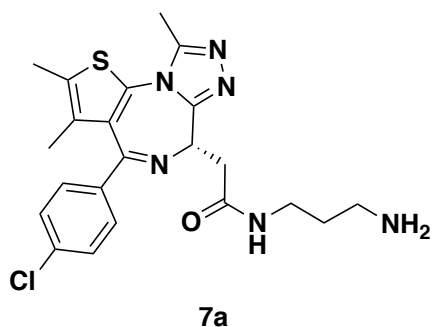
(S)-N-(3-aminopropyl)-2-(4-(4-chlorophenyl)-2,3,9-trimethyl-6H-thieno[3,2-f][1,2,4]triazolo[4,3-a][1,4]diazepin-6-yl)acetamide (7a): (S)-2-(4-(4-chlorophenyl)-2,3,9-trimethyl-6H-thieno[3,2-f][1,2,4]triazolo[4,3-a][1,4]diazepin-6-yl)acetic acid was coupled to tert-butyl (3-aminopropyl)carbamate following General Procedure A to provide **7a** (55mg, 0.123 mmol, 82%) as a tan solid. **LC/MS** [M+H]$^+$ *m/z* calc. 457.2, found 457.1. **1H NMR** (400 MHz, DMSO) δ 8.20 (t, J = 5.7 Hz, 1H), 7.50 (d, J = 8.6 Hz, 2H), 7.42 (d, J = 8.7 Hz, 2H), 4.50 (dd, J = 8.1, 6.0 Hz, 1H), 3.30 – 3.08 (m, 6H), 2.64 – 2.55 (m, 5H), 2.41 (s, 3H), 1.62 (s, 3H), 1.52 (q, J = 6.9 Hz, 2H).
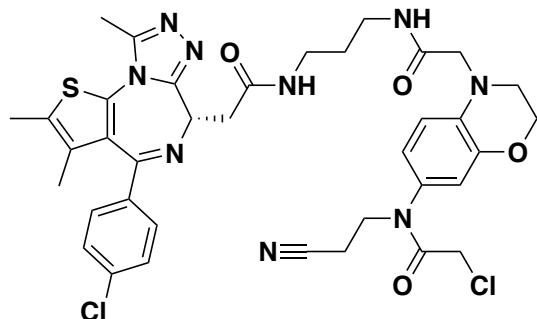
NJH-2-088

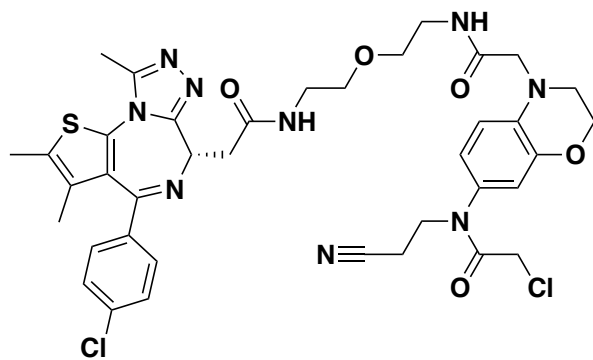**(S)-2-chloro-N-(4-(2-((2-(2-(2-(4-(4-chlorophenyl)-2,3,9-trimethyl-6H-thieno[3,2-f][1,2,4]triazolo[4,3-a][1,4]diazepin-6-yl)acetamido)ethoxy)ethyl)amino)-2-oxoethyl)-3,4-dihydro-2H-benzo[b][1,4]oxazin-7-yl)-N-(2-cyanoethyl)acetamide (NJH-2-088):** Intermediate **6** (22.9 mg, 0.043 mmol) was hydrolyzed and coupled to **7a** (13 mg, 0.0085 mmol) following General Procedure B to provide NJH-2-088 (6.6 mg, 8.5 μmol, 29%) as a clear colorless oil. **HRMS** [M+H]⁺ *m/z* calc. 776.2222, found 776.2288. **1H NMR** (600 MHz, CDCl3) δ 7.44 (t, J = 6.3 Hz, 1H), 7.39 (d, J = 8.2 Hz, 2H), 7.33 (d, J = 8.6 Hz, 2H), 7.02 (t, J = 6.3 Hz, 1H), 6.71 (dd, J = 8.5, 2.5 Hz, 1H), 6.66 (d, J = 2.5 Hz, 1H), 6.56 (d, J = 8.5 Hz, 1H), 4.53 (dd, J = 8.6, 5.0 Hz, 1H), 4.35 (dd, J = 5.6, 3.5 Hz, 2H), 3.92 – 3.81 (m, 6H), 3.52 – 3.42 (m, 3H), 3.38 – 3.30 (m, 1H), 3.30 – 3.20 (m, 3H), 3.20 – 3.12 (m, 1H), 2.67 – 2.62 (m, 5H), 2.42 (s, 3H), 1.68 (s, 3H), 1.63 (p, J = 6.3 Hz, 2H). **13C NMR** (151 MHz, CDCl3) δ 171.1, 169.0, 167.1, 164.1, 155.6, 150.0, 145.0, 137.0, 136.4, 135.7, 132.1, 131.1, 130.9, 130.7, 130.4, 129.8, 128.8, 121.0, 117.6, 115.7, 112.9, 64.7, 56.0, 54.4, 48.6, 46.0, 41.9, 39.3, 36.3, 35.9, 30.9, 29.7, 29.5, 16.2, 14.4, 13.1, 11.8.
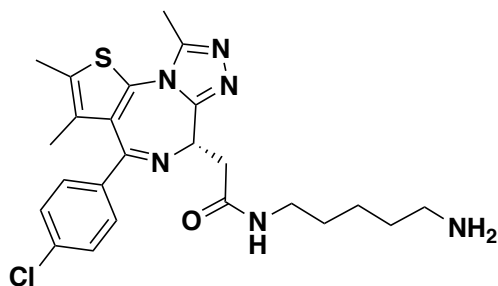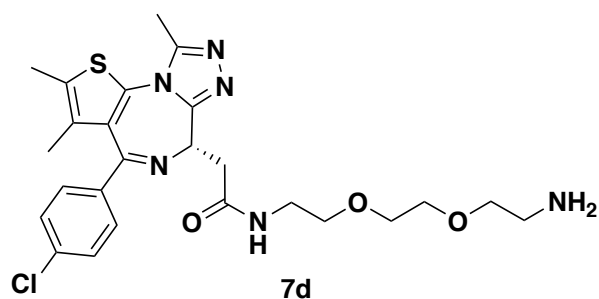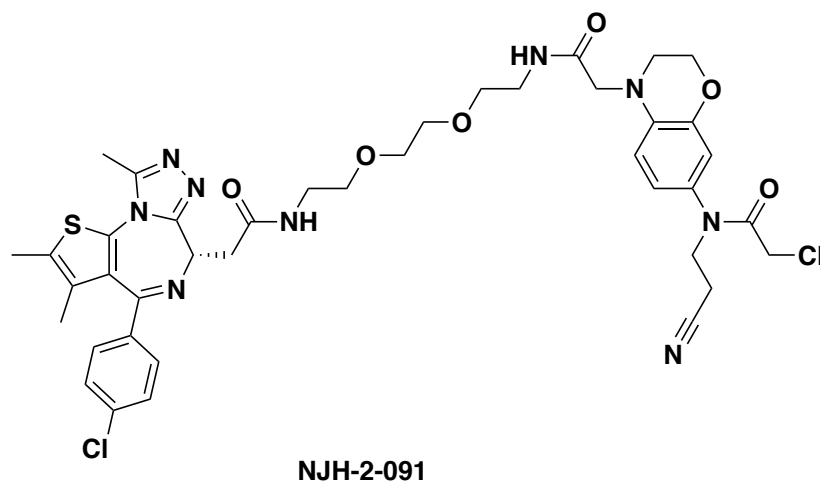

7b

(S)-N-(5-aminopentyl)-2-(4-(4-chlorophenyl)-2,3,9-trimethyl-6H-thieno[3,2-f][1,2,4]triazolo[4,3-a][1,4]diazepin-6-yl)acetamide (7b): (S)-2-(4-(4-chlorophenyl)-2,3,9-trimethyl-6H-thieno[3,2-f][1,2,4]triazolo[4,3-a][1,4]diazepin-6-yl)acetic acid (JQ1-acid, 50 mg, 0.13 mmol) and 1-Boc-1,5-diaminopentane were dissolved in DMF (2 mL). DIEA (113 μL, 0.65 mmol) was added, followed by HATU (100 mg, 0.26 mmol) at rt and the solution was stirred for 20 minutes. Water was added and the mixture extracted with EtOAc, combined organic extracts were washed with brine, dried over Na₂SO₄, concentrated and the crude residue was purified by silica gel chromatography to provide

the Boc-protected amine as a colorless oil. LC/MS [M+H]$^+$ calc 585.2, found 585.2. This oil was then dissolved in DCM (0.5 mL) and TFA (0.5 mL) was added and the solution stirred for 2 hours before volatiles were evaporated, the residue redissolved in DCM and this solution washed with aqueous sat. NaHCO$_3$. The DCM was then evaporated to provide the title compound as a colorless oil (31mg, 0.063 mmol, 48% over two steps). **LC/MS** [M+H]$^+$ *m/z* calc 485.2, found 485.2. **1H NMR** (400 MHz, CDCl3) δ 7.44 (d, J = 8.5 Hz, 2H), 7.37 (d, J = 8.6 Hz, 2H), 6.96 (s, 1H), 4.68 (dd, J = 8.3, 5.9 Hz, 1H), 3.62 (dd, J = 14.3, 8.4 Hz, 1H), 3.31 (m), 2.78 (t, J = 6.7 Hz, 2H), 2.70 (s, 3H), 2.44 (s, 3H), 2.30 (s, 3H), 1.71 (s, 3H), 1.66 – 1.47 (m, 3H), 1.43 (q, J = 7.4 Hz, 2H).

NJH-01-106
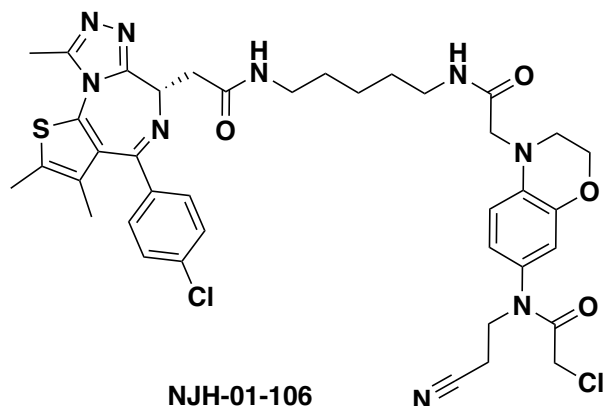
(S)-2-chloro-N-(4-(2-((5-(2-(4-(4-chlorophenyl)-2,3,9-trimethyl-6H-thieno[3,2-f][1,2,4]triazolo[4,3-a][1,4]diazepin-6-yl)acetamido)pentyl)amino)-2-oxoethyl)-3,4-dihydro-2H-benzo[b][1,4]oxazin-7-yl)-N-(2-cyanoethyl)acetamide (NJH-1-106): Chloroacetamide **6** (22 mg, 0.064 mmol) was dissolved in MeOH (600 µL) and treated with aqueous LiOH (400 µL, 0.5 M, 0.2 mmol) at rt for 1h. The mixture diluted with DCM (5 mL) and acidified with aqueous HCl (400 µL, 1 M) and the mixture extracted with DCM. Combined organic extracts were dried over Na$_2$SO$_4$, concentrated, and the crude residue dissolved in DMF (0.5 mL). DIEA (55 µL, 0.32 mmol) was added followed by **7b** (31mg, 0.064 mmol) then HATU (49 mg, 0.13 mmol). The resulting solution was stirred for 5 minutes before it was diluted with EtOAc (0.5 mL) and purified by silica gel chromatography (0-10% MeOH/DCM) followed by preparatory thin layer chromatography (7% MeOH/DCM) to obtain the title compound (26 mg, 0.032 mmol, 50%) as a white lyophilized solid. **HRMS** [M+H]$^+$ *m/z* calc 804.2535, found 804.2669. **1H NMR** (400 MHz, CDCl3) δ 7.44 – 7.31 (m, 4H), 7.04 – 6.96 (m, 1H), 6.74 (dd, J = 8.5, 2.5 Hz, 2H), 6.68 (d, J = 2.5 Hz, 1H), 6.59 (d, J = 8.5 Hz, 1H), 4.62 (dd, J = 8.8, 5.3 Hz, 1H), 4.30 (t, J = 4.5 Hz, 2H), 3.89 (d, J = 5.5 Hz, 6H), 3.55 (dd, J = 14.4, 8.8 Hz, 1H), 3.46 (dq, J = 7.7, 3.8, 3.2 Hz, 1H), 3.43 – 3.32 (m, 1H), 3.32 – 3.24 (m, 1H), 3.23 – 3.13 (m, 2H), 2.69 (dd, J = 6.9, 2.9 Hz, 2H), 2.67 (s, 3H), 2.41 (d, J = 0.9 Hz, 3H), 1.70 – 1.65 (m, 3H), 1.55 – 1.41 (m, 6H), 1.35 (h, J = 6.0, 5.5 Hz, 2H). **13C NMR** (151 MHz, CDCl3) δ 170.49, 169.20, 167.15, 164.08, 155.65, 149.90, 145.04, 136.92, 136.55, 135.77, 132.05, 131.07, 130.96, 130.94, 130.48, 129.85, 128.78, 121.05, 117.68, 115.75, 113.37, 64.79, 56.08, 55.58, 54.53, 48.69, 46.11, 41.91, 39.32, 39.15, 39.04, 28.70, 23.78, 18.65, 17.30, 16.28, 14.38, 13.11, 11.81.

7c
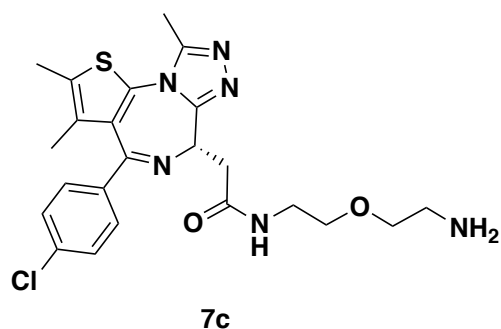
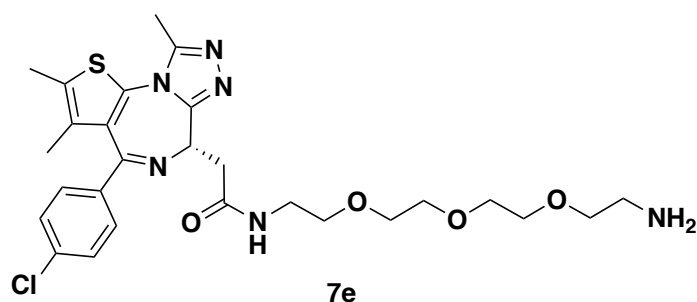**(S)-N-(2-(2-aminoethoxy)ethyl)-2-(4-(4-chlorophenyl)-2,3,9-trimethyl-6H-thieno[3,2-f][1,2,4]triazolo[4,3-a][1,4]diazepin-6-yl)acetamide (7c):**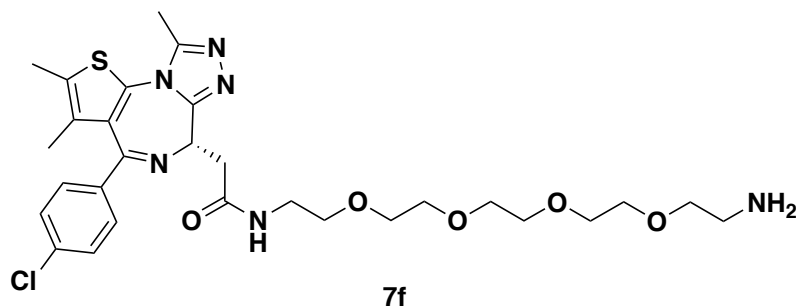 (S)-2-(4-(4-chlorophenyl)-2,3,9-trimethyl-6H-thieno[3,2-f][1,2,4]triazolo[4,3-a][1,4]diazepin-6-yl)acetic acid and tert-butyl (2-(2-aminoethoxy)ethyl)carbamate were combined using General Procedure A to provide **7c** (56.4 mg, 0.099 mmol, 99% over two steps) as a tan solid. **LC/MS** [M+H]$^+$ *m/z* calc. 487.2, found 287.2. **1H NMR** (400 MHz, DMSO) δ 8.31 (d, J = 5.2 Hz, 1H), 7.50 (d, 2H), 7.43 (d, J = 8.3 Hz, 2H), 4.51 (dd, J = 8.0, 6.1 Hz, 1H), 3.49 – 3.39 (m, 4H), 3.34 – 3.17 (m, 6H), 2.74 (t, J = 5.6 Hz, 2H), 2.60 (d, J = 2.6 Hz, 3H), 2.42 (s, 3H), 1.63 (s, 3H).

NJH-2-090

(S)-2-chloro-N-(4-(2-((2-(2-(2-(4-(4-chlorophenyl)-2,3,9-trimethyl-6H-thieno[3,2-f][1,2,4]triazolo[4,3-a][1,4]diazepin-6-yl)acetamido)ethoxy)ethyl)amino)-2-oxoethyl)-3,4-dihydro-2H-benzo[b][1,4]oxazin-7-yl)-N-(2-cyanoethyl)acetamide (NJH-2-090): Intermediate **6** (22.9 mg, 0.043 mmol) was hydrolysed and coupled to **7c** (14 mg, 0.029 mmol) following General Procedure B to provide NJH-2-090 (13.6 mg, 0.017 mmol, 58%) as as a clear colorless oil. **HRMS** [M+H]$^+$ *m/z* calc. 806.2328, found 806.2396. **1H NMR** (600 MHz, DMSO) δ 8.24 (t, J = 5.6 Hz, 1H), 8.09 (t, J = 5.7 Hz, 1H), 7.49 (d, J = 8.6 Hz, 2H), 7.43 (d, J = 8.6 Hz, 2H), 6.78 – 6.73 (m, 2H), 6.54 (d, J = 8.4 Hz, 1H), 4.52 (dd, J = 7.9, 6.2 Hz, 1H), 4.24 (t, J = 3.8 Hz, 2H), 3.99 (s, 2H), 3.91 (s, 2H), 3.78 (t, J = 6.7 Hz, 2H), 3.49 – 3.42 (m, 6H), 3.30 – 3.21 (m, 6H), 2.66 (t, J = 6.7 Hz, 2H), 2.60 (s, 3H), 2.41 (s, 3H), 1.62 (s, 3H). **13C NMR** (151 MHz, DMSO) δ 170.2, 169.6, 166.5, 163.5, 155.6, 150.3, 144.1, 137.2, 136.2, 135.7, 132.7, 131.2, 130.6,

130.3, 130.0, 129.6, 128.9, 121.3, 119.2, 115.7, 112.2, 69.4, 69.3, 64.6, 54.3, 54.0, 48.0, 45.5, 42.8, 39.0, 38.9, 38.0, 16.2, 14.5, 13.2, 11.8.

7d

**(S)-N-(2-(2-(2-aminoethoxy)ethoxy)ethyl)-2-(4-(4-chlorophenyl)-2,3,9-trimethyl-6H-thieno[3,2-f][1,2,4]triazolo[4,3-a][1,4]diazepin-6-yl)acetamide (7d):** (S)-2-(4-(4-chlorophenyl)-2,3,9-trimethyl-6H-thieno[3,2-f][1,2,4]triazolo[4,3-a][1,4]diazepin-6-yl)acetic acid and tert-butyl (2-(2-(2-aminoethoxy)ethoxy)ethyl)carbamate were combined using General Procedure A to provide **7d** (41.9 mg, 0.070 mmol, 70% over two steps) as a clear colorless oil. **LC/MS** [M+H]$^+$ *m/z* found 531.2, found 531.2. **1H NMR** (400 MHz, DMSO) δ 8.31 (t, J = 5.5 Hz, 1H), 7.50 (d, J = 8.7 Hz, 2H), 7.43 (d, J = 8.5 Hz, 2H), 4.57 − 4.45 (m, 1H), 3.58 − 3.43 (m, 6H), 3.41 − 3.35 (m, 5H), 3.29 − 3.15 (m, 4H), 2.65 (t, J = 5.8 Hz, 2H), 2.60 (s, 2H), 2.42 (s, 3H), 1.63 (s, 3H).


NJH-2-091

(S)-2-chloro-N-(4-(14-(4-(4-chlorophenyl)-2,3,9-trimethyl-6H-thieno[3,2-f][1,2,4]triazolo[4,3-a][1,4]diazepin-6-yl)-2,13-dioxo-6,9-dioxa-3,12-diazatetradecyl)-3,4-dihydro-2H-benzo[b][1,4]oxazin-7-yl)-N-(2-cyanoethyl)acetamide (NJH-2-091): Intermediate **6** (22.9 mg, 0.043 mmol) was hydrolyzed and coupled to **7d** (15 mg, 0.016 mmol) following General Procedure B to provide **NJH-2-091** (13.5 mg, 0.016 mmol, 55%) as as a clear colorless oil. **HRMS** [M+H]$^+$ *m/z* calc. 850.2591, found 850.2657. **1H NMR** (600 MHz, CDCl3) δ 7.70 (t, J = 5.8 Hz, 1H), 7.44 (d, J = 8.4 Hz, 2H), 7.36 (d, J = 8.7 Hz, 2H), 7.21 (t, J = 5.5 Hz, 1H), 6.73 (dd, J = 8.5, 2.5 Hz, 1H), 6.70 − 6.63 (m, 2H),

4.57 (dd, J = 9.8, 4.5 Hz, 1H), 4.31 – 4.24 (m, 2H), 3.98 (d, J = 3.1 Hz, 2H), 3.89 (s, 4H), 3.70 – 3.59 (m, 3H), 3.58 – 3.48 (m, 5H), 3.48 – 3.34 (m, 3H), 3.28 (dd, J = 13.8, 4.5 Hz, 1H), 2.72 – 2.65 (m, 5H), 2.43 (s, 3H), 1.70 (s, 3H). **13C NMR** (151 MHz, CDCl3) δ 170.5, 169.6, 167.2, 164.1, 155.8, 150.0, 144.9, 137.0, 136.4, 136.0, 131.9, 131.2, 131.0, 130.6, 130.4, 129.9, 128.8, 120.9, 117.6, 115.6, 113.0, 69.7, 69.1, 64.7, 55.3, 54.7, 48.6, 46.1, 41.9, 39.7, 39.4, 39.3, 38.6, 30.9, 29.7, 16.2, 14.4, 13.1, 11.8.

7e

(S)-N-(2-(2-(2-(2-aminoethoxy)ethoxy)ethoxy)ethyl)-2-(4-(4-chlorophenyl)-2,3,9-trimethyl-6H-thieno[3,2-f][1,2,4]triazolo[4,3-a][1,4]diazepin-6-yl)acetamide (7e): (S)-2-(4-(4-chlorophenyl)-2,3,9-trimethyl-6H-thieno[3,2-f][1,2,4]triazolo[4,3-a][1,4]diazepin-6-yl)acetic acid and tert-butyl (2-(2-(2-(2-aminoethoxy)ethoxy)ethoxy)ethyl)carbamate were combined using General Procedure A to provide **7e** (50.8 mg, 0.079 mmol, 79% over two steps) as a clear colorless oil. **LC/MS** [M+H]+ *m/z* calc. 575.1, found 575.2. **1H NMR** (400 MHz, DMSO) δ 8.31 (t, J = 5.5 Hz, 1H), 7.49 (d, J = 8.4 Hz, 2H), 7.43 (d, J = 8.3 Hz, 2H), 4.50 (t, J = 7.0 Hz, 1H), 3.54 (d, J = 3.6 Hz, 8H), 3.50 – 3.40 (m, 4H), 3.29 – 3.15 (m, 6H), 2.77 (t, J = 5.6 Hz, 2H), 2.60 (s, 3H), 2.41 (s, 3H), 1.63 (s, 3H).
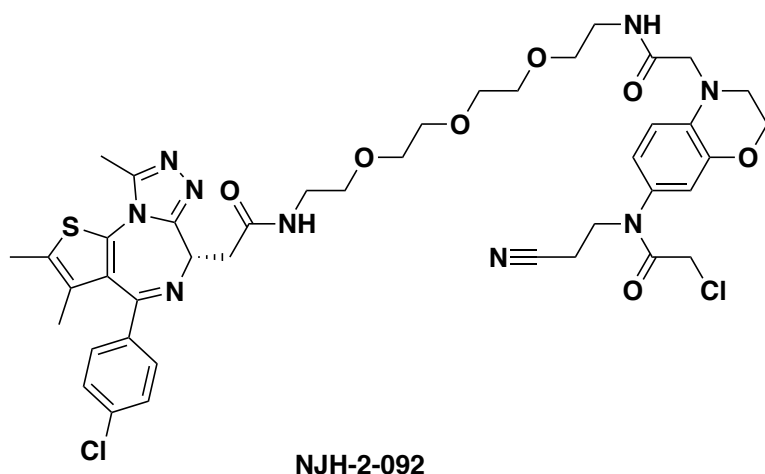
NJH-2-092

(S)-2-chloro-N-(4-(17-(4-(4-chlorophenyl)-2,3,9-trimethyl-6H-thieno[3,2-f][1,2,4]triazolo[4,3-a][1,4]diazepin-6-yl)-2,16-dioxo-6,9,12-trioxa-3,15-diazaheptadecyl)-3,4-dihydro-2H-benzo[b][1,4]oxazin-7-yl)-N-(2-cyanoethyl)acetamide (NJH-2-092): Intermediate **6** (22.9 mg, 0.043 mmol) was hydrolyzed and coupled to **7e** (15 mg, 0.016 mmol) following General Procedure B to

provide **NJH-2-092** (11.8 mg, 0.013 mmol, 56%) as a clear colorless oil. **HRMS** [M+H]$^+$ *m/z* calc. 894.3, found 894.2922. **1H NMR** (400 MHz, CDCl3) δ 7.45 (d, J = 8.2 Hz, 2H), 7.42 (s, 2H), 7.38 (d, J = 8.7 Hz, 2H), 6.77 – 6.68 (m, 2H), 6.58 (d, J = 8.8 Hz, 1H), 4.70 (d, J = 7.4 Hz, 1H), 4.37 – 4.30 (m, 2H), 4.00 – 3.86 (m, 6H), 3.78 – 3.31 (m, 20H), 2.76 – 2.67 (m, 5H), 2.45 (s, 3H), 1.72 (s, 3H). **13C NMR** (151 MHz, DMSO) δ 170.1, 169.5, 166.5, 163.5, 155.6, 150.3, 144.2, 137.2, 136.2, 135.7, 132.7, 131.2, 130.6, 130.3, 130.0, 129.6, 128.9, 121.3, 119.3, 115.7, 112.3, 70.2, 70.1, 70.1, 69.7, 69.5, 64.7, 54.3, 54.1, 48.0, 45.5, 42.8, 39.1, 38.9, 38.0, 29.5, 16.2, 14.5, 13.2, 11.8. 21

7f

(S)-N-(14-amino-3,6,9,12-tetraoxatetradecyl)-2-(4-(4-chlorophenyl)-2,3,9-trimethyl-6H-thieno[3,2-f][1,2,4]triazolo[4,3-a][1,4]diazepin-6-yl)acetamide (7f): (S)-2-(4-(4-chlorophenyl)-2,3,9-trimethyl-6H-thieno[3,2-f][1,2,4]triazolo[4,3-a][1,4]diazepin-6-yl)acetic acid and tert-butyl (14-amino-3,6,9,12-tetraoxatetradecyl)carbamate were combined using General Procedure A to provide **7f** (49.8 mg, 0.072 mmol, 72% over two steps) as a yellow oil. **LC/MS** [M+H]$^+$ *m/z* calc. 619.2, found 619.3. **1H NMR** (400 MHz, DMSO) δ 8.32 (s, 1H), 7.50 (d, J = 8.4 Hz, 2H), 7.43 (d, J = 8.3 Hz, 2H), 4.51 (t, J = 7.1 Hz, 1H), 3.62 – 3.42 (m, 14H), 3.29 – 3.15 (m, 6H), 2.64 (t, J = 5.8 Hz, 2H), 2.60 (s, 3H), 2.42 (s, 3H), 1.63 (s, 3H).
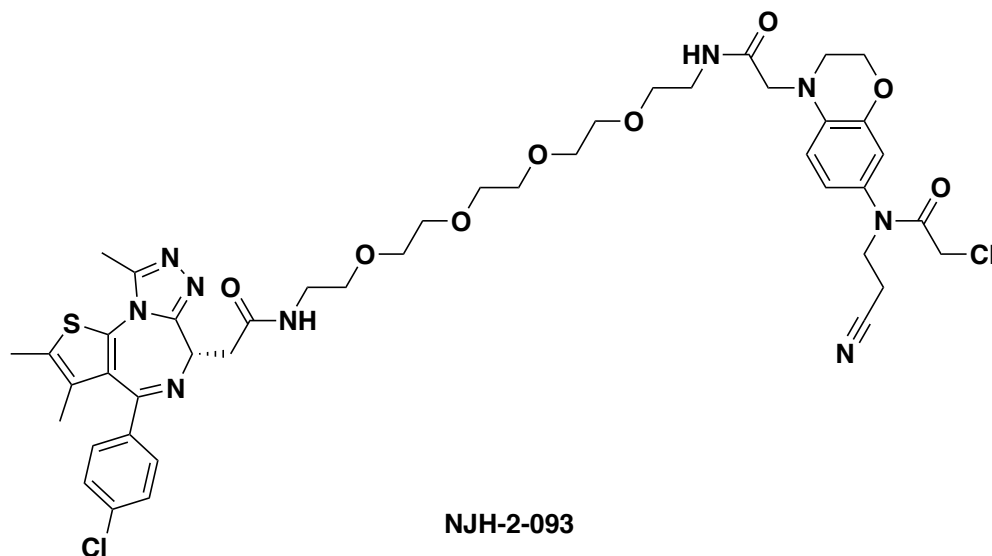
NJH-2-093

(S)-2-chloro-N-(4-(20-(4-(4-chlorophenyl)-2,3,9-trimethyl-6H-thieno[3,2-f][1,2,4]triazolo[4,3-a][1,4]diazepin-6-yl)-2,19-dioxo-6,9,12,15-tetraoxa-3,18-diazaicosyl)-3,4-dihydro-2H-benzo[b][1,4]oxazin-7-yl)-N-(2-cyanoethyl)acetamide (NJH-2-093): Intermediate **6** (22.9 mg, 0.043 mmol) was hydrolyzed and coupled to **7f** (13 mg, 0.023 mmol) following General Procedure B to provide **NJH-2-093** (4.4 mg, 4.7 µmol, 16%) as a clear colorless oil. **HRMS** [M+H]⁺ *m/z* calc. 938.3115, found 938.3187. **1H NMR** (600 MHz, CDCl3) δ 7.44 (d, J = 8.4 Hz, 2H), 7.36 (d, J = 8.7 Hz, 2H), 7.34 – 7.29 (m, 2H), 6.71 (dd, J = 8.4, 2.5 Hz, 1H), 6.69 (d, J = 2.5 Hz, 1H), 6.55 (d, J = 8.5 Hz, 1H), 4.63 (t, J = 6.7 Hz, 1H), 4.35 (t, J = 4.5 Hz, 2H), 3.93 – 3.87 (m, 6H), 3.76 – 3.42 (m, 23H), 3.36 (dd, J = 14.7, 6.5 Hz, 1H), 2.73 – 2.64 (m, 5H), 2.44 (s, 3H), 1.71 (s, 3H). **13C NMR** (151 MHz, CDCl3) δ 167.2, 155.6, 149.9, 145.1, 137.0, 136.5, 135.9, 132.0, 131.0, 130.7, 130.5, 129.9, 128.8, 120.8, 117.7, 115.6, 113.1, 64.9, 60.4, 55.7, 54.2, 48.5, 46.1, 41.9, 39.3, 39.0, 29.7, 16.2, 14.4, 13.1, 11.8.
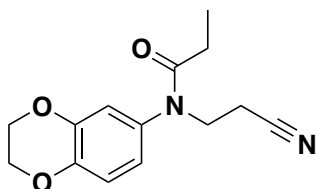
NJH-2-082

N-(2-cyanoethyl)-N-(2,3-dihydrobenzo[b][1,4]dioxin-6-yl)propionamide (NJH-2-082): 2,3-dihydrobenzo[b][1,4]dioxin-6-amine (302 mg, 2.0 mmol) and basic alumina (408 mg, 4.0 mmol) were added to acrylonitrile (3 mL), and the resulting suspension was stirred stirred at 80 C for 24h. The mixture was filtered through a celite pad to remove the alumina, and the acrylonitrile was removed under vacuum. The crude oil was redissolved in DCM (10 mL) and the solution cooled to 0 C. DIEA (522 µL, 3.0 mmol) was added, followed by propionyl chloride (174 µL, 2.0 mmol). After stirring at 0 °C for 30 minutes, water was added, and the mixture was extracted three times with DCM. Combined organic extracts were washed with brine, dried over sodium sulfate, concentrated, and purified by silica gel chromatography (0-30% EtOAc/Hex) to provide NJH-2-082 (74 mg, 0.28 mmol, 14% over two steps) as a tan oil. **HRMS** [M+H]⁺ *m/z* calc. 261.1161, found 261.1232. **1H NMR** (400 MHz, CDCl3) δ 6.91 (d, J = 8.5 Hz, 1H), 6.78 – 6.68 (m, 2H), 4.30 (s, 4H), 3.91 (t, J = 6.9 Hz, 2H), 2.69 (t, J = 7.0 Hz, 2H), 2.12 (q, J = 7.5 Hz, 2H), 1.06 (t, J = 7.5 Hz, 3H). **13C NMR** (151 MHz, CDCl₃) δ 174.6, 144.2, 143.8, 135.0, 121.1, 118.3, 117.9, 116.9, 64.3, 45.4, 27.6, 16.5, 9.4.

8
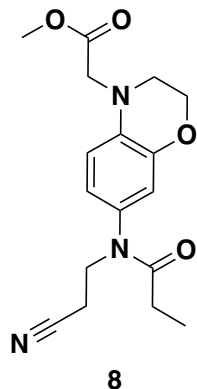
methyl 2-(7-(N-(2-cyanoethyl)propionamido)-2,3-dihydro-4H-benzo[b][1,4]oxazin-4-yl)acetate (8): Intermediate **5** (411 mg, 1.77 mmol) was dissolved in acrylonitrile (6 mL) and basic alumina (361 mg, 3.54 mmol) was added. The reaction mixture was stirred for 40 hrs at reflux before being cooled and filtered through a Celite pad to remove alumina. The solution was concentrated to remove acrylonitrile, and the crude residue was dissolved in DCM (8 mL). At 0 ºC, DIEA (0.85 μL, 4.88 mmol) was added followed by propionyl chloride (0.21 μL, 2.43 mmol). This reaction mixture was stirred for 30 min at 0 ºC before water was added. The mixture was then extracted three times with DCM. Organic extracts were combined, washed with brine, dried over sodium sulfate, and concentrated. The crude residue was purified by silica gel chromatography to provide Intermediate **8** (317 mg, 0.96 mmol, 54% over two steps) as an amber oil. **LC/MS** [M+H]$^+$ *m/z* calc. 332.2, found 332.2. **1H NMR** (400 MHz, CDCl3) δ 6.72 – 6.64 (m, 2H), 6.51 (d, J = 8.5 Hz, 1H), 4.34 (t, J = 4.4 Hz, 2H), 4.09 (s, 2H), 3.92 (t, J = 7.0 Hz, 2H), 3.80 (s, 3H), 3.55 (t, J = 4.4 Hz, 2H), 2.69 (t, J = 7.1 Hz, 2H), 2.14 (q, J = 7.5 Hz, 2H), 1.07 (t, J = 7.5 Hz, 3H).
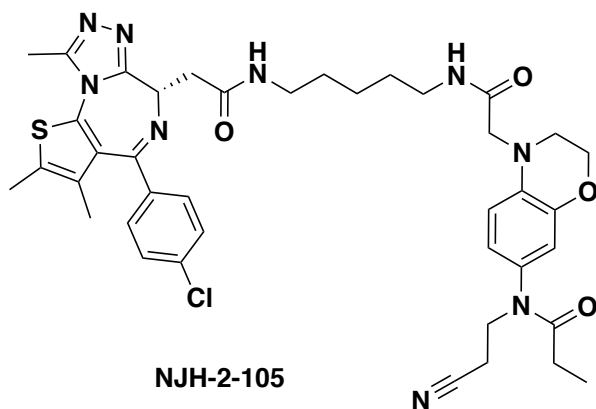
NJH-2-105

(S)-N-(4-(2-((5-(2-(4-(4-chlorophenyl)-2,3,9-trimethyl-6H-thieno[3,2-f][1,2,4]triazolo[4,3-a][1,4]diazepin-6-yl)acetamido)pentyl)amino)-2-oxoethyl)-3,4-dihydro-2H-benzo[b][1,4]oxazin-7-yl)-N-(2-cyanoethyl)propionamide (NJH-2-105): Intermediate **8** (15 mg, 0.045 mmol) was hydrolyzed and coupled to Intermediate **7b** (11 mg, 0.022 mmol) according to General Procedure B. The crude residue was purified by silica gel chromatography (0-6% MeOH/DCM), then by prep. TLC (7% MeOH/DCM) to provide **NJH-2-105** (4.9 mg, 6.25 μmol, 28%) as a clear colorless oil. **HRMS** [M+H]$^+$ *m/z* calc. 784.3082, found 784.3145. **1H NMR** (600 MHz, CDCl3) δ 7.43 (d, J = 8.1 Hz, 2H),

7.36 (d, J = 8.1 Hz, 2H), 6.95 (t, J = 6.0 Hz, 1H), 6.70 (dd, J = 8.5, 2.4 Hz, 1H), 6.68 – 6.61 (m, 2H), 6.59 (d, J = 8.5 Hz, 1H), 4.63 (dd, J = 8.8, 5.4 Hz, 1H), 4.32 (t, J = 4.5 Hz, 2H), 3.94 – 3.83 (m, 4H), 3.59 (dd, J = 14.2, 8.9 Hz, 1H), 3.50 – 3.27 (m, 5H), 3.26 – 3.18 (m, 2H), 2.69 – 2.64 (m, 5H), 2.43 (d, J = 0.8 Hz, 3H), 2.11 (q, J = 7.4 Hz, 2H), 1.70 (d, J = 0.8 Hz, 3H), 1.60 – 1.50 (m, 4H), 1.38 (ddd, J = 15.7, 8.7, 6.8 Hz, 2H), 1.04 (t, J = 7.5 Hz, 3H). **13C NMR** (151 MHz, CDCl3) δ 174.8, 170.4, 169.2, 164.0, 155.7, 149.9, 145.0, 136.9, 136.6, 135.0, 133.1, 132.1, 131.0, 130.9, 130.5, 129.8, 128.8, 121.2, 118.0, 116.1, 113.5, 77.2, 77.0, 76.8, 64.8, 56.5, 54.6, 48.9, 45.4, 39.5, 39.2, 39.0, 30.9, 29.7, 29.1, 28.8, 27.6, 23.8, 16.5, 14.4, 14.1, 13.1, 11.8, 9.5.
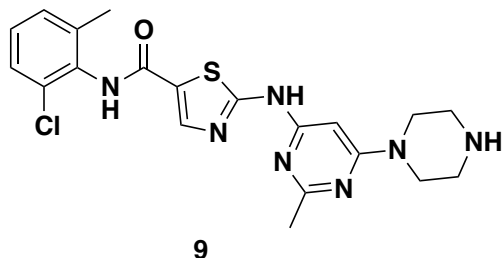
9

N-(2-chloro-6-methylphenyl)-2-((2-methyl-6-(piperazin-1-yl)pyrimidin-4-yl)amino)thiazole-5-carboxamide was synthesized according to published procedures by Veach et al. J Med Chem 2007, 50, 5853-5857: Synthesis and Biological Evaluation of a Fluorine-18 Derivative of Dasatinib.
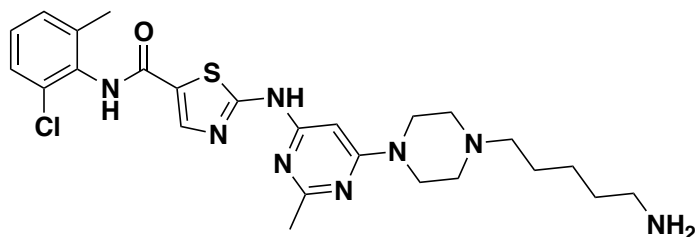
10a

2-((6-(4-(5-aminopentyl)piperazin-1-yl)-2-methylpyrimidin-4-yl)amino)-N-(2-chloro-6-methylphenyl)thiazole-5-carboxamide (10a): N-(2-chloro-6-methylphenyl)-2-((2-methyl-6-(piperazin-1-yl)pyrimidin-4-yl)amino)thiazole-5-carboxamide **(9)** was alkylated and deprotected using tert-butyl (5-bromopentyl)carbamate following general procedure C to provide Intermediate **9** (37 mg, 0.058 mmol, 85% over two steps). **LC/MS** [M+H]+ *m/z* calc. 592.2, found 592.2. **1H NMR** (400 MHz, DMSO) δ 11.68 (s, 1H), 9.93 (s, 2H), 8.25 (s, 1H), 7.73 (s, 2H), 7.41 (dd, J = 7.4, 2.0 Hz, 1H), 7.33 – 7.22 (m, 2H), 6.16 (s, 1H), 4.37 (d, J = 13.9 Hz, 2H), 3.59 (d, J = 11.9 Hz, 2H), 3.23 (t, J = 13.1 Hz, 2H), 3.09 (s, 4H), 2.80 (q, J = 6.9, 6.5 Hz, 2H), 2.46 (s, 3H), 2.24 (s, 3H), 1.79 – 1.62 (m, 2H), 1.56 (p, J = 7.7 Hz, 2H), 1.34 (p, J = 7.9 Hz, 2H).
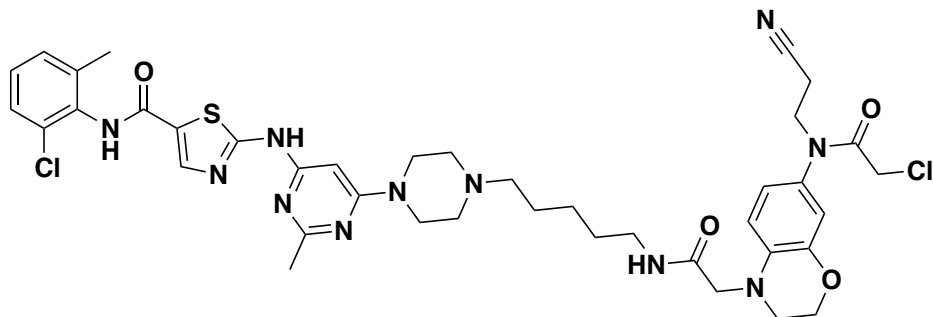
NJH-2-142

N-(2-chloro-6-methylphenyl)-2-((6-(4-(5-(2-(7-(2-chloro-N-(2-cyanoethyl)acetamido)-2,3-dihydro-4H-benzo[b][1,4]oxazin-4-yl)acetamido)pentyl)piperazin-1-yl)-2-methylpyrimidin-4-yl)amino)thiazole-5-carboxamide (NJH-2-142): Intermediate **6** (15 mg, 0.043 mmol) was hydrolyzed and coupled to Intermediate **10a** (13 mg, 0.024 mmol) following general procedure B and purified by silica gel chromatography (0-10% MeOH/DCM) to provide **NJH-2-142** (11 mg, 0.013 mmol, 56%) as a white solid. **HRMS** [M+H]$^+$ *m/z* calc. 848.2910, found 848.2980. **1H NMR** (600 MHz, DMSO) δ 11.46 (s, 1H), 9.87 (s, 1H), 8.23 (s, 1H), 7.99 (t, J = 5.8 Hz, 1H), 7.40 (dd, J = 7.8, 1.7 Hz, 1H), 7.32 – 7.23 (m, 2H), 6.81 – 6.74 (m, 2H), 6.53 (d, J = 8.5 Hz, 1H), 6.06 (s, 1H), 4.26 (dd, J = 5.2, 3.6 Hz, 2H), 4.01 (s, 2H), 3.88 (s, 2H), 3.80 (t, J = 6.6 Hz, 2H), 3.51 (s, 4H), 3.47 (t, J = 4.4 Hz, 2H), 3.09 (q, J = 6.6 Hz, 2H), 2.68 (t, J = 6.6 Hz, 2H), 2.41 (s, 6H), 2.28 (d, J = 7.9 Hz, 2H), 2.25 (s, 3H), 1.44 (dq, J = 15.0, 7.2, 6.4 Hz, 4H), 1.27 (ddd, J = 17.6, 8.8, 6.2 Hz, 3H). **13C NMR** (151 MHz, DMSO) δ 169.2, 166.5, 165.6, 163.0, 162.8, 160.4, 157.4, 144.2, 141.3, 139.3, 136.2, 134.0, 132.9, 129.6, 129.5, 128.6, 127.5, 126.2, 121.2, 119.3, 115.7, 112.2, 83.1, 64.7, 58.3, 54.2, 52.8, 48.0, 45.5, 44.1, 42.8, 38.8, 29.5, 26.4, 26.0, 24.7, 18.8, 16.2.
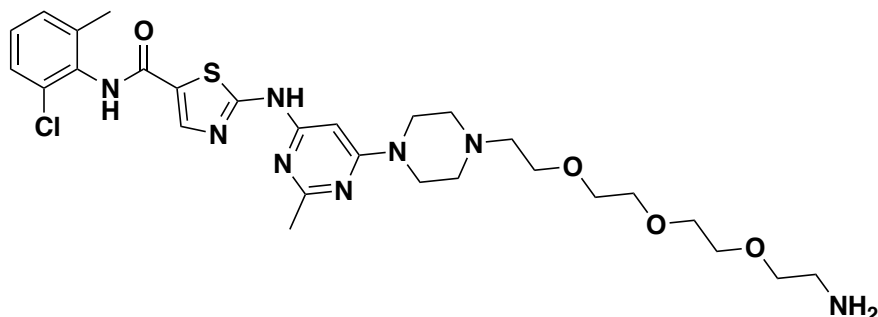
10b

2-((6-(4-(2-(2-(2-(2-aminoethoxy)ethoxy)ethoxy)ethyl)piperazin-1-yl)-2-methylpyrimidin-4-yl)amino)-N-(2-chloro-6-methylphenyl)thiazole-5-carboxamide (10b): N-(2-chloro-6-methylphenyl)-2-((2-methyl-6-(piperazin-1-yl)pyrimidin-4-yl)amino)thiazole-5-carboxamide (**9**) was alkylated using tert-butyl (5-bromopentyl)carbamate and deprotected following general procedure C to provide Intermediate **9** (37 mg, 0.058 mmol, 85% over two steps). **LC/MS** [M+H]$^+$ *m/z* calc. 619.3, found 619.2. **1H NMR** (400 MHz, DMSO) δ 11.69 (s, 1H), 10.02 (s, 1H), 9.93 (s, 1H), 8.25 (s, 1H), 7.81 (s, 2H), 7.41 (dd, J = 7.5, 2.0 Hz, 1H), 7.33 – 7.22 (m, 2H), 6.16

(s, 1H), 4.34 (s, 2H), 3.78 (t, J = 4.9 Hz, 2H), 3.65 – 3.54 (m, 12H), 3.36 (s, 2H), 3.27 (d, J = 12.9 Hz, 2H), 3.13 (s, 2H), 2.99 (q, J = 5.6 Hz, 2H), 2.46 (s, 3H), 2.24 (s, 3H).
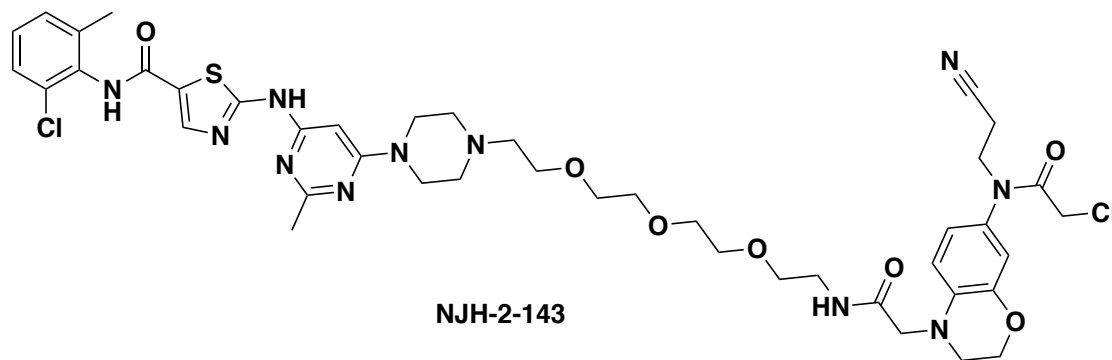
NJH-2-143

N-(2-chloro-6-methylphenyl)-2-((6-(4-(1-(7-(2-chloro-N-(2-cyanoethyl)acetamido)-2,3-dihydro-4H-benzo[b][1,4]oxazin-4-yl)-2-oxo-6,9,12-trioxa-3-azatetradecan-14-yl)piperazin-1-yl)-2-methylpyrimidin-4-yl)amino)thiazole-5-carboxamide (NJH-2-143): Intermediate **6** (15 mg, 0.043 mmol) was hydrolyzed and coupled to Intermediate **10b** (15 mg, 0.024 mmol) following general procedure B and purified by silica gel chromatography (0-10% MeOH/DCM) to provide **NJH-2-143** (14 mg, 0.015 mmol, 62%) as a colorless oil. **HRMS** [M+H]$^+$ *m/z* calc. 938.3227, found 938.3302. **1H NMR** (600 MHz, DMSO) δ 11.46 (s, 1H), 9.87 (s, 1H), 8.23 (s, 1H), 8.06 (t, J = 5.7 Hz, 1H), 7.40 (d, J = 7.9 Hz, 1H), 7.32 – 7.23 (m, 2H), 6.80 – 6.74 (m, 2H), 6.54 (d, J = 8.5 Hz, 1H), 6.06 (s, 1H), 4.24 (d, J = 4.2 Hz, 2H), 4.09 (q, J = 5.2 Hz, 1H), 4.01 (s, 2H), 3.90 (s, 2H), 3.80 (t, J = 6.6 Hz, 2H), 3.59 – 3.38 (m, 21H), 3.25 (q, J = 5.9 Hz, 2H), 3.18 (d, J = 5.2 Hz, 2H), 2.68 (t, J = 6.6 Hz, 2H), 2.41 (s, 3H), 2.25 (s, 3H). **13C NMR** (151 MHz, DMSO) δ 169.5, 166.5, 165.6, 163.0, 162.8, 160.4, 157.4, 144.2, 141.3, 139.3, 136.2, 134.0, 132.9, 129.6, 129.5, 128.6, 127.5, 126.2, 121.3, 119.3, 115.7, 112.3, 83.1, 70.2, 70.1, 70.1, 69.5, 68.8, 64.7, 57.6, 55.4, 54.1, 53.1, 49.1, 48.0, 45.5, 44.1, 42.8, 39.0, 36.2, 26.0, 18.8, 16.2.

Appendix B – Supplementary information for Chapter 3

B.1 Supplementary Table Legends
B.2 Supplementary Figures
B.3 Materials and Methods
B.4 Chemical Synthesis and Characterization

B.1. Supplementary Table Legends

Table S3.1 Chemoproteomic analysis of DUBs.
Table of all probe-modified cysteines identified for 65 DUBs from 455 distinct isoTOP-ABPP experiments. These data are from our research group's aggregate chemoproteomic experiments from various human cell lines wherein cell lysates were labeled with an IA-alkyne probe and taken through the isoTOP-ABPP procedure. Shown are the DUBs, probe-modified peptides, the site of the modified cysteine, the aggregate spectral counts for each particular probe-modified site identified across 455 experiments and the total numbers of experiments for which the probe-modified peptide was observed.

Table S3.2. Structures of covalent ligands screened against OTUB1.
Covalent ligand screen of cysteine-reactive libraries competed against IA-rhodamine labeling of recombinant OTUB1 to identify binders to OTUB1 by gel-based ABPP. Vehicle DMSO or cysteine-reactive covalent ligands (50 µM) were preincubated with OTUB1 for 30 min at room temperature before IA-rhodamine labeling (500 nM for 30 min at room temperature). OTUB1 was then separated by SDS–PAGE, and in-gel fluorescence was assessed and quantified. Gel-based ABPP data are shown in Extended Data Fig. 1a. Quantification of gel-based ABPP data normalized to the average of DMSO vehicle-treated controls in each gel is shown in tab 1.

Table S3.3. TMT-based quantitative proteomic profiling of NJH-2-057 treatment.
CFBE41o-4.7 cells expressing ΔF508-CFTR were treated with vehicle DMSO or NJH-2-057 (tabs 1 and 2) or EN523 or lumacaftor (tabs 3 and 4) (10 µM) for 24 h. Data shown are from n = 3 biologically independent samples per group.

Table S3.4. IsoTOP-ABPP analysis of NJH-2-057.
CFBE41o-4.7 cells expressing ΔF508-CFTR were treated with vehicle DMSO or NJH-2-057 (10 µM) for 8 h. Resulting cell lysates were labeled with IA-alkyne (200 µM) for 1 h and taken through the isoTOP-ABPP procedure Shown in red are the probe-modified peptides that showed isotopically light/heavy or control/NJH-2-57 ratios >4 with adjusted P values of <0.05. The data are from n = 3 biologically independent samples per group.

B.2. Supplementary Figures.

a

total spectral counts

b

c

d

OTUB1 C23
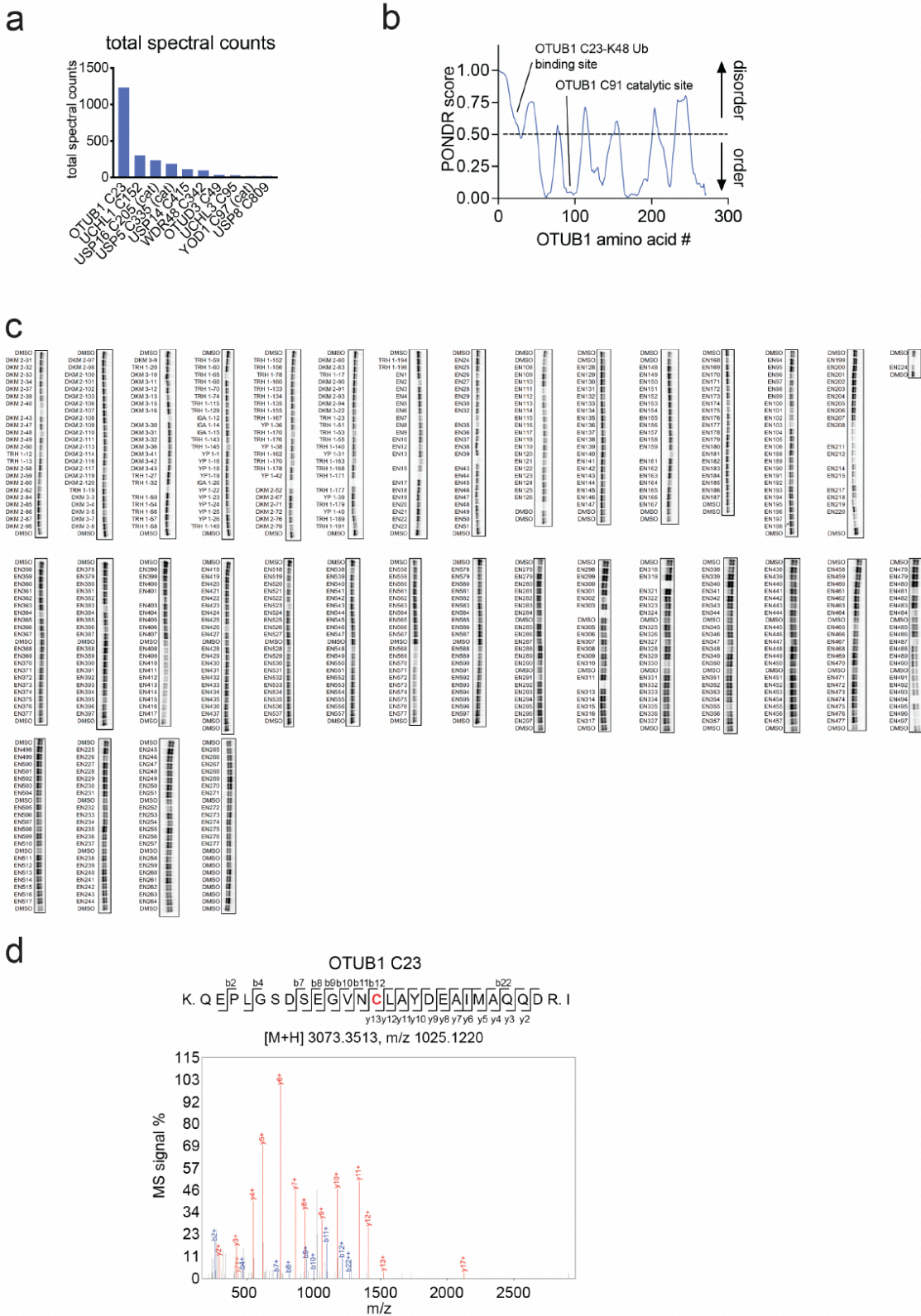
Figure S3.1. Primary covalent ligand screen against OTUB1.
(a) Analysis of aggregate chemoproteomic data for DUBs. Top 10 candidate DUBs described in Figure 1c for total aggregate spectral counts of the particular probe-modified cysteine found in our aggregate chemoproteomic data showing OTUB1 C23 appears far more frequently in chemoproteomic datasets compared to the other DUBs. (b) C23 belongs to an intrinsically disordered region within OTUB1 as assessed by PONDR. (c) Covalent ligand screen of cysteine-reactive libraries competed against IA-rhodamine labeling of recombinant OTUB1 to identify binders to OTUB1 by gel-based ABPP. Vehicle DMSO or cysteine-reactive covalent ligands (50 µM) were preincubated with OTUB1 for 30 min at room temperature prior to IA-rhodamine labeling (500 nM, 30 min room temperature). OTUB1 was then separated by SDS/PAGE and in-gel fluorescence was assessed and quantified.
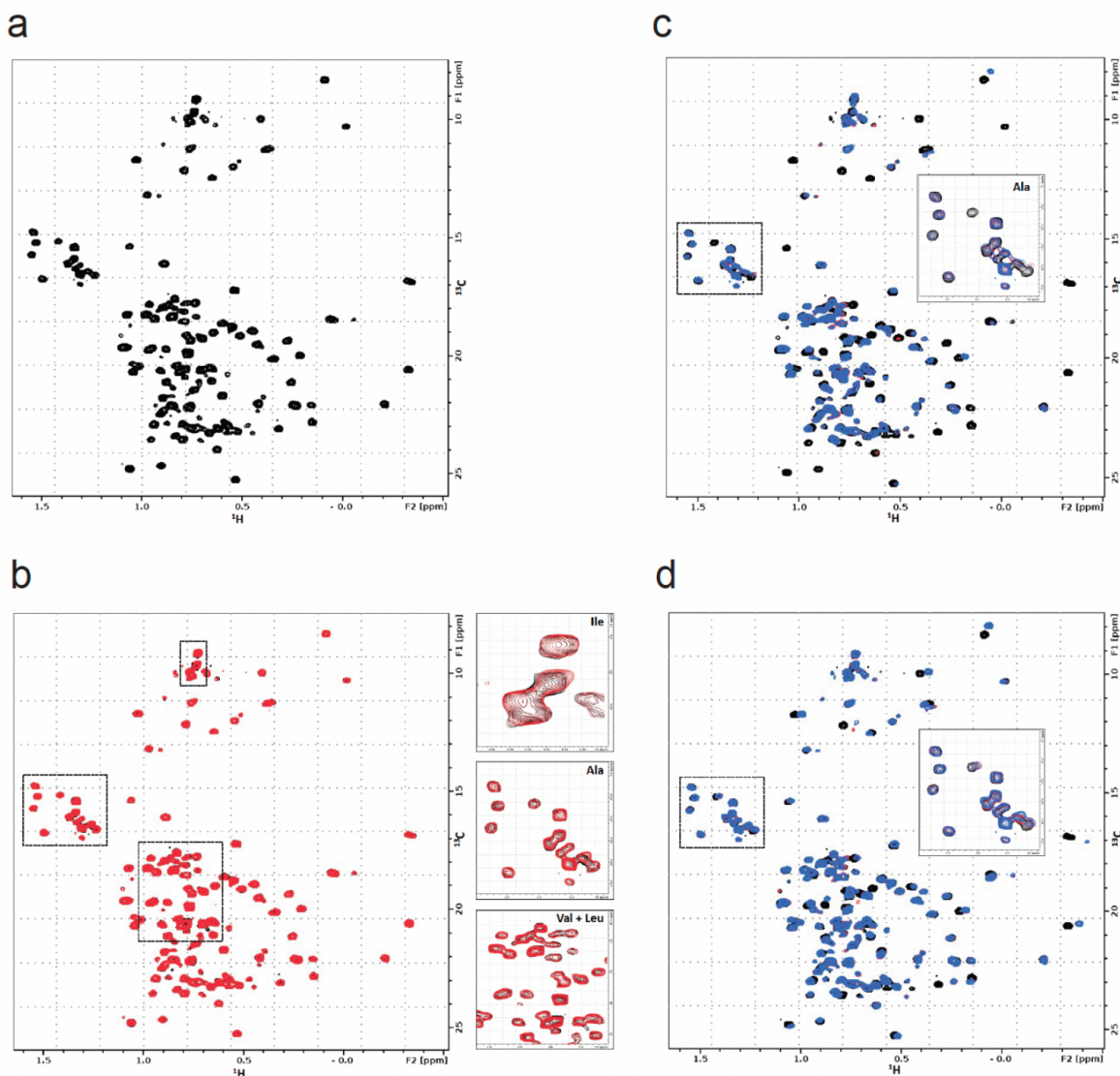
Figure S3.2. NMR analysis of OTUB1, EN523, and UBE2D2.
(a) 13C-HMQC spectrum of OTUB1 labeled on methyl groups of isoleucine, alanine, valine and leucine residues. The presence of peaks with negative proton chemical shifts indicates that the protein is properly folded. (b) Overlay of HMQC spectra of apo-OTUB1 (black) and EN523-bound

OTUB1 (red). While both spectra are mostly identical, we identified small but clear chemical shift perturbations of alanine, isoleucine, valine and leucine peaks. Some of these signal changes are shown in the respective blow-up boxes. (c) Overlay of HMQC spectra of apo-OTUB1 (black), UBE2D2 bound OTUB1 (red) and EN523/UBE2D2-bound OTUB1 (blue). The strong chemical shift perturbations (CSPs) are evidence of specific interactions between OTUB1 and the ubiquitinylated ubiquitinconjugating enzyme. The lack of significant differences between spectra recorded in the presence and absence of EN523 prove that the covalent ligand does not interfere with the protein-protein interaction. Differing peak shift pattern are only seen for peaks directly affected by compound binding (see inlay for blowup of Ala region). (d) Overlay of HMQC spectra of apo-OTUB1 (black), Ub-UBE2D2 bound OTUB1 (red) and EN523/Ub-UBE2D2-bound OTUB1 (blue). The strong CSPs are evidence of specific interactions between OTUB1 and the ubiquitin-conjugating enzyme. The lack of significant differences between spectra recorded in the presence and absence of EN523 prove that the covalent ligand does not interfere with the protein-protein interaction. Differing peak shift pattern are only seen for peaks directly affected by compound binding (see inlay for blow-up of Ala region).
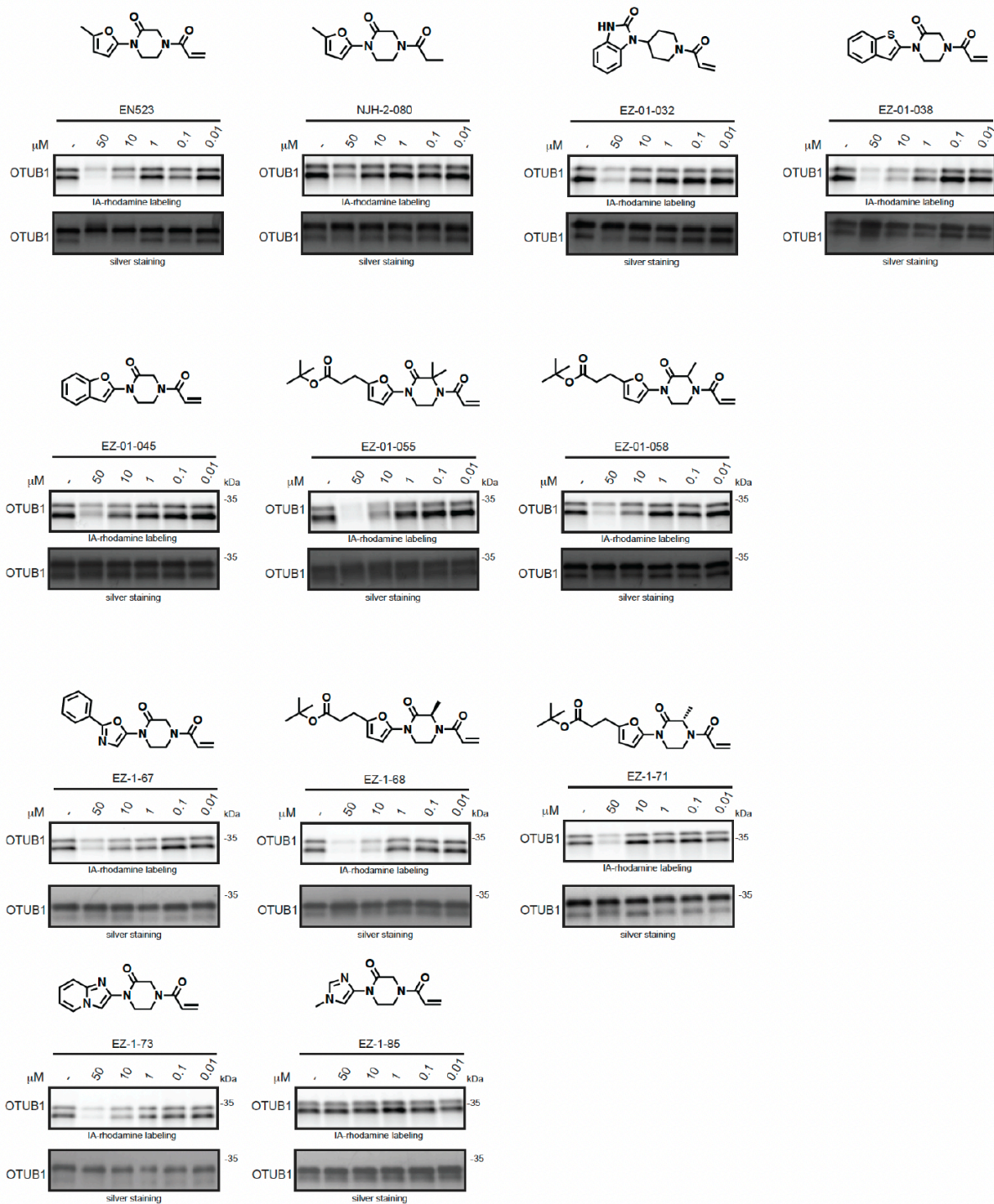
Figure S3.3. Structure-activity relationships of EN523 analogs with OTUB1.
Gel-based ABPP analysis EN523 analogs against OTUB1. Vehicle DMSO or EN523 analogs were pre-incubated with recombinant OTUB1 for 30 min at 37 °C prior to IA-rhodamine labeling (100 nM, 30 min room temperature). OTUB1 was then separated by SDS/PAGE and in-gel fluorescence was assessed. Also shown is silver staining showing protein loading. Shown are representative gels of n=3 biologically independent samples/group.
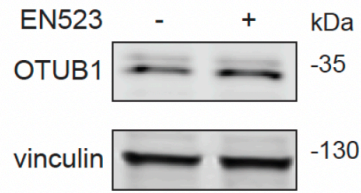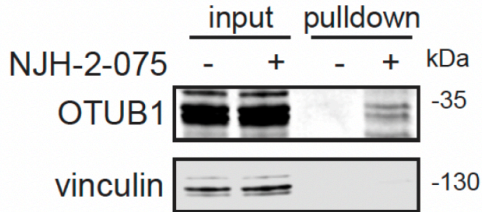
Figure S3.4. EN523 does not alter ORUB1 levels and NJH-2-075 engages OTUB1 in CFBE41o-4.7 cells expressing DF508-CFTR.

(a) CFBE41o-4.7 cells expressing DF508-CFTR were treated with vehicle DMSO or EN523 (10 µM) for 24 h and OTUB1 and loading control vinculin levels were assessed by Western blotting. (b) NJH-2-075 engagement of OTUB1 in CFBE41o-4.7 cells expressing DF508-CFTR. Cells were treated with DMSO vehicle or NJH-2-075 (50 µM) for 2 h, after which cell lysates were subjected to CuAAC with biotin picolyl azide and NJH-2-075 labeled proteins were subjected to avidin pulldown, eluted, separated by SDS/PAGE, and blotted for OTUB1 and vinculin. Both input lysate and pulldown levels are shown. Blots shown are representative blots from n=3 biologically independent samples/group.
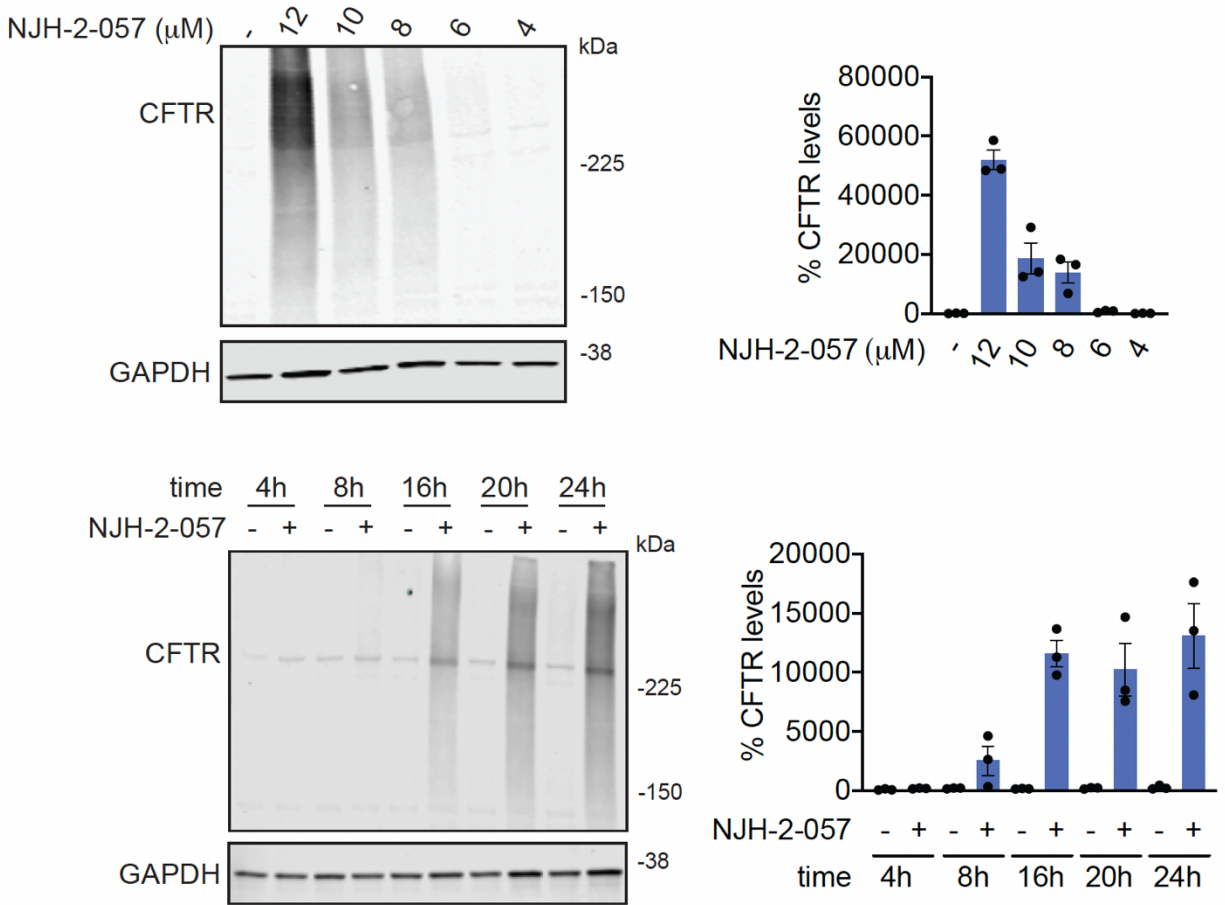
Figure S3.5. Effect of DUBTACs on mutant CFTR levels.
CFBE41o-4.7 cells expressing DF508-CFTR were treated with vehicle DMSO or NJH-2-057 and CFTR and loading control GAPDH levels were assessed by Western blotting. For dose-response studies, NJH-2-057 was treated for 24 h. For timecourse studies, NJH-2-057 was treated at 10 µM. Dose-response and time-course data gels are representative of n=3 biologically independent samples/group and are quantified in the bar graphs to the right. Data in bar graphs show individual biological replicate values and average ± sem from n=3 biologically independent samples/group.
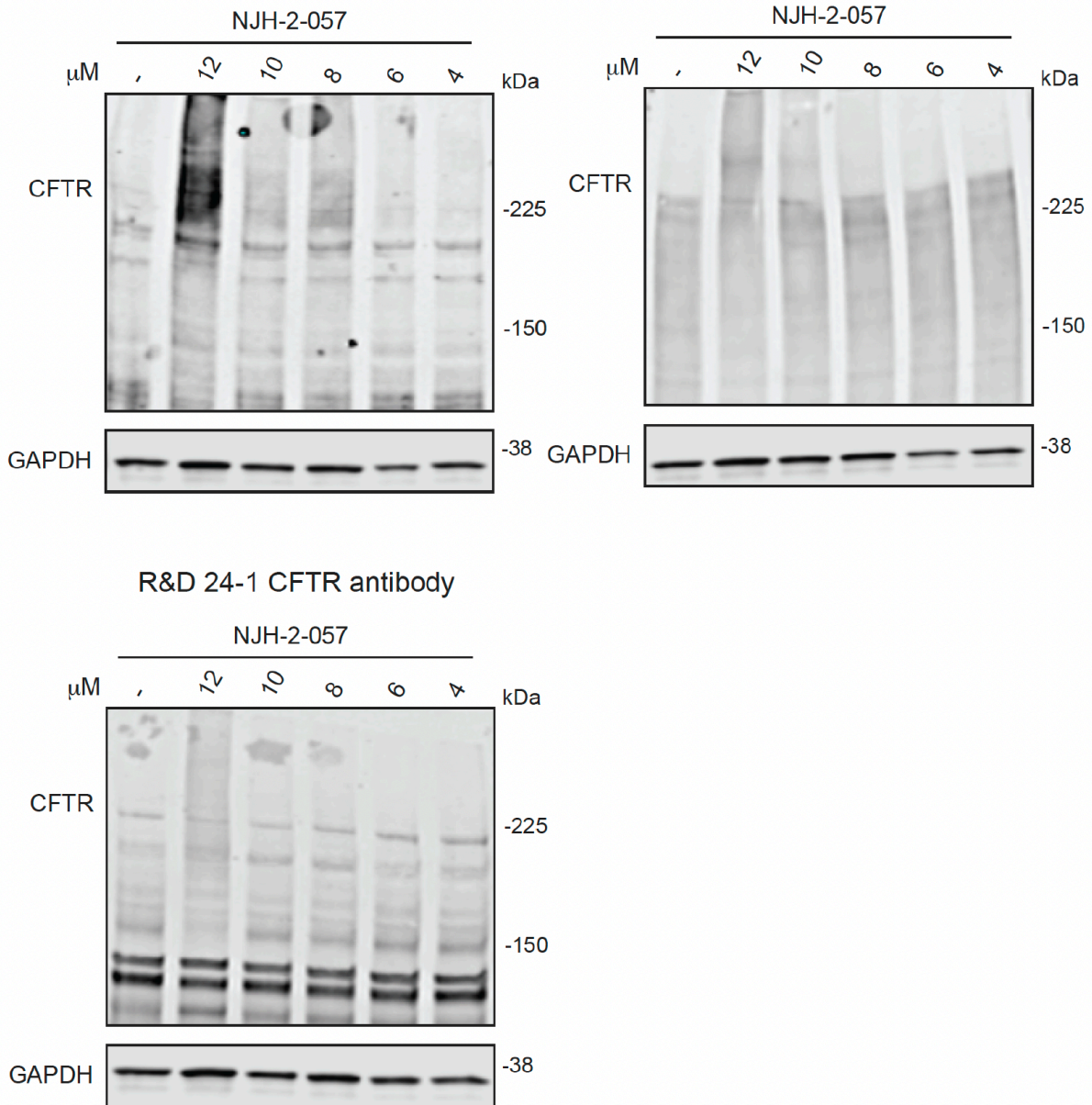
Figure S3.6. Antibodies detecting the effect of DUBTACs on mutant CFTR levels.
CFBE41o-4.7 cells expressing DF508-CFTR were treated with vehicle DMSO or NJH-2-057 and CFTR and loading control GAPDH levels were assessed by Western blotting using three different antibodies against CFTR from the ones used for the main figures. NJH-2-057 was treated for 24 h. Gels are representative of n=3 biologically independent samples/group.
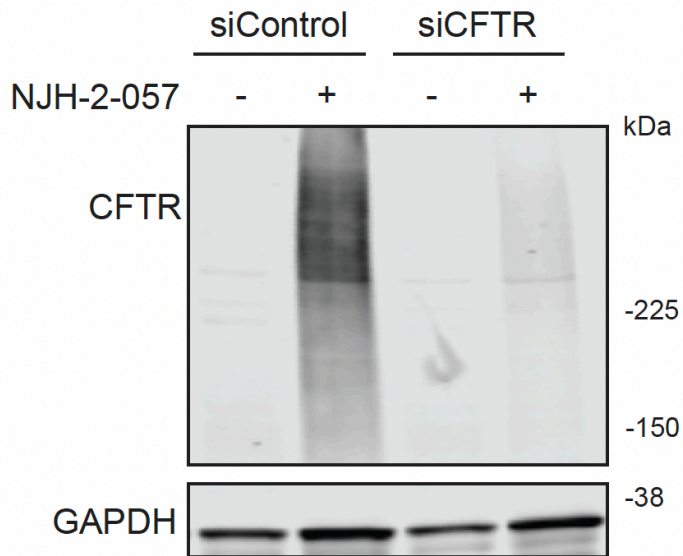
Figure S3.7. Effect of DUBTACs on mutant CFTR levels in siControl and siCFTR cells.
CFBE41o-4.7 cells expressing DF508-CFTR were treated with vehicle DMSO or NJH-2-057 (10 µM) for 24 h and CFTR and loading control GAPDH levels were assessed by Western blotting. Blot is representative of n=3 biologically independent samples/group.
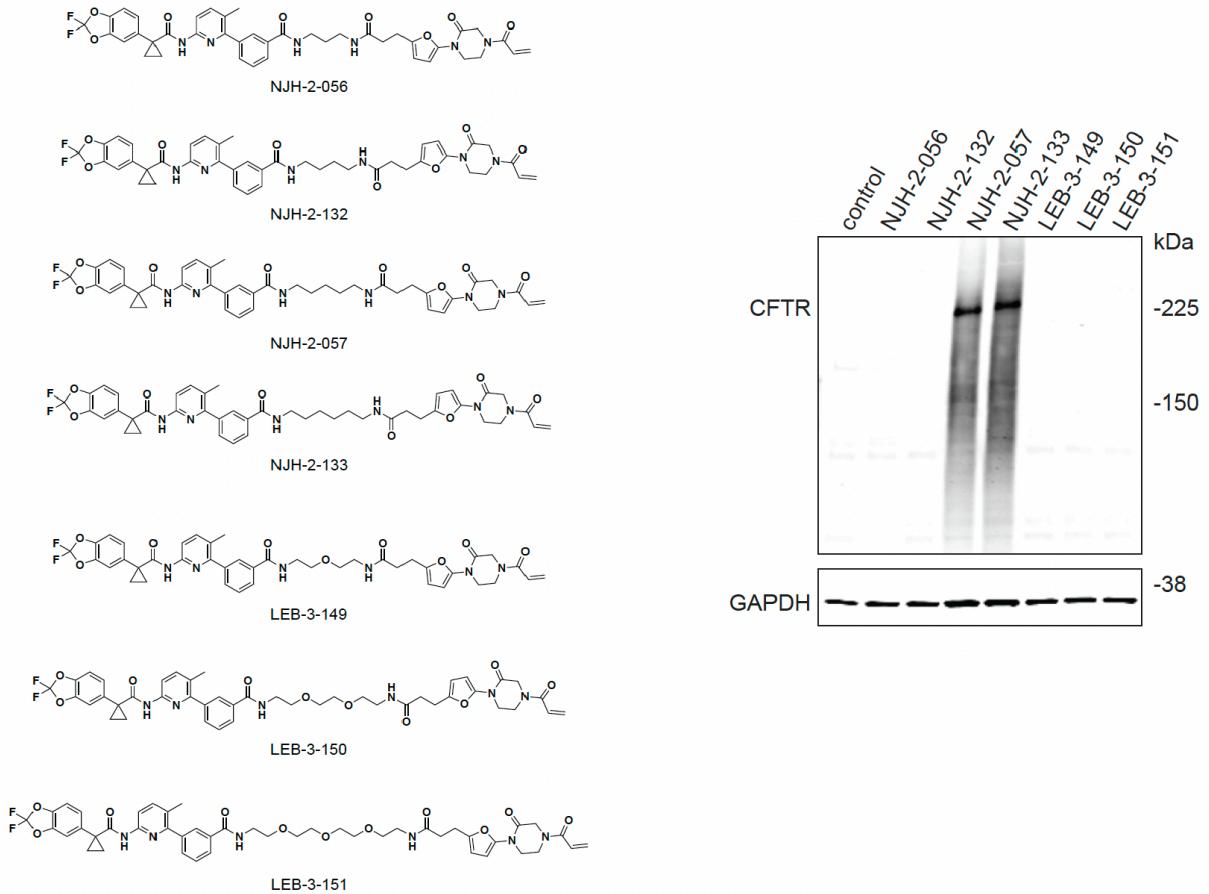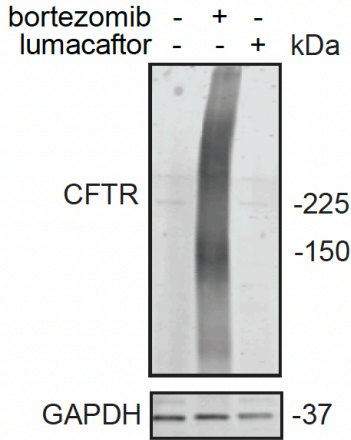
**Figure S3.8. SAR of CFTR DUBTACs.**
CFBE41o-4.7 cells expressing DF508-CFTR were treated with vehicle DMSO or DUBTACs (10 µM) for 24 h and CFTR and loading control GAPDH levels were assessed by Western blotting. Blot is representative of n=3 biologically independent samples/group.

a

GL-01

GL-02

GL-03

GL-04

GL-05

GL-06

GL-07

GL-08

b

CFTR

actin

% CFTR levels

% CFTR levels
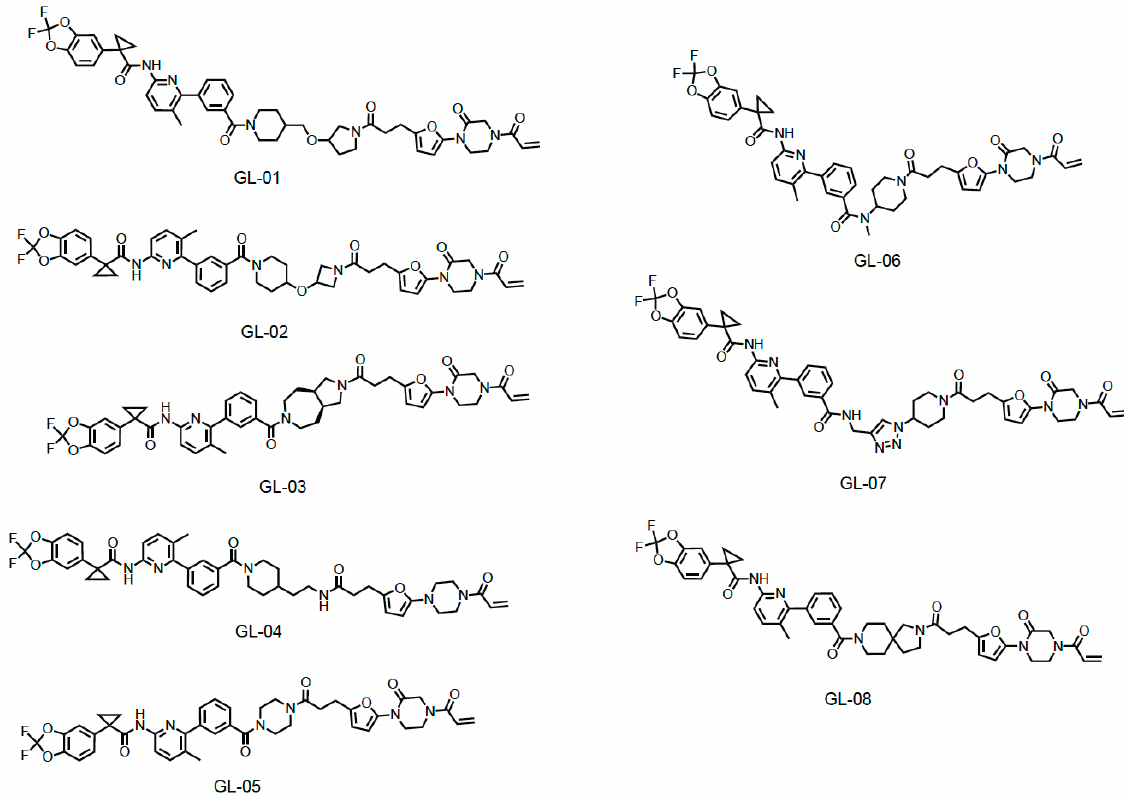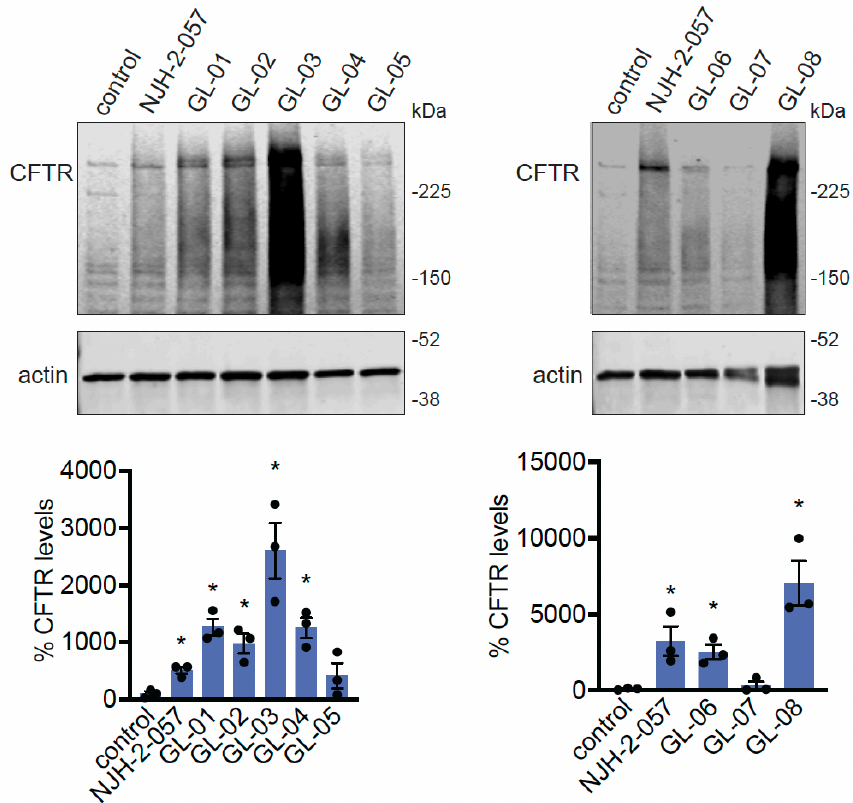
Figure S3.9. SAR of CFTR DUBTACs with more rigid linkers.
CFBE41o-4.7 cells expressing DF508-CFTR were treated with vehicle DMSO or DUBTACs (10 µM) for 24 h and CFTR and loading control actin levels were assessed by Western blotting. Blot is representative of n=3 biologically independent samples/group. Bar graphs show quantification of CFTR levels shown as individual biological replicate data and average ± sem. Statistical significance was calculated with unpaired two-tailed Student's t-tests compared to vehicle-treated controls and is expressed as *p<0.05.

NJH-2-057

NJH-2-106

NJH-2-075
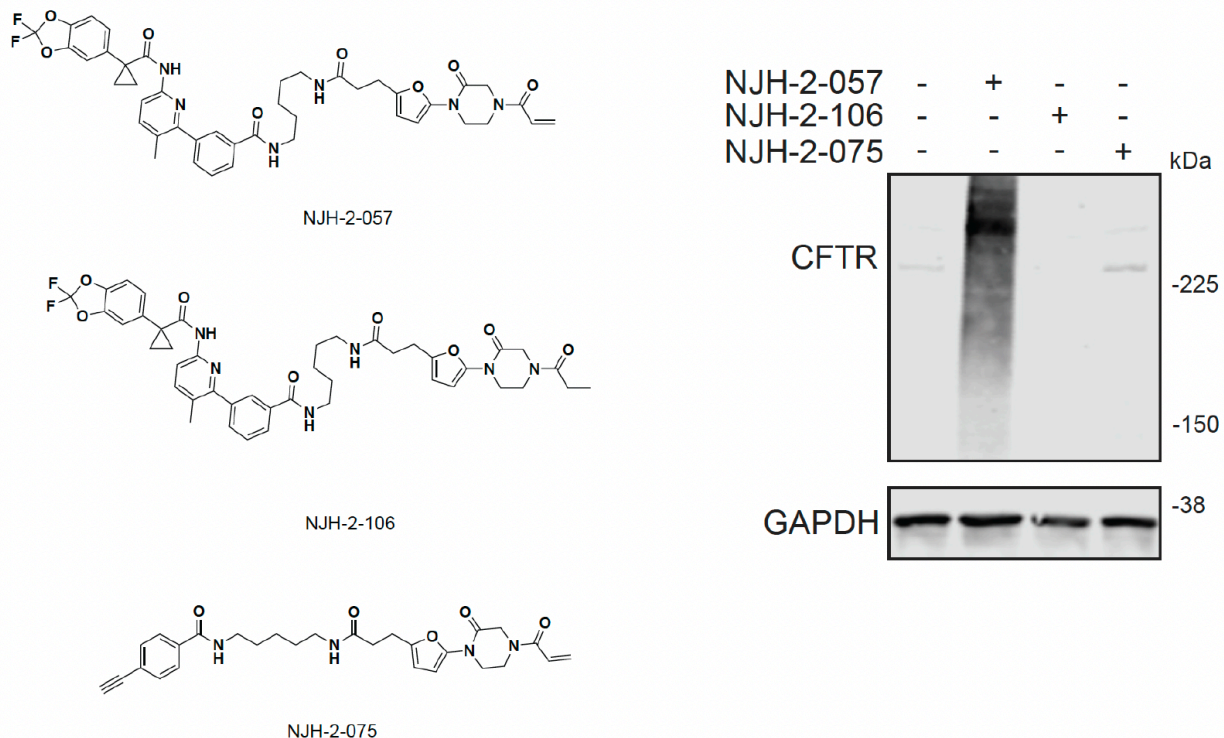
Figure S3.10. Negative control compounds no not stabilize CFTR.
CFBE41o-4.7 cells expressing DF508-CFTR were treated with vehicle DMSO or compounds (10 µM) for 24 h and CFTR and loading control GAPDH levels were assessed by Western blotting. Blot is representative of n=3 biologically independent samples/group.

Figure S3.11. Effect of bortezomib and lumacaftor on mutant CFTR levels.
CFBE41o-4.7 cells expressing DF508-CFTR were treated with vehicle DMSO, bortezomib (1 µM), or lumacaftor (1 µM) for 24 h and CFTR and loading control GAPDH levels were assessed by Western blotting. The gel shown is representative of n=3 biologically independent samples/group.
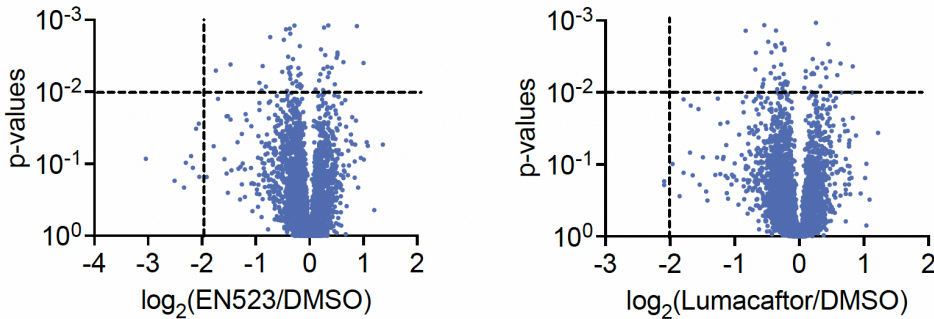
Figure S3.12. TMT-based quantitative proteomic profiling of EN523 or Lumacaftor treatment.
CFBE41o-4.7 cells expressing DF508-CFTR were treated with vehicle DMSO or EN523 or Lumacaftor (10 µM) for 24 h. Data shown are from n=3 biologically independent samples/group. Full data for this experiment can be found in Table S3.
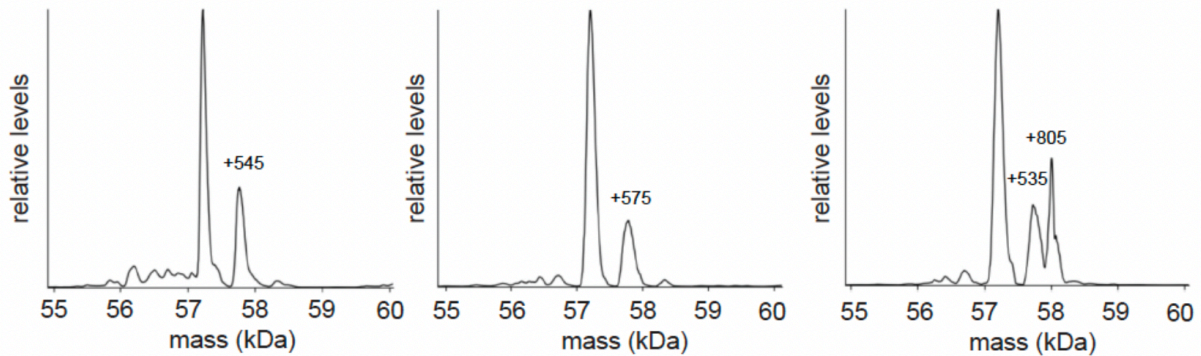
Figure S3.13. Native MS analysis of DUBTAC-mediated ternary complex formation.
OTUB1 (2 µM) and the CFTR-nucleotide binding domain (2 µM) were incubated with DMSO vehicle, EN523 (50 µM), or NJH-2-057 (50 µM) in 150 mM ammonium acetate with MgCl2 (100 µM) and ATP

(100 µM). Zoomed in spectra of just the ternary complex is shown for each biologically independent replicate showing the minor peaks next to the OTUB1-CFTR complex mass of 57,225 Da.
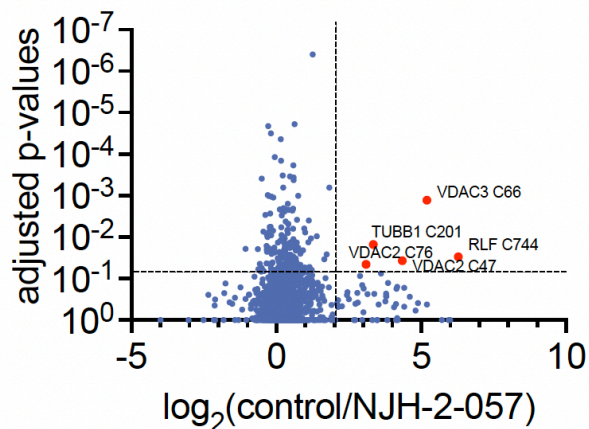
Figure S3.14. IsoTOP-ABPP analysis of NJH-2-057.
CFBE41o-4.7 cells expressing DF508- CFTR were treated with vehicle DMSO or NJH-2-057 for 8 h. Resulting cell lysates were labeled with IA-alkyne (200 µM) for 1 h and taken through the isoTOP-ABPP procedure. Shown in red are the probe-modified peptides that showed isotopically light/heavy or control/NJH-2-57 ratios >4 with adjusted p-values <0.05. The data are from n=3 biologically independent samples/group. The full isoTOP-ABPP dataset can be found in Table S4.

B.3. Materials and Methods

Cysteine-reactive covalent ligand libraries were either previously synthesized and described or, for the compounds starting with 'EN', were purchased from Enamine, including EN523 (refs. 31,34,48–51). Lumacaftor was purchased from MedChemExpress.

Cell culture. CFBE41o-4.7 ΔF508-CFTR human cystic fibrosis bronchial epithelial cells were purchased from Millipore Sigma (SCC159). CFBE41o-4.7 ΔF508-CFTR human cystic fibrosis bronchial epithelial cells were cultured in MEM (Gibco) containing 10% (vol/vol) FBS and maintained at 37 °C with 5% CO2.

Gel-based activity-based protein profiling. Recombinant OTUB1 (0.1 µg per sample) was pretreated with either DMSO vehicle or covalent ligand or DUBTACs at 37 °C for 30 min in 25 µl of PBS and subsequently treated with IA-rhodamine (concentrations are designated in the figure legends; Setareh Biotech) at room temperature for 1 h. The reaction was stopped by addition of 4× reducing Laemmli SDS sample loading buffer (Alfa Aesar). After boiling at 95 °C for 5 min, the samples were separated on precast 4–20% Criterion TGX gels (Bio-Rad). Probe-labeled proteins were analyzed by in-gel fluorescence using a ChemiDoc MP (Bio-Rad).

NJH-2-057 probe labeling of recombinant OTUB1. Recombinant and pure OTUB1 protein (0.5 µg) per sample per replicate was suspended in 50 µl of PBS. One microliter of either DMSO or NJH-2-075 (to give final concentrations of 50, 10, 1 and 0.1 µM) was added, followed by a 1.5-h incubation at 37 °C. Next, 7.8 µl of a solution composed of 9.4 µl of 5 mM azide-Fluor 545 (in DMSO), 112 µl of tris(benzyltriazolylmethyl)amine (TBTA) ligand (stock 1.7 mM in four parts tert-butanol + one part DMSO), 37.5 µl of 50 mM TCEP (in water) and 37.5 µl of 50 mM copper(II) sulfate was added to each sample, and the samples were incubated for 1 h at room temperature. Following CuAAC, 30 µl of Laemmli sample buffer (4×) was added to each sample, vortexed and boiled for 6 min at 95 °C. Samples were loaded on an SDS–PAGE gel and analyzed for in-gel fluorescence.

Deubiquitinase activity assay. Previously described methods were used to assess EN523 effects on OTUB1 activity23. Recombinant OTUB1 (500 nM) was preincubated with DMSO or EN523 (50 µM) for 1 h. To initiate the assay, pretreated OTUB1 enzyme was mixed 1:1 with diubiquitin reaction mix for final concentrations of 250 nM OTUB1, 1.5 µM   diubiquitin, 12.5 µM UBE2D1 and 5 mM DTT. The appearance of monoubiquitin was monitored by western blotting over time by removing a portion of the reaction mix and adding Laemmli's buffer to terminate the reaction. The blot shown is a representative gel from n = 3 biologically independent experiments per group.

Bio-nuclear magnetic resonance analysis of EN523–OTUB1 interactions. We recorded all NMR spectra on a Bruker 600-MHz spectrometer equipped with a 5-mm QCI-F cryo probe with a z gradient, and the temperature was kept constant at 298 K during all experiments. To probe compound and E2 ligase binding to OTUB1, we

recorded 1H-1D and 13C-SOFAST-HMQC experiments. We used 3-mm NMR tubes filled   with 160 µl of 50 µM ILVA, U-15N U-13C labeled OTUB1, 25 mM d-Tris, pH 7.5, 150 mM NaCl, 5% heavy water (to lock), 100 µM sodium trimethylsilylpropanesulfonate   (DSS; internal standard), 75 µM EN523 (dissolved in 100% d6-DMSO; for compound-binding study) and/or 100 µM E2 D2/UBE2D2 (for ligase-binding studies). To allow for complete binding of the compound to OTUB1, we chose an incubation period of ~40 h. We also recorded reference spectra with the adequate volumes of pure d6-DMSO and/or E2 buffer to compensate for solvent-induced effects and repeated experiments after 40 h to make sure that any spectral changes were not related to protein oxidation.

Labeling of endogenous OTUB1 in HEK293T cells with NJH-2-075 probe. One plate of 70% confluent HEK293T cells per condition per replicate were treated with either DMSO vehicle or NJH-02-075 (50 µM) for 2 h. Cells were collected by scraping, suspended in 600 µl of PBS, lysed by probe sonication and centrifuged for 10 min at 5,000 r.p.m. to remove debris. Lysate was normalized to 3.1 mg ml–1, and 85 µl was removed for western blotting analysis of input. Lysate (500 µl) was then incubated for 1 h at room temperature with 10 µl of 5 mM biotin picolyl azide (in water), 10 µl of 50 mM TCEP (in water), 30 µl of TBTA ligand (stock 1.7 mM in four parts tert-butanol + one part DMSO) and 10 µl of 50 mM copper(II) sulfate. Following CuAAC, precipitated proteins were washed three times with cold methanol and resolubilized in 200 µl of 1.2% SDS/PBS. To ensure solubility, proteins were heated to 90 °C for 5 min following resuspension. PBS (1 ml) was then added to each sample, followed by 50 µl of high-capacity streptavidin beads. Samples were then incubated overnight on a rocker at 4 °C. The following morning, the samples were warmed to room temperature, and non-specific binding proteins were washed away with three PBS washes followed by three water washes. Beads were then resuspended in 100 µl of PBS and 30 µl of Laemmli sample buffer (4×) and boiled for 13 min at 95 °C. Samples were vortexed and loaded onto an SDS– PAGE gel along with saved input samples for western blotting analysis.

Western blotting. Proteins were resolved by SDS–PAGE and transferred to nitrocellulose membranes using the Trans-Blot Turbo transfer system (Bio-Rad). Membranes were blocked with 5% BSA in Tris-buffered saline containing Tween 20 (TBS-T) solution for 30 min at room temperature, washed in TBS-T and probed with primary antibody diluted in the recommended diluent, per the manufacturer's instructions, overnight at 4 °C. After three washes with TBS-T, the membranes were incubated in the dark with IR680- or IR800-conjugated secondary antibodies at a 1:10,000 dilution in 5% BSA in TBS-T at room temperature for 1 h. After three additional washes with TBS-T, blots were visualized using an Odyssey Li-Cor fluorescent scanner. The membranes were stripped using ReBlot Plus Strong Antibody Stripping Solution (EMD Millipore) when additional primary antibody incubations were performed. Antibodies used in this study were CFTR (Cell Signaling Technologies, rabbit monoclonal antibody 78335, 1:1,000 dilution in 5% BSA; Figs. 3 and 4), CFTR (R&D Systems, mouse monoclonal antibody, MAB25031, 1 µg ml–1 in 5% BSA; Supplementary Fig. 3), CFTR (Millipore, mouse monoclonal antibody, MAB3484, 1 µg ml–1 in 5% BSA; Supplementary Fig. 3), CFTR (Prestige, rabbit polyclonal antibody,

HPA021939, 1:1,000 dilution in 5% BSA; Supplementary Fig. 3), GAPDH (Proteintech, mouse monoclonal antibody, 1:10,000 dilution in 5% BSA, 60004-1-Ig), OTUB1 (Abcam, rabbit monoclonal antibody, ab175200, 1:1,000 dilution in 5% BSA, EPR13028(B)), CTNNB1 (Cell Signaling Technologies, 1:1,000 dilution in 5% BSA, rabbit monoclonal antibody, 8480) and WEE1 (Cell Signaling Technologies, 1:1,000 dilution in 5% BSA, 4936).

Native mass spectrometry analysis of ternary complex formation. Native MS experiments were performed on a Thermo QE UHMR equipped with a nano-electrospray ionization source (Advion TriVersa NanoMate). Recombinant OTUB1 was first buffer exchanged into 150 mM ammonium acetate, 100 µM MgCl2 and 100 µM ATP at pH 6.7. OTUB1 (4 µM) was then preincubated at room temperature for 24 h with DMSO, EN523 (100 µM) or NJH-2-057 (100 µM). After 24 h, 4 µM CFTR, in the same buffer, was added to the OTUB1 solution, for final concentrations of 2 µM of each protein with either DMSO or 50 µM compound. The solution was then allowed to incubate for 30 min before analysis on the mass spectrometer. Mass spectra were recorded in positive ion mode with a mass range of 1,000–8,000 m/z. Each spectrum was then deconvoluted, and relevant peaks were integrated to determine percent ternary complex formed. All experiments were performed in triplicate.

Isotopic tandem orthogonal proteolysis activity-based protein profiling chemoproteomic experiments. IsoTOP-ABPP studies were done as previously reported[15,31,52]. Our aggregate chemoproteomic data analysis of DUBs was obtained from 455 distinct isoTOP-ABPP experiments performed by the Nomura Research Group. These data are aggregated from various human cell lines, including 231MFP, A549, HeLa, HEK293T, HEK293A, UM-Chor1, PaCa2, PC3, HUH7, NCI-H460, THP1, SKOV3, U2OS and K562 cells. Some of the chemoproteomic data have been previously reported as part of other studies[31,34,48–56]. All of the isoTOP-ABPP datasets were prepared as previously reported using the IA-alkyne probe[15,31,52].

Knockdown studies. RNA interference was performed using siRNA purchased from Dharmacon. CFBE41o-4.7 cells were seeded at 400,000 cells per 6-cm plate and allowed to adhere overnight. Cells were transfected with 33 nM of either non-targeting (ON-TARGETplus Non-targeting Control Pool, Dharmacon, D-001810-10-20) or anti-CFTR siRNA (Dharmacon, custom) using 8 µl of transfection reagent (DharmaFECT 1 (Dharmacon, T-2001-02), DharmaFECT 4 (Dharmacon, T-2004-02) or Lipofectamine 2000 (Thermo Fisher, 11668027)). Transfection reagent was added to OPTIMEM (Thermo Fisher, 31985070) medium and allowed to incubate for 5 min at room temperature. Meanwhile siRNA was added to an equal amount of OPTIMEM. Solutions of transfection reagent and siRNA in OPTIMEM were then combined and allowed to incubate for 30 min at room temperature. These combined solutions were diluted with complete MEM to provide 33 nM siRNA and 8 µl of transfection reagent per 4 ml of MEM, and the medium was exchanged. Cells were incubated with transfection reagents for 24 h, at which point the medium was replaced with medium containing DMSO or 10 µM NJH-2-057 and incubated for another 24 h. Cells were then collected, and protein abundance was analyzed by western blotting.

Transepithelial conductance assays in human bronchial epithelial cells. Human bronchial epithelial cells from individuals with cystic fibrosis bearing the △F508-CFTR mutation were cultured at 37 °C and 5% CO2 in bronchial epithelial cell growth basal medium (BEGM) with SingleQuots Supplements and Growth Factors (Lonza, CC-3170). Cells were maintained in cell culture flasks (Corning, 430641U) for 1 week, and medium was replaced every 2 to 3 d. Cells were washed with Dulbecco's PBS (Thermo Fisher Scientific, 14040141) and trypsinized for 5 to 10 min with 0.05% Trypsin-EDTA (Thermo Fisher Scientific, 25300120), after which Trypsin Neutralizing Solution (Thermo Fisher Scientific, R002100) was added. Cells were pelleted at 300g for 5 min and resuspended in BEGM with DMEM (Thermo Fisher Scientific, 11965092) and plated at 1×106 cells per plate in 24-well transwell plates (Corning, 3526). Cells were grown submerged in BEGM with DMEM for 1 week with medium changed every 2 to 3 d, at which time they were taken to air liquid interface and grown another 2 weeks before being ready to use. Cells were treated with either DMSO vehicle, 10 µM VX-809 or 10 µM DUBTAC 24 h before the experiment. Cells were then submerged in Ham's F12 buffer (Thermo Fisher Scientific, 21700075) with 20 mM HEPES (Thermo Fisher Scientific, 15630080) at pH 7.4 and mounted into the assay system. Transepithelial resistance was recorded using a 24-channel transepithelial current clamp amplifier (TECC24, EP Design). Resistance measurements were taken at intervals of approximately 6 min. Four values were taken to determine baseline resistance, and another four measurements were taken after each of the following additions: 10 µM amiloride (Millipore Sigma, A7410) added apically, 20 µM forskolin (Millipore Sigma, F6886) added apically and 0.5 µM VX770 added both apically and basolaterally. CFTR(inh)-172 (Millipore Sigma, 219672) was then added, and a final six measurements were taken. Transepithelial conductance (G) was calculated from resistance measurements (G = 1/R). Chloride ion transport across the epithelial monolayer is mediated by CFTR, and activation or inhibition of functional CFTR therefore causes changes in transepithelial conductance. In this way, ΔG can be used to measure functional CFTR expression and the functional rescue of CFTR through compound addition.

Quantitative tandem mass tags proteomics analysis. Quantitative TMT-based proteomic analysis was performed as previously described[31]. Acquired MS data was processed using Proteome Discoverer v. 2.4.0.305 software (Thermo) utilizing the Mascot v 2.5.1 search engine (Matrix Science) together with Percolator validation node for peptide–spectral match filtering[57]. Data were searched against the UniProt protein database (canonical human sequences, EBI) supplemented with sequences of common contaminants. Peptide search tolerances were set to 10 ppm for precursors and 0.8 Da for fragments. Trypsin cleavage specificity (cleavage at lysine, arginine except if followed by proline)　　allowed for up to two missed cleavages. Carbamidomethylation of cysteine was set as a fixed modification, and methionine oxidation and TMT modification of N termini and lysine residues were set as variable modifications. Data validation of peptide and protein identifications was done at the level of the complete dataset consisting of combined Mascot search results for all individual samples per experiment via the Percolator validation node in Proteome Discoverer. Reporter ion ratio calculations were performed using summed abundances, with the

most confident centroid selected from a 20-ppm window. Only peptide-to-spectrum matches that are unique assignments to a given identified protein within the total dataset were considered for protein quantitation. High-confidence protein identifications were reported using a Percolator estimated <1% false discovery rate cutoff. Differential abundance significance was estimated using an analysis of variance test with a Benjamini–Hochberg correction to determine adjusted P values.

B.4. Chemical Synthesis and Characterization

Starting materials, reagents and solvents were purchased from commercial suppliers and were used without further purification unless otherwise noted. All reactions were monitored by TLC (TLC Silica gel 60 F_{254}, Sepulco Millipore Sigma). Reaction products were purified by flash column chromatography using a Biotage Isolera with Biotage Sfar® or Silicycle normal-phase silica flash columns (5 g, 10 g, 25 g, or 40 g). 1H NMR and 13C NMR spectra were recorded on a 400 MHz Bruker Avance I spectrometer or a 600 MHz Bruker Avance III spectrometer equipped with a 5 mm 1H/BB Prodigy cryo-probe. Chemical shifts are reported in parts per million (ppm, δ) downfield from tetramethylsilane (TMS). Coupling constants (J) are reported in Hz. Spin multiplicities are described as br (broad), s (singlet), d (doublet), t (triplet), q (quartet) and m (multiplet).

General Procedure A:
Carboxylic acid (1.0 Eq.) was dissolved in DCM (0.1 M). An amine (1.25 Eq.) was added, followed by DIEA (4.0 Eq.), HOBt (0.2 Eq.) and EDCI (2.0 Eq.). The reaction mixture was stirred overnight at rt, water was added, and the mixture extracted three times with DCM. Combined organic extracts were washed with 1M HCl, washed with brine, dried over sodium sulfate, and concentrated. The crude product was purified by silica gel chromatography to provide the amide.

General Procedure B:
Boc-protected amine was dissolved in DCM (0.1 M), and TFA was added to give a 1:2 TFA:DCM ratio. The solution was allowed to stir for 1h. The volatiles were then evaporated, and the resulting oil redissolved in DCM and treated with aqueous saturated $NaHCO_3$. The resulting mixture was then extracted with DCM three times, the combined organic extracts dried over Na_2SO_4, and concentrated to provide the amine without further purification.

General Procedure C:
Tert-butyl ester such as Intermediate 3 (30 mg, 0.086 mmol, 3.0 Eq) was dissolved in DCM (600 µL). TFA (300 µL) was added and the solution stirred for 1h. Volatiles were evaporated under vacuum, and DCM (1 mL) was added and evaporated to give the carboxylic acid intermediate, though some excess TFA remained. This intermediate was dissolved in DMF (500 µL) and DIEA (150 µL, 30 Eq.) and the appropriate amine (0.029 mmol, 1.0 Eq) were added, followed by HATU (30 mg, 0.079 mmol, 2.7 Eq.). The reaction mixture was allowed to stir for 1h at rt. Water was added, and the mixture extracted three times with EtOAc for CFTR DUBTACS, or 4:1 $CHCl_3$:IPA for WEE1 DUBTACs. Organic extracts were combined, washed with brine, dried over sodium sulfate, and concentrated. Crude residues were purified by silica gel chromatography to provide the final compounds.

General Procedure D:

To a solution of the appropriate bromide dissolved in dioxane, N,N'-dimethylethylenediamine (0.25 eq), K_2CO_3 (3.0 eq), CuI (0.1 eq), and the appropriate amide coupling partner (1.0 eq) were added. The reaction mixture was degassed, the atmosphere exchanged for nitrogen, and stirred at 100 °C overnight. Saturated NH_4Cl was added to the completed reaction mixture once cooled, which was stirred for 20 minutes, then filtered through celite and the celite pad was washed with EtOAc. The mixture was extracted with EtOAc three times, washed with brine twice, and dried by $NaSO_4$, before concentration *in vacuo*. Resulting crude mixtures were purified via silica gel column chromatography.

General Procedure E:
The appropriate amine was dissolved in THF and water (2:1 THF:H_2O) with potassium carbonate (3.0 eq). Benzyl chloroformate (1-2 eq) was added dropwise to the reaction mixture, which was then stirred vigorously overnight at room temperature. Water was added and the mixture extracted with EtOAc three times. Organic extracts were combined, washed with brine twice, concentrated and the resulting crude purified using flash column chromatography.

General Procedure F:
The coupled product was dissolved in DCM, followed by a dropwise addition of trifluoroacetic acid (1:2 TFA:DCM) until consumption of starting material was observed via TLC (15-30 min). The mixture was then washed with DCM twice and immediately used without further purification.

General Procedure G:
Pd/C (10% wt.) was added to a mixture of the Cbz-protected compound in EtOH (0.2 M), and the atmosphere was exchanged for H_2 (balloon). The reaction mixture was stirred vigorously overnight, before being diluted with DCM, filtered through a syringe filter (0.45 um), concentrated, and purified using silica gel column chromatography.

General Procedure H:
The amine starting material was dissolved in DCM on ice. TEA (3.0 eq) and acryloyl chloride (1.5 eq) were then added to the reaction mixture until consumption of the starting material was observed by TLC (0.5 – 2 hrs). Water was added, and the reaction mixture was extracted with DCM three times. Organic extracts were combined, washed with H_2O then brine, concentrated, and purified via silica gel column chromatography.
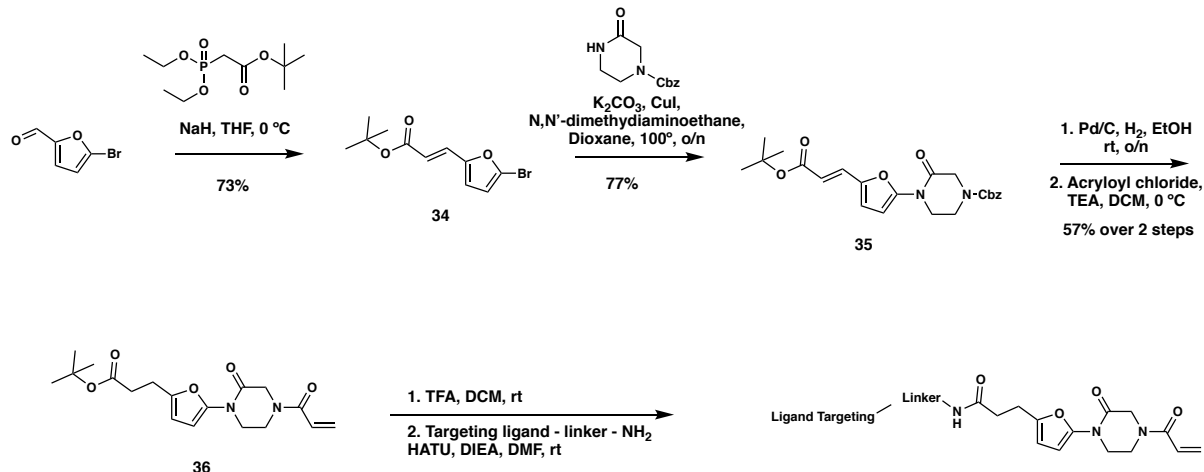
Scheme 1. General scheme describing synthetic route to bifunctional DUBTACs containing EN523 as an OTUB1 recruiter.

SYNTHESIS OF CFTR DUBTACs

34
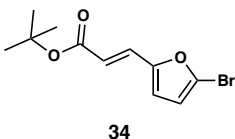
tert-butyl (*E*)-3-(5-bromofuran-2-yl)acrylate (34): tert-butyl diethylphosphonoacetate (971 mg, 0.908 mL, 3.85 mmol) was dissolved in THF (22 mL) and the solution cooled to 0 ºC. Then, 5-bromofuran-2-carbaldehyde (613 mg, 3.50 mmol) was added portion-wise over 5 minutes. The reaction was stirred for 20 minutes at 0 ºC as a gummy solid precipitated. Water was added and the resulting mixture was extracted with EtOAc three times. Combined organic extracts were washed with brine, dried over Na_2SO_4, and concentrated. The crude residue was purified by silica gel chromatography (0-15% EtOAc/Hex) to provide the title compound as a light yellow oil (782 mg, 2.86 mmol, 82%).

1H NMR (400 MHz, CDCl$_3$) δ 7.26 (d, J = 15.7 Hz, 1H), 6.55 (d, J = 3.5 Hz, 1H), 6.42 (d, J = 3.4 Hz, 1H), 6.29 (d, J = 15.7 Hz, 1H), 1.55 (s, 9H).

35
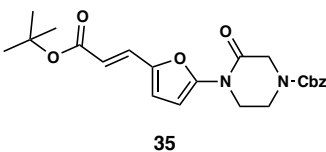
benzyl (*E*)-4-(5-(3-(tert-butoxy)-3-oxoprop-1-en-1-yl)furan-2-yl)-3-oxopiperazine-1-carboxylate (35): tert-butyl (*E*)-3-(5-bromofuran-2-yl)acrylate (1.62 g, 5.94 mmol) was dissolved in dioxane (30 mL) and benzyl 3-oxopiperazine-1-carboxylate (1.4 g, 5.94 mmol), K_2CO_3 (2.46 g, 17.8 mmol), *N,N'*-dimethyldiaminoethane (0.167 mL, 1.49 mmol),

and CuI (114 mg, 0.59 mmol) were added. The mixture was stirred under nitrogen at reflux for 40 h, then cooled to rt. 5 mL saturated aq. NH$_4$Cl was added and the mixture stirred for 30 min. Then the mixture was diluted in EtOAc, filtered through celite, water was added, the mixture partitioned, and the aqueous layer extracted with EtOAc. The extracts were combined, washed with brine, dried over Na$_2$SO$_4$, concentrated, and purified by silica gel chromatography (0-35% EtOAc/Hex) to provide the title compound as an orange oil (1.95 g, 4.59 mmol, 77%).

LC/MS: [M+2H-tBu]$^+$ m/z calc. 371.18, found 373.1.

1H NMR (400 MHz, DMSO) δ 7.45 – 7.24 (m, 6H), 6.98 (s, 1H), 6.57 (s, 1H), 6.08 (dd, J = 15.7, 3.4 Hz, 1H), 5.14 (dd, J = 4.4, 2.3 Hz, 2H), 4.22 (s, 2H), 4.01 (s, 2H), 3.77 (s, 2H), 1.47 (s, 9H).

36
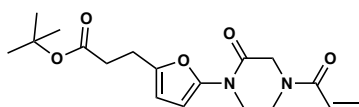
tert-butyl 3-(5-(4-acryloyl-2-oxopiperazin-1-yl)furan-2-yl)propanoate (36): benzyl (*E*)-4-(5-(3-(tert-butoxy)-3-oxoprop-1-en-1-yl)furan-2-yl)-3-oxopiperazine-1-carboxylate (1.95 g, 4.59 mmol) was dissolved in EtOH (25 mL) and Pd/C (200 mg, 10% wt. Pd) was added. The reaction was placed under an atmosphere of H$_2$ and stirred vigorously overnight, before being filtered through celite twice and then concentrated. The crude product was then redissolved in DCM (25 mL), cooled to 0 ºC and treated with TEA (1.28 mL, 9.18 mmol) before a solution of acryloyl chloride (445 µL, 5.51 mmol) in DCM (5 mL) was added over 2 minutes. After stirring for 20 min, water was added, and the mixture extracted with DCM three times. Combined organic extracts were washed with brine, dried over Na$_2$SO$_4$, concentrated, and the resulting crude oil was purified by silica gel chromatography (0-75% EtOAc/Hex) to obtain the title compound as a light yellow oil (846 mg, 2.43 mmol, 53% over two steps).

1H NMR (400 MHz, CDCl$_3$) δ 6.64 – 6.46 (m, 1H), 6.41 (dd, J = 16.7, 2.0 Hz, 1H), 6.29 (d, J = 3.2 Hz, 1H), 6.04 (d, J = 3.3 Hz, 1H), 5.82 (dd, J = 10.2, 2.0 Hz, 1H), 4.42 (d, J = 24.9 Hz, 2H), 4.06 – 3.82 (m, 4H), 2.88 (t, J = 7.8 Hz, 2H), 2.54 (d, J = 7.6 Hz, 2H), 1.44 (s, 9H).

LC/MS: [M+2H-tBu]$^+$ m/z calc. 293.1, found 293.1.

Note: Intermediate 36 is prone to decomposition, likely through polymerization. Care should be taken to store at -20 °C. Attempts to dry thoroughly (e.g. leaving on vacuum at rt overnight) occasionally led to decomposition of ~50% of the material.
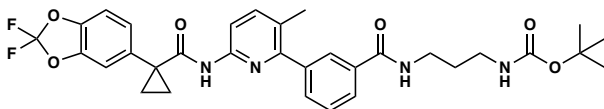
37

tert-butyl (3-(3-(6-(1-(2,2-difluorobenzo[d][1,3]dioxol-5-yl)cyclopropane-1-carboxamido)-3-methylpyridin-2-yl)benzamido)propyl)carbamate (37): Lumacaftor (3-(6-(1-(2,2-difluorobenzo[d][1,3]dioxol-5-yl)cyclopropane-1-carboxamido)-3-methylpyridin-2-yl)benzoic acid) (18 mg, 0.04 mmol), tert-butyl (3-aminopropyl)carbamate (14 mg, 0.08 mmol), DIEA (35 µL, 0.20 mmol), and HOBt (5.4 mg, 0.04 mmol) were dissolved in DCM (1 mL), followed by the addition of EDCI HCl (15 mg, 0.05 mmol). The reaction was stirred at rt for 2 days before water was added, the mixture partitioned, and the aqueous layer extracted with DCM twice. The combined organic extracts were washed with brine, dried over Na_2SO_4, concentrated, and the resulting crude oil was purified by silica gel chromatography (0-60% EtOAc/Hex) to obtain the **37** as a clear oil (23 mg, 0.038 mmol, 94%).

1H NMR (400 MHz, CDCl$_3$) δ 8.13 (d, J = 8.4 Hz, 1H), 7.95 (s, 1H), 7.88 (d, J = 7.6 Hz, 1H), 7.74 (s, 1H), 7.62 (d, J = 8.5 Hz, 1H), 7.60 − 7.49 (m, 2H), 7.34 (s, 1H), 7.30 − 7.18 (m, 2H), 7.11 (d, J = 8.2 Hz, 1H), 4.96 (s, 1H), 3.54 (q, J = 6.2 Hz, 2H), 3.27 (q, J = 6.3 Hz, 2H), 2.31 (s, 3H), 1.78 (q, J = 3.9 Hz, 2H), 1.76 − 1.70 (m, 2H), 1.47 (s, 9H), 1.19 (q, J = 3.9 Hz, 2H).

LC/MS: [M+H]$^+$ m/z calc. 609.24, found 609.3.

38

N-(3-aminopropyl)-3-(6-(1-(2,2-difluorobenzo[d][1,3]dioxol-5-yl)cyclopropane-1-carboxamido)-3-methylpyridin-2-yl)benzamide (38): Intermediate **37** (23 mg, 0.038 mmol) was dissolved in DCM (1 mL) and TFA (1 mL) was added and the solution stirred for 2 hours. The volatiles were then evaporated and the resulting oil redissolved in DCM and treated with aqueous saturated NaHCO$_3$. The resulting mixture was then extracted with DCM three times, combined organic extracts dried over Na_2SO_4, concentrated to provide **38** (15 mg, 0.029 mmol, 78%) as a colorless oil which was used in the next step without further purification.

1H NMR (400 MHz, CDCl$_3$) δ 10.73 (s, 1H), 8.96 (s, 1H), 8.66 (t, J = 5.7 Hz, 1H), 7.95 − 7.85 (m, 3H), 7.79 − 7.66 (m, 2H), 7.60 (d, J = 7.6 Hz, 1H), 7.56 − 7.49 (m, 2H), 7.41 − 7.30 (m, 2H), 3.33 (q, J = 6.4 Hz, 2H), 2.88 − 2.77 (m, 2H), 2.21 (s, 3H), 1.79 (p, J = 6.9 Hz, 2H), 1.52 (dd, J = 4.9, 2.5 Hz, 2H), 1.19 − 1.15 (m, 2H).

LC/MS: [M+H]$^+$ m/z calc. 509.19, found 509.2.
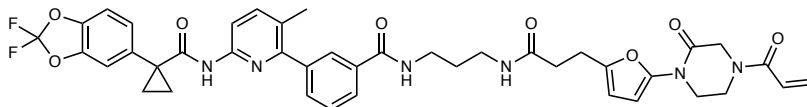
14
NJH-2-056

***N*-(3-(3-(5-(4-acryloyl-2-oxopiperazin-1-yl)furan-2-yl)propanamido)propyl)-3-(6-(1-(2,2-difluorobenzo[d][1,3]dioxol-5-yl)cyclopropane-1-carboxamido)-3-methylpyridin-2-yl)benzamide (NJH-2-056) (14):** Intermediate **36** (tert-butyl 3-(5-(4-acryloyl-2-oxopiperazin-1-yl)furan-2-yl)propanoate) (14 mg, 0.04 mmol) was dissolved in DCM (0.6 mL) and TFA (0.3 mL) was added and the solution was stirred for 1 h at rt

until starting material was consumed as monitored by TLC. Volatiles were evaporated, DCM was added and evaporated again. The residue was dissolved in DCM (1.5 mL) and DIEA (140 µL, 0.80 mmol) was added followed by **38** (*N*-(3-aminopropyl)-3-(6-(1-(2,2-difluorobenzo[d][1,3]dioxol-5-yl)cyclopropane-1-carboxamido)-3-methylpyridin-2-yl)benzamide) (5.4 mg, 0.1 mmol). EDCI HCl (15 mg, 0.08 mmol) was then added, and the mixture stirred for 16h. Water was added and the resulting suspension was extracted with DCM three times. Combined organic extracts were washed with brine and dried over Na_2SO_4 before being concentrated. The crude residue was purified by silica gel chromatography (0-5% MeOH/DCM) to obtain **NJH-2-056** (9.5 mg, 0.012 mmol, 30%) as a white powder following lyophilization from 1:1 water:acetonitrile (2 mL).

1H NMR (400 MHz, CDCl$_3$) δ 8.09 (d, J = 8.4 Hz, 1H), 7.93 – 7.87 (m, 1H), 7.83 (dt, J = 7.5, 1.6 Hz, 1H), 7.72 (s, 1H), 7.59 (d, J = 8.5 Hz, 1H), 7.57 – 7.45 (m, 2H), 7.29 (s, 1H), 7.23 (dd, J = 8.2, 1.8 Hz, 1H), 7.19 (d, J = 1.7 Hz, 1H), 7.07 (d, J = 8.1 Hz, 1H), 6.50 (s, 1H), 6.43 – 6.33 (m, 2H), 6.19 (d, J = 3.2 Hz, 1H), 6.07 (d, J = 3.3 Hz, 1H), 5.81 (d, J = 10.1 Hz, 1H), 4.47 – 4.31 (m, 2H), 4.04 – 3.78 (m, 4H), 3.36 (q, J = 6.2 Hz, 2H), 3.32 – 3.23 (m, 2H), 2.96 (t, J = 7.2 Hz, 2H), 2.55 (t, J = 7.2 Hz, 2H), 2.26 (s, 3H), 1.74 (q, J = 3.9 Hz, 2H), 1.69 – 1.58 (m, 2H), 1.16 (q, J = 3.9 Hz, 2H).

13C NMR (151 MHz, CDCl$_3$) δ 172.5, 171.8, 167.4, 165.0, 155.5, 149.8, 148.9, 145.0, 144.1, 143.6, 141.0, 140.2, 134.9, 134.6, 131.8, 131.7, 130.0, 128.5, 127.8, 127.0, 126.6, 126.5, 126.3, 112.9, 112.4, 110.2, 107.6, 101.3, 36.0, 35.9, 35.2, 31.2, 29.5, 24.4, 19.2, 17.2.

HRMS: [M+H]$^+$ m/z calc. 783.2949, found 783.2954.

Synthesis of NJH-2-132 (17)
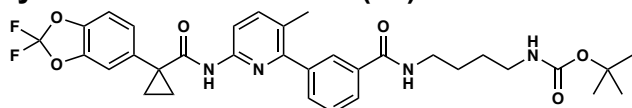
39

tert-butyl (4-(3-(6-(1-(2,2-difluorobenzo[d][1,3]dioxol-5-yl)cyclopropane-1-carboxamido)-3-methylpyridin-2-yl)benzamido)butyl)carbamate (39): Lumacaftor (100 mg, 0.22 mmol), tert-butyl (4-aminobutyl)carbamate were reacted according to General Procedure A and purified by silica gel chromatography (0-60% EtOAc/Hex) to obtain **39** as a clear colorless oil (128 mg, 0.20 mmol, 93%).

1H NMR (400 MHz, CDCl3) δ 8.14 (d, J = 8.4 Hz, 1H), 7.87 (s, 1H), 7.83 (d, J = 7.7 Hz, 1H), 7.74 (s, 1H), 7.63 (d, J = 8.5 Hz, 1H), 7.57 (dt, J = 7.7, 1.5 Hz, 1H), 7.51 (t, J = 7.6 Hz, 1H), 7.27 (dd, J = 8.1, 1.8 Hz, 1H), 7.23 (d, J = 1.7 Hz, 1H), 7.12 (d, J = 8.2 Hz, 1H), 6.58 (s, 1H), 4.68 (s, 1H), 3.52 (q, J = 6.4 Hz, 2H), 3.20 (q, J = 6.6 Hz, 2H), 2.29 (s, 3H), 1.79 (q, J = 3.9 Hz, 2H), 1.71 – 1.67 (m, 2H), 1.65 (s, 9H), 1.65 – 1.57 (m, 2H), 1.20 (q, J = 3.9 Hz, 2H).

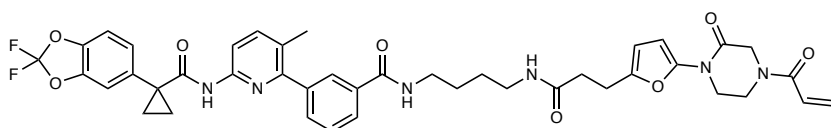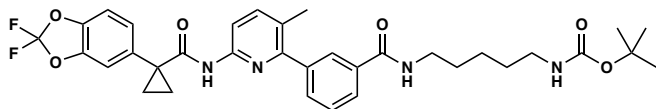**LC/MS:** [M+H]+ *m/z* calc. 623.3, found 623.3.
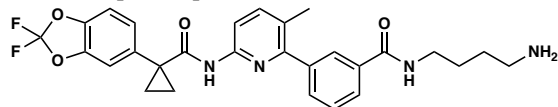
40

N-(4-aminobutyl)-3-(6-(1-(2,2-difluorobenzo[d][1,3]dioxol-5-yl)cyclopropane-1-carboxamido)-3-methylpyridin-2-yl)benzamide (40): **39** (128 mg, 0.20 mmol)was deprotected according to General Procedure B to provide the amine **40** (104 mg, 0.20 mmol, quant.) as a colorless oil.

1H NMR (400 MHz, CDCl3) δ 8.13 (dd, J = 8.4, 1.7 Hz, 1H), 7.85 (tt, J = 8.5, 1.8 Hz, 1H), 7.81 (dt, J = 7.6, 1.6 Hz, 1H), 7.73 (s, 1H), 7.62 (dd, J = 8.5, 2.1 Hz, 1H), 7.56 (ddt, J = 7.7, 2.9, 1.5 Hz, 1H), 7.50 (td, J = 7.6, 3.0 Hz, 1H), 7.27 (dd, J = 8.2, 1.8 Hz, 1H), 7.22 (t, J = 1.8 Hz, 1H), 7.11 (d, J = 8.1 Hz, 1H), 7.03 (d, J = 5.3 Hz, 1H), 3.57 – 3.46 (m, 2H), 3.27 (d, J = 6.7 Hz, 1H), 2.80 (t, J = 6.7 Hz, 1H), 2.28 (d, J = 2.5 Hz, 3H), 1.98 (d, J = 1.4 Hz, 1H), 1.86 (s, 1H), 1.79 (q, J = 3.9 Hz, 2H), 1.72 (dd, J = 8.1, 6.3 Hz, 1H), 1.63 – 1.53 (m, 1H), 1.20 (qd, J = 4.0, 1.1 Hz, 2H).

LC/MS: [M+H]⁺ *m/z* calc. 523.2, found 523.2.

17
NJH-2-132

N-(4-(3-(5-(4-acryloyl-2-oxopiperazin-1-yl)furan-2-yl)propanamido)butyl)-3-(6-(1-(2,2-difluorobenzo[d][1,3]dioxol-5-yl)cyclopropane-1-carboxamido)-3-methylpyridin-2-yl)benzamide (NJH-2-132) (17): Intermediate 36 (tert-butyl 3-(5-(4-acryloyl-2-oxopiperazin-1-yl)furan-2-yl)propanoate) (30 mg, 0.086 mmol) was dissolved in DCM (0.6 mL) and TFA (0.3 mL) was added and the solution stirred for 1 h until starting material was consumed. Volatiles were evaporated, DCM was added and evaporated again. The residue was dissolved in DCM (1.5 mL) and DIEA (150 µL, 0.86 mmol) was added followed by N-(4-aminobutyl)-3-(6-(1-(2,2-difluorobenzo[d][1,3]dioxol-5-yl)cyclopropane-1-carboxamido)-3-methylpyridin-2-yl)benzamide **(40)** (15 mg, 0.029 mmol). HATU (30mg, 0.079 mmol) was then added and the mixture stirred for 16h. Water was added and the resulting suspension was extracted with DCM three times. Combined organic extracts were washed brine and dried over sodium sulfate before being concentrated. The crude residue was purified by silica gel chromatography (0-5% MeOH/DCM) to obtain the title compound (9.5 mg, 0.012 mmol, 30%) as a white solid.

1H NMR (400 MHz, CDCl3) δ 8.12 (d, J = 8.4 Hz, 1H), 7.88 (t, J = 1.8 Hz, 1H), 7.84 (dt, J = 7.6, 1.6 Hz, 1H), 7.74 (s, 1H), 7.62 (d, J = 8.5 Hz, 1H), 7.56 (dt, J = 7.7, 1.5 Hz, 1H), 7.51 (t, J = 7.6 Hz, 1H), 7.26 (dd, J = 8.2, 1.7 Hz, 1H), 7.22 (d, J = 1.7 Hz, 1H), 7.11 (d, J = 8.2 Hz, 1H), 6.80 (s, 1H), 6.53 (d, J = 24.7 Hz, 1H), 6.41 (dd, J = 16.7, 2.0 Hz, 1H), 6.20 (d, J = 3.2 Hz, 1H), 6.07 (d, J = 3.3 Hz, 2H), 5.83 (dd, J = 10.2, 2.0 Hz, 1H), 4.38 (d, J = 28.2 Hz, 2H), 4.07 – 3.79 (m, 4H), 3.73 (tt, J = 9.8, 4.9 Hz, 1H), 3.45 (q, J = 6.4 Hz, 2H), 3.27 (q, J = 6.2 Hz, 2H), 3.20 (qd, J = 7.4, 3.4 Hz, 1H), 2.94 (q, J = 6.1, 5.0 Hz, 2H), 2.52 (t, J = 7.2 Hz, 2H), 2.28 (s, 3H), 1.77 (q, J = 3.9 Hz, 2H), 1.63 – 1.51 (m, 2H), 1.19 (q, J = 3.9 Hz, 2H).

13C NMR (151 MHz, CDCl3) δ 171.8, 167.4, 165.0, 155.5, 149.9, 148.9, 144.7, 144.1, 143.6, 141.0, 140.2, 134.9, 134.7, 133.4, 131.8, 131.7, 128.5, 127.6, 127.0, 126.6, 126.4, 112.9, 112.4, 110.2, 107.4, 101.2, 55.5, 43.5, 39.6, 39.0, 34.9, 31.2, 26.8, 26.7, 24.3, 19.2, 18.6, 17.2, 17.2, 12.5.

HRMS (ESI): *m/z* calc. 797.3032, found 797.3109.
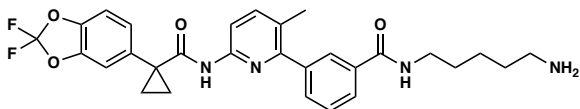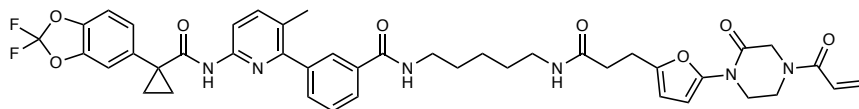
Synthesis of NJH-2-057 (15)

41

tert-butyl (5-(3-(6-(1-(2,2-difluorobenzo[d][1,3]dioxol-5-yl)cyclopropane-1-carboxamido)-3-methylpyridin-2-yl)benzamido)pentyl)carbamate (41): Lumacaftor (3-(6-(1-(2,2-difluorobenzo[d][1,3]dioxol-5-yl)cyclopropane-1-carboxamido)-3-methylpyridin-2-yl)benzoic acid) (181 mg, 0.40 mmol), tert-butyl (5-aminopentyl)carbamate (121 mg, 0.60 mmol), DIEA (350 µL, 2.00 mmol), and HOBt (54 mg, 0.4mmol) were dissolved in DCM (6 mL), followed by addition of EDCI HCl (153 mg, 0.50 mmol). The reaction was stirred at rt for 16 hours before water was added, the mixture partitioned, and the aqueous layer extracted with DCM twice. The combined organic extracts were washed with brine, dried over Na_2SO_4, concentrated, and the resulting crude oil was purified by silica gel chromatography (0-50% EtOAc/Hex) to obtain Intermediate **41** as a clear oil (240 mg, 0.38 mmol, 95%).

1H NMR (400 MHz, CDCl$_3$) δ 8.14 (d, J = 8.4 Hz, 1H), 7.84 (s, 1H), 7.80 (dt, J = 7.6, 1.6 Hz, 1H), 7.73 (s, 1H), 7.63 (d, J = 8.5 Hz, 1H), 7.57 (dt, J = 7.7, 1.5 Hz, 1H), 7.51 (t, J = 7.6 Hz, 1H), 7.27 (dd, J = 8.1, 1.8 Hz, 1H), 7.23 (d, J = 1.7 Hz, 1H), 7.12 (d, J = 8.2 Hz, 1H), 6.25 (s, 1H), 3.17 (d, J = 6.8 Hz, 2H), 4.61 (s, 1H), 3.49 (q, J = 7.0, 6.8, 6.3 Hz, 2H), 2.29 (s, 3H), 1.79 (q, J = 3.9 Hz, 2H), 1.56 (q, J = 7.2 Hz, 2H), 1.46 (s, 11H), 1.36 – 1.27 (m, 2H), 1.20 (q, J = 3.9 Hz, 2H), 0.97 – 0.89 (m, 2H).

LC/MS [M+H]$^+$ m/z calc. 637.28, found 637.3.

42

***N*-(5-aminopentyl)-3-(6-(1-(2,2-difluorobenzo[d][1,3]dioxol-5-yl)cyclopropane-1-carboxamido)-3-methylpyridin-2-yl)benzamide (42):** Intermediate **41** (240 mg, 0.038 mmol) was dissolved in DCM (2 mL) and TFA (2 mL) was added and the solution stirred for 2 hours. The volatiles were then evaporated and the resulting oil redissolved in DCM and treated with aqueous saturated $NaHCO_3$. The layers were separated and the aqueous layer was then extracted with DCM three times. The combined organic extracts were dried over Na_2SO_4, and concentrated to provide the title compound (184 mg, 0.34 mmol, 85% over two steps) as a colorless oil which was used in the next step without further purification.

1H NMR (400 MHz, CDCl$_3$) δ 8.09 (d, J = 8.4 Hz, 1H), 7.80 (t, J = 1.8 Hz, 1H), 7.76 (dd, J = 7.7, 1.5 Hz, 1H), 7.69 (s, 1H), 7.59 (d, J = 8.5 Hz, 1H), 7.57 – 7.50 (m, 1H), 7.47 (t, J = 7.6 Hz, 1H), 7.23 (dd, J = 8.2, 1.7 Hz, 1H), 7.19 (d, J = 1.8 Hz, 1H), 7.08 (d, J = 8.2 Hz, 1H), 6.30 (s, 1H), 3.45 (q, J = 6.7 Hz, 2H), 2.74 (t, J = 6.8 Hz, 2H), 2.25 (s, 3H),

1.65 – 1.59 (m, 2H), 1.57 – 1.47 (m, 2H), 1.48 – 1.40 (m, 2H), 1.33 – 1.23 (m, 2H), 1.20 – 1.12 (m, 2H), 0.91 – 0.85 (m, 2H).
**LC/MS** [M+H]$^+$ m/z calc. 537.22, found 537.2.

15
NJH-2-057

***N*-(5-(3-(5-(4-acryloyl-2-oxopiperazin-1-yl)furan-2-yl)propanamido)pentyl)-3-(6-(1-(2,2-difluorobenzo[d][1,3]dioxol-5-yl)cyclopropane-1-carboxamido)-3-methylpyridin-2-yl)benzamide (NJH-2-057) (15):** Intermediate **36** (tert-butyl 3-(5-(4-acryloyl-2-oxopiperazin-1-yl)furan-2-yl)propanoate) (70 mg, 0.20 mmol) was dissolved in DCM (1.0 mL) and TFA (0.8 mL) was added and the solution stirred for 1 h until starting material was consumed as monitored by TLC. The volatiles were evaporated, DCM was added and evaporated again. The residue was dissolved in DMF (1.5 mL) and DIEA (150 µL, 0.86 mmol) was added followed by intermediate **42** (N-(5-aminopentyl)-3-(6-(1-(2,2-difluorobenzo[d][1,3]dioxol-5-yl)cyclopropane-1-carboxamido)-3-methylpyridin-2-yl)benzamide) (54 mg, 0.1 mmol). HATU (152 mg, 0.4mmol) was then added and the mixture stirred for 1 h. Water was added, and the resulting suspension was extracted with DCM three times. Combined organic extracts were washed twice with 1M HCl twice, saturated NaHCO$_3$, twice with 5% LiCl, brine, and dried over Na$_2$SO$_4$ before being concentrated. The crude residue was purified by silica gel chromatography (0-4% MeOH/DCM) to obtain the title compound (35 mg, 0.043 mmol, 43%) as a white powder following lyophilization from 1:1 water:acetonitrile (2 mL).
1H NMR (600 MHz, CDCl$_3$) δ 8.11 (d, J = 8.4 Hz, 1H), 7.85 (t, J = 1.8 Hz, 1H), 7.81 (dt, J = 7.8, 1.5 Hz, 1H), 7.71 (s, 1H), 7.61 (d, J = 8.5 Hz, 1H), 7.55 (dt, J = 7.7, 1.4 Hz, 1H), 7.49 (t, J = 7.6 Hz, 1H), 7.25 (dd, J = 8.2, 1.8 Hz, 1H), 7.21 (d, J = 1.8 Hz, 1H), 7.10 (d, J = 8.2 Hz, 1H), 6.53 (s, 1H), 6.41 (dd, J = 16.7, 1.8 Hz, 2H), 6.22 (d, J = 3.3 Hz, 1H), 6.03 (d, J = 3.3 Hz, 1H), 5.82 (dd, J = 10.4, 1.8 Hz, 2H), 4.54 – 4.32 (m, 2H), 4.07 – 3.79 (m, 4H), 3.45 (q, J = 6.6 Hz, 2H), 3.24 (q, J = 6.6 Hz, 2H), 2.91 (t, J = 7.3 Hz, 2H), 2.46 (t, J = 7.3 Hz, 2H), 2.27 (s, 3H), 1.77 (q, J = 3.9 Hz, 2H), 1.65 – 1.59 (m, 2H), 1.52 (p, J = 7.0 Hz, 2H), 1.40 – 1.32 (m, 2H), 1.18 (q, J = 3.9 Hz, 2H).
13C NMR (151 MHz, CDCl$_3$) δ 171.7, 167.4, 165.0, 155.5, 148.9, 144.8, 144.1, 143.6, 141.0, 140.2, 134.9, 134.8, 131.8, 128.4, 127.5, 127.0, 126.6, 126.6, 126.3, 112.9, 112.4, 110.2, 107.4, 100.9, 39.7, 39.1, 31.2, 29.0, 24.2, 23.7, 19.2, 17.2.
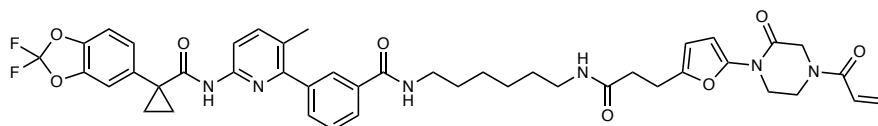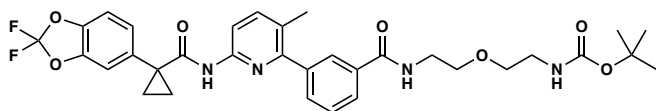**HRMS** [M+H]$^+$ m/z calc. 811.3262, found 811.3267.
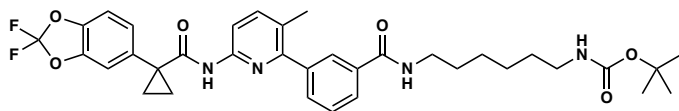
43

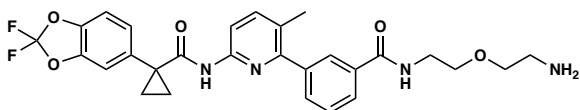**tert-butyl (6-(3-(6-(1-(2,2-difluorobenzo[d][1,3]dioxol-5-yl)cyclopropane-1-carboxamido)-3-methylpyridin-2-yl)benzamido)hexyl)carbamate (43):** Lumacaftor

(100 mg, 0.22 mmol) and tert-butyl (6-aminohexyl)carbamate were reacted according to General Procedure A and purified by silica gel chromatography (0-60% EtOAc/Hex) to obtain **43** (114 mg, 0.18 mmol, 80%) as a clear colorless oil.

1H NMR (400 MHz, CDCl3) δ 8.14 (d, J = 8.4 Hz, 1H), 7.86 (s, 1H), 7.82 (d, J = 7.7 Hz, 1H), 7.72 (s, 1H), 7.63 (d, J = 8.5 Hz, 1H), 7.57 (dt, J = 7.6, 1.5 Hz, 1H), 7.51 (t, J = 7.6 Hz, 1H), 7.27 (dd, J = 8.2, 1.8 Hz, 1H), 7.23 (d, J = 1.7 Hz, 1H), 7.12 (d, J = 8.1 Hz, 1H), 6.37 (s, 1H), 4.58 (s, 1H), 3.48 (q, J = 6.7 Hz, 2H), 3.17 (q, J = 6.7 Hz, 2H), 2.29 (s, 3H), 1.79 (q, J = 3.9 Hz, 2H), 1.69 – 1.64 (m, 1H), 1.58 – 1.49 (m, 1H), 1.46 (s, 9H), 1.45 – 1.38 (m, 6H), 1.20 (q, J = 3.9 Hz, 2H).

LC/MS [M+H]$^+$ *m/z* calc. 651.3, found 651.2.
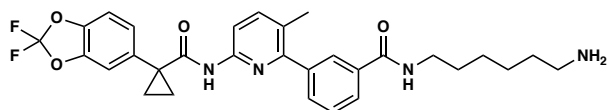
44

N-(6-aminohexyl)-3-(6-(1-(2,2-difluorobenzo[d][1,3]dioxol-5-yl)cyclopropane-1-carboxamido)-3-methylpyridin-2-yl)benzamide) (44): **43** (114 mg, 0.18 mmol) was deprotected according to General Procedure B to provide the amine **44** (99 mg, 0.18 mmol, quant.) as a colorless oil.

1H NMR (400 MHz, CDCl3) δ 8.10 (d, J = 8.4 Hz, 1H), 7.78 (s, 1H), 7.74 (dt, J = 7.5, 1.6 Hz, 1H), 7.69 (s, 1H), 7.59 (d, J = 8.4 Hz, 1H), 7.53 (dt, J = 7.7, 1.5 Hz, 1H), 7.47 (t, J = 7.6 Hz, 1H), 7.22 (dd, J = 8.2, 1.8 Hz, 1H), 7.18 (d, J = 1.6 Hz, 1H), 7.07 (d, J = 8.2 Hz, 1H), 6.17 (s, 1H), 3.44 (td, J = 7.2, 5.8 Hz, 2H), 2.68 (t, J = 6.8 Hz, 2H), 2.24 (s, 3H), 1.99 (s, 1H), 1.81 (s, 1H), 1.74 (q, J = 3.9 Hz, 2H), 1.67 – 1.55 (m, 3H), 1.51 – 1.33 (m, 5H), 1.16 (q, J = 3.9 Hz, 2H).

LC/MS [M+H]$^+$ *m/z* calc. 551.2, found 551.2.

16
NJH-2-133

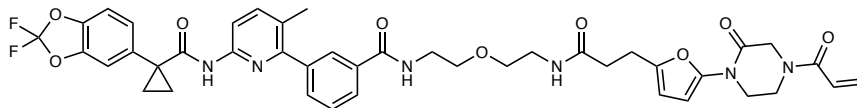**N-(6-(3-(5-(4-acryloyl-2-oxopiperazin-1-yl)furan-2-yl)propanamido)hexyl)-3-(6-(1-(2,2-difluorobenzo[d][1,3]dioxol-5-yl)cyclopropane-1-carboxamido)-3-methylpyridin-2-yl)benzamide (NJH-2-133) (16):** Intermediate **36** (30 mg, 0.086 mmol) was deprotected and coupled to intermediate **44** (16 mg, 0.029 mmol) following General Procedure C to provide **NJH-2-133** (17.4 mg, 0.021 mmol, 73%) as a clear colorless oil.

1H NMR (400 MHz, CDCl3) δ 8.12 (d, J = 8.4 Hz, 1H), 7.89 – 7.79 (m, 2H), 7.73 (s, 1H), 7.62 (d, J = 8.5 Hz, 1H), 7.56 (dt, J = 7.7, 1.5 Hz, 1H), 7.51 (t, J = 7.6 Hz, 1H), 7.27 (dd, J = 8.2, 1.8 Hz, 1H), 7.22 (d, J = 1.7 Hz, 1H), 7.11 (d, J = 8.2 Hz, 1H), 6.54 (d, J = 31.0 Hz, 2H), 6.41 (dd, J = 16.8, 1.9 Hz, 1H), 6.25 (d, J = 3.3 Hz, 1H), 6.07 (d, J = 3.3 Hz, 1H), 5.98 (d, J = 39.7 Hz, 1H), 5.83 (dd, J = 10.3, 2.0 Hz, 1H), 4.42 (d, J = 21.6 Hz, 2H), 4.05 – 3.81 (m, 4H), 3.74 (p, J = 6.7 Hz, 2H), 3.45 (q, J = 6.7 Hz, 2H), 3.22 (dq, J = 13.2, 6.9 Hz, 3H), 2.94 (q, J = 6.4, 5.5 Hz, 2H), 2.52 (t, J = 7.4 Hz, 2H), 2.28 (s, 3H),

1.78 (q, J = 3.9 Hz, 2H), 1.61 (p, J = 6.9 Hz, 2H), 1.42 – 1.30 (m, 3H), 1.20 (q, J = 3.9 Hz, 2H).

13C NMR (151 MHz, CDCl3) δ 171.8, 167.3, 155.5, 149.7, 148.9, 144.7, 144.1, 143.6, 141.0, 140.2, 134.9, 134.9, 133.4, 131.7, 131.7, 130.0, 128.5, 127.5, 127.0, 126.6, 126.6, 126.4, 112.9, 112.4, 110.2, 107.3, 100.8, 55.6, 43.6, 39.6, 39.1, 34.8, 31.2, 29.4, 29.3, 26.0, 25.9, 24.2, 19.1, 18.6, 17.2, 12.5.

HRMS (ESI): [M+H]$^+$ *m/z* calc. 825.3345, found 825.3425.

45

tert-butyl (2-(2-(3-(6-(1-(2,2-difluorobenzo[d][1,3]dioxol-5-yl)cyclopropane-1-carboxamido)-3-methylpyridin-2-yl)benzamido)ethoxy)ethyl)carbamate (45):
Lumacaftor (100 mg, 0.22 mmol) and tert-butyl (2-(2-aminoethoxy)ethyl)carbamate (57 mg, 0.28 mmol) were reacted according to General Procedure A and purified by silica gel chromatography (0-60% EtOAc/Hex) to obtain intermediate **45** (122 mg, 0.19 mmol, 87%) as a clear colorless oil.

1H NMR (400 MHz, Chloroform-d) δ 8.14 (d, J = 8.4 Hz, 1H), 7.88 (t, J = 1.8 Hz, 1H), 7.81 (dt, J = 7.5, 1.6 Hz, 1H), 7.72 (s, 1H), 7.63 (d, J = 8.5 Hz, 1H), 7.59 (dt, J = 7.7, 1.5 Hz, 1H), 7.52 (t, J = 7.6 Hz, 1H), 7.27 (dd, J = 8.2, 1.8 Hz, 1H), 7.23 (d, J = 1.7 Hz, 1H), 7.12 (d, J = 8.2 Hz, 1H), 6.60 (s, 1H), 4.87 (s, 1H), 3.74 – 3.62 (m, 4H), 3.58 (t, J = 5.2 Hz, 2H), 3.41 – 3.31 (m, 2H), 2.29 (s, 3H), 1.79 (q, J = 3.9 Hz, 2H), 1.46 (s, 9H), 1.20 (q, J = 3.9 Hz, 2H).

LC/MS [M+H]+ m/z calc. 639.3, found 639.2.

46

N-(2-(2-aminoethoxy)ethyl)-3-(6-(1-(2,2-difluorobenzo[d][1,3]dioxol-5-yl)cyclopropane-1-carboxamido)-3-methylpyridin-2-yl)benzamide (46):
Intermediate **45** (122 mg, 0.19 mmol) was deprotected according to General Procedure B to provide the amine **46** (102 mg, 0.19 mmol, quant.) as a colorless oil.

1H NMR (400 MHz, Chloroform-d) δ 8.14 (d, J = 8.4 Hz, 1H), 7.88 (t, J = 1.7 Hz, 1H), 7.85 (s, 1H), 7.77 (s, 1H), 7.63 (d, J = 8.5 Hz, 1H), 7.57 (dt, J = 7.7, 1.5 Hz, 1H), 7.51 (t, J = 7.6 Hz, 1H), 7.27 (dd, J = 8.1, 1.8 Hz, 1H), 7.23 (d, J = 1.7 Hz, 1H), 7.12 (d, J = 8.2 Hz, 1H), 6.91 (s, 0H), 3.70 (tdd, J = 7.9, 4.0, 1.2 Hz, 4H), 3.55 (t, J = 5.2 Hz, 2H), 2.91 (t, J = 5.2 Hz, 2H), 2.29 (s, 3H), 1.79 (q, J = 3.9 Hz, 2H), 1.20 (q, J = 3.9 Hz, 2H).

**LC/MS:** [M+H]$^+$ *m/z* calc. 539.2 found 639.2.

18
LEB-3-149

N-(2-(2-(3-(5-(4-acryloyl-2-oxopiperazin-1-yl)furan-2-yl)propanamido)ethoxy)ethyl)-3-(6-(1-(2,2-difluorobenzo[d][1,3]dioxol-5-yl)cyclopropane-1-carboxamido)-3-methylpyridin-2-yl)benzamide (LEB-03-149) (**18**). Intermediate **36** (30 mg, 0.086 mmol) was deprotected and coupled to intermediate **46** (23 mg, 0.043 mmol) following General Procedure C to provide **LEB-03-149** (10.9 mg, 0.0134 mmol, 31% yield) as a white foam.

^{1}H NMR (600 MHz, Chloroform-d) δ 8.10 (d, J = 8.4 Hz, 1H), 7.88 (t, J = 1.8 Hz, 1H), 7.82 (dt, J = 7.7, 1.5 Hz, 1H), 7.72 (s, 1H), 7.60 (d, J = 8.5 Hz, 1H), 7.55 (dt, J = 7.6, 1.4 Hz, 1H), 7.48 (t, J = 7.7 Hz, 1H), 7.25 (dd, J = 8.2, 1.8 Hz, 1H), 7.21 (d, J = 1.7 Hz, 1H), 7.09 (d, J = 8.2 Hz, 1H), 6.86 (s, 1H), 6.39 (dd, J = 16.7, 1.8 Hz, 1H), 6.20 (d, J = 3.3 Hz, 1H), 6.02 (d, J = 3.2 Hz, 1H), 5.81 (dd, J = 10.4, 1.8 Hz, 1H), 3.82 (s, 2H), 3.73 (hept, J = 6.6 Hz, 2H), 3.63 (d, J = 4.1 Hz, 4H), 3.53 (t, J = 5.1 Hz, 2H), 3.41 (q, J = 5.3 Hz, 2H), 3.19 (q, J = 7.4 Hz, 2H), 2.89 (t, J = 7.5 Hz, 2H), 2.47 (t, J = 7.3 Hz, 2H), 2.26 (s, 3H), 1.48 (t, J = 7.4 Hz, 3H), 1.18 (q, J = 3.9 Hz, 2H), 0.12 – 0.06 (m, 1H).
^{13}C NMR (151 MHz, CDCl3) δ 171.77, 167.53, 165.03, 155.44, 149.75, 148.91, 144.71, 144.11, 143.59, 140.95, 140.22, 134.94, 134.55, 131.91, 131.68, 128.46, 127.72, 126.98, 126.64, 126.36, 112.96, 112.39, 110.21, 107.27, 100.91, 69.63, 69.50, 55.72, 53.43, 43.65, 39.83, 39.18, 34.69, 31.20, 24.08, 19.14, 17.18, 12.52.
HRMS (ESI): [M+H]$^+$ *m/z* calc. 813.31, found 813.3055.
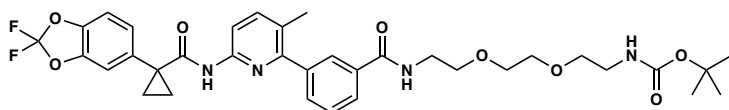
47

tert-butyl (2-(2-(2-(3-(6-(1-(2,2-difluorobenzo[d][1,3]dioxol-5-yl)cyclopropane-1-carboxamido)-3-methylpyridin-2-yl)benzamido)ethoxy)ethoxy)ethyl)carbamate (47): Lumacaftor (100 mg, 0.22 mmol) and tert-butyl (2-(2-(2-aminoethoxy)ethoxy)ethyl)carbamate (70 mg, 0.28 mmol) were reacted according to General Procedure A and purified by silica gel chromatography (0-80% EtOAc/Hex) to obtain intermediate **47** (127 mg, 0.19 mmol, 85%) as a clear colorless oil.
1H NMR (400 MHz, Chloroform-d) δ 8.14 (d, J = 8.4 Hz, 1H), 7.88 (s, 1H), 7.80 (d, J = 7.5 Hz, 1H), 7.77 – 7.72 (m, 1H), 7.63 (d, J = 8.4 Hz, 1H), 7.57 (d, J = 7.5 Hz, 1H), 7.52 (t, J = 7.6 Hz, 1H), 7.27 (dd, J = 8.2, 1.8 Hz, 1H), 7.23 (d, J = 1.7 Hz, 1H), 7.11 (d, J = 8.2 Hz, 1H), 6.74 (s, 1H), 5.02 (s, 1H), 3.75 – 3.61 (m, 8H), 3.56 (t, J = 5.4 Hz, 2H), 3.31 (d, J = 5.8 Hz, 2H), 2.28 (s, 3H), 1.79 (q, J = 3.9 Hz, 2H), 1.45 (s, 9H), 1.20 (q, J = 3.9 Hz, 2H).
LC/MS: [M+H]$^+$ *m/z* calc. 683.3, found 683.3.
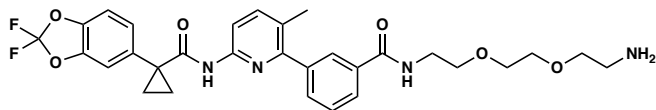
48

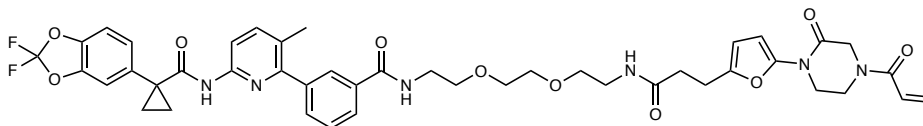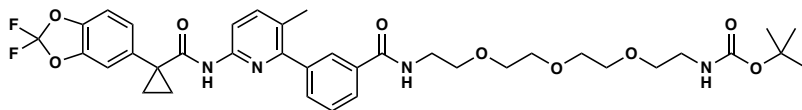## N-(2-(2-(2-aminoethoxy)ethoxy)ethyl)-3-(6-(1-(2,2-difluorobenzo[d][1,3]dioxol-5-yl)cyclopropane-1-carboxamido)-3-methylpyridin-2-yl)benzamide (48):

Intermediate **47** (127 mg, 0.19 mmol) was deprotected according to General Procedure B to provide the amine **48** (111 mg, 0.19 mmol, quant.) as a colorless oil.

1H NMR (400 MHz, Chloroform-d) δ 8.13 (d, J = 8.4 Hz, 1H), 7.89 (t, J = 1.7 Hz, 1H), 7.83 (dt, J = 7.7, 1.5 Hz, 1H), 7.78 (s, 1H), 7.63 (d, J = 8.5 Hz, 1H), 7.56 (dt, J = 7.7, 1.5 Hz, 1H), 7.51 (t, J = 7.6 Hz, 1H), 7.27 (dd, J = 8.2, 1.7 Hz, 1H), 7.23 (d, J = 1.7 Hz, 1H), 7.12 (d, J = 8.2 Hz, 1H), 7.08 (s, 1H), 3.73 – 3.62 (m, 9H), 3.51 (t, J = 5.2 Hz, 2H), 2.82 (t, J = 5.1 Hz, 2H), 2.28 (s, 3H), 1.79 (q, J = 3.9 Hz, 2H), 1.20 (q, J = 3.9 Hz, 2H).

LC/MS: [M+H]$^+$ *m/z* calc. 583.2, found 583.3.

19
LEB-3-150

N-(2-(2-(2-(3-(5-(4-acryloyl-2-oxopiperazin-1-yl)furan-2-yl)propanamido)ethoxy)ethoxy)ethyl)-3-(6-(1-(2,2-difluorobenzo[d][1,3]dioxol-5-yl)cyclopropane-1-carboxamido)-3-methylpyridin-2-yl)benzamide (LEB-03-150)

(19). Intermediate **36** (30 mg, 0.086 mmol) was deprotected and coupled to intermediate **48** (25 mg, 0.043 mmol) following General Procedure C to **provide LEB-03-150** (11.6 mg, 0.0134 mmol, 31% yield) as a clear colorless oil.

¹H NMR (600 MHz, Chloroform-d) δ 8.11 (d, J = 8.4 Hz, 1H), 7.86 (tt, J = 1.8, 1.2 Hz, 1H), 7.79 (ddd, J = 7.7, 1.8, 1.2 Hz, 1H), 7.72 (s, 1H), 7.62 – 7.58 (m, 1H), 7.55 (ddd, J = 7.6, 1.7, 1.2 Hz, 1H), 7.48 (td, J = 7.7, 0.6 Hz, 1H), 7.25 (dd, J = 8.2, 1.8 Hz, 1H), 7.21 (d, J = 1.7 Hz, 1H), 7.09 (d, J = 8.2 Hz, 1H), 6.83 (d, J = 5.8 Hz, 1H), 6.41 (dd, J = 16.7, 1.8 Hz, 1H), 6.24 (d, J = 3.2 Hz, 1H), 6.18 (s, 1H), 6.05 (dd, J = 3.3, 1.0 Hz, 1H), 5.82 (dd, J = 10.5, 1.8 Hz, 1H), 5.32 (s, 1H), 4.40 (d, J = 39.8 Hz, 2H), 3.94 (d, J = 47.9 Hz, 1H), 3.85 (s, 2H), 3.70 – 3.58 (m, 7H), 3.50 (dd, J = 5.6, 4.8 Hz, 2H), 3.39 (q, J = 5.4 Hz, 2H), 2.93 (t, J = 7.5 Hz, 2H), 2.47 (t, J = 7.5 Hz, 2H), 2.25 (s, 3H), 2.19 (s, 1H), 1.76 (q, J = 3.8 Hz, 2H), 1.47 (d, J = 12.2 Hz, 1H), 1.18 (p, J = 3.8 Hz, 2H).

¹³C NMR 151 MHz, CDCl3) δ 171.78, 171.54, 167.31, 164.98, 155.46, 148.91, 144.68, 144.12, 143.60, 140.94, 140.25, 134.93, 134.64, 131.88, 131.68, 128.46, 127.72, 126.98, 126.63, 126.51, 126.34, 113.00, 112.39, 110.19, 107.18, 100.77, 70.23, 70.18, 69.80, 55.62, 53.43, 43.58, 39.81, 39.16, 34.67, 31.20, 30.92, 23.97, 19.13, 17.19, 12.47, 1.02.

HRMS (ESI): [M+H]$^+$ *m/z* calc. 857.33, found 857.3319.

49

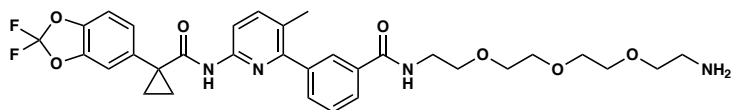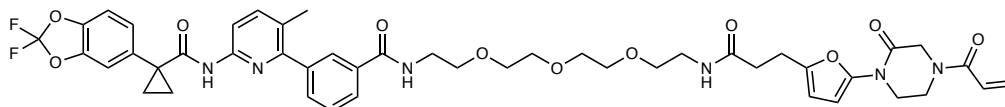**tert-butyl (1-(3-(6-(1-(2,2-difluorobenzo[d][1,3]dioxol-5-yl)cyclopropane-1-carboxamido)-3-methylpyridin-2-yl)phenyl)-1-oxo-5,8,11-trioxa-2-azatridecan-13-yl)carbamate (49):** Lumacaftor (100 mg, 0.22 mmol) and tert-butyl (2-(2-(2-(2-aminoethoxy)ethoxy)ethoxy)ethyl)carbamate (82 mg, 0.28 mmol) were reacted according to General Procedure A and purified by silica gel chromatography (0-100% EtOAc/Hex) to obtain intermediate **49** (139 mg, 0.19 mmol, 87%) as a colorless oil.
1H NMR (400 MHz, Chloroform-d) δ 8.14 (d, J = 8.4 Hz, 1H), 7.89 (s, 1H), 7.82 (d, J = 7.5 Hz, 1H), 7.73 (s, 1H), 7.63 (d, J = 8.5 Hz, 1H), 7.57 (d, J = 7.5 Hz, 1H), 7.51 (t, J = 7.6 Hz, 1H), 7.27 (dd, J = 8.2, 1.8 Hz, 1H), 7.23 (d, J = 1.7 Hz, 1H), 7.12 (d, J = 8.2 Hz, 1H), 6.80 (s, 1H), 3.73 – 3.66 (m, 9H), 3.64 (dd, J = 6.1, 3.2 Hz, 2H), 3.59 (dd, J = 6.1, 3.2 Hz, 2H), 3.50 (t, J = 5.1 Hz, 2H), 3.30 (d, J = 5.7 Hz, 2H), 2.28 (s, 3H), 1.79 (q, J = 3.9 Hz, 2H), 1.46 (s, 9H), 1.20 (q, J = 3.9 Hz, 2H).
LC/MS: [M+H]$^+$ m/z calc. 727.3, found 727.2.

50

N-(2-(2-(2-(2-aminoethoxy)ethoxy)ethoxy)ethyl)-3-(6-(1-(2,2-difluorobenzo[d][1,3]dioxol-5-yl)cyclopropane-1-carboxamido)-3-methylpyridin-2-yl)benzamide (50): Intermediate **49** (139 mg, 0.19 mmol) was deprotected according to General Procedure B to provide the amine **50** (119 mg, 0.19 mmol, quant.) as a colorless oil.
1H NMR (400 MHz, Chloroform-d) δ 8.13 (d, J = 8.4 Hz, 1H), 7.93 (t, J = 1.8 Hz, 1H), 7.87 (dt, J = 7.6, 1.6 Hz, 1H), 7.76 (s, 1H), 7.62 (d, J = 8.5 Hz, 1H), 7.60 (s, 1H), 7.55 (dt, J = 7.7, 1.5 Hz, 1H), 7.50 (t, J = 7.6 Hz, 1H), 7.27 (dd, J = 8.2, 1.7 Hz, 1H), 7.23 (d, J = 1.7 Hz, 1H), 7.12 (d, J = 8.2 Hz, 1H), 3.73 – 3.63 (m, 9H), 3.61 (dt, J = 6.0, 1.8 Hz, 4H), 3.48 – 3.43 (m, 2H), 2.82 – 2.75 (m, 2H), 2.29 (s, 3H), 1.79 (q, J = 3.9 Hz, 2H), 1.20 (q, J = 3.9 Hz, 2H).
LC/MS: [M+H]$^+$ m/z calc. 627.3, found 627.3.

20
LEB-3-151

N-(15-(5-(4-acryloyl-2-oxopiperazin-1-yl)furan-2-yl)-13-oxo-3,6,9-trioxa-12-azapentadecyl)-3-(6-(1-(2,2-difluorobenzo[d][1,3]dioxol-5-yl)cyclopropane-1-carboxamido)-3-methylpyridin-2-yl)benzamide (LEB-03-151) (20). Intermediate **36** (30 mg, 0.086 mmol) was deprotected and coupled to intermediate **50** (27 mg, 0.043

mmol) following General Procedure C to provide **LEB-03-151** (13.7 mg, 0.0152 mmol, 35% yield) as a colorless oil.

¹H NMR 1H NMR (600 MHz, Chloroform-d) δ 8.10 (d, J = 8.5 Hz, 1H), 7.87 (t, J = 1.8 Hz, 1H), 7.80 (dt, J = 7.8, 1.5 Hz, 1H), 7.73 (s, 1H), 7.60 (d, J = 8.5 Hz, 1H), 7.54 (dt, J = 7.7, 1.4 Hz, 1H), 7.48 (t, J = 7.7 Hz, 1H), 7.25 (dd, J = 8.2, 1.8 Hz, 1H), 7.21 (d, J = 1.7 Hz, 1H), 7.09 (d, J = 8.2 Hz, 1H), 6.93 (d, J = 6.0 Hz, 1H), 6.41 (dd, J = 16.7, 1.8 Hz, 1H), 6.25 (d, J = 3.2 Hz, 1H), 6.05 (d, J = 3.3 Hz, 1H), 5.82 (dd, J = 10.4, 1.8 Hz, 1H), 4.41 (d, J = 35.7 Hz, 2H), 3.95 (d, J = 50.4 Hz, 3H), 3.85 (s, 2H), 3.70 – 3.62 (m, 8H), 3.62 – 3.57 (m, 2H), 3.57 – 3.52 (m, 2H), 3.47 (dd, J = 5.6, 4.6 Hz, 2H), 3.39 (q, J = 5.3 Hz, 2H), 2.93 (t, J = 7.6 Hz, 2H), 2.47 (t, J = 7.6 Hz, 2H), 2.25 (s, 3H), 2.19 (s, 1H), 1.76 (q, J = 3.9 Hz, 2H), 1.18 (q, J = 3.9 Hz, 2H).

¹³C NMR (151 MHz, CDCl3) δ 171.78, 171.50, 167.25, 164.97, 155.52, 148.90, 144.64, 144.13, 143.60, 140.92, 140.21, 134.93, 134.65, 133.37, 131.81, 131.68, 129.98, 128.40, 127.78, 126.98, 126.62, 126.59, 126.35, 112.96, 112.38, 110.20, 107.12, 100.70, 70.43, 70.38, 70.18, 70.07, 69.85, 69.82, 53.43, 39.81, 39.19, 34.59, 31.20, 30.92, 23.93, 19.13, 17.18.

HRMS (ESI): [M+H]⁺ *m/z* calc. 901.36, found 901.3584.

Synthesis of WEE1 DUBTACs:
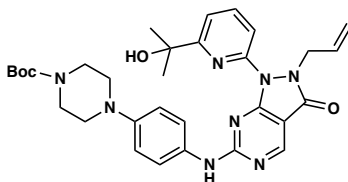
51

tert-butyl 4-(4-((2-allyl-1-(6-(2-hydroxypropan-2-yl)pyridin-2-yl)-3-oxo-2,3-dihydro-1H-pyrazolo[3,4-d]pyrimidin-6-yl)amino)phenyl)piperazine-1-carboxylate (51).
Commercially available 2-allyl-1-(6-(2-hydroxypropan-2-yl)pyridin-2-yl)-6-(methylthio)-1,2-dihydro-3H-pyrazolo[3,4-d]pyrimidin-3-one (250 mg, 0.7 mmol) was dissolved in 7mL of toluene and cooled to 0°C. meta-Chloroperoxybenzoic acid (190 mg, 0.77 mmol) was added to the reaction mixture on ice, and the reaction mixture was warmed to room temperature and stirred for 1 hour. N,N-Diisopropylethylamine (365 µL, 2.1 mmol) and 1-Piperazinecarboxylic acid, 4-(4-aminophenyl)-, 1,1-dimethylethyl ester (232 mg, 0.84 mmol) were then added slowly and the reaction mixture was stirred overnight. The reaction mixture was extracted in EtOAc, washed 3X with brine, and dried on silica. Purification by flash column chromatography (DCM/Hexane 5:95) yielded **51** (0.445 mmol, 64% yield).

¹H NMR (400 MHz, Chloroform-d) δ 8.99 (s, 1H), 7.95 (t, J = 7.9 Hz, 1H), 7.80 (dd, J = 8.1, 0.8 Hz, 1H), 7.44 (dd, J = 7.7, 0.8 Hz, 1H), 5.83 – 5.65 (m, 1H), 5.13 – 5.04 (m, 1H), 4.97 (dq, J = 17.1, 1.4 Hz, 1H), 4.85 (dt, J = 6.2, 1.4 Hz, 2H), 3.80 (s, 1H), 2.63 (s, 3H), 1.63 (s, 6H).
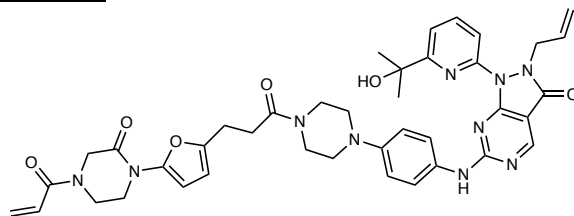
.
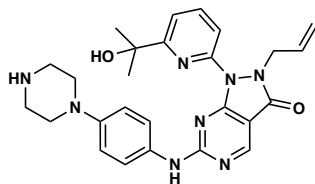
52

2-allyl-1-(6-(2-hydroxypropan-2-yl)pyridin-2-yl)-6-((4-(piperazin-1-yl)phenyl)amino)-1,2-dihydro-3H-pyrazolo[3,4-d]pyrimidin-3-one (52). Intermediate **51** (261 mg, 0.445 mmol) was dissolved in 4mL of DCM and cooled to 0°C. 1mL of trifluoroacetic acid was added dropwise on ice. The reaction mixture was stirred at room temperature for 1 hour, then extracted in DCM, washed 3X with brine, and dried on silica. Purification by flash column chromatography (DCM/Hexane 5:95) yielded **52** (0.398 mmol, 89% yield).
^{1}H NMR (400 MHz, Chloroform-d) δ 8.84 (s, 1H), 7.86 (t, J = 7.9 Hz, 1H), 7.75 (d, J = 8.1 Hz, 1H), 7.48 (d, J = 8.5 Hz, 2H), 7.34 (d, J = 7.6 Hz, 1H), 6.93 (d, J = 9.0 Hz, 2H), 5.78 – 5.59 (m, 1H), 5.04 (d, J = 10.2 Hz, 1H), 4.94 (d, J = 17.0 Hz, 1H), 4.74 (d, J = 6.2 Hz, 2H), 3.94 (s, 1H), 3.60 (t, J = 5.1 Hz, 4H), 3.11 (t, J = 5.1 Hz, 4H), 2.05 (s, 1H), 1.59 (s, 6H), 1.49 (s, 9H).

Synthesis of LEB-03-153 (30)

30
LEB-03-153

6-((4-(4-(3-(5-(4-acryloyl-2-oxopiperazin-1-yl)furan-2-yl)propanoyl)piperazin-1-yl)phenyl)amino)-2-allyl-1-(6-(2-hydroxypropan-2-yl)pyridin-2-yl)-1,2-dihydro-3H-pyrazolo[3,4-d]pyrimidin-3-one (LEB-03-153) (30). Intermediate **51** (0.0449 mmol) was dissolved in 3mL of DCM and the reaction mixture was cooled on ice. 1mL of trifluoroacetic acid was added dropwise and the solution was warmed to room temperature and stirred for 1 hour. The deprotected amine salt was washed twice with DCM and dried under vacuum. Immediately following deprotection, the crude product was dissolved in 0.5 mL DMF and **deprotected intermediate 36** (.0898 mmol) was added to the mixture, followed by DIPEA (0.449 mmol) and HATU (0.0898 mmol). The reaction was stirred for 30 minutes before water was added. The mixture was extracted three times with EtOAc, and combined organic extracts were washed with brine, dried over sodium sulfate, and concentrated. Purification by flash column chromatography (MeOH:DCM 8:92) yielded **LEB-03-153** as a light-yellow solid (12.9 mg, 0.0169 mmol, 38% yield).
**^{1}H NMR** (600 MHz, Chloroform-d) δ 8.76 (s, 1H), 7.80 (t, J = 7.9 Hz, 1H), 7.66 (d, J = 8.0 Hz, 1H), 7.43 (d, J = 8.4 Hz, 2H), 7.29 (d, J = 7.6 Hz, 1H), 7.19 (s, 1H), 6.87 – 6.82 (m, 2H), 6.45 (s, 1H), 6.34 (dd, J = 16.7, 1.8 Hz, 1H), 6.20 (d, J = 3.2 Hz, 1H), 6.01 (d, J = 3.2 Hz, 1H), 5.74 (t, J = 11.1, 10.6 Hz, 1H), 5.67 – 5.59 (m, 1H), 5.23 (s, 1H), 4.97 (dd, J = 9.8, 0.8 Hz, 1H), 4.87 (dd, J = 17.4, 0.8 Hz, 1H), 4.67 (d, J = 6.2 Hz, 2H), 4.38

(s, 1H), 4.31 (s, 1H), 3.73 (t, *J* = 5.2 Hz, 2H), 3.55 (t, *J* = 5.1 Hz, 2H), 3.06 (t, *J* = 5.2 Hz, 4H), 2.92 (t, *J* = 7.8 Hz, 2H), 2.62 (d, *J* = 8.4 Hz, 2H), 1.59 (s, 4H), 1.52 (s, 6H).
^{13}**C NMR** (151 MHz, Chloroform-d) δ 169.96, 165.90, 165.00, 162.18, 161.36, 161.26, 156.36, 150.16, 147.68, 147.51, 144.67, 138.85, 131.56, 131.29, 126.30, 119.07, 117.20, 116.21, 116.12, 107.23, 101.12, 72.46, 50.15, 49.85, 49.49, 47.67, 45.40, 41.64, 31.55, 30.56, 23.71.
HRMS (ESI): [M+H]$^+$ *m/z* calc. 761.35, found 761.3522.

Synthesis of LEB-03-144 (31)

53
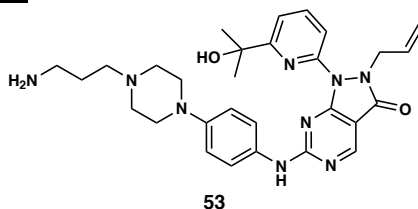
2-allyl-6-((4-(4-(3-aminopropyl)piperazin-1-yl)phenyl)amino)-1-(6-(2-hydroxypropan-2-yl)pyridin-2-yl)-1,2-dihydro-3H-pyrazolo[3,4-d]pyrimidin-3-one (53). Intermediate **52** (40 mg, 0.0823 mmol) was dissolved in 0.5 mL of DMF. tert-butyl (3-bromopropyl)carbamate (24 mg, 1.2 eq, 0.0987 mmol) and potassium carbonate (34 mg, 3.0 eq, 0.247 mmol) were added to the mixture, and the reaction was warmed to 50°C and stirred overnight. Water was added, the mixture extracted three times with EtOAc, combined organic extracts were washed with brine, and dried over sodium sulfate, and concentrated. Purification by flash column chromatography (EtOAc:Hexanes 50:50) yielded the boc-protected intermediate. This was immediately dissolved in 3mL of DCM and the reaction mixture was cooled on ice. 1 mL of trifluoroacetic acid was added dropwise and the solution was warmed to room temperature and stirred for 1 hour. The deprotected amine TFA salt was washed twice with DCM and dried under vacuum to yield **53** (33 mg, 0.0497 mmol, 60% yield over two steps) as a yellow oil.
^{1}**H NMR** (300 MHz, Chloroform-d) δ 8.80 (s, 1H), 7.92 (t, J = 7.9 Hz, 1H), 7.63 (d, J = 8.0 Hz, 1H), 7.54 (d, J = 8.4 Hz, 3H), 6.90 (d, J = 8.9 Hz, 2H), 5.75 – 5.54 (m, 1H), 5.05 (d, J = 10.2 Hz, 1H), 4.89 (d, J = 17.1 Hz, 1H), 4.75 (d, J = 6.2 Hz, 2H), 3.66 (s, 1H), 3.43 (s, 9H), 3.28 (q, J = 9.4, 8.5 Hz, 2H), 3.19 (s, 1H), 3.06 (t, J = 7.1 Hz, 2H), 2.23 (d, J = 8.2 Hz, 3H), 1.59 (s, 6H).
**LC/MS:** [M+H]$^+$ *m/z* calc. 544.3, found 544.3.
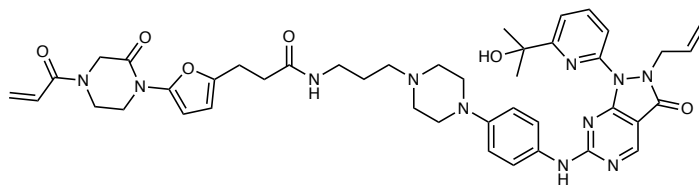
31
LEB-03-144

3-(5-(4-acryloyl-2-oxopiperazin-1-yl)furan-2-yl)-N-(3-(4-(4-((2-allyl-1-(6-(2-hydroxypropan-2-yl)pyridin-2-yl)-3-oxo-2,3-dihydro-1H-pyrazolo[3,4-d]pyrimidin-6-yl)amino)phenyl)piperazin-1-yl)propyl)propenamide (LEB-03-144) (31).
Intermediate 36 (19 mg, 0.0558 mmol) and **53** (0.0497 mmol) were reacted according to general procedure C. After hydrolysis, deprotected **36** and **53** were dissolved in DMF

(0.5 mL), followed by DIPEA (43 μL, 0.249 mmol) and HATU (23 mg, 0.0596 mmol). The reaction was stirred for 30 minutes. Water was added and the mixture extracted three times with 4:1 CHCl$_3$:IPA. Combined organic extracts were washed with brine, and dried over sodium sulfate, and concentrated. Purification by prep TLC (10% MeOH in DCM) yielded **LEB-03-144** as a light-yellow solid (8.1 mg, 0.0099 mmol, 20% yield).
^{1}H NMR (600 MHz, DMSO) δ 10.07 (s, 1H), 8.75 (s, 1H), 7.97 (s, 1H), 7.83 (t, J = 5.6 Hz, 1H), 7.68 (d, J = 8.1 Hz, 1H), 7.54 (d, J = 7.7 Hz, 1H), 7.51 (s, 2H), 6.85 (d, J = 8.6 Hz, 2H), 6.80 – 6.72 (m, 1H), 6.16 – 6.08 (m, 2H), 6.04 (d, J = 3.2 Hz, 1H), 5.71 – 5.66 (m, 1H), 5.64 – 5.55 (m, 1H), 5.24 (s, 1H), 4.92 (d, J = 10.2 Hz, 1H), 4.76 (d, J = 17.0 Hz, 1H), 4.61 (d, J = 6.0 Hz, 2H), 4.27 (d, J = 93.6 Hz, 2H), 3.95 – 3.63 (m, 4H), 3.02 (q, J = 6.4 Hz, 6H), 2.73 (t, J = 7.5 Hz, 2H), 2.31 (t, J = 7.5 Hz, 2H), 2.24 (t, J = 7.2 Hz, 2H), 1.55 – 1.47 (m, 2H), 1.39 (s, 2H), 1.17 (s, 6H), 0.80 – 0.74 (m, 2H).
^{13}C NMR (151 MHz, DMSO) δ 171.0, 168.0, 164.6, 161.6, 156.5, 150.1, 139.3, 132.7, 131.3, 128.8, 118.7, 116.8, 115.9, 106.9, 100.5, 72.8, 55.9, 53.2, 49.2, 47.6, 47.1, 46.9, 42.5, 37.4, 34.7, 33.8, 31.4, 30.9, 29.5, 26.9, 25.3, 24.0, 22.6, 22.5, 14.4.
HRMS (ESI): [M+H]$^+$ *m/z* calc. 818.41, found 818.4101.

Synthesis of LEB-3-145 (32)
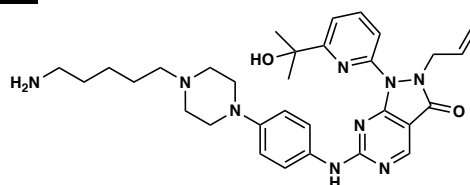
54

2-allyl-6-((4-(4-(5-aminopentyl)piperazin-1-yl)phenyl)amino)-1-(6-(2-hydroxypropan-2-yl)pyridin-2-yl)-1,2-dihydro-3H-pyrazolo[3,4-d]pyrimidin-3-one (54). Intermediate **52** (40 mg, 0.0823 mmol) was dissolved in 0.5 mL of DMF. tert-butyl (5-bromopentyl)carbamate (26 mg, 1.2 eq, 0.0987 mmol) and potassium carbonate (34 mg, 3.0 eq, 0.247 mmol) were added to the mixture, and the reaction was warmed to 50°C and stirred overnight. Water was added, the mixture extracted three times with EtOAc, combined organic extracts were washed with brine, and dried over sodium sulfate, and concentrated. Purification by flash column chromatography (EtOAc:Hexanes 50:50) yielded boc-protected intermediate. This was immediately dissolved in 3mL of DCM and the reaction mixture was cooled on ice. 1mL of trifluoroacetic acid was added dropwise and the solution was warmed to room temperature and stirred for 1 hour. The deprotected amine TFA salt was washed twice with DCM and dried under vacuum to yield **54** (21 mg, 0.0307 mmol, 37% yield over two steps) as a yellow oil.
^{1}H NMR (300 MHz, Chloroform-d) δ 8.80 (s, 1H), 8.12 (s, 1H), 7.94 (t, J = 7.9 Hz, 1H), 7.64 (d, J = 8.0 Hz, 1H), 7.56 (d, J = 8.2 Hz, 3H), 6.92 (d, J = 8.8 Hz, 2H), 5.67 (dd, J = 16.8, 10.4 Hz, 1H), 5.07 (d, J = 10.2 Hz, 1H), 4.90 (d, J = 17.1 Hz, 1H), 4.76 (d, J = 6.2 Hz, 2H), 3.69 (s, 1H), 3.55 – 3.47 (m, 8H), 3.22 (s, 1H), 3.19 – 2.89 (m, 4H), 1.91 – 1.66 (m, 4H), 1.61 (s, 6H), 1.51 (s, 2H), 1.27 (s, 1H).
LC/MS: [M+H]$^+$ *m/z* calc. 572.3, found 572.3.
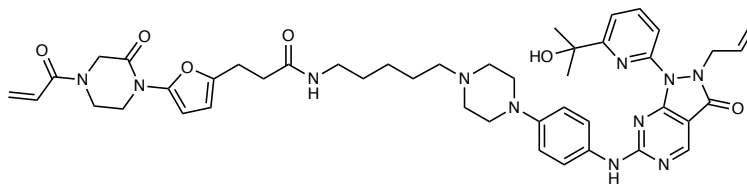
32
LEB-03-145

3-(5-(4-acryloyl-2-oxopiperazin-1-yl)furan-2-yl)-N-(5-(4-(4-((2-allyl-1-(6-(2-hydroxypropan-2-yl)pyridin-2-yl)-3-oxo-2,3-dihydro-1H-pyrazolo[3,4-d]pyrimidin-6-yl)amino)phenyl)piperazin-1-yl)pentyl)propanamide (LEB-03-145) (32).
**Intermediate 36** (19 mg, 0.0558 mmol) and **54** (21 mg, 0.0307 mmol) were coupled according to general procedure C. After hydrolysis, deprotected **36** and **54** were dissolved in DMF (0.5 mL), followed by DIPEA (27 µL, 0.153 mmol) and HATU (14 mg, 0.0368 mmol). Water was added and the mixture extracted three times with 4:1 CHCl$_3$:IPA. Combined organic extracts were washed with brine, and dried over sodium sulfate, and concentrated. Purification by prep TLC (8% MeOH in DCM) yielded **LEB-03-145** as a light-yellow solid (10.1 mg, 0.0119 mmol, 39% yield).
^{1}H NMR (600 MHz, DMSO-d6) δ 10.15 (s, 1H), 8.83 (s, 1H), 8.05 (s, 1H), 7.86 (t, J = 5.6 Hz, 1H), 7.78 – 7.72 (m, 1H), 7.61 (d, J = 7.7 Hz, 2H), 7.58 (s, 2H), 6.92 (d, J = 8.7 Hz, 2H), 6.88 – 6.76 (m, 1H), 6.24 – 6.19 (m, 1H), 6.10 (d, J = 3.2 Hz, 1H), 5.76 (q, J = 9.8, 8.3 Hz, 1H), 5.72 – 5.61 (m, 1H), 5.36 – 5.26 (m, 1H), 5.00 (dq, J = 10.3, 1.3 Hz, 1H), 4.84 (dq, J = 17.2, 1.5 Hz, 1H), 4.69 (d, J = 6.0 Hz, 2H), 4.43 (s, 1H), 4.27 (s, 1H), 3.95 (d, J = 5.8 Hz, 1H), 3.86 (s, 1H), 3.82 – 3.73 (m, 2H), 3.13 – 3.08 (m, 4H), 3.08 – 3.01 (m, 2H), 2.80 (t, J = 7.5 Hz, 2H), 2.38 (t, J = 7.5 Hz, 2H), 2.30 (t, J = 7.4 Hz, 2H), 1.47 (s, 6H), 1.45 – 1.37 (m, 2H), 1.26 – 1.21 (m, 6H), 0.89 – 0.81 (m, 2H).
^{13}C NMR (151 MHz, DMSO) δ 170.97, 168.04, 161.64, 156.46, 150.07, 139.28, 132.67, 128.77, 118.72, 115.93, 106.92, 100.44, 72.78, 58.33, 53.28, 49.17, 47.57, 47.06, 46.88, 42.46, 38.88, 33.80, 30.92, 29.54, 29.48, 29.16, 26.48, 24.81, 24.00, 22.56, 14.42.
HRMS (ESI): [M+H]$^+$ *m/z* calc. 846.44, found 846.4395.
<u>**Synthesis of LEB-3-146 (33)**</u>
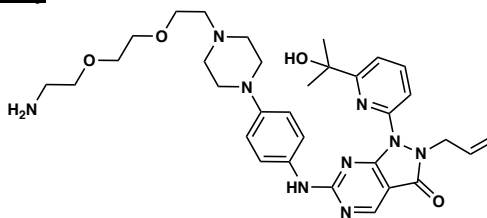
55

2-allyl-6-((4-(4-(2-(2-(2-aminoethoxy)ethoxy)ethyl)piperazin-1-yl)phenyl)amino)-1-(6-(2-hydroxypropan-2-yl)pyridin-2-yl)-1,2-dihydro-3H-pyrazolo[3,4-d]pyrimidin-3-one (55). Intermediate **52** (40 mg, 0.0823 mmol) was dissolved in 0.5 mL of DMF. tert-butyl (2-(2-(bromomethoxy)ethoxy)ethyl)carbamate (31 mg, 1.2 eq, 0.0987 mmol) and potassium carbonate (34 mg, 3.0 eq, 0.247 mmol) were added to the mixture, and the reaction was warmed to 50°C and stirred overnight. Water was added, the mixture extracted three times with EtOAc, combined organic extracts were washed with brine, and dried over sodium sulfate, and concentrated. Purification by flash column chromatography (EtOAc:Hexanes 50:50) yielded boc-protected intermediate. This was

immediately dissolved in 3mL of DCM and the reaction mixture was cooled on ice. 1mL of trifluoroacetic acid was added dropwise and the solution was warmed to room temperature and stirred for 1 hour. The deprotected amine TFA salt was washed twice with DCM and dried under vacuum to yield **55** (28 mg, 0.0389 mmol, 47% yield).
^{1}H NMR (300 MHz, Chloroform-d) δ 10.99 (s, 1H), 8.74 (s, 1H), 8.25 (s, 1H), 7.97 (t, J = 7.9 Hz, 1H), 7.60 (t, J = 8.9 Hz, 2H), 7.50 (d, J = 8.5 Hz, 2H), 6.87 (d, J = 8.7 Hz, 2H), 5.66 (ddd, J = 16.5, 10.3, 5.6 Hz, 1H), 5.07 (d, J = 10.2 Hz, 1H), 4.90 (d, J = 17.1 Hz, 1H), 4.75 (d, J = 6.3 Hz, 4H), 3.87 (d, J = 4.6 Hz, 4H), 3.76 – 3.69 (m, 4H), 3.65 (s, 4H), 3.39 – 3.10 (m, 8H), 1.61 (s, 6H).
LC/MS: [M+H]$^+$ *m/z* calc. 618.3, found 618.3.
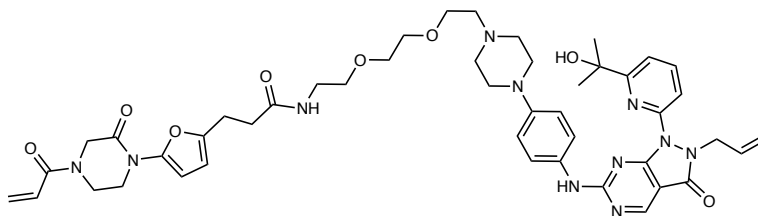
33
LEB-03-146

3-(5-(4-acryloyl-2-oxopiperazin-1-yl)furan-2-yl)-N-(2-(2-(2-(4-(4-((2-allyl-1-(6-(2-hydroxypropan-2-yl)pyridin-2-yl)-3-oxo-2,3-dihydro-1H-pyrazolo[3,4-d]pyrimidin-6-yl)amino)phenyl)piperazin-1-yl)ethoxy)ethoxy)ethyl)propanamide (LEB-03-146) (33). Intermediate 36 (19 mg, 0.0558 mmol) and **55** (28 mg, 0.0389 mmol) were coupled according to general procedure C. After hydrolysis, deprotected **36** and **55** were dissolved in DMF (0.5 mL), followed by DIPEA (34 µL, 0.195 mmol) and HATU (18 mg, 0.0466 mmol). The reaction was stirred for 30 minutes. Water was added and the mixture extracted three times with 4:1 CHCl$_3$:IPA. Combined organic extracts were washed with brine, and dried over sodium sulfate, and concentrated. Purification by prep TLC (8% MeOH in DCM) yielded **LEB-03-146** as a light-yellow solid (8.3 mg, 0.0093 mmol, 17% yield).
^{1}H NMR (600 MHz, DMSO-d6) δ 8.83 (s, 1H), 8.05 (s, 1H), 7.97 (t, J = 5.8 Hz, 1H), 7.76 (s, 1H), 7.61 (d, J = 7.8 Hz, 1H), 7.58 (s, 3H), 6.92 (d, J = 8.5 Hz, 2H), 6.81 (d, J = 12.8 Hz, 1H), 6.23 – 6.15 (m, 2H), 6.10 (d, J = 3.2 Hz, 1H), 5.76 (d, J = 7.0 Hz, 2H), 5.67 (ddt, J = 16.5, 10.8, 6.0 Hz, 1H), 5.31 (s, 1H), 5.04 – 4.97 (m, 1H), 4.87 – 4.80 (m, 1H), 4.69 (s, 2H), 4.42 (s, 1H), 4.26 (s, 1H), 3.94 (s, 1H), 3.85 (s, 1H), 3.77 (d, J = 24.8 Hz, 2H), 3.56 (t, J = 5.8 Hz, 2H), 3.54 – 3.49 (m, 6H), 3.42 (t, J = 5.9 Hz, 2H), 3.22 (q, J = 5.8 Hz, 2H), 3.09 (d, J = 5.8 Hz, 4H), 2.79 (t, J = 7.6 Hz, 2H), 2.58 (t, J = 4.8 Hz, 4H), 2.44 – 2.36 (m, 4H), 1.47 (s, 6H), 0.86 (d, J = 7.4 Hz, 1H).
^{13}C NMR (151 MHz, DMSO) δ 171.31, 168.04, 161.64, 156.46, 150.02, 139.28, 132.68, 128.76, 118.72, 115.93, 106.93, 100.44, 72.78, 70.12, 70.04, 69.58, 68.89, 57.72, 53.63, 49.14, 47.07, 46.88, 42.46, 39.07, 33.65, 30.92, 29.49, 23.89, 14.42.
HRMS (ESI): [M+H]$^+$ *m/z* calc. 892.45, found 892.4454.

Synthesis of NJH-2-106 (29)
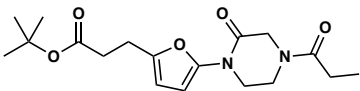
56

tert-butyl 3-(5-(2-oxo-4-propionylpiperazin-1-yl)furan-2-yl)propanoate (56):
Intermediate **35** (benzyl (E)-4-(5-(3-(tert-butoxy)-3-oxoprop-1-en-1-yl)furan-2-yl)-3-oxopiperazine-1-carboxylate) (85 mg, 0.20 mmol) was dissolved in EtOH (5 mL) and Pd/C (10 mg, 10% wt.) was added. The atmosphere was exchanged for hydrogen (balloon) and the mixture was stirred vigorously overnight. After 16h, the suspension was diluted with DCM and filtered through Celite to remove Pd/C, then concentrated. The crude residue was redissolved in DCM (2 mL), and TEA (83 µL, 0.60 mmol) was added. The solution was then cooled to 0 °C and propionyl chloride (25 µL, 0.31 mmol) was added and the mixture stirred for 30 min at 0 °C. Water was added and the mixture was extracted with DCM three times. Organic extracts were combined, washed with brine, dried over sodium sulfate, and concentrated. The crude residue was purified by silica gel chromatography to provide **56** (48 mg, 0.14 mmol, 69% yield over two steps) as a white solid.
1H NMR (600 MHz, CDCl3) δ 6.28 (d, J = 3.2 Hz, 1H), 6.04 (d, J = 3.2 Hz, 1H), 4.40 (s, 1H), 4.29 (s, 1H), 3.91 (dt, J = 30.8, 5.3 Hz, 2H), 3.85 – 3.78 (m, 2H), 2.88 (t, J = 7.6 Hz, 2H), 2.54 (t, J = 7.5 Hz, 2H), 2.43 – 2.34 (m, 2H), 1.44 (s, 9H), 1.19 (q, J = 6.9 Hz, 3H).
LC/MS: [M+H]$^+$ *m/z* calc. 351.2, found 351.2.
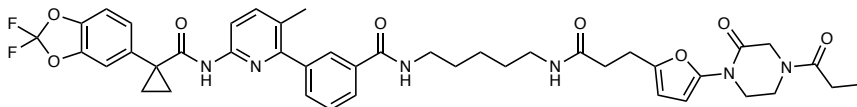

29
NJH-2-106

3-(6-(1-(2,2-difluorobenzo[d][1,3]dioxol-5-yl)cyclopropane-1-carboxamido)-3-methylpyridin-2-yl)-N-(5-(3-(5-(2-oxo-4-propionylpiperazin-1-yl)furan-2-yl)propanamido)pentyl)benzamide (NJH-2-106) (29): Intermediate **56** (15 mg, 0.043 mmol) and Intermediate **42** (15 mg, 0.029 mmol) were reacted according to General Procedure C to provide **NJH-2-106** (18 mg, 0.022 mmol, 76%) as a clear colorless oil.
1H NMR (400 MHz, CDCl3) δ 8.10 (d, J = 8.4 Hz, 1H), 7.82 (s, 1H), 7.79 (d, J = 7.6 Hz, 1H), 7.72 (s, 1H), 7.59 (d, J = 8.5 Hz, 1H), 7.52 (d, J = 7.7 Hz, 1H), 7.46 (t, J = 7.6 Hz, 1H), 7.22 (dd, J = 8.1, 1.8 Hz, 1H), 7.19 (d, J = 1.7 Hz, 1H), 7.07 (d, J = 8.1 Hz, 1H), 6.51 – 6.39 (m, 1H), 6.22 – 6.15 (m, 1H), 6.02 – 5.97 (m, 1H), 5.88 – 5.76 (m, 1H), 4.31 (d, J = 50.6 Hz, 2H), 3.96 – 3.71 (m, 4H), 3.42 (q, J = 6.6 Hz, 2H), 3.21 (q, J = 6.5 Hz, 2H), 2.92 – 2.82 (m, 2H), 2.44 (t, J = 7.4 Hz, 2H), 2.41 – 2.29 (m, 2H), 2.24 (s, 3H), 1.74 (q, J = 3.9 Hz, 2H), 1.64 – 1.56 (m, 2H), 1.53 – 1.43 (m, 2H), 1.38 – 1.26 (m, 2H), 1.21 – 1.09 (m, 5H).
13C NMR (151 MHz, CDCl3) δ 206.9, 172.2, 171.8, 167.3, 155.4, 149.8, 148.9, 144.9, 144.1, 143.6, 141.0, 140.1, 134.9, 134.8, 131.7, 131.7, 128.4, 127.5, 127.0, 126.6, 113.0, 112.4, 110.2, 107.3, 100.9, 53.4, 49.3, 47.2, 42.4, 39.7, 39.1, 38.7, 34.9, 31.2, 29.0, 26.5, 24.2, 23.8, 19.1, 17.2, 9.0.

HRMS (ESI): [M+H]⁺ *m/z* calc. 813.3345, found 813.3422.

## Synthesis of NJH-2-080 (2):
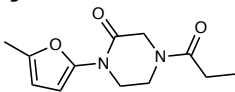
2
NJH-2-080

1-(5-methylfuran-2-yl)-4-propionylpiperazin-2-one (NJH-2-080) (2): 1-(5-methylfuran-2-yl)piperazin-2-one (30 mg, 0.17 mmol) was dissolved in DCM (2 mL). The solution was cooled to 0 °C and TEA (69 µL, 0.50 mmol) and propionyl chloride (21 µL, 0.25 mmol) were added. After stirring at 0 °C for 30 min, water was added, and the reaction extracted three times with DCM. Organic extracts were combined, washed with brine, dried over sodium sulfate, and concentrated. The crude residue was purified by silica gel chromatography (0-100% EtOAc/Hex) to provide **NJH-2-080** (17.3 mg, 0.073 mmol, 43%) as a white solid.

1H NMR (600 MHz, CDCl3) δ 6.25 (d, J = 3.2 Hz, 1H), 6.00 (d, J = 2.2 Hz, 1H), 4.41 (s, 1H), 4.29 (s, 1H), 3.97 – 3.86 (m, 2H), 3.82 (t, J = 5.5 Hz, 2H), 2.45 – 2.34 (m, 2H), 2.27 (s, 3H), 1.23 – 1.16 (m, 3H). 13C NMR (151 MHz, CDCl3) δ 172.2, 163.4, 147.5, 144.4, 107.2, 101.0, 49.3, 46.9, 38.8, 26.5, 13.4, 9.0.

13C NMR (151 MHz, CDCl3) δ 172.2, 163.4, 147.5, 144.4, 107.2, 101.0, 49.3, 46.9, 38.8, 26.5, 13.4, 9.0.

HRMS (ESI): [M+H]⁺ *m/z* calc. 259.1160, found 259.1053.

Synthesis of NJH-2-075 (13):
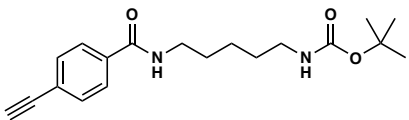
57

tert-butyl (5-(4-ethynylbenzamido)pentyl)carbamate (57): 4-ethynylbenzoic acid (27 mg, 0.19 mmol), N-Boc-1,5-diaminopentane (47 mg, 0.23 mmol), HOBt (26 mg, 0.19 mmol), and DIEA (165 µL, 0.95 mmol) were dissolved in DCM (1.5 mL) and EDCI•HCl (73 mg, 0.38 mmol) was added. After stirring the mixture for 16h at rt, water was added, the mixture partitioned, and the aqueous phase extracted with DCM. Combined organic extracts were washed with brine and dried over Na₂SO₄, concentrated, and the crude residue was purified by silica gel chromatography (0-50% EtOAc/Hex) to obtain the Boc-protected amine **57** (27 mg, 0.082 mmol, 43%) as a white solid.

1H NMR (300 MHz, CDCl₃) δ 7.78 (d, J = 8.3 Hz, 2H), 7.59 (d, J = 8.7 Hz, 2H), 6.32 (s, 1H), 4.63 (s, 1H), 3.50 (td, J = 7.0, 5.7 Hz, 2H), 3.23 (s, 1H), 3.18 (q, J = 6.5 Hz, 2H), 1.70 (d, J = 7.5 Hz, 2H), 1.62 – 1.52 (m, 2H), 1.46 (s, 11H).

LC/MS [M+H]+ m/z calc. 331.19, found 331.1.

58
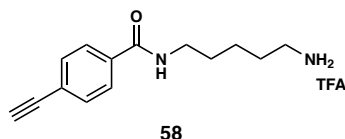
N-(5-aminopentyl)-4-ethynylbenzamide (58): tert-butyl (5-(4-ethynylbenzamido)pentyl)carbamate **57** (27 mg, 0.082 mmol) was dissolved in DCM (1 mL) and TFA (0.5 mL) was added. After stirring at rt for 2h, the mixture was diluted in DCM and evaporated repeatedly to remove volatiles and provide the amine as a TFA salt and an orange oil (32 mg, 0.096 mmol, 117%), which was used without further purification.

1H NMR (400 MHz, DMSO) δ 8.55 (t, J = 5.7 Hz, 1H), 7.84 (d, J = 8.2 Hz, 2H), 7.63 (s, 2H), 7.57 (d, J = 8.1 Hz, 2H), 4.39 (s, 1H), 3.26 (q, J = 6.6 Hz, 2H), 2.83 – 2.74 (m, 2H), 1.62 – 1.48 (m, 4H), 1.40 – 1.32 (m, 2H).

LC/MS [M+H]$^+$ m/z calc. 231.14, found 231.1.

13
NJH-2-075
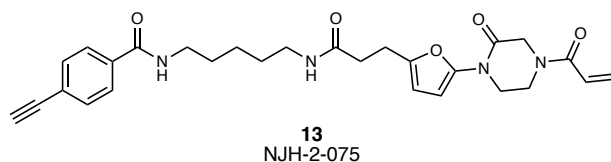
N-(5-(3-(5-(4-acryloyl-2-oxopiperazin-1-yl)furan-2-yl)propanamido)pentyl)-4-ethynylbenzamide (NJH-2-075) (13): Intermediate 36, tert-butyl 3-(5-(4-acryloyl-2-oxopiperazin-1-yl)furan-2-yl)propanoate, (20 mg, 0.057 mmol) was dissolved in DCM (0.5 mL) and treated with TFA (0.25 mL). The mixture was stirred at rt for 45 minutes until the starting material was consumed, followed by dilution with DCM and evaporation to remove volatiles. The carboxylic acid was then dissolved in DMF, and intermediate **58** N-(5-aminopentyl)-4-ethynylbenzamide TFA (22 mg, 0.062 mmol), DIEA (50 µL, 0.29 mmol), and HATU (43 mg, 0.11 mmol) were added. After stirring the mixture at rt for 1 h, water was added. The resulting suspension was extracted three times with DCM. Combined organic extracts were washed brine and dried over Na$_2$SO$_4$, concentrated, and the crude residue was purified by silica gel chromatography (0-4% MeOH/DCM) to obtain **NJH-2-075** (7.6 mg, 0.016 mmol, 27%) as a pale yellow oil.

1H NMR (300 MHz, CDCl$_3$) δ 7.82 (d, J = 8.3 Hz, 2H), 7.58 (d, J = 8.3 Hz, 2H), 6.77 – 6.50 (m, 2H), 6.43 (dd, J = 16.7, 2.1 Hz, 1H), 6.24 (d, J = 3.2 Hz, 1H), 6.06 (d, J = 3.3 Hz, 1H), 5.93 (s, 1H), 5.86 (dd, J = 10.1, 2.1 Hz, 1H), 4.44 (d, J = 17.4 Hz, 2H), 4.01 (s, 2H), 3.91 – 3.84 (m, 2H), 3.46 (q, J = 6.6 Hz, 2H), 3.32 – 3.19 (m, 3H), 2.93 (t, J = 7.2 Hz, 2H), 2.50 (t, J = 7.3 Hz, 2H), 1.72 – 1.61 (m, 2H), 1.60 – 1.46 (m, 2H), 1.44 – 1.35 (m, 2H).

13C NMR (151 MHz, DMSO) δ 171.0, 165.7, 164.6, 150.1, 135.2, 132.1, 128.8, 127.9, 124.7, 106.9, 100.5, 83.4, 83.1, 38.9, 33.8, 29.3, 29.2, 24.3, 24.0.

HRMS [M+H]$^+$ m/z calc. 380.1586, found 380.1581.

Synthesis of EZ-1-032 (3)
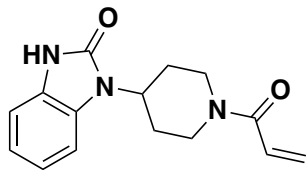
**1-(1-acryloylpiperidin-4-yl)-1,3-dihydro-2H-benzo[d]imidazol-2-one (EZ-1-032) (3):**
1-(piperidin-4-yl)-1,3-dihydro-2*H*-benzo[*d*]imidazol-2-one (50 mg, 0.23 mmol) was acylated via general procedure H and the crude residue was purified by silica gel chromatography (0 to 20% MeOH/DCM) to afford the title compound as a clear yellow oil (11.8 mg, 0.043 mmol, 19%).
1H NMR (400 MHz, DMSO) δ 10.87 (s, 1H), 7.29 – 7.17 (m, 1H), 7.05 – 6.95 (m, 3H), 6.88 (ddd, J = 16.1, 10.5, 3.3 Hz, 1H), 6.16 (d, J = 2.4 Hz, 1H), 5.70 (dd, J = 10.4, 2.4 Hz, 1H), 4.61 (d, J = 13.1 Hz, 1H), 4.44 (tt, J = 12.0, 3.9 Hz, 1H), 4.21 (d, J = 13.8 Hz, 1H), 3.21 (t, J = 13.3 Hz, 1H), 2.76 (t, J = 12.9 Hz, 1H), 2.34 – 2.07 (m, 2H), 1.75 (d, J = 12.4 Hz, 2H).
13C NMR (151 MHz, DMSO) δ 164.8, 154.2, 129.7, 129.0, 129.0, 127.7, 121.1, 120.9, 109.3, 109.0, 50.3, 45.1, 41.6, 29.9, 29.0.
HRMS (ESI): [M+H]⁺ *m/z* calc. 272.14, found 272.1394.
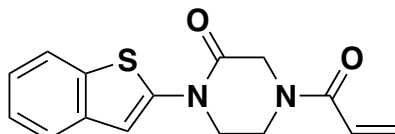
Synthesis of EZ-1-038 (4)
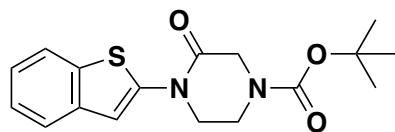
***tert*-butyl 4-(benzo[*b*]thiophen-2-yl)-3-oxopiperazine-1-carboxylate** (**59**): 2-bromobenzo[*b*]thiophene (100 mg, 0.47 mmol) was coupled to *tert*-butyl 3-oxopiperazine-1-carboxylate (93.5 mg, 0.47 mmol) via general procedure D and the crude residue was purified by silica gel chromatography (0 to 100% EtOAc/hexane) to yield a pale yellow solid (22.3 mg, 0.116 mmol, 14%).
1H NMR (400 MHz, CDCl3) δ 7.81 (d, J = 7.8 Hz, 1H), 7.72 (d, J = 7.7 Hz, 1H), 7.30 (s, 2H), 6.92 (s, 1H), 4.40 (s, 2H), 4.01 (t, J = 5.4 Hz, 2H), 3.92 (t, J = 5.4 Hz, 2H), 1.54 (s, 9H).
**LC/MS:** [M+H]⁺ *m/z* calc. 333.1, found 333.1

4-acryloyl-1-(benzo[b]thiophen-2-yl)piperazin-2-one (EZ-1-038) (4): *tert*-butyl 4-(benzo[*b*]thiophen-2-yl)-3-oxopiperazine-1-carboxylate (**59**) (18 mg, 0.05 mmol) was deprotected and acylated via general procedures F and H respectively. The crude residue was purified by silica gel chromatography (0 to 100% EtOAc/Hex) to afford the title compound as a pale yellow solid (6.6 mg, 0.023 mmol, 46%).

1H NMR (400 MHz, DMSO) δ 7.86 (d, J = 7.9 Hz, 1H), 7.74 (t, J = 7.2 Hz, 1H), 7.45 – 7.32 (m, 1H), 7.28 (q, J = 6.8 Hz, 1H), 7.11 (s, 1H), 6.98 – 6.77 (m, 1H), 6.21 (d, J = 16.7 Hz, 1H), 5.83 – 5.74 (m, 1H), 4.50 (d, J = 68.5 Hz, 2H), 4.18 – 3.91 (m, 4H).
13C NMR (151 MHz, DMSO) δ 164.7, 142.0, 136.7, 136.2, 128.9, 128.0, 124.9, 123.9, 122.8, 122.1, 108.0, 49.2, 48.4, 47.6, 46.8.
**HRMS (ESI):** [M+Na]$^+$ *m/z* calc. 309.0674, found 309.0667.

Synthesis of EZ-1-045 (5)
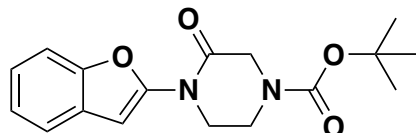
***tert*-butyl 4-(benzofuran-2-yl)-3-oxopiperazine-1-carboxylate (60):** 2-bromobenzofuran (200 mg, 1.02 mmol) was coupled with *tert*-butyl 3-oxopiperazine-1-carboxylate (204.24 mg, 1.02 mmol) via general procedure D and purified by silica gel chromatography (0 to 50% EtOAc/hexane) to yield a yellow solid (44.3 mg, 0.14 mmol, 14%).
1H NMR (400 MHz, CDCl3) δ 7.65 – 7.52 (m, 1H), 7.48 – 7.39 (m, 1H), 7.26 (dd, J = 6.0, 3.3 Hz, 2H), 6.96 (d, J = 1.2 Hz, 1H), 4.35 (s, 2H), 4.19 – 4.05 (m, 2H), 3.86 (d, J = 5.6 Hz, 2H), 1.53 (d, J = 1.6 Hz, 9H).
**LC/MS:** [M+H]$^+$ *m/z* calc. 316.1, found 316.2
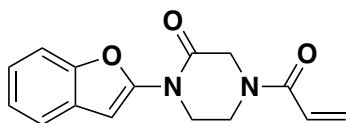
4-acryloyl-1-(benzofuran-2-yl)piperazin-2-one (EZ-1-045) (5): *tert*-butyl 4-(benzofuran-2-yl)-3-oxopiperazine-1-carboxylate (**60**) (44.3 mg, 0.14 mmol) was deprotected and acylated via general procedures F and H and purified by silica gel chromatography (0 to 50% EtOAc/hexane) to afford the title compound as a pale yellow solid (9.3 mg, 0.034 mmol, 25%).
1H NMR (300 MHz, CDCl3) δ 7.63 – 7.51 (m, 1H), 7.43 (dt, J = 7.1, 3.8 Hz, 1H), 7.29 (td, J = 6.3, 2.8 Hz, 2H), 6.98 (d, J = 1.0 Hz, 1H), 6.57 (d, J = 9.8 Hz, 1H), 6.47 (dd, J = 16.7, 2.2 Hz, 1H), 5.88 (dd, J = 10.1, 2.2 Hz, 1H), 4.52 (s, 2H), 4.24 – 3.92 (m, 4H).
13C NMR (151 MHz, DMSO) δ 165.0, 150.1, 149.5, 129.0, 128.8, 128.1, 123.9, 123.9, 121.2, 111.1, 94.6, 49.5, 47.1, 46.6, 42.4.
**HRMS (ESI):** [M+H]$^+$ *m/z* calc. 271.1004, found 271.1078.

Synthesis of EZ-1-055 (9)
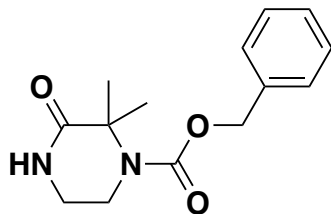
benzyl 2,2-dimethyl-3-oxopiperazine-1-carboxylate (61): 3,3-dimethylpiperazin-2-one (400 mg, 3.12 mmol) was protected with benzyl chloroformate via general procedure E and purified by silica gel chromatography (0 to 10% MeOH/DCM) to yield a fluffy white powder (492.1 mg, 1.88 mmol, 60%).
1H NMR (300 MHz, CDCl3) δ 7.41 (s, 5H), 6.02 (s, 1H), 5.19 (s, 2H), 3.87 – 3.74 (m, 2H), 3.49 – 3.35 (m, 2H), 1.75 (s, 6H).
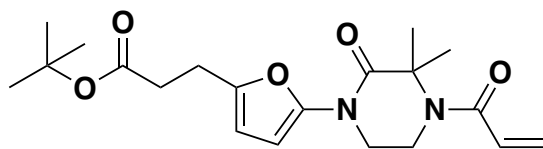**LC/MS:** [M+H]+ *m/z* calc. 263.1, found 263.1.
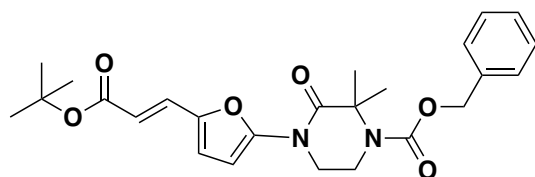
benzyl (*E*)-4-(5-(3-(*tert*-butoxy)-3-oxoprop-1-en-1-yl)furan-2-yl)-2,2-dimethyl-3-oxopiperazine-1-carboxylate (62): *tert*-butyl (E)-3-(5-bromofuran-2-yl)acrylate (Intermediate **2**) (104 mg, 0.38 mmol) and benzyl 2,2-dimethyl-3-oxopiperazine-1-carboxylate (**61**) (100 mg, 0.38 mmol) were coupled via general procedure D and purified by silica gel chromatography (0 to 50% EtOAc/hexane) to yield a clear yellow oil that solidified upon standing (133.7 mg, 0.29 mmol, 77%).
1H NMR (400 MHz, CDCl3) δ 7.43 (d, J = 5.1 Hz, 6H), 6.66 (q, J = 3.6 Hz, 2H), 6.12 (d, J = 15.6 Hz, 1H), 5.22 (s, 2H), 4.04 – 3.98 (m, 2H), 3.91 (d, J = 5.2 Hz, 2H), 1.80 (s, 6H), 1.56 (d, J = 4.0 Hz, 9H).
**LC/MS:** [M+H]+ *m/z* calc. 455.2, found 455.2

***tert*-butyl 3-(5-(4-acryloyl-3,3-dimethyl-2-oxopiperazin-1-yl)furan-2-yl)propanoate (EZ-1-055) (9):** benzyl (*E*)-4-(5-(3-(*tert*-butoxy)-3-oxoprop-1-en-1-yl)furan-2-yl)-2,2-dimethyl-3-oxopiperazine-1-carboxylate (**62**) (30 mg, 0.066 mmol) was deprotected and acylated via general procedures G and H and purified by silica gel chromatography (0-70% EtOAc/hexane) to afford the title compound as a clear colorless oil (7.2 mg, 0.019 mmol, 29% over two steps).
1H NMR (400 MHz, CDCl3) δ 6.51 (ddd, J = 16.8, 10.6, 2.3 Hz, 1H), 6.29 (t, J = 2.9 Hz, 1H), 6.23 (dt, J = 16.8, 2.1 Hz, 1H), 6.03 (d, J = 3.2 Hz, 1H), 5.70 (dt, J = 10.5, 2.1 Hz, 1H), 3.88 (dd, J = 6.4, 3.4 Hz, 2H), 3.78 (dd, J = 6.1, 3.6 Hz, 2H), 2.87 (t, J = 7.6 Hz, 2H), 2.54 (td, J = 7.9, 2.3 Hz, 2H), 1.83 (d, J = 2.3 Hz, 6H), 1.44 (d, J = 2.3 Hz, 9H).
13C NMR (151 MHz, DMSO) δ 171.6, 171.1, 166.3, 149.1, 146.2, 131.5, 127.2, 107.2, 99.7, 80.4, 63.6, 47.5, 42.7, 28.2, 23.8, 23.5.

**HRMS (ESI):** [M+Na]$^+$ *m/z* calc. 399.1896, found 399.1883.

Synthesis of EZ-1-058 (10)
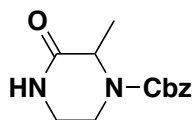
Benzyl 2-methyl-3-oxopiperazine-1-carboxylate (63): 3-methylpiperazin-2-one (400 mg, 3.5 mmol) was protected with benzyl chloroformate via general procedure E and purified by silica gel chromatography (0 to 10% MeOH/DCM) to yield a pale yellow solid (123.9 mg, 0.5 mmol, 14%).
1H NMR (300 MHz, CDCl3) δ 7.36 (s, 5H), 5.96 (s, 1H), 5.16 (s, 2H), 4.69 (s, 1H), 4.18 (s, 1H), 3.47 (d, J = 12.1 Hz, 1H), 3.27 (d, J = 12.2 Hz, 2H), 1.46 (d, J = 7.1 Hz, 3H).
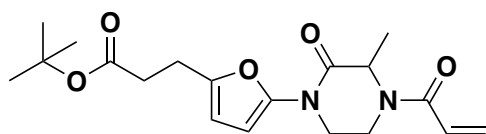**LC/MS:** [M+H]$^+$ *m/z* calc. 249.1, found 249.1.
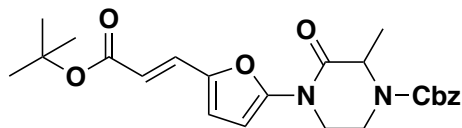
benzyl (E)-4-(5-(3-(tert-butoxy)-3-oxoprop-1-en-1-yl)furan-2-yl)-2-methyl-3-oxopiperazine-1-carboxylate (64): Benzyl 2-methyl-3-oxopiperazine-1-carboxylate (**63**) (60 mg, 0.24 mmol) and *tert*-butyl (E)-3-(5-bromofuran-2-yl)acrylate (EZ-1-048) (66 mg, 0.24 mmol) were coupled via general procedure D and purified by silica gel chromatography (0 to 50% EtOAc/hexane) to yield a yellow solid (69.3 mg, 0.16 mmol, 66%).
1H NMR (400 MHz, CDCl3) δ 7.42 (s, 5H), 7.32 – 7.24 (m, 1H), 6.70 – 6.62 (m, 2H), 6.12 (d, J = 15.4 Hz, 1H), 5.23 (d, J = 2.5 Hz, 2H), 4.89 (s, 1H), 4.35 (s, 1H), 4.00 (d, J = 13.9 Hz, 2H), 3.50 (s, 1H), 1.72 – 1.49 (m, 12H).
LC/MS: [M+H]$^+$ *m/z* calc. 441.2, found 441.2.

**tert-butyl 3-(5-(4-acryloyl-3-methyl-2-oxopiperazin-1-yl)furan-2-yl)propanoate (EZ-1-058) (10):**
benzyl (E)-4-(5-(3-(tert-butoxy)-3-oxoprop-1-en-1-yl)furan-2-yl)-2-methyl-3-oxopiperazine-1-carboxylate (**64**) (52.3 mg, 0.12 mmol) was deprotected and acylated via general procedures G and H and purified by silica gel chromatography (0-100% EtOAc/hexane) to yield the title compound as a clear colorless oil (17.9 mg, 0.05 mmol, 42% over two steps).
1H NMR (400 MHz, CDCl3) δ 6.66 – 6.51 (m, 1H), 6.46 (d, J = 16.7 Hz, 1H), 6.32 (d, J = 3.2 Hz, 1H), 6.07 (dd, J = 3.2, 1.0 Hz, 1H), 5.84 (d, J = 9.8 Hz, 1H), 4.74 (s, 1H), 4.23 – 3.23 (m, 4H), 2.91 (t, J = 7.6 Hz, 2H), 2.57 (dd, J = 8.2, 6.9 Hz, 3H), 1.63 (s, 3H), 1.47 (s, 9H).

13C NMR (151 MHz, DMSO) δ 171.6, 167.6, 164.2, 149.5, 145.9, 128.7, 128.2, 107.2, 100.7, 80.4, 60.2, 54.5, 52.0, 48.2, 33.4, 28.2, 23.5, 17.0.
**HRMS (ESI):** [M+Na]+ *m/z* calc. 385.1739, found 385.1728.

Synthesis of EZ-1-067 (6)
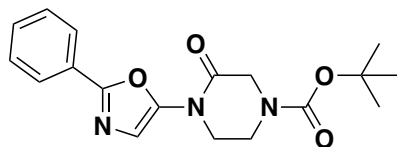
***tert*-butyl 3-oxo-4-(2-phenyloxazol-5-yl)piperazine-1-carboxylate (65):** 5-bromo-2-phenyloxazole (50 mg, 0.22 mmol) was coupled with *tert*-butyl 3-oxopiperazine-1-carboxylate (44.7 mg, 0.22 mmol) via general procedure D and purified by silica gel chromatography (0 to 60% EtOAc/hexane) to yield a white solid (40.4 mg, 0.117 mmol, 54%).
1H NMR (400 MHz, CDCl3) δ 8.05 – 7.98 (m, 2H), 7.49 (dd, J = 5.7, 1.8 Hz, 3H), 7.38 (s, 1H), 4.36 (s, 2H), 4.04 (t, J = 5.4 Hz, 2H), 3.89 (t, J = 5.3 Hz, 2H), 1.55 (s, 9H).
**LC/MS:** [M+H]+ *m/z* calc. 344.2, found 344.1.
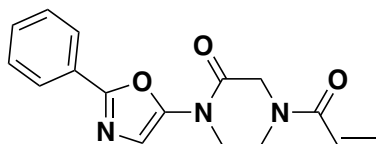
4-acryloyl-1-(2-phenyloxazol-5-yl)piperazin-2-one (EZ-1-067) (6): *tert*-butyl 3-oxo-4-(2-phenyloxazol-5-yl)piperazine-1-carboxylate (**65**) (40.4 mg, 0.117 mmol) was deprotected and acylated via general procedures F and H and purified by silica gel chromatography (0 to 80% EtOAc/hexane) to afford the title compound as a yellow solid (34.6 mg, 0.116 mmol, 45% over two steps)
1H NMR (300 MHz, CDCl3) δ 8.01 (dd, *J* = 6.8, 3.0 Hz, 2H), 7.54 – 7.46 (m, 3H), 7.39 (s, 1H), 6.59 (s, 1H), 6.54 – 6.42 (m, 1H), 5.90 (d, *J* = 11.6 Hz, 1H), 4.53 (s, 2H), 4.10 (s, 4H).
13C NMR (151 MHz, DMSO) δ 164.6, 155.1, 146.6, 130.8, 129.6, 128.9, 128.3, 128.1, 127.1, 125.9, 116.2, 49.4, 47.2, 46.9.
HRMS (ESI): [M+H]+ *m/z* calc. 298.1113, found 298.1187.

Synthesis of EZ-1-068 (11)
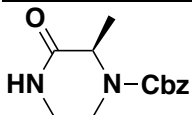
phenyl (*R*)-2-methyl-3-oxopiperazine-1-carboxylate (65): (*R*)-3-methylpiperazin-2-one (100 mg, 0.88 mmol) was protected with benzyl chloroformate (186 µL, 0.876 mmol) via general procedure E and purified by silica gel chromatography (0 to 100% EtOAc/hexane) to yield a white solid (47.2 mg, 0.25 mmol, 22%).
1H NMR (400 MHz, CDCl3) δ 6.15 (s, 1H), 5.21 (s, 2H), 4.73 (s, 1H), 4.24 (s, 1H), 3.51 (d, J = 12.5 Hz, 1H), 3.31 (d, J = 12.6 Hz, 2H), 1.50 (d, J = 7.0 Hz, 3H).
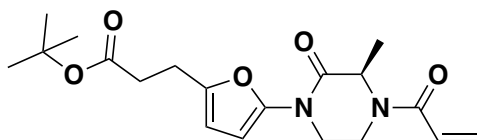
LC/MS: [M+H]$^+$ *m/z* calc. 248.1, found 248.1.
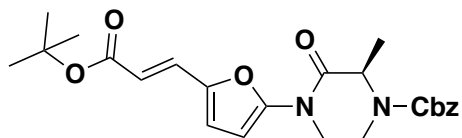
benzyl (R,E)-4-(5-(3-(tert-butoxy)-3-oxoprop-1-en-1-yl)furan-2-yl)-2-methyl-3-oxopiperazine-1-carboxylate (66): phenyl (*R*)-2-methyl-3-oxopiperazine-1-carboxylate (**65**) (44.6 mg, 0.18 mmol) was coupled to *tert*-butyl (E)-3-(5-bromofuran-2-yl)acrylate (EZ-1-048) (49.1 mg, 0.18 mmol) via general procedure D and purified by silica gel chromatography (0 to 35% EtOAc/hexane) to yield a clear yellow oil (56.7 mg, 0.13 mmol, 72%).
1H NMR (400 MHz, CDCl3) δ 7.42 (d, J = 5.3 Hz, 5H), 7.30 (s, 1H), 6.74 – 6.62 (m, 2H), 6.12 (d, J = 15.6 Hz, 1H), 5.23 (d, J = 2.3 Hz, 2H), 4.89 (s, 1H), 4.34 (s, 1H), 4.02 (s, 2H), 3.49 (s, 1H), 1.61 (s, 3H), 1.56 (d, J = 5.5 Hz, 9H).
**LC/MS:** [M+H]$^+$ *m/z* calc. 441.2, found 441.2.

tert-butyl (R)-3-(5-(4-acryloyl-3-methyl-2-oxopiperazin-1-yl)furan-2-yl)propanoate (EZ-1-068) (11): benzyl (R,E)-4-(5-(3-(tert-butoxy)-3-oxoprop-1-en-1-yl)furan-2-yl)-2-methyl-3-oxopiperazine-1-carboxylate (**66**) (31.2 mg, 0.07 mmol) was deprotected and acylated via general procedures F and H and purified by silica gel chromatography (0 to 100% EtOAc/hexane) to afford the title compound as a yellow solid (18.9 mg, 0.052 mmol, 68% over two steps).
1H NMR (300 MHz, CDCl3) δ 6.65 – 6.40 (m, 2H), 6.33 (d, J = 3.4 Hz, 1H), 6.08 (d, J = 3.3 Hz, 1H), 5.90 – 5.81 (m, 1H), 4.76 (s, 1H), 3.93 – 3.34 (m, 4H), 2.92 (t, J = 7.5 Hz, 2H), 2.58 (dd, J = 8.3, 6.8 Hz, 2H), 2.22 (s, 3H), 1.48 (s, 9H).
13C NMR (151 MHz, DMSO) δ 171.6, 167.6, 164.2, 149.4, 145.9, 128.7, 128.2, 107.2, 100.6, 80.4, 52.0, 48.2, 47.2, 33.4, 28.2, 23.5.
**HRMS (ESI):** [M+Na]$^+$ *m/z* calc. 385.1739, found 385.1730.

Synthesis of EZ-1-071 (12)
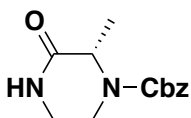
benzyl (S)-2-methyl-3-oxopiperazine-1-carboxylate (68): (*S*)-3-methylpiperazin-2-one (100mg , 0.88mmol) was protected with benzyl chloroformate (149.4 mg, 0.88 mmol) via general procedure E and purified by silica gel chromatography (0 to 100% EtOAc/hexane) to yield a white solid (89.4 mg, 0.36 mmol, 41%).

1H NMR (400 MHz, CDCl3) δ 7.40 (d, J = 4.6 Hz, 5H), 6.13 (s, 1H), 5.21 (s, 2H), 4.72 (s, 1H), 4.24 (s, 1H), 3.53 (s, 1H), 3.31 (d, J = 12.5 Hz, 2H).
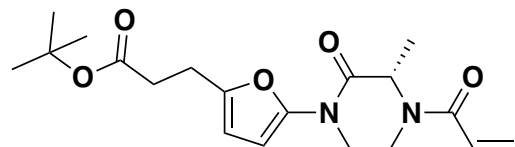**LC/MS:** [M+H]$^+$ *m/z* calc. 248.1, found 248.1.
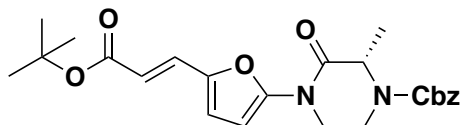
benzyl (S,E)-4-(5-(3-(tert-butoxy)-3-oxoprop-1-en-1-yl)furan-2-yl)-2-methyl-3-oxopiperazine-1-carboxylate (69): benzyl (S)-2-methyl-3-oxopiperazine-1-carboxylate (**68**) (41.6 mg, 0.17 mmol) was coupled to *tert*-butyl (E)-3-(5-bromofuran-2-yl)acrylate (EZ-1-048) (46.8 mg, 0.17 mmol) via general procedure D and purified by silica gel chromatography (0 to 50% EtOAc/hexane) to yield a clear yellow oil (41.3 mg, 0.09 mmol, 56%).
1H NMR (300 MHz, CDCl3) δ 7.45 – 7.37 (m, 5H), 7.31 (d, J = 1.3 Hz, 1H), 6.72 – 6.61 (m, 2H), 6.12 (d, J = 15.6 Hz, 1H), 5.23 (d, J = 1.3 Hz, 2H), 4.90 (s, 1H), 4.34 (s, 1H), 4.05 – 3.92 (m, 2H), 3.49 (s, 1H), 1.62 (s, 3H), 1.56 (d, J = 3.1 Hz, 9H).
**LC/MS:** [M+H]$^+$ *m/z* calc. 441.2, found 441.2.

tert-butyl (S)-3-(5-(4-acryloyl-3-methyl-2-oxopiperazin-1-yl)furan-2-yl)propanoate (EZ-1-071) (12): benzyl (S,E)-4-(5-(3-(tert-butoxy)-3-oxoprop-1-en-1-yl)furan-2-yl)-2-methyl-3-oxopiperazine-1-carboxylate (**69**) (35.4 mg, 0.08 mmol) was deprotected and acylated via general procedures F and H and purified by silica gel chromatography (0 to 100% EtOAc/hexane) to afford the title compound as a clear colorless oil (16.9 mg, 0.047 mmol, 58% over two steps).
1H NMR (400 MHz, CDCl3) δ 6.63 – 6.41 (m, 2H), 6.32 (d, J = 3.4 Hz, 1H), 6.07 (d, J = 3.5 Hz, 1H), 5.85 (d, J = 10.3 Hz, 1H), 4.77 (s, 2H), 3.88 (s, 2H), 3.34 (s, 1H), 2.91 (t, J = 7.5 Hz, 2H), 2.58 (dt, J = 8.8, 5.2 Hz, 2H), 1.74 (s, 3H), 1.48 (d, J = 4.0 Hz, 9H).
13C NMR (151 MHz, DMSO) δ 171.6, 164.2, 149.5, 145.9, 128.7, 128.1, 107.2, 100.7, 80.4, 54.4, 52.0, 48.2, 33.4, 28.2, 23.5.
HRMS (ESI): [M+Na]$^+$ *m/z* calc. 385.1739, found 385.1726.
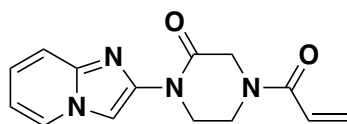
Synthesis of EZ-1-073 (7)
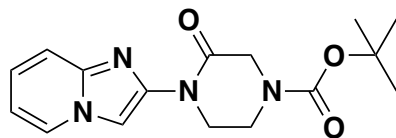
***tert*-butyl 4-(imidazo[1,2-*a*]pyridin-2-yl)-3-oxopiperazine-1-carboxylate (70):** 2-bromoimidazo[1,2-*a*]pyridine (50 mg, 0.25 mmol) was coupled to *tert*-butyl 3-oxopiperazine-1-carboxylate (50.8 mg, 0.25 mmol) via general procedure D and purified

by silica gel chromatography (0 to 80% EtOAc/hexane) to yield a clear colorless oil (35.7 mg, 0.11 mmol, 45%).
1H NMR (400 MHz, CDCl3) δ 8.33 (s, 1H), 8.15 (d, J = 6.7 Hz, 1H), 7.54 (d, J = 9.1 Hz, 1H), 7.22 (ddd, J = 8.7, 6.9, 1.4 Hz, 1H), 6.85 (td, J = 6.8, 1.3 Hz, 1H), 4.34 (s, 2H), 4.31 (t, J = 5.5 Hz, 2H), 3.83 (t, J = 5.4 Hz, 2H), 1.53 (s, 9H).
**LC/MS:** [M+H]$^+$ *m/z* calc. 317.2, found 317.2.

4-acryloyl-1-(imidazo[1,2-a]pyridin-2-yl)piperazin-2-one (EZ-1-073) (7): *tert*-butyl 4-(imidazo[1,2-*a*]pyridin-2-yl)-3-oxopiperazine-1-carboxylate (**70**) (23.4 mg, 0.074 mmol) was deprotected and acylated via general procedures F and H and purified by silica gel chromatography (0 to 100% EtOAc/hexane) to afford the title compound as an off white solid (3.8 mg, 0.014 mmol, 19% over two steps).
1H NMR (400 MHz, CDCl3) δ 8.32 (s, 1H), 8.15 (d, J = 6.9 Hz, 1H), 7.55 (d, J = 9.0 Hz, 1H), 7.24 (t, J = 7.9 Hz, 1H), 6.87 (t, J = 6.8 Hz, 1H), 6.62 (s, 1H), 6.46 (d, J = 16.7 Hz, 1H), 5.86 (d, J = 10.5 Hz, 1H), 4.53 (d, J = 23.7 Hz, 2H), 4.38 (s, 2H), 4.04 (d, J = 33.0 Hz, 2H).
HRMS (ESI): [M+H]$^+$ *m/z* calc. 271.1117, found 271.1190.

Synthesis of EZ-1-085 (8)
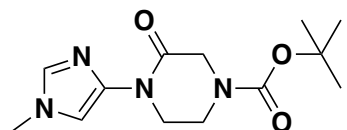
***tert*-butyl 4-(1-methyl-1*H*-imidazol-4-yl)-3-oxopiperazine-1-carboxylate (71):** 4-bromo-1-methyl-1*H*-imidazole (155 µL, 1.55 mmol) was coupled to *tert*-butyl 3-oxopiperazine-1-carboxylate (311 mg, 1.55 mmol) via general procedure D and the crude residue was purified by silica gel chromatography (0-100% EtOAc/Hex) to yield a pale yellow solid (412 mg, 1.47 mmol, 95%).
1H NMR (400 MHz, CDCl3) δ 7.58 – 7.50 (m, 1H), 7.39 – 7.26 (m, 1H), 4.27 (d, J = 9.5 Hz, 2H), 4.18 – 4.06 (m, 3H), 3.80 – 3.61 (m, 4H), 1.51 (d, J = 4.1 Hz, 9H).
LC/MS: [M+H]$^+$ *m/z* calc. 281.2, found 281.2.
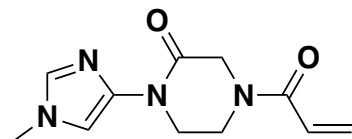
4-acryloyl-1-(1-methyl-1H-imidazol-4-yl)piperazin-2-one (EZ-1-085) (8): *tert*-butyl 4-(1-methyl-1*H*-imidazol-4-yl)-3-oxopiperazine-1-carboxylate (**71**) (100 mg, 0.36 mmol) was deprotected and acylated via general procedures F and H and the crude residue

was purified by silica gel chromatography (0 to 10% MeOH/DCM) to afford the title compound as a white solid (27.7 mg, 0.12 mmol, 33%).

1H NMR (300 MHz, CDCl3) δ 7.54 (s, 1H), 7.27 (s, 1H), 6.58 (s, 1H), 6.44 (dd, J = 16.7, 2.0 Hz, 1H), 5.88 – 5.81 (m, 1H), 4.46 (d, J = 16.0 Hz, 2H), 4.18 (s, 2H), 3.99 (d, J = 23.0 Hz, 2H), 3.73 (s, 3H).

13C NMR (151 MHz, DMSO) δ 163.4, 162.9, 138.9, 133.9, 128.6, 128.5, 128.2, 46.9, 44.9, 42.6, 33.7.

HRMS (ESI): [M+H]⁺ *m/z* calc. 235.1117, found 235.1190.

GL-01 (21): N-(6-(3-(4-(((1-(3-(5-(4-acryloyl-2-oxopiperazin-1-yl)furan-2-yl)propanoyl)pyrrolidin-3-yl)oxy)methyl)piperidine-1-carbonyl)phenyl)-5-methylpyridin-2-yl)-1-(2,2-difluorobenzo[d][1,3]dioxol-5-yl)cyclopropane-1-carboxamide
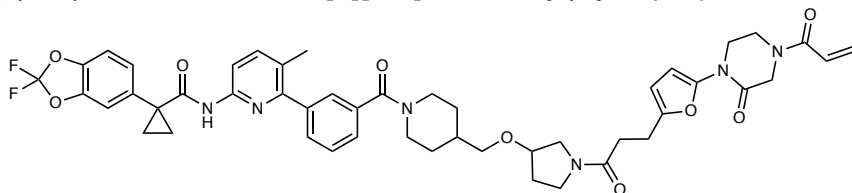
21
GL-01

1H NMR (400 MHz, CDCl₃) δ 8.09 (d, *J* = 8.3 Hz, 1H), 7.68 (s, 1H), 7.59 (d, *J* = 8.4 Hz, 1H), 7.47 – 7.42 (m, 3H), 7.39 (d, *J* = 1.8 Hz, 1H), 7.23 (dd, *J* = 8.2, 1.8 Hz, 1H), 7.19 (d, *J* = 1.7 Hz, 1H), 7.08 (d, *J* = 8.1 Hz, 1H), 6.52 (s, 1H), 6.40 (dd, *J* = 16.7, 2.0 Hz, 1H), 6.26 (dd, *J* = 3.2, 1.2 Hz, 1H), 6.05 (d, *J* = 3.2 Hz, 1H), 5.81 (dd, *J* = 10.2, 2.0 Hz, 1H), 4.72 (s, 1H), 4.48 – 4.34 (m, 2H), 4.10 – 3.75 (m, 6H), 3.66 – 3.58 (m, 1H), 3.54 – 3.39 (m, 3H), 3.34 – 3.22 (m, 2H), 3.05 – 2.87 (m, 3H), 2.81 – 2.70 (m, 1H), 2.60 – 2.50 (m, 2H), 2.26 (s, 3H), 2.12 – 1.95 (m, 2H), 1.94 – 1.71 (m, 5H), 1.21 – 1.04 (m, 4H)

13C NMR (101 MHz, CDCl3) δ 171.78, 170.23, 170.02, 169.92, 164.97, 150.29, 148.82, 144.50, 144.13, 143.61, 141.08, 136.23, 134.92, 134.24, 131.69, 130.09, 128.33, 127.73, 127.69, 127.02, 126.67, 126.31, 112.85, 112.44, 110.20, 107.03, 100.93, 78.63, 73.53, 73.39, 52.05, 50.93, 44.59, 43.69, 42.18, 39.06, 36.74, 36.70, 33.03, 32.80, 31.66, 31.21, 29.66, 23.29, 19.25, 17.23.

19F: (376 MHz, CDCl3) δ -49.51, -49.52

HRMS (TOF, ES+): m/z calcd for C48H51F2N6O9 (M+H)⁺ 893.3686; found 893.3688

GL-02 (22): N-(6-(3-(4-((1-(3-(5-(4-acryloyl-2-oxopiperazin-1-yl)furan-2-yl)propanoyl)azetidin-3-yl)oxy)piperidine-1-carbonyl)phenyl)-5-methylpyridin-2-yl)-1-(2,2-difluorobenzo[d][1,3]dioxol-5-yl)cyclopropane-1-carboxamide
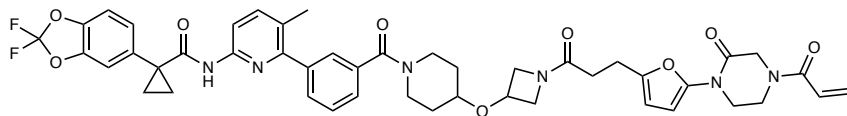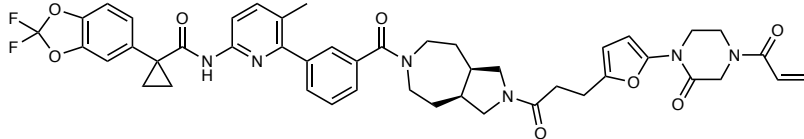
22
GL-02

1H NMR (400 MHz, CDCl₃) δ 8.09 (d, *J* = 8.4 Hz, 1H), 7.68 (s, 1H), 7.59 (d, *J* = 8.4 Hz, 1H), 7.50 – 7.42 (m, 3H), 7.39 (dt, *J* = 7.0, 1.8 Hz, 1H), 7.23 (dd, *J* = 8.2, 1.8 Hz, 1H), 7.19 (d, *J* = 1.7 Hz, 1H), 7.09 (d, *J* = 8.2 Hz, 1H), 6.52 (s, 1H), 6.40 (dd, *J* = 16.7, 2.0 Hz, 1H), 6.26 (d, *J* = 3.3 Hz, 1H), 6.05 (d, *J* = 3.3 Hz, 1H), 5.82 (dd, *J* = 10.3, 2.0 Hz, 1H), 4.50 – 4.34 (m, 3H), 4.27 – 4.16 (m, 2H), 4.12 – 3.81 (m, 7H), 3.71 – 3.54 (m, 2H), 3.45 (d, *J* = 21.9 Hz, 1H), 3.22 (s, 1H), 2.96 – 2.86 (m, 2H), 2.39 (t, *J* = 7.6 Hz, 2H), 2.26 (s, 3H), 1.88 (s, 1H), 1.80 – 1.72 (m, 3H), 1.51 (s, 2H), 1.17 (q, *J* = 3.9 Hz, 2H)
13C NMR (101 MHz, CDCl3) δ 171.78, 171.58, 169.98, 164.97, 163.22, 155.21, 149.95, 148.84, 144.63, 144.12, 143.61, 141.12, 135.90, 134.94, 134.24, 131.69, 130.25, 129.98, 129.15, 128.43, 127.63, 127.01, 126.69, 126.29, 112.89, 112.46, 110.20, 107.21, 101.04, 73.90, 65.51, 58.03, 55.96, 49.46, 46.72, 44.80, 39.10, 31.96, 31.21, 30.09, 23.25, 19.22, 17.25.
19F: (376 MHz, CDCl3) δ -49.52

HRMS (TOF, ES+): m/z calcd for C46H47F2N6O9 (M+H)⁺ 865.3373; found 865.3416

GL-03 (23): N-(6-(3-((3aR,8aS)-2-(3-(5-(4-acryloyl-2-oxopiperazin-1-yl)furan-2-yl)propanoyl)decahydropyrrolo[3,4-d]azepine-6-carbonyl)phenyl)-5-methylpyridin-2-yl)-1-(2,2-difluorobenzo[d][1,3]dioxol-5-yl)cyclopropane-1-carboxamide

23
GL-03

1H NMR (400 MHz, CDCl₃) δ 8.09 (d, *J* = 8.4 Hz, 1H), 7.66 (s, 1H), 7.59 (d, *J* = 8.4 Hz, 1H), 7.48 – 7.42 (m, 3H), 7.38 (dt, *J* = 6.3, 2.0 Hz, 1H), 7.23 (dd, *J* = 8.2, 1.8 Hz, 1H), 7.19 (d, *J* = 1.7 Hz, 1H), 7.08 (d, *J* = 8.2 Hz, 1H), 6.52 (s, 1H), 6.40 (dd, *J* = 16.7, 2.0 Hz, 1H), 6.25 (d, *J* = 1.8 Hz, 1H), 6.05 (d, *J* = 3.3 Hz, 1H), 5.81 (dd, *J* = 10.2, 2.0 Hz, 1H), 4.52 – 4.28 (m, 2H), 4.06 – 3.79 (m, 5H), 3.74 – 3.45 (m, 4H), 3.37 – 3.25 (m, 2H), 3.22 – 3.11 (m, 1H), 2.95 (t, *J* = 7.6 Hz, 2H), 2.56 (t, *J* = 8.3 Hz, 3H), 2.53 – 2.38 (m, 2H), 2.25 (s, 3H), 2.11 – 1.97 (m, 1H), 1.85 – 1.72 (m, 5H), 1.16 (q, *J* = 3.9 Hz, 2H)
13C NMR (101 MHz, CDCl3) δ 171.77, 170.94, 170.04, 164.97, 163.22, 155.29, 150.26, 148.85, 144.58, 144.11, 143.60, 141.07, 140.07, 136.55, 134.94, 134.23, 131.68, 130.08, 129.14, 128.43, 127.48, 126.99, 126.70, 126.53, 126.31, 112.89, 112.46, 110.20, 107.11, 100.98, 52.48, 51.83, 51.57, 51.14, 49.46, 47.76, 43.17, 42.94, 40.49, 39.10, 32.86, 31.20, 30.18, 23.39, 19.24, 17.26.
19F: (376 MHz, CDCl3) δ -49.55

HRMS (TOF, ES+): m/z calcd for C46H47F2N6O8 (M+H)⁺ 849.3423; found 849.3475

GL-04 (24): N-(6-(3-(4-(2-(3-(5-(4-acryloyl-2-oxopiperazin-1-yl)furan-2-yl)propanamido)ethyl)piperidine-1-carbonyl)phenyl)-5-methylpyridin-2-yl)-1-(2,2-difluorobenzo[d][1,3]dioxol-5-yl)cyclopropane-1-carboxamide
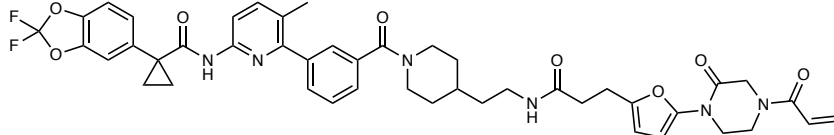
24
GL-04

1H NMR (400 MHz, CDCl3) δ 8.10 (s, 1H), 7.82 – 7.54 (m, 2H), 7.49 – 7.42 (m, 3H), 7.39 (dd, J = 5.4, 3.2 Hz, 1H), 7.23 (dd, J = 8.2, 1.7 Hz, 1H), 7.19 (d, J = 1.7 Hz, 1H), 7.09 (d, J = 8.1 Hz, 1H), 6.52 (s, 1H), 6.41 (dd, J = 16.7, 2.0 Hz, 1H), 6.20 (d, J = 3.2 Hz, 1H), 6.05 (d, J = 3.2 Hz, 1H), 5.82 (dd, J = 10.2, 2.0 Hz, 1H), 5.61 (s, 1H), 4.67 (s, 1H), 4.51 – 4.32 (m, 2H), 4.05 – 3.72 (m, 5H), 3.25 (q, J = 6.9 Hz, 2H), 2.99 – 2.87 (m, 3H), 2.73 (s, 1H), 2.48 (t, J = 7.3 Hz, 2H), 2.26 (s, 3H), 1.83 – 1.72 (m, 3H), 1.57 – 1.47 (m, 2H), 1.42 (q, J = 7.1 Hz, 2H), 1.23 – 1.00 (m, 4H)
13C NMR (101 MHz, CDCl3) δ 171.45, 169.80, 164.99, 149.89, 148.76, 144.92, 144.14, 143.64, 136.32, 134.87, 134.24, 131.69, 130.07, 129.17, 128.37, 127.68, 127.09, 126.69, 126.26, 112.93, 112.46, 110.21, 107.37, 101.10, 47.99, 42.42, 39.06, 36.98, 36.12, 35.02, 33.69, 32.67, 31.74, 31.26, 24.26, 19.18, 17.25.
19F: (376 MHz, CDCl3) δ -49.50

HRMS (TOF, ES+): m/z calcd for C45H47F2N6O8 (M+H)$^+$ 837.3423, found 837.3448

GL-05 (25): N-(6-(3-(4-(3-(5-(4-acryloyl-2-oxopiperazin-1-yl)furan-2-yl)propanoyl)piperazine-1-carbonyl)phenyl)-5-methylpyridin-2-yl)-1-(2,2-difluorobenzo[d][1,3]dioxol-5-yl)cyclopropane-1-carboxamide
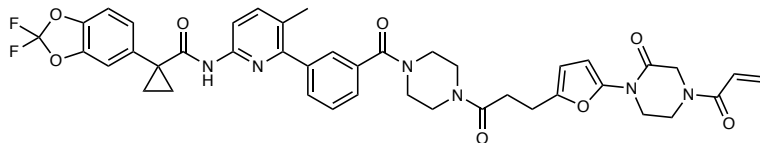

25
GL-05

1H NMR (400 MHz, CDCl$_3$) δ 8.08 (d, *J* = 8.4 Hz, 1H), 7.65 (s, 1H), 7.59 (d, *J* = 8.4 Hz, 1H), 7.54 – 7.45 (m, 3H), 7.40 (dt, *J* = 7.4, 1.6 Hz, 1H), 7.23 (dd, *J* = 8.2, 1.7 Hz, 1H), 7.19 (d, *J* = 1.7 Hz, 1H), 7.10 (d, *J* = 8.2 Hz, 1H), 6.52 (s, 1H), 6.41 (dd, *J* = 16.7, 2.0 Hz, 1H), 6.26 (d, *J* = 3.3 Hz, 1H), 6.07 (d, *J* = 3.3 Hz, 1H), 5.82 (dd, *J* = 10.2, 2.0 Hz, 1H), 4.48 – 4.36 (m, 2H), 4.05 – 3.83 (m, 4H), 3.80 – 3.37 (m, 8H), 2.97 (dd, *J* = 8.8, 6.4 Hz, 2H), 2.65 (d, *J* = 9.4 Hz, 2H), 2.26 (s, 3H), 1.74 (q, *J* = 3.9 Hz, 2H), 1.16 (q, *J* = 3.9 Hz, 2H)
**13C NMR** (101 MHz, CDCl3) δ 171.75, 170.24, 170.14, 164.97, 155.06, 149.93, 148.92, 144.72, 144.13, 143.62, 141.11, 140.28, 135.04, 134.94, 134.23, 131.68, 130.70,

129.99, 129.14, 128.49, 128.00, 126.94, 126.84, 126.62, 126.29, 112.94, 112.44, 110.26, 107.31, 101.08, 49.46, 46.83, 39.06, 31.56, 31.19, 23.60, 19.28, 17.23.
19F: (376 MHz, CDCl3) δ -49.54
HRMS (TOF, ES+): m/z calcd for C42H41F2N6O8 (M+H)$^+$ 795.2954, found 795.2943

GL-06 (26): N-(1-(3-(5-(4-acryloyl-2-oxopiperazin-1-yl)furan-2-yl)propanoyl)piperidin-4-yl)-3-(6-(1-(2,2-difluorobenzo[d][1,3]dioxol-5-yl)cyclopropane-1-carboxamido)-3-methylpyridin-2-yl)-N-methylbenzamide
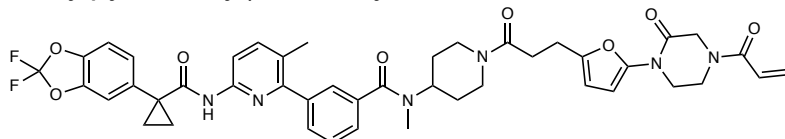

26
GL-06

1H NMR (400 MHz, CDCl$_3$) δ 8.10 (s, 1H), 7.76 – 7.55 (m, 1H), 7.51 – 7.43 (m, 3H), 7.39 (d, *J* = 6.9 Hz, 1H), 7.23 (dd, *J* = 8.2, 1.7 Hz, 1H), 7.19 (d, *J* = 1.7 Hz, 1H), 7.08 (d, *J* = 8.2 Hz, 1H), 6.50 (s, 1H), 6.41 (dd, *J* = 16.7, 2.0 Hz, 1H), 6.27 (d, *J* = 3.2 Hz, 1H), 6.07 (d, *J* = 3.2 Hz, 1H), 5.82 (dd, *J* = 10.2, 2.0 Hz, 1H), 4.77 (s, 2H), 4.50 – 4.32 (m, 2H), 4.09 – 3.71 (m, 6H), 3.17 (s, 1H), 2.96 (t, *J* = 7.7 Hz, 2H), 2.93 – 2.75 (m, 3H), 2.66 (s, 2H), 2.27 (s, 3H), 1.81 – 1.72 (m,3H), 1.59 (s, 2H), 1.37 – 1.28 (m, 1H), 1.18 (s, 2H)
13C NMR (101 MHz, CDCl3) δ 169.70, 164.97, 150.17, 144.62, 144.16, 143.65, 131.69, 130.14, 128.39, 126.68, 126.30, 112.46, 110.21, 107.16, 100.94, 69.02, 49.37, 44.78, 39.08, 31.50, 29.72, 23.72, 19.21, 17.26.
19F: (376 MHz, CDCl3) δ -49.56
HRMS (TOF, ES+): m/z calcd for C44H45F2N6O8 (M+H)$^+$ 823.3267; found 823.3247

GL-07 (27): N-((1-(1-(3-(5-(4-acryloyl-2-oxopiperazin-1-yl)furan-2-yl)propanoyl)piperidin-4-yl)-1H-1,2,3-triazol-4-yl)methyl)-3-(6-(1-(2,2-difluorobenzo[d][1,3]dioxol-5-yl)cyclopropane-1-carboxamido)-3-methylpyridin-2-yl)benzamide
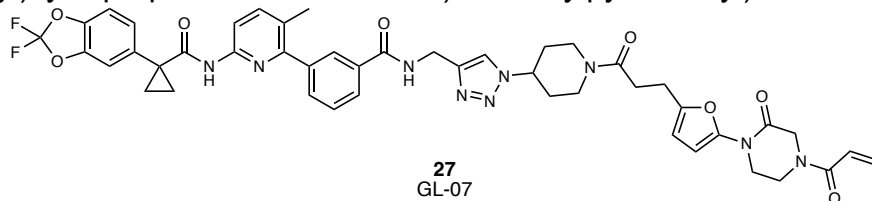
27
GL-07

1H NMR (400 MHz, CDCl$_3$) δ 8.18 (br s, 1H), 8.01 – 7.59 (m, 5H), 7.58 – 7.44 (m, 3H), 7.23 (dd, *J* = 8.2, 1.8 Hz, 1H), 7.18 (d, *J* = 1.7 Hz, 1H), 7.08 (d, *J* = 8.2 Hz, 1H), 6.50 (d, *J* = 11.6 Hz, 1H), 6.39 (dd, *J* = 16.7, 1.9 Hz, 1H), 6.25 (d, *J* = 3.2 Hz, 1H), 6.07 (d, *J* = 3.2 Hz, 1H), 5.80 (dd, *J* = 10.3, 1.9 Hz, 1H), 4.78 – 4.67 (m, 3H), 4.63 (tt, *J* = 11.3, 4.1 Hz, 1H), 4.47 – 4.33 (m, 2H), 4.07 – 3.79 (m, 5H), 3.22 (ddd, *J* = 14.2, 11.9, 2.8 Hz, 1H), 2.97 (td, *J* = 7.6, 2.8 Hz, 2H), 2.90 – 2.78 (m, 1H), 2.68 (q, *J* = 7.4 Hz, 2H), 2.41 – 2.13 (m, 5H), 2.01 – 1.84 (m, 2H), 1.77 (q, *J* = 4.0 Hz, 2H), 1.21 (s, 2H)
**13C NMR** (101 MHz, CDCl3) δ 169.91, 167.08, 164.98, 150.02, 144.71, 144.20, 143.75, 134.23, 131.97, 131.69, 129.94, 129.15, 128.68, 126.71, 126.33, 120.54, 112.46,

110.24, 107.36, 101.06, 57.82, 49.45, 46.82, 44.13, 40.51, 35.57, 32.74, 32.09, 31.98, 31.45, 23.78, 19.02, 17.43.

19F: (376 MHz, CDCl3) δ -49.46

HRMS (TOF, ES+): m/z calcd for $C_{46}H_{46}F_2N_9O_8$ (M+H)$^+$ 890.3437; found 890.3433.

GL-08 (28): N-(6-(3-(2-(3-(5-(4-acryloyl-2-oxopiperazin-1-yl)furan-2-yl)propanoyl)-2,8-diazaspiro[4.5]decane-8-carbonyl)phenyl)-5-methylpyridin-2-yl)-1-(2,2-difluorobenzo[d][1,3]dioxol-5-yl)cyclopropane-1-carboxamide

28
GL-08
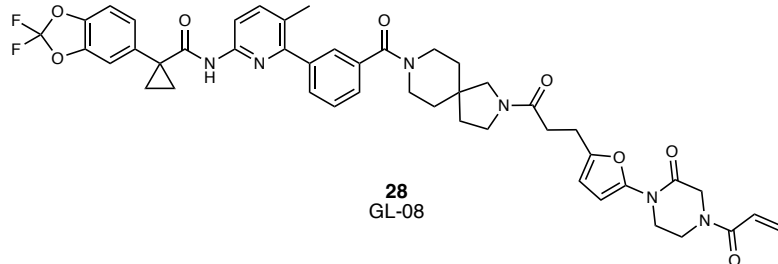
1H NMR (400 MHz, CDCl3) δ 8.11 (d, J = 8.4 Hz, 1H), 7.83 (s, 1H), 7.61 (d, J = 8.5 Hz, 1H), 7.49 – 7.43 (m, 3H), 7.42 – 7.38 (m, 1H), 7.25 – 7.20 (m, 1H), 7.19 (t, J = 1.7 Hz, 1H), 7.08 (dd, J = 8.2, 3.9 Hz,1H), 6.52 (s, 1H), 6.44 – 6.36 (m, 1H), 6.25 (dd, J = 3.2, 2.2 Hz, 1H), 6.05 (t, J = 2.5 Hz, 1H), 5.82 (d, J = 1.5 Hz, 1H), 4.49 – 4.36 (m, 2H), 4.06 – 3.76 (m, 5H), 3.62 – 3.17 (m, 7H), 2.96 (t, J = 7.6 Hz, 2H), 2.57 (dd, J = 8.7, 6.4 Hz, 2H), 2.26 (s, 3H), 2.11 (d, J = 15.1 Hz, 2H), 1.91 – 1.78 (m, 2H), 1.75 (q, J = 3.8 Hz, 2H), 1.54 – 1.39 (m, 2H), 1.17 (q, J = 4.1 Hz, 2H)

13C NMR (101 MHz, CDCl3) δ 171.83, 170.42, 170.19, 169.97, 169.92, 164.98, 154.97, 150.26, 148.76, 144.60, 144.12, 143.62, 141.43, 139.60, 135.93, 135.85, 134.85, 131.69, 130.31, 130.23, 128.45, 127.68, 127.12, 126.82, 126.68, 126.29, 113.10, 112.42, 110.20, 107.11, 101.12, 56.64, 54.66, 44.71, 44.04, 41.63, 39.62, 36.60, 33.97, 33.08, 32.74, 31.23, 29.72, 23.40,19.18, 17.27.

19F: (376 MHz, CDCl3) δ -49.52

HRMS (TOF, ES+): m/z calcd for $C_{46}H_{47}F_2N_6O_8$ (M+H)$^+$ 849.3423; found 849.3419

Appendix C – Supplementary information for Chapter 4

C.1 Supplementary Figures
C.2 Materials and Methods
C.3 Chemical Synthesis and Characterization

C.1. Supplementary Figures
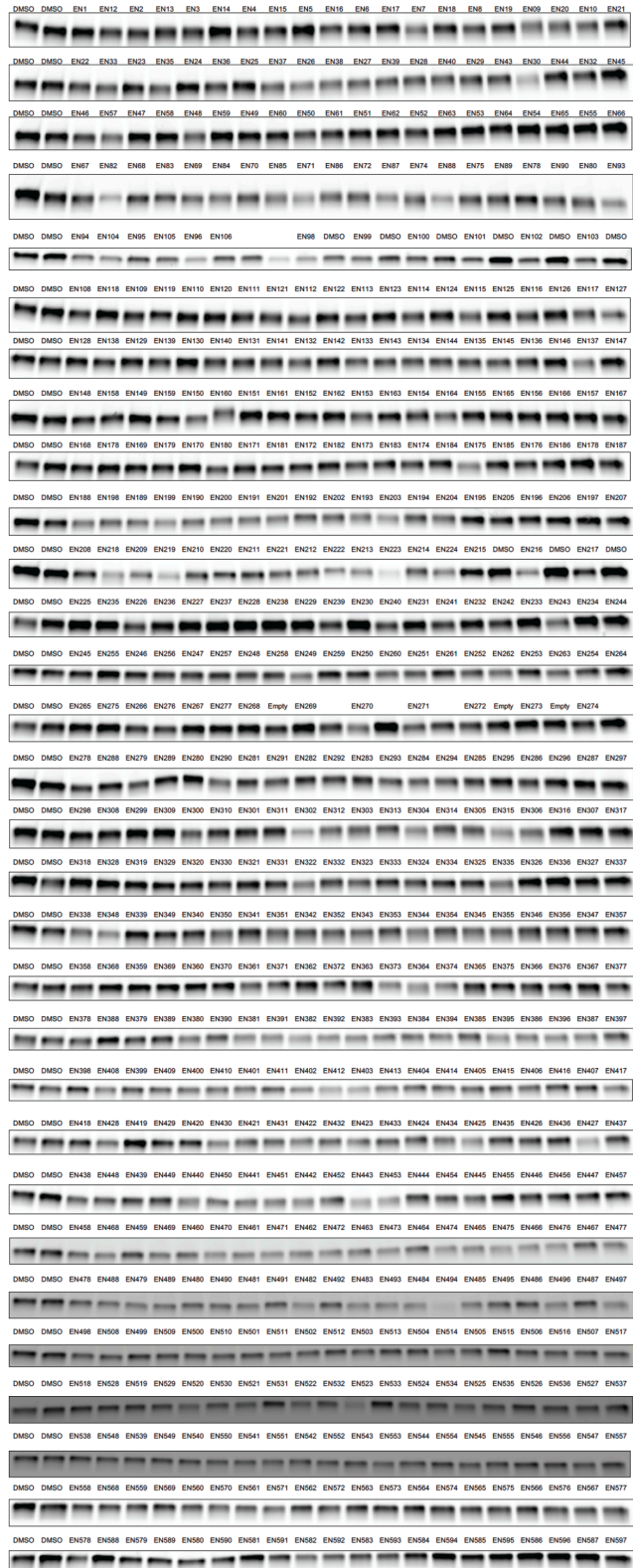
Figure S4.1. Gel-based ABPP screen of cysteine-reactive covalent ligands against Mpro enzyme.
Pure SARS-CoV-2 Mpro protein was pre-incubated with DMSO vehicle or cysteine-reactive covalent ligands (50 μM, 30 min) prior to addition of a rhodamine-conjugated iodoacetamide (IA-rhodamine) probe (100 nM) for 1 hr after which reactions were quenched with SDS/PAGE loading buffer, resolved on SDS/PAGE and visualized by in-gel fluorescence.

Figure S4.2. Hit confirmation of initial gel-based ABPP screen.
Pure SARS-CoV-2 Mpro protein was pre-incubated with DMSO vehicle or cysteine-reactive covalent ligands (50 mM, 30 min) prior to addition of a rhodamine-conjugated iodoacetamide (IA-rhodamine) probe (100 nM) for 1hr min after which reactions were quenched with SDS/PAGE loading buffer, resolved on SDS/PAGE and visualized by in-gel fluorescence.
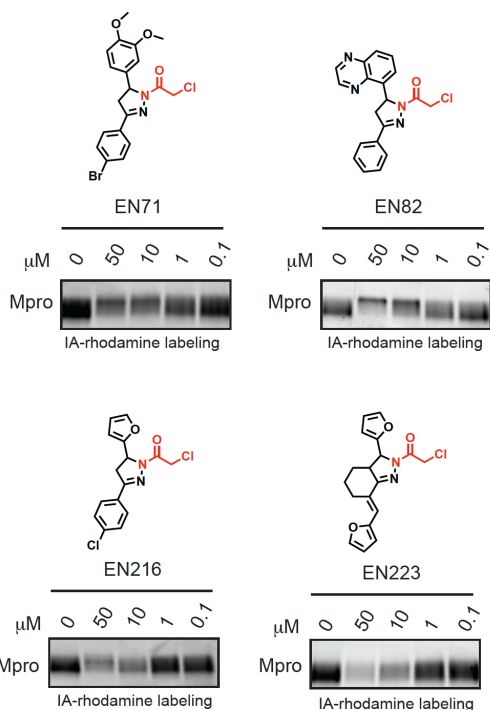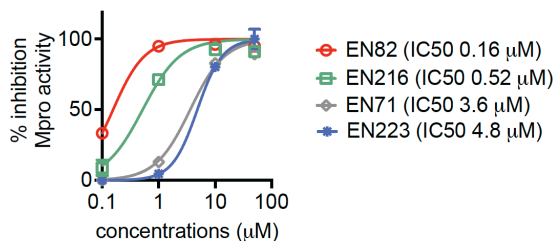
Figure S4.3. Testing reproducible hit compounds in dose-response gel-based ABPP and Mpro substrate activity assays.
(A) Gel-based ABPP studies with reproducible hit compounds. Pure SARS-CoV-2 Mpro protein was pre-incubated with DMSO vehicle or cysteine-reactive covalent ligands (30 min) prior to addition of a rhodamine-conjugated iodoacetamide (IA-rhodamine) probe (100 nM) for 1 hr after which reactions were quenched with SDS/PAGE loading buffer, resolved on SDS/PAGE and visualized by in-gel fluorescence. **(B)** Mpro substrate activity assay using an FRET-based peptide probe. Activity assays in **(B)** are from n=3 biological replicates/group and values are expressed as average ± sem.

IC50 (μM)

|	EN82	(R)-EN82	(S)-EN82	CMZ-15	CMZ-35	CMZ-13	NJH-1-147	NJH-1-159
SARS-CoV-2	0.025	0.30	0.17	0.010	0.0046	0.0027	0.058	0.02
HCoV-HKU1	0.0066	0.0027	0.0052	0.0031	0.0023	0.0098	0.026	0.0089
HCoV-229E	0.029	0.015	0.053	0.011	0.0037	0.0045	0.054	0.019
MERS-CoV	1.56	0.67	2.4	0.18	0.14	0.31	7.2	0.96
PorCoV-HKU15	10	>25	7.4	8.2	1.6	5.0	11	9.3
HCoV-NL63	0.24	0.13	0.55	0.11	0.016	0.0038	0.33	0.11

IC50 (μM)

	LEB-2-172	LEB-3-004
SARS-CoV-2	0.00089	0.0016
HCoV-HKU1	0.00096	0.0023
HCoV-229E	0.0055	0.0053
MERS-CoV	0.038	0.10
PorCoV-HKU15	—	2.1
HCoV-NL63	0.011	0.025

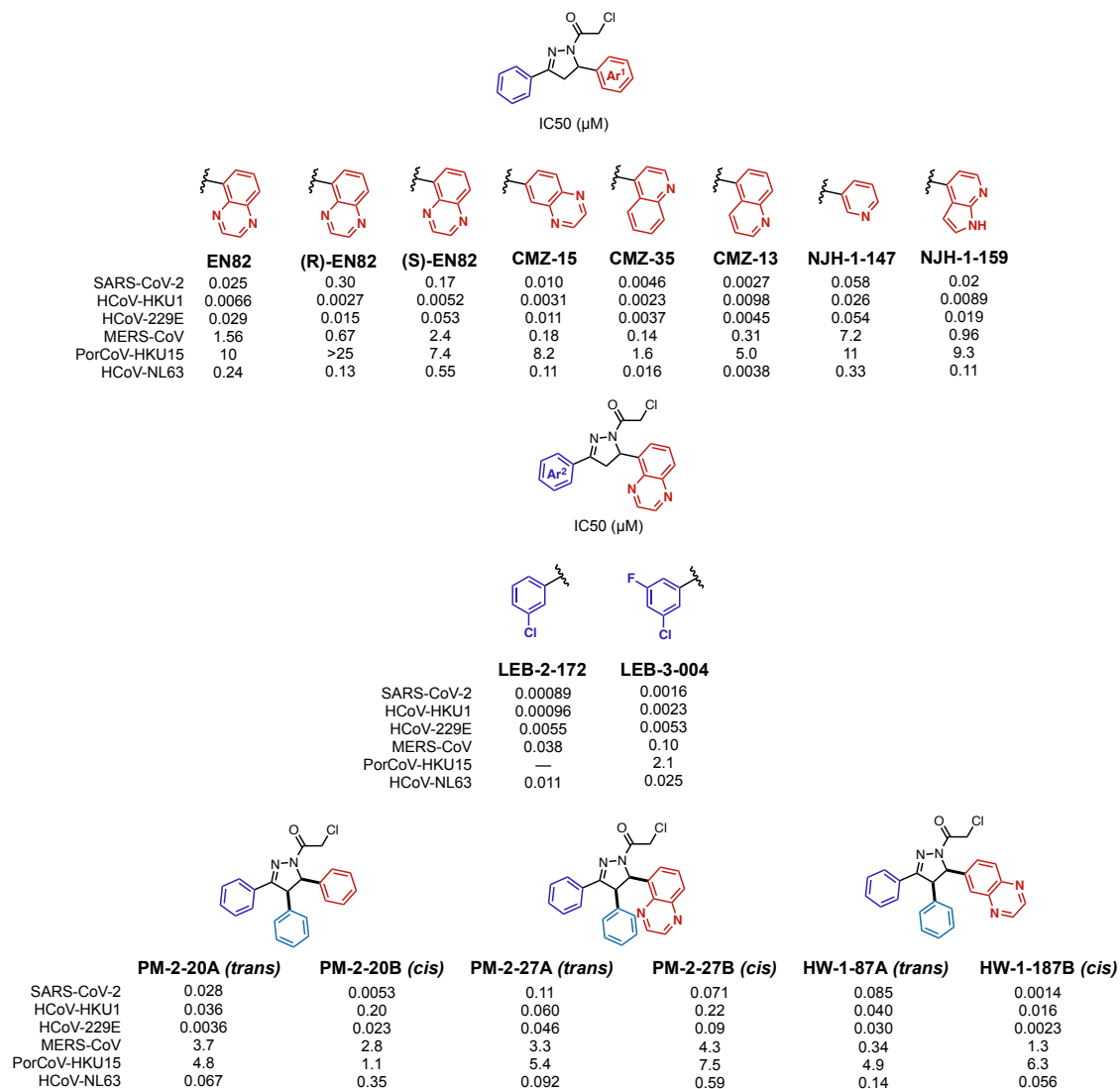|	PM-2-20A (trans)	PM-2-20B (cis)	PM-2-27A (trans)	PM-2-27B (cis)	HW-1-87A (trans)	HW-1-187B (cis)
SARS-CoV-2	0.028	0.0053	0.11	0.071	0.085	0.0014
HCoV-HKU1	0.036	0.20	0.060	0.22	0.040	0.016
HCoV-229E	0.0036	0.023	0.046	0.09	0.030	0.0023
MERS-CoV	3.7	2.8	3.3	4.3	0.34	1.3
PorCoV-HKU15	4.8	1.1	5.4	7.5	4.9	6.3
HCoV-NL63	0.067	0.35	0.092	0.59	0.14	0.056

Figure S4.4. Potency of inhibitors against MPro enzymes from other coronaviruses.
The Mpro activity assays were performed with a MS-based substrate activity assay.

C.2. Methods and Materials

Production of authentic SARS-CoV-2 Main Proteases

The coding sequence for SARS-CoV-2 main protease was codon-optimized for *E. coli* and synthesized by Integrated DNA Technologies. The sequence was amplified by PCR and cloned into the pGEX6P-1 vector, downstream of GST and an HRV 3C protease cleavage site, using the Gibson Assembly Master Mix kit (New England BioLabs, Inc). To ensure authentic termini, the amino acids AVLQ were added to the N-terminus of the main protease by addition of their coding sequence to the 5′ end of the gene product. This sequence reconstitutes the NSP4/5 cleavage site, resulting in auto-cleavage by the main protease protein product and removal of the GST tag. We also added a GP-6xHis tag (to enable IMAC purification) on the C-terminus (the GP completes a non-consensus 3C cleavage site along with the C-terminus of the main protease which allows for cleavage of the his tag after purification, resulting in an authentic C-terminus).

Hi Control BL21(DE3) cells were transformed with the expression plasmid using standard techniques. We used Hi Control cells as we observed expression of the main protease was toxic in other standard *E. coli* cell lines. A single colony was used to start an overnight culture in LB + carbenicillin media. This culture was used to inoculate 2 x 1 L cultures in Terrific Broth, supplemented with 50 mM sodium phosphate pH 7.0 and 100 µg/mL carbenicillin. These cultures grew in Fernbach flasks at 37 °C while shaking at 225 rpm, until the OD600 reached approximately 2.0, at which point the temperature was reduced to 20 °C and 0.5 mM IPTG (final) was added to each culture. The cells were allowed to grow overnight.

The next day, the cultures were centrifuged at 6,000 x *g* for 20 minutes at 4 °C, and the resulting cell pellets were resuspended in IMAC_A buffer (50 mM Tris pH 8.0, 400 mM NaCl, 1 mM TCEP). Cells were lysed with two passes through a cell homogenizer (Microfluidics model M-110P) at 18,000 psi. The lysate was clarified with centrifugation at 42,000 x *g* for 30 minutes and the cleared lysate was loaded onto 3 x 5 mL HiTrap Ni-NTA columns (GE) pre-equilibrated with IMAC_A buffer, using an AKTA Pure FPLC. After loading, the columns were washed with IMAC_A buffer until the A280 levels reached a sustained baseline. The protein was then eluted with a linear gradient with IMAC_B buffer (50 mM Tris pH 8.0, 400 mM NaCl, 500 mM imidazole, 1 mM TCEP) across 25 column volumes, while 2 mL fractions were collected automatically. Peak fractions were analyzed by SDS-PAGE and those containing SARS-CoV-2 main protease were pooled. Importantly, auto-cleavage of the N-terminal GST tag was observed and the eluted protein had a mass consistent with SARS-CoV-2 main protease along with the C-terminal GP-6xHis tag, as determined by ESI-LC/MS.

Pooled fractions were treated with HRV 3C protease (also known as "PreScission" protease) while dialyzing against IMAC_A buffer at room temperature (2 x 2 L dialyses). Room temperature dialysis was important as we observed a tendency for the main protease protein to precipitate with prolonged exposure to 4 °C. Cleavage of the C-terminal GP-6xHis tag was confirmed after 2 hours by ESI-LC/MS. The dialyzed and cleaved protein was then re-run through a 5 mL HiTrap Ni-NTA column pre-

equilibrated with IMAC_A buffer. The main protease eluted in the flow-through as expected.

The protein was then concentrated to approximately 5 mL and loaded onto a Superdex 75 16/60 column pre-equilibrated with SEC Buffer (25 mM HEPES pH 7.5, 150 mM NaCl, 1 mM TCEP). The protein was run through the column at 1 mL/min and eluted as one large peak well in the included volume (at ~75 mL). Fractions from this peak were analyzed by SDS-PAGE and pure fractions were pooled and concentrated to 10 mg/mL, aliquotted, and stored at -80 °C. Final yield was typically in the realm of 60-70 mg/L of culture.

Crystallography of Compounds with Mpro

Co-crystallization of Covid-19^{Mpro} with compounds EN82 and PM-02-20B was performed with 10mg/ml Covid-19^{Mpro} (25 mM Hepes pH 7.5, 150 mM NaCl, 1 mM EDTA) was inhibited at 10X molar excess and incubated on ice for 1hr, solution was spun down for 10min at 10,000 rpm. Crystals were grown by hanging-drop vapor diffusion method at 18℃ by mixing 1:1, 1:2 and 2:1 ratio of protein to well solution. Crystal grew out of well solution composed of 25% w/v Peg 1500, 100 mM MIB buffer pH 7.0, from PACT screen (Nextal Biotechnologies). After 24 hr, crystals were harvested and cryo-protected using 20% Glycerol and well solution, flash-cooled in liquid nitrogen for data collection. EN82 was collected using in-house radiation source using an R-AXIS detector (Rigaku) and Cu Kα X-ray source (FR-E SuperBright High-Brilliance Rotating Anode Generator). Data was collected on a single crystal cooled to 100K. For PM-2-20B, data collection was completed at APS, IMCA-CAT beamline 17-ID-B.

X-ray data collection, processing and structure refinement: EN82 PM-2-20b

The diffraction images for both structures were processed using autoPROC, [Vonrhein, C., Flensburg, C., Keller, P., Sharff, A., Smart, O., Paciorek, W., Womack, T. & Bricogne, G. (2011). Data processing and analysis with the autoPROC toolbox. Acta Cryst. D67, 293-302.]. The Molecular Replacement solution was solved with Phaser (as implemented in CCP4I) using an in-house structure as the input model. This initial structure was built and refined by iterative cycles of manual rebuilding and subsequent structure refinement in Coot and autoBuster, respectively. Ligands were then placed and the structures further refined to convergence.

Table C.2.1 Data collection, processing and refinement statistics.

	EN-82 R stereoisomer	PM-20-20b
PDB ID		
Data Collection		
Resolution range	56.1 - 2.00 (2.10 - 2.00)	48.31 - 1.88 (1.98-1.88)
Space group	C 1 2 1	C 1 2 1
Mol. in the ASU	1	1
Unit cell	114.51 53.74 45.59 90.00 101.53 90.00	114.662 53.531 44.962 90.00 101.89 90.00
Total reflections	120409 (8386)	63010 (2506)
Unique reflections	17088 (1652)	18050 (1065)
Multiplicity	7.0 (5.1)	3.5 (2.4)
Completeness (%)	92.2 (62.1)	82.7 (33.5)
Mean I/sigma(I)	15.5 (1.3)	18.6 (1.3)
Wilson B-factor	39.19	36.09
R-merge	0.072 (0.967)	0.032 (0.573)
R-meas	0.084 (1.237)	0.044 (0.811)
R-pim	0.044 (0.755)	0.030 (0.573)
CC1/2	0.999 (0.442)	0.999 (0.623)
CC*		
Refinement		
Reflections used in refinement	17064 (388)	18025 (392)
Reflections used for R-free	890 (27)	929 (22)
R-work	0.1936 (0.3067)	0.1844 (0.3120)
R-free	0.2359 (0.2941)	0.2307 (0.3530)
CC(work)	0.958	0.96
CC(free)	0.943	0.943
Number of non-hydrogen atoms	2467	2535
protein atoms	2310	2335
solvent	128	174
Protein residues	306	306
RMS(bonds)	0.008	0.008
RMS(angles)	0.95	0.99
Ramachandran favored (%)	99.01	99.01
Ramachandran allowed (%)	0.66	0
Ramachandran outliers (%)	0.33	0.99
Rotamer outliers (%)	0.4	0

Clashscore	4.37	5.82
Average B-factor	42.22	37.04

Gel-Based ABPP Screens

Recombinant Mpro (100 nM) was pre-treated with either DMSO vehicle or covalent ligand at room temperatue for 30 min in 25 µL of PBS, and subsequently treated with Tetramethylrhodamine-5-iodoacetamide dihydroiodide (IA-rhodamine) (500 nM) (ThermoFisher Scientific) at room temperature for 1 h. The reaction was stopped by addition of 4×reducing Laemmli SDS sample loading buffer (Alfa Aesar). After boiling at 95 °C for 5 min, the samples were separated on precast 4−20% Criterion TGX gels (Bio-Rad). Probe-labeled proteins were analyzed by in-gel fluorescence using a ChemiDoc MP (Bio-Rad).

SARS CoV2 MPro Activity Assay using a Fluorescent Substrate Peptide Probe (FRET-based assay)

Compounds were made up in DMSO to 50X the desired screening concentration. DMSO was used as a solvent control. MPro protein was diluted in assay buffer (Tris buffered saline with 1 mM EDTA) to a concentration of 115 nM and was aliquoted to each well of a 96-well plate. Each well was treated with compound or vehicle and the plate was incubated for 30 min at room temperature. During the compound incubation the quenched fluorescent peptide probe (7-methoxycoumarin-4-ylacetyl) MCA-ABLQSGFR-Lys(2,4,-dinitrophenyl (Dnp))-Lys-NH was added from a 80 µM stock solution to a final concentration of 10 µM. Values were read-out on a Tecan Spark plate-reader.

SARS CoV2 MPro Activity Assay using a Fluorescent Substrate Peptide Probe (Rhodamine-based assay)

Compounds were made up in DMSO to 50X the desired screening concentration. DMSO was used as a solvent control. MPro protein was diluted in assay buffer (50 mM HEPES, pH 7.5, 150 mM NaCl, 1 mM EDTA, 0,01% pluronic acid F127) to a concentration of 30 nM and 24.5 µL of diluted protein was aliquoted to each well of a black 384 well plate (Corning 384-Well, Flat-Bottom Microplate). Each well was treated with 0.5 µL of compound or vehicle and the plate was incubated for 30 min at room temperature. During the compound incubation the peptide probe KTSAVLQ-(Rhodamine-110 (Rh-110))-gammaGlu (Biosyntan) was diluted from 5mM DMSO stock into assay buffer. After pre-incubation 5 µL of 75 µM Rh-110 probe was added to each well. RFU value was immediately measured on a Tecan Spark plate reader with an excitation wavelength of 488 nm and an emission wavelength of 535 nm at 30 °C for 30 min.

SARS CoV2 MPro Activity Assay using an Agilent RapidFire Mass Spectrometer (MS-based assay)

Compound IC_{50} values for the Coranavirus main protease (Mpro) panel were determined in a Rapidfire-Mass spectrometry (RFMS) assay using an Agilent Rapidfire 365 autosampler coupled to Sciex 6500 triplequad (QQQ) mass spectrometer. Initially,

Mpro was diluted in assay buffer (50 mM HEPES, pH 7.3, 150 mM NaCl, 1 mM EDTA, 0.01% pluronic acid F127) and added to a 384 well plate where it was pre-incubated with compound for 15 minutes prior to addition of substrate. To initiate the reaction, substrate was added to the compound plate and incubated for between 2-3 hrs depending on the Mpro (see table) at RT. Conditions were kept similar for each Mpro and were based off original conditions established for CoV2. Final incubation time was chosen when 10% substrate turnover was observed. After incubation the reaction was quenched with 2% acetic acid solution and then submitted to the RFMS. Samples were loaded onto a C18 SPE cartridge (Agilent) with H_2O with 0.1% formic acid at a flow rate of 1.5 mL/min. They were then eluted with 75:20:5 ACN:H_2O:IPA with 0.1% formic acid at flow rate of 1.0 mL/min. MRM (multiple reaction monitoring) transitions corresponding to the substrate and the related products, along with $^{13}C_3$ ^{15}N AVLQ (for signal normalization) were monitored and peaks integrated using Sciex Multiquant. Corresponding peptides (Vivitide) monitored for each Mpro are listed in the table.

Panel protein	Substrate	Product	Final enzyme conc. (nM)	Final substrate conc. (µM)	Incubation time (h)
IBV	SRLQAGFKKL	SRLQ	5	10	2.5
HCoV-NL63	STLQSGLKKM	STLQ	10	10	3
HCoV-229E	STLQAGLRKM	STLQ	10	10	3
PorCoV-HKU15	TKLQAGIKILL	TKLQ	5	10	2.5
HCoV-OC43	SFLQSGIVKM	SFLQ	5	5	2
SARS-CoV-2	AVLQSGFRKM	AVLQ	5	5	2
SARS-CoV-1	AVLQSGFRKM	AVLQ	5	5	2.5
HCoV-HKU1	SFLQSGIVKM	SFLQ	5	5	2

Cysteine profiling via rapid covalent chemoproteomics

SARS-CoV-2 Mpro was spiked into HEK293T lysate (200ul at 5ug/ul) with a final concentration of 1uM followed by treatment with DMSO or EN82 at 10 µM for 6h in triplicate. This was followed by treatment with acid-cleavable biotin-PEG4-DADPS-C6-iodoacetamide probe at 100 µM for 1h at room temperature. Excess biotin probe was removed by cleanup through Zeba 7K MWCO columns. Lysates were denatured with 200 µL 8M urea, reduced with 10 mM DTT for 15 minutes and alkylated with 55 mM iodoacetamide for 1h. The denatured, alkylated proteins were digested with 20µg LysC/trypsin (Promega) for 4h at 37C. After dilution to 1M urea, biotinylated peptides were

enriched by incubating with 100 µL ultralink streptavidin agarose (Thermo) for 1h at RT on a rotator. Beads were then transferred to 1.2 µM filter plate and washed 5x with 1 mL 0.1% SDS, 5x 1ml PBS and 5x with 1 mL water. 300 uL 10% formic acid were added and the samples incubated for 1h at RT to cleave the DADPS linker. Cysteinyl peptides were collected by centrifugation and dried by speedvac. After resuspension in 40 µL 50 mM HEPES pH 8, 60 µL acetonitrile and 50 µL TMT reagent in acetonitrile (Thermo) were added and the samples were incubated for 1hr at room temperature. TMT-labeled samples were pooled and 10% of the total material directly analyzed by nanoLC-SPS-using an Easy-nLC 1200 high-performance liquid chromatography system (Thermo) interfaced with an Orbitrap Eclipse Tribrid mass spectrometer (Thermo). A Kasil-fritted trapping column (75 µm x 15 mm) packed with 5 um ReproSil-Pur 120 C18-AQ, was used together with a fused silica spraying capillary pulled to a tip diameter of 8-10 um using a P-2000 capillary puller (Sutter Instruments). The capillary tubing (75 µm I.D.) was packed with a 120 mm separation column comprised of 3 um ReproSil-Pur C18 AQ. Samples (10 µL) were injected onto the trapping column using 0.1% formic acid/2% acetonitrile in water at a flow rate of 2.5 µL/min. Trapped peptides were then introduced into the separation column and eluted at 300 nL/min using a gradient of 3-45% mobile phase B (98% acetonitrile + 0.1% formic acid in water) over 90 min (mobile phase A: 2% acetonitrile + 0.1% formic acid in water). SPS-MS3 analysis of the TMT labeled peptides was performed using MS1 scans that were acquired from m/z 400-1600 at 120,000 mass resolution with a triggering intensity threshold of 400,000 ions. MS2 scans were acquired using Turbo CID with 1.2 Da isolation and AGC target of 1E4 and a collision energy of 30%. For SPS the top 10 ions were selected for MS3 analysis using a collision energy of 55% with an orbitrap resolution of 60,000. Raw files were processed using Proteome Discoverer 2.4. Data were searched against the Uniprot human protein database including the SARS-CoV-2 Mpro sequence using Mascot.

C.3 Chemical Synthesis and Characterization

All non-aqueous reactions were performed under an inert atmosphere of dry nitrogen in flame dried glassware sealed with a rubber septum unless stated otherwise. Nitrogen was supplied through a glass manifold. Reactions were stirred magnetically and monitored by thin layer chromatography (TLC). Analytical thin layer chromatography was performed using MERCK Silica Gel 60 F254 TLC glass plates and visualized by ultraviolet light (UV). Additionally, TLC plates were stained with aqueous potassium permanganate ($KMnO_4$) [1.5 g $KMnO_4$, 200 mL H_2O, 10 g K_2CO_3, 1.25 mL 10% NaOH]. Concentration under reduced pressure was performed by rotator evaporation at 40 °C at the appropriate pressure. Chromatographic purification was performed as flash chromatography on MERCK silica gel 60 Å (230 x 400 mesh) at 0.2–0.5 bar overpressure. Purified compounds were dried further under high vacuum (0.01-0.1 mbar). Yields refer to the purified compound.

Chemicals
All chemicals and solvents were used as received from the commercial supplier without further purification unless mentioned otherwise. CH_2Cl_2 was purified by passage through an activated alumina column under an atmosphere of dry argon.

Analytics
Nuclear Magnetic Resonance (NMR) spectra were recorded on BRUKER AV (600 MHz and 300 MHz), AVB (400 MHz), AVQ (400 MHz) and NEO (500 MHz) spectrometers. Measurements were carried out at ambient temperature. Chemical shifts ($δ$) are reported in ppm with the residual solvent signal as internal standard (chloroform at 7.26 and 77.00 ppm for ^1H NMR and ^{13}C NMR spectroscopy, respectively). The data is reported as (s = singlet, d = doublet, t = triplet, q = quartet, p = quintet, m = multiplet or unresolved, br = broad signal, coupling constant(s) in Hz, integration). ^{13}C NMR spectra were recorded with broadband ^1H decoupling.

Mass spectrometry (MS) analyses were obtained at the Catalysis Center at the College of Chemistry, University of California, Berkeley.

General Procedures
Synthesis of α,β-Unsaturated Ketones

General Procedure A
The ketone (1.0 equiv) and aldehyde (2.0 equiv) were taken up in EtOH (0.6 M) and cooled to 0 °C. 40% NaOH (10 equiv) was added dropwise, and the resulting reaction mixture was stirred at ambient temperature for 4 h. The precipitated solid was filtered, washed with cold water and cold EtOH and dried under high vacuum. Where necessary, the crude product was recrystallized from hot EtOH to afford the corresponding α,β-unsaturated ketone.

General Procedure B
LiOH·H_2O (10 mol%) was added to a solution of the ketone (1.0 equiv) in EtOH (1 M) and the resulting mixture was stirred for 10 min at ambient temperature. The aldehyde (1.0 equiv) was then added, and the reaction mixture was stirred at ambient temperature

for 30 min to 1 h before it was concentrated under reduced pressure. Purification by column chromatography afforded the corresponding the corresponding α,β-unsaturated ketone.

General Procedure C

A mixture of the aldehyde (1.0 equiv) and deoxybenzoin (3.0 equiv) in toluene (0.4 M) was treated with acetic acid (0.9 equiv) and piperidine (0.2 equiv). Powdered 4 Å molecular sieves (500 mg/mmol) was added, and the resulting reaction mixture was stirred at reflux temperature for 7 to 16 h. It was then allowed to cool to ambient temperature, quenched with NaHCO$_3$ solution (sat. aqueous) and extracted with EtOAc (3 x). The combined organic phases were washed with NaCl solution (sat. aqueous), dried over Na$_2$SO$_4$, filtered and concentrated under reduced pressure. Purification by column chromatography afforded the corresponding α,β-unsaturated ketone.
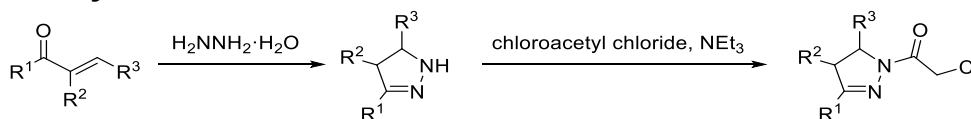
General Procedure D

A mixture of the aldehyde (1.0 equiv) and propiophenone (1.0 equiv) in EtOH (0.3 M) was heated gently until both starting materials dissolved. A solution of NaOH (1.2 equiv) in EtOH/H$_2$O (1:1 v/v, 0.3 M) was added dropwise, and the resulting reaction mixture was stirred at ambient temperature for 1 h, then at 60 °C for 16 h. The reaction mixture was allowed to cool to ambient temperature, diluted with water and extracted with CH$_2$Cl$_2$ (3 x). The combined organic phases were washed with NaCl solution (sat. aqueous), dried over Na$_2$SO$_4$, filtered and concentrated under reduced pressure. Purification by column chromatography afforded the corresponding α,β-unsaturated ketone.

General Procedure E
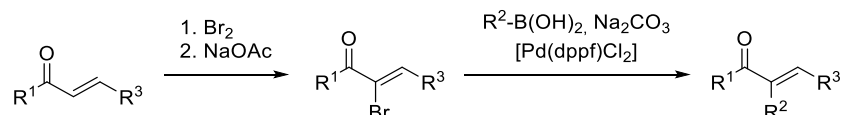
A solution of the chalcone (1.0 equiv) in CH$_2$Cl$_2$ (0.1 M) was cooled to 0 °C. A solution of bromine (1.2 equiv) in CH$_2$Cl$_2$ (1 M) was added dropwise over 3 min, and the resulting reaction mixture was stirred at 0 °C for 15 min, then at ambient temperature for 15 min. It was then quenched with Na$_2$S$_2$O$_3$ solution (sat. aqueous) and the resulting mixture was extracted with CH$_2$Cl$_2$ (3 x). The combined organic phases were washed with NaCl solution (sat. aqueous), dried over Na$_2$SO$_4$, filtered and concentrated under reduced pressure.

The crude dibromide was dissolved in EtOH (0.3 M) and sodium acetate (1.2 equiv) was added. The resulting reaction mixture was stirred at reflux temperature for 1.5 h before the solvent was removed under reduced pressure. The residue was partitioned between CH$_2$Cl$_2$ and NaHCO$_3$ solution (sat. aqueous), the phases were separated and the aqueous phase was extracted with CH$_2$Cl$_2$ (2 x). The combined organic phases were washed with NaCl solution (sat. aqueous), dried over Na$_2$SO$_4$, filtered and concentrated under reduced pressure.

A mixture of the crude vinyl bromide (1.0 equiv), the boronic acid (1.3 equiv), sodium carbonate (2.0 equiv) and Pd(dppf)Cl$_2$ (5 mol%) was taken up in toluene/H$_2$O (4:1 v/v, 0.2 M). The resulting suspension was sparged with nitrogen for 10 min. The flask was sealed and the reaction mixture was stirred at 100 °C for 1 h. It was then allowed to cool to ambient temperature and partitioned between CH$_2$Cl$_2$ and 1 M NaOH. The phases were separated and the aqueous phase was extracted with CH$_2$Cl$_2$ (2 x). The combined organic phases were washed with NaCl solution (sat. aqueous), dried over Na$_2$SO$_4$,

filtered and concentrated under reduced pressure. Purification by column chromatography afforded the corresponding α,β-unsaturated ketone.
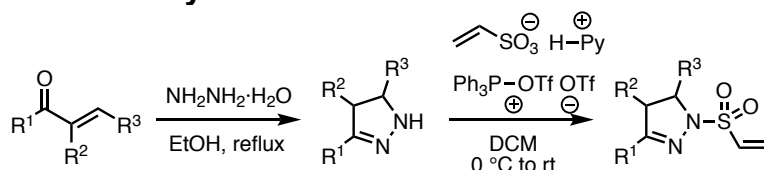
Synthesis of Pyrazoline Chloroacetamides

General Procedure F

Hydrazine monohydrate (2.0 equiv) was added to a suspension of the α,β-unsaturated ketone (1.0 equiv) in EtOH (0.3 M). The resulting reaction mixture was stirred at reflux temperature for 2.5 to 4 h before it was concentrated under reduced pressure. The crude pyrazoline was then dissolved in CH_2Cl_2 (0.2 M) and cooled to 0 °C. Triethylamine (3.0 equiv) was added dropwise, followed by chloroacetyl chloride (1.5 equiv). The resulting reaction mixture was stirred at ambient temperature for 30 min before it was diluted with CH_2Cl_2. The organic phase was sequentially washed with $NaHCO_3$ solution (sat. aqueous) and NaCl solution (sat. aqueous), dried over Na_2SO_4, filtered and concentrated under reduced pressure. Purification by column chromatography afforded the corresponding chloroacetamide.
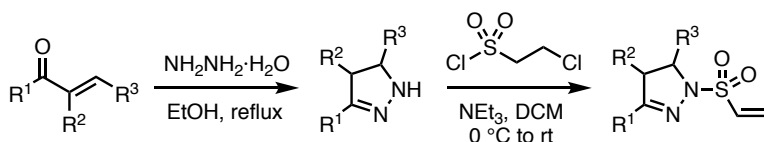
Synthesis of Pyrazoline Vinyl Sulfonamides

General Procedure G

Step 1: Hydrazine monohydrate (2.0 equiv) was added to a suspension of the α,β-unsaturated ketone (1.0 equiv) in EtOH (0.3 M) at rt. The reaction mixture was then stirred at reflux for 2h, then allowed to cool to rt and concentrated under reduced pressure to give the crude pyrazoline. This was used in the next step without further purification.

Step 2: A solution of triphenylphosphine oxide (2.2 equiv) in dichloromethane (0.25 M) was degassed at rt. Trifluoromethanesulfonic anhydride (1.0 equiv) was added at rt and the resultant mixture was stirred at this temperature for 15 min. In a separate flask, pyridine (1.0 equiv) was added to a solution of vinyl sulfonic acid (1.0 equiv) in dichloromethane (0.15 M) at rt and the mixture was then concentrated *in vacuo* to give a white solid. A solution of the vinyl sulfonic acid-pyridinium salt in dichloromethane (0.30 M) was added to the reaction mixture at rt and the resultant mixture was stirred at this temperature for 30 min. A solution of the crude pyrazoline (1.0 equiv) and triethylamine (2.0 equiv) in dichloromethane (0.20 M) was then added to the reaction mixture at 0 °C and the resultant mixture was allowed to warm to rt and stirred at rt for 16 h. The mixture was then diluted with dichloromethane and washed sequentially with 2.0 M aq HCl, sat aq $NaHCO_3$ and brine, then dried and concentrated under reduced pressure. Purification *via* flash column chromatography using both normal-phase (gradient elution, EtOAc in hexane) and reverse-phase (gradient elution, acetonitrile in water) conditions afforded the vinyl sulfonamides.

General Procedure H

Hydrazine monohydrate (2.0 equiv) was added to a suspension of the α,β-unsaturated ketone (1.0 equiv) in EtOH (0.3 M). The resulting reaction mixture was stirred at reflux temperature for 1 to 4 h before it was concentrated under reduced pressure. The crude pyrazoline. The crude pyrazoline was dissolved in CH_2Cl_2 (0.2 M) and cooled to 0 °C. Triethylamine (3.0 equiv) was added dropwise, followed by 2-chloroethanesulfonyl chloride (1.2–1.5 equiv). The resulting reaction mixture was stirred at room temperature 1 h before it was diluted with CH_2Cl_2. The organic phase was sequentially washed with 1M HCl, sat. aq. $NaHCO_3$ and brine, dried over Na_2SO_4, filtered and concentrated under reduced pressure. Purification by column chromatography or preparative TLC afforded the corresponding vinyl sulfonamide.

Stereoselective Synthesis of Pyrazoline Chloroacetamides
General Procedure I

(E)-1-phenyl-3-(quinoxalin-5-yl)prop-2-en-1-one (1.0 eq.), tert-butyl carbazate (1.1 eq.), potassium phosphate (1.3 eq.), indicated catalyst (10 mol%) were combined in THF (0.5 M) under nitrogen and stirred at 0 °C for 18h. The mixture was diluted with EtOAc, filtered to remove salts, concentrated and purified by silica gel chromatography to provide the stereoenriched pyrazoline.
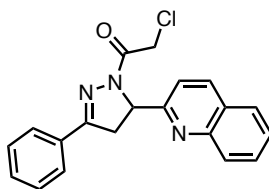
General Procedure J

Boc-protected pyrazoline (1.0 eq) was dissolved in DCM (0.2 M), cooled to 0 °C, and 4.0 M HCl in dioxane (10.0 eq.) was added under nitrogen. The mixture was stirred at room temperature for several hours (2-3) until starting material was consumed, then additional DCM was added (reducing HCl to 0.1 M). At 0 °C, chloroacetyl chloride (3.0 eq.) was added followed by TEA (13.0 eq.), and the reaction allowed to warm to room temperature and stirred for 1h. Water was added and the mixture extracted with DCM. Extracts were combined, washed with brine, dried over Na_2SO_4, concentrated under vacuum and purified by silica gel chromatography.

Formylation of Aryl Bromides
General Procedure K

Aryl bromide (1.0 Eq.) was dissolved in THF (to 0.2 M) and cooled to -78 ºC. n-BuLi (2.5 M in hexanes) was added dropwise, the reaction turned red-brown, and was stirred for 20 minutes at -78 ºC. Then, DMF (2.0 Eq.) was added dropwise. The reaction was removed from the -78 ºC bath and allowed to stir for 2h at room temperature. To quench the reaction the flask was cooled to -78 ºC quickly, sat. NH_4Cl (2 mL) was added dropwise, and the reaction allowed to warm to rt again. Water was added and the mixture was extracted with ethyl acetate. Combined organic extracts were washed with brine, dried over sodium sulfate, concentrated, and purified by silica gel chromatography to provide the resulting aldehyde.
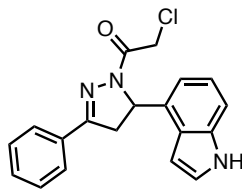
Characterization Data

HW-01-146

2-Chloro-1-(3-phenyl-5-(quinolin-2-yl)-4,5-dihydro-1*H*-pyrazol-1-yl)ethan-1-one.
General Procedure B was followed starting from acetophenone (0.30 mL, 2.6 mmol) and quinoline-2-carbaldehyde (445 mg, 2.83 mmol). Purification by column chromatography (EtOAc/hexane, 15:85) afforded the corresponding chalcone (326 mg) as a white solid. General Procedure F was followed starting from the above product (0.20 g, 0.77 mmol). Purification by column chromatography (EtOAc/hexane, 30:70) afforded the corresponding chloroacetamide (158 mg, 29% over three steps) as a white solid.
^{1}H NMR (400 MHz, CDCl$_3$): δ 8.15 (d, J = 8.5 Hz, 1H), 8.01 (dd, J = 8.5, 1.0 Hz, 1H), 7.80 (ddd, J = 6.9, 4.0, 1.6 Hz, 3H), 7.68 (ddd, J = 8.4, 6.9, 1.5 Hz, 1H), 7.55–7.49 (m, 2H), 7.49–7.43 (m, 3H), 5.88 (dd, J = 10.9, 6.1 Hz, 1H), 4.64 (d, J = 2.1 Hz, 2H), 3.89 – 3.71 (m, 2H); **^{13}C NMR** (151 MHz, CD$_2$Cl$_2$) δ 164.5, 159.6, 156.5, 148.3, 137.4, 131.3, 131.1, 130.1, 129.5, 129.2, 128.0, 128.0, 127.3, 127.0, 119.9, 62.7, 42.9, 40.6. **HRMS** (ESI): exact mass calculated for C$_{20}$H$_{17}$ClN$_3$O [(M+H)$^+$] 350.1055, found 350.1048.
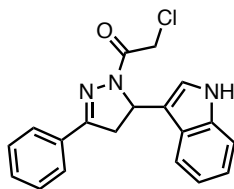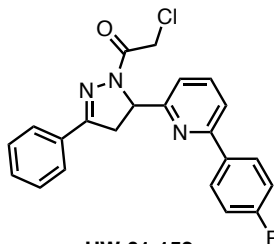

HW-01-151

1-(5-(1*H*-Indol-4-yl)-3-phenyl-4,5-dihydro-1*H*-pyrazol-1-yl)-2-chloroethan-1-one.
General Procedure B was followed starting from acetophenone (0.30 mL, 2.6 mmol) and indole-4-carbaldehyde (373 mg, 2.57 mmol). Purification by column chromatography (EtOAc/hexane, 30:70) afforded the corresponding chalcone (375 mg) as a yellow solid. General Procedure F was followed starting from the above product (0.20 g, 0.81 mmol). Purification by column chromatography (EtOAc/hexane, 30:70) afforded the corresponding chloroacetamide (100 mg, 20% over three steps) as a yellowish solid.
^{1}H NMR (600 MHz, CDCl$_3$): δ 8.27 (s, br, 1H), 7.83–7.71 (m, 2H), 7.52–7.39 (m, 3H), 7.32 (dt, J = 8.2, 1.0 Hz, 1H), 7.19 (dd, J = 3.3, 2.5 Hz, 1H), 7.14 (t, J = 7.7 Hz, 1H), 7.02 (d, J = 7.2 Hz, 1H), 6.43 (ddd, J = 3.2, 1.9, 0.9 Hz, 1H), 5.94 (dd, J = 11.9, 5.4 Hz, 1H), 4.74–4.51 (m, 2H), 3.85 (dd, J = 17.8, 12.0 Hz, 1H), 3.38 (dd, J = 17.8, 5.4 Hz, 1H); **^{13}C NMR** (151 MHz, CDCl$_3$): δ 164.0, 155.8, 136.4, 132.0, 131.0, 130.7, 128.8, 126.8, 124.4, 124.3, 122.1, 117.4, 111.0, 100.2, 59.9, 42.3, 41.5; **HRMS** (ESI): exact mass calculated for C$_{19}$H$_{17}$ClN$_3$O [(M+H)$^+$] 338.1055, found 338.1026.

HW-01-161

1-(5-(1*H*-Indol-3-yl)-3-phenyl-4,5-dihydro-1*H*-pyrazol-1-yl)-2-chloroethan-1-one.
General Procedure B was followed starting from acetophenone (0.10 mL, 0.86 mmol) and indole-3-carbaldehyde (124 mg, 0.857 mmol). The stirring time was prolonged to 22 h at ambient temperature followed by 1 h at 40 °C. Purification by column chromatography (EtOAc/hexane, 35:65) afforded the corresponding chalcone (22 mg) as a yellow solid.
General Procedure F was followed starting from the above product (22 mg, 89 μmol). Purification by column chromatography (EtOAc/hexane, 40:60) afforded the corresponding chloroacetamide (19 mg, 6% over three steps) as a white solid.
^{1}H NMR (600 MHz, CDCl$_3$): δ 8.48 (s, br, 1H), 7.84–7.77 (m, 2H), 7.53–7.43 (m, 3H), 7.34 (ddd, J = 8.9, 8.0, 1.0 Hz, 2H), 7.20–7.07 (m, 2H), 7.01 (ddd, J = 8.0, 7.0, 1.0 Hz, 1H), 5.92 (dd, J = 11.8, 4.8 Hz, 1H), 4.63 (d, J = 13.8 Hz, 1H), 4.57 (d, J = 13.8 Hz, 1H), 3.76 (dd, J = 17.8, 11.8 Hz, 1H), 3.48 (dd, J = 17.8, 4.8 Hz, 1H); **^{13}C NMR** (151 MHz, CDCl$_3$): δ 164.1, 156.1, 136.9, 131.0, 130.8, 128.9, 126.9, 124.2, 123.5, 122.2, 119.8, 118.5, 114.6, 111.8, 54.6, 42.5, 40.4; **HRMS** (ESI): exact mass calculated for C$_{19}$H$_{17}$ClN$_3$O [(M+H)$^+$] 338.1055, found 338.1032.


HW-01-152

2-Chloro-1-(5-(6-(4-fluorophenyl)pyridin-2-yl)-3-phenyl-4,5-dihydro-1*H*-pyrazol-1-yl)-ethan-1-one. General Procedure B was followed starting from acetophenone (50 μL, 0.43 mmol) and 6-(4-fluorophenyl)picolinaldehyde (86 mg, 0.43 mmol). Purification by column chromatography (EtOAc/hexane, 15:85) afforded the corresponding chalcone (108 mg) as a white solid.
General Procedure F was followed starting from the above product (60 mg, 0.20 mmol). Purification by column chromatography (EtOAc/hexane, 30:70) afforded the corresponding chloroacetamide (57 mg, 61% over three steps) as a white solid.
^{1}H NMR (400 MHz, CDCl$_3$): δ 7.98–7.88 (m, 2H), 7.84–7.76 (m, 2H), 7.72 (t, J = 7.7 Hz, 1H), 7.59 (d, J = 7.8 Hz, 1H), 7.51–7.40 (m, 3H), 7.32 (d, J = 7.6 Hz, 1H), 7.08 (t, J = 8.7 Hz, 2H), 5.76 (dd, J = 10.9, 5.5 Hz, 1H), 4.63 (d, J = 1.1 Hz, 2H), 3.84–3.63 (m, 2H); **^{13}C NMR** (151 MHz, CD$_2$Cl$_2$) δ 164.4, 164.0 (d, J = 247.8 Hz), 158.8, 156.6, 156.4, 138.1, 135.6 (d, J = 3.2 Hz), 131.5, 131.1, 129.2, 129.1 (d, J = 8.4 Hz), 127.3, 120.5, 119.5, 115.8 (d, J = 21.6 Hz), 62.1, 42.9, 40.7. **HRMS** (ESI): exact mass calculated for C$_{22}$H$_{18}$ClFN$_3$O [(M+H)$^+$] 394.1117, found 394.1099.
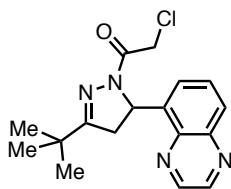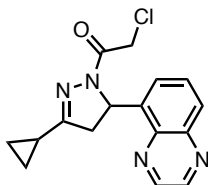
HW-1-174

1-(3-(*tert*-Butyl)-5-(quinoxalin-5-yl)-4,5-dihydro-1*H*-pyrazol-1-yl)-2-chloroethan-1-one. General Procedure A was followed starting from pinacolone (20 µL, 0.16 mmol) and quinoxaline-5-carbaldehyde (50 mg, 0.32 mmol). The crude α,β-unsaturated ketone (27 mg) was used in the following transformation without further purification.

General Procedure F was followed starting from the above product (26 mg, 0.11 mmol). Purification by column chromatography (EtOAc/hexane, 40:60) afforded the corresponding chloroacetamide (18 mg, 35% over three steps) as a white solid.

¹H NMR (300 MHz, CDCl₃): δ 8.88 (d, J = 1.8 Hz, 1H), 8.83 (d, J = 1.8 Hz, 1H), 8.04 (d, J = 8.6 Hz, 1H), 7.81–7.66 (m, 1H), 7.48 (d, J = 7.1 Hz, 1H), 6.46 (dd, J = 11.7, 4.9 Hz, 1H), 4.69–4.43 (m, 2H), 3.63 (dd, J = 18.1, 11.7 Hz, 1H), 2.79 (dd, J = 18.1, 5.0 Hz, 1H), 1.20 (s, 9H); **¹³C NMR** (151 MHz, CD₂Cl₂) δ 168.4, 164.1, 145.6, 144.4, 143.9, 140.5, 139.5, 130.2, 129.5, 125.9, 56.91, 42.8, 42.0, 34.5, 28.1. **HRMS** (ESI): exact mass calculated for $C_{17}H_{20}ClN_4O$ [(M+H)$^+$] 331.1320, found 331.1343.


HW-01-185

2-Chloro-1-(3-cyclopropyl-5-(quinoxalin-5-yl)-4,5-dihydro-1*H*-pyrazol-1-yl)ethan-1-one. General Procedure A was followed starting from cyclopropyl methyl ketone (20 µL, 0.20 mmol) and quinoxaline-5-carbaldehyde (64 mg, 0.40 mmol). Upon completion of the reaction, the reaction mixture was diluted with water (10 mL) and extracted with diethyl ether (3 x 20 mL). The combined organic phases were washed with NaCl solution (20 mL, sat. aqueous), dried over Na₂SO₄, filtered and concentrated under reduced pressure. Purification by column chromatography (EtOAc/hexane, 30:70) afforded the corresponding α,β-unsaturated ketone (53 mg) as a white solid.

General Procedure F was followed starting from the above product (23 mg, 0.10 mmol). Purification by column chromatography (EtOAc/hexane, 50:50) afforded the corresponding chloroacetamide (16 mg, 50% over three steps) as a white solid.

¹H NMR (300 MHz, CDCl₃): δ 8.87 (d, J = 1.8 Hz, 1H), 8.82 (d, J = 1.8 Hz, 1H), 8.03 (dd, J = 8.5, 1.4 Hz, 1H), 7.73 (dd, J = 8.5, 7.2 Hz, 1H), 7.56–7.42 (m, 1H), 6.47 (dd, J = 11.7, 4.9 Hz, 1H), 4.69–4.36 (m, 2H), 3.49 (dd, J = 18.0, 11.6 Hz, 1H), 2.57 (dd, J = 18.0, 4.9 Hz, 1H), 1.81 (ddd, J = 13.3, 8.4, 5.0 Hz, 1H), 1.04–0.66 (m, 4H); **¹³C NMR** (151 MHz, CD₂Cl₂) δ 163.6, 163.5, 145.6, 144.4, 143.9, 140.4, 139.3, 130.2, 129.5, 125.8, 56.3, 42.9, 42.7, 11.7, 7.4, 7.0. **HRMS** (ESI): exact mass calculated for $C_{16}H_{15}ClN_4NaO$ [(M+MeCN+Na)$^+$] 378.1082, found 378.1055.

PM-02-20A   **PM-02-20B**
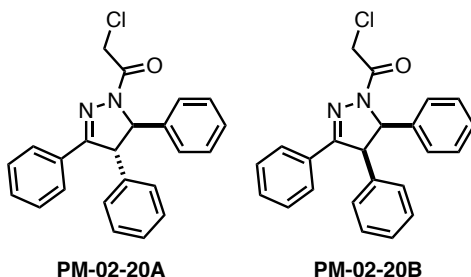
2-chloro-1-(3,4,5-triphenyl-4,5-dihydro-1*H*-pyrazol-1-yl)ethan-1-one. General Procedure C was followed starting from deoxybenzoin (235 mg, 1.2 mmol) and benzaldehyde (0.12 mL, 1.2 mmol). Purification by column chromatography (EtOAc/hexane, 10:90) afforded the corresponding α,β-unsaturated ketone (126 mg) as a mixture with benzaldehyde. This mixture was used in the following transformation without further purification.

General Procedure F was followed starting from the above product (120 mg, 0.42 mmol). Purification by column chromatography (EtOAc/hexane, 0:100 to 20:80) afforded the *trans*-substituted chloroacetamide **PM-02-20A** (13 mg, 2% over three steps) as a colorless film and the *cis*-substituted chloroacetamide **PM-02-20B** (8 mg, 1% over three steps) as a colorless film.

PM-02-20A [trans] : ^{1}H NMR (300 MHz, CDCl$_3$) δ 7.71 – 7.63 (m, 2H), 7.40 – 7.27 (m, 9H), 7.25 – 7.10 (m, 4H), 5.36 (d, *J* = 3.6 Hz, 1H), 4.68 (d, *J* = 2.7 Hz, 2H), 4.55 (d, *J* = 3.5 Hz, 1H). ^{13}**C NMR** (126 MHz, CDCl$_3$) δ 164.2, 157.2, 140.2, 139.3, 130.6, 130.2, 129.7, 129.3, 128.8, 128.3, 128.2, 127.6, 127.1, 125.5, 70.7, 61.5, 42.3. **HRMS** (ESI): exact mass calculated for C$_{23}$H$_{20}$ClN$_2$O [(M+H)$^+$] 375.1259, found 375.1253.

PM-02-20B [cis]: ^{1}H NMR (300 MHz, C$_6$D$_6$) δ 7.56 (dd, *J* = 6.9, 2.8 Hz, 2H), 6.96 (t, *J* = 3.4 Hz, 3H), 6.89 – 6.69 (m, 5H), 6.69 – 6.60 (m, 3H), 6.45 (dd, *J* = 6.3, 2.7 Hz, 2H), 5.46 (d, *J* = 11.8 Hz, 1H), 4.54 – 4.40 (m, 2H), 4.34 (d, *J* = 11.7 Hz, 1H). ^{13}**C NMR** (151 MHz, C$_6$D$_6$) δ 164.4, 155.8, 136.2, 135.3, 131.2, 130.1, 129.9, 128.6, 127.2, 127.2, 127.2, 66.9, 57.2, 42.2. **HRMS** (ESI): exact mass calculated for C$_{23}$H$_{20}$ClN$_2$O [(M+H)$^+$] 375.1259, found 375.1280.

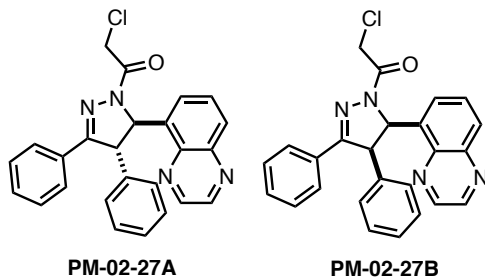**PM-02-43A**   **PM-02-43B**
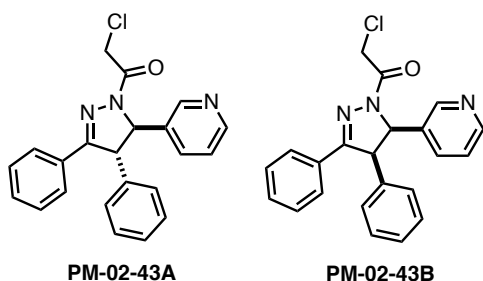
2-chloro-1-(3,4-diphenyl-5-(pyridin-3-yl)-4,5-dihydro-1*H*-pyrazol-1-yl)ethan-1-one. General procedure E was followed starting from 1-phenyl-3-(pyridin-3-yl)prop-2-en-1-one (630 mg, 3.0 mmol, 1 equiv.). The intermediate product 2-bromo-1-phenyl-3-(pyridin-3-yl)prop-2-en-1-one was obtained as a light orange oil (896 mg, 99%). ^{1}**H NMR** (300 MHz, CDCl$_3$) δ 8.86 (d, *J* = 2.3 Hz, 1H), 8.65 (dd, *J* = 4.8, 1.6 Hz, 1H), 8.38 (dt, *J* = 7.8, 1.9 Hz, 1H), 7.87 – 7.80 (m, 2H), 7.65 (s, 1H), 7.65 – 7.58 (m, 1H), 7.51 (m, 2H), 7.46 – 7.37 (m, 1H).

A mixture of 2-bromo-1-phenyl-3-(pyridin-3-yl)prop-2-en-1-one (58 mg, 0.20 mmol, 1.0 equiv), phenylboronic acid (32 mg, 0.26 mmol, 1.3 equiv), sodium carbonate (43 mg, 0.40 mmol, 2.0 equiv) and Pd(dppf)Cl$_2$ (7 mg, 10 µmol, 5 mol%) was taken up in toluene/H$_2$O (4:1 v/v, 1 mL). The resulting suspension was sparged with nitrogen for 10 min. The flask was sealed and the reaction mixture was stirred at 100 °C for 1 h. The reaction mixture was then allowed to cool to ambient temperature and partitioned between CH$_2$Cl$_2$ (20 mL) and 1 M NaOH (10 mL). The phases were separated and the aqueous phase was extracted with CH$_2$Cl$_2$ (2 x 20 mL). The combined organic phases were washed with NaCl solution (20 mL, sat. aqueous), dried over Na$_2$SO$_4$, filtered and concentrated under reduced pressure. Purification by column chromatography (EtOAc/hexane, 40:60 to 100:0) afforded the corresponding phenyl-substituted α,β-unsaturated ketone (41 mg, 72%). **¹H NMR** (300 MHz, CDCl$_3$) δ 8.54 – 8.32 (m, 2H), 7.96 (dt, J = 8.4, 1.2 Hz, 1H), 7.85 (dt, J = 7.0, 1.3 Hz, 1H), 7.59 – 7.50 (m, 1H), 7.50 – 7.40 (m, 2H), 7.40 – 7.22 (m, 6H), 7.14 (d, J = 2.7 Hz, 1H), 7.06 (dd, J = 8.6, 4.3 Hz, 1H).
General Procedure F was followed starting from the above product (41 mg, 0.14 mmol). Purification by column chromatography (7% to 9% MeOH/DCM) afforded the *trans*-substituted chloroacetamide **PM-02-43A** (18 mg, 25% over three steps) as a colorless film. Further purification (EtOAc/hexane, 20:80 to 100:0) afforded the *cis*-substituted chloroacetamide **PM-02-43B** (8 mg, 11% over three steps) as a colorless film.
PM-02-43A [trans] : ¹H NMR (600 MHz, C$_6$D$_6$) δ 8.61 (d, J = 2.3 Hz, 1H), 8.45 (dd, J = 4.8, 1.6 Hz, 1H), 7.56 – 7.48 (m, 2H), 7.11 (dt, J = 8.0, 2.0 Hz, 1H), 6.94 (ddt, J = 11.0, 8.6, 4.4 Hz, 6H), 6.83 – 6.77 (m, 2H), 6.66 (dd, J = 7.9, 4.7 Hz, 1H), 5.31 (d, J = 3.9 Hz, 1H), 4.39 – 4.26 (m, 2H), 4.19 (d, J = 4.0 Hz, 1H). **¹³C NMR** (151 MHz, C$_6$D$_6$) δ 164.0, 156.2, 149.9, 148.2, 139.4, 136.2, 132.8, 130.5, 130.5, 129.9, 128.8, 128.3, 127.8, 127.2, 123.8, 68.9, 61.3, 41.8. **HRMS** (ESI): exact mass calculated for C$_{22}$H$_{19}$ClN$_3$O [(M+H)$^+$] 376.1211, found 376.1196.
PM-02-43B [cis] : ¹H NMR (500 MHz, C$_6$D$_6$) δ 8.29 (d, J = 2.5 Hz, 1H), 8.15 (dd, J = 4.8, 1.7 Hz, 1H), 7.56 – 7.48 (m, 2H), 7.04 – 6.89 (m, 3H), 6.78 (dt, J = 7.9, 2.1 Hz, 1H), 6.65 (dd, J = 5.2, 2.8 Hz, 3H), 6.44 – 6.34 (m, 3H), 5.30 (d, J = 11.6 Hz, 1H), 4.47 – 4.36 (m, 2H), 4.30 (d, J = 11.7 Hz, 1H). **¹³C NMR** (126 MHz, C$_6$D$_6$) δ 164.8, 155.8, 149.1, 148.8, 134.9, 133.7, 131.7, 130.9, 130.3, 129.6, 128.7, 128.6, 128.6, 127.5, 122.5, 64.8, 56.9, 42.2. **HRMS** (ESI): exact mass calculated for C$_{22}$H$_{19}$ClN$_3$O [(M+H)$^+$] 376.1211, found 376.1211.
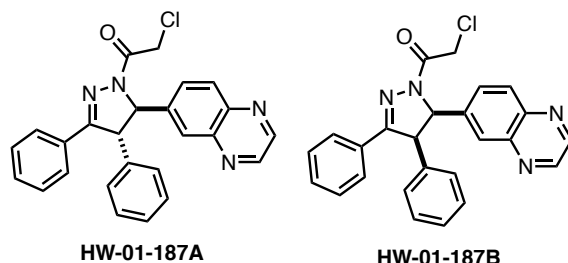

PM-02-27A   PM-02-27B

2-chloro-1-(3,4-diphenyl-5-(quinoxalin-5-yl)-4,5-dihydro-1*H*-pyrazol-1-yl)ethan-1-one. General Procedure C was followed starting from deoxybenzoin (39 mg, 0.20 mmol) and quinoxaline-6-carbaldehyde (32 mg, 0.20 mmol). Purification by column chromatography (EtOAc/hexane, 1:4) afforded the corresponding α,β-unsaturated ketone

(22 mg) as a mixture with quinoxaline-6-carbaldehyde. This mixture was used in the following transformation without further purification.

General Procedure F was followed starting from the above product (22 mg, 0.066 mmol). Purification by column chromatography (EtOAc/hexane, 0:100 to 40:60) afforded the *trans*-substituted chloroacetamide **PM-02-27A** (10 mg, 12% over three steps) as a colorless film and the *cis*-substituted chloroacetamide **PM-02-27B** (1.4 mg, 2% over three steps) as a colorless film.

PM-02-27A [trans]: ^{1}H NMR (300 MHz, CD$_2$Cl$_2$) δ 8.87 (dd, J = 22.7, 1.8 Hz, 2H), 8.08 (d, J = 8.4 Hz, 1H), 7.81 – 7.61 (m, 3H), 7.51 (d, J = 7.3 Hz, 1H), 7.46 – 7.13 (m, 8H), 6.47 (d, J = 3.0 Hz, 1H), 4.92 – 4.71 (m, 2H), 4.61 (d, J = 3.1 Hz, 1H). ^{13}**C NMR** (151 MHz, CD$_2$Cl$_2$) δ 164.3, 158.4, 145.8, 144.5, 144.1, 140.6, 139.5, 137.8, 130.9, 130.8, 130.2, 129.9, 129.6, 129.0, 128.3, 128.0, 127.8, 125.8, 66.8, 61.3, 42.7.**HRMS** (ESI): exact mass calculated for C$_{25}$H$_{20}$ClN$_4$O [(M+H)$^+$] 427.1320, found 427.1293.

PM-02-27B [cis]: ^{1}H NMR (300 MHz, C$_6$D$_6$) δ 8.26 – 8.16 (m, 2H), 7.71 (d, J = 8.4 Hz, 1H), 7.60 (dd, J = 6.8, 2.9 Hz, 1H), 7.24 (d, J = 7.2 Hz, 1H), 7.05 – 6.87 (m, 5H), 6.43 (m, 4H), 5.00 (d, J = 11.7 Hz, 1H), 4.68 (d, J = 12.8 Hz, 1H), 4.40 (d, J = 12.8 Hz, 1H). ^{13}**C NMR** (126 MHz, C$_6$D$_6$) δ 165.2, 156.2, 144.8, 143.4, 143.2, 140.3, 135.9, 135.3, 131.2, 130.1, 129.3, 129.2, 128.9, 128.6, 128.6, 127.7, 127.6, 127.1, 62.6, 57.1, 42.6. **HRMS** (ESI): exact mass calculated for C$_{25}$H$_{20}$ClN$_4$O [(M+H)$^+$] 427.1320, found 427.1338.


HW-01-187A   **HW-01-187B**

2-Chloro-1-(3,4-diphenyl-5-(quinoxalin-6-yl)-4,5-dihydro-1*H*-pyrazol-1-yl)ethan-1-one. General Procedure C was followed starting from deoxybenzoin (118 mg, 0.599 mmol) and quinoxaline-6-carbaldehyde (32 mg, 0.20 mmol). Purification by column chromatography (EtOAc/hexane, 40:60) afforded the corresponding α,β-unsaturated ketone (57 mg) containing impurities. This product was used in the following transformation without further purification. ^{1}**H NMR** (300 MHz, CDCl$_3$) δ 8.83 – 8.71 (m, 2H), 8.02 (d, J = 7.5 Hz, 2H), 7.96 – 7.82 (m, 2H), 7.74 – 7.29 (m, 10H).

General Procedure F was followed starting from the above product (57 mg). Purification by column chromatography (EtOAc/hexane, 45:55) afforded the *trans*-substituted chloroacetamide **HW-01-187A** (33 mg, 39% over three steps) as a white solid and the *cis*-substituted chloroacetamide **HW-01-187B** (6 mg, 7% over three steps) as a colorless film.

HW-01-187A [trans]: ^{1}H NMR (600 MHz, CDCl$_3$): δ 8.84 (s, 2H), 8.15 (d, J = 8.7 Hz, 1H), 7.97 (d, J = 2.0 Hz, 1H), 7.68 (ddd, J = 8.8, 4.9, 1.6 Hz, 3H), 7.42–7.27 (m, 6H), 7.24–7.16 (m, 2H), 5.61 (d, J = 3.8 Hz, 1H), 4.75 (d, J = 13.4 Hz, 1H), 4.71 (d, J = 13.4 Hz, 1H), 4.64 (d, J = 3.8 Hz, 1H); ^{13}**C NMR** (151 MHz, CDCl$_3$): δ 164.3, 156.9, 145.4, 145.2, 143.1, 142.7, 142.1, 138.7, 130.9, 130.7, 129.8, 129.8, 128.7, 128.3, 127.7, 127.6, 127.0, 125.8, 70.3, 61.5, 42.0; **HRMS** (ESI): exact mass calculated for C$_{25}$H$_{20}$ClN$_4$O [(M+MeCN+H)$^+$] 468.1585, found 468.1574.

HW-01-187B [cis]: ^{1}H NMR (600 MHz, CDCl$_3$): δ 8.75 (d, J = 1.8 Hz, 1H), 8.73 (d, J = 1.8 Hz, 1H), 7.74–7.70 (m, 2H), 7.64–7.60 (m, 2H), 7.37–7.33 (m, 1H), 7.31–7.27 (m, 2H), 7.20 (dd, J = 8.8, 2.0 Hz, 1H), 6.87 (s, 3H), 6.78 (s, 2H), 6.08 (d, J = 11.7 Hz, 1H), 5.34 (d, J = 11.7 Hz, 1H), 4.80 (d, J = 13.5 Hz, 1H), 4.67 (d, J = 13.5 Hz, 1H); ^{13}**C NMR** (151 MHz, CD$_2$Cl$_2$) δ 165.4, 157.0, 145.6, 145.5, 142.8, 142.4, 138.7, 134.7, 130.8, 130.7, 130.0 (2C), 129.2 (2C), 128.9, 128.6, 128.1, 127.7, 66.8, 57.7, 43.0. **HRMS** (ESI): exact mass calculated for C$_{25}$H$_{19}$ClN$_4$NaO [(M+MeCN+Na)$^+$] 490.1405, found 490.1400.

HW-01-198A   HW-01-198B
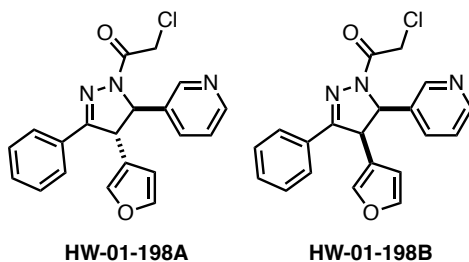
2-Chloro-1-(4-(furan-3-yl)-3-phenyl-5-(pyridin-3-yl)-4,5-dihydro-1H-pyrazol-1-yl)ethan-1-one. General procedure E was followed starting from 1-phenyl-3-(pyridin-3-yl)prop-2-en-1-one (630 mg, 3.0 mmol, 1 equiv.). The intermediate product 2-bromo-1-phenyl-3-(pyridin-3-yl)prop-2-en-1-one was obtained as a light orange oil (896 mg, 99%). A mixture of 2-bromo-1-phenyl-3-(pyridin-3-yl)prop-2-en-1-one (58 mg, 0.20 mmol, 1.0 equiv), 3-furanylboronic acid (29 mg, 0.26 mmol, 1.3 equiv), sodium carbonate (43 mg, 0.40 mmol, 2.0 equiv) and Pd(dppf)Cl$_2$ (7 mg, 10 µmol, 5 mol%) was taken up in toluene/H$_2$O (4:1 v/v, 1 mL). The resulting suspension was sparged with nitrogen for 10 min. The flask was sealed and the reaction mixture was stirred at 100 °C for 1 h. More portions of 3-furanylboronic acid (29 mg, 0.26 mmol, 1.3 equiv), sodium carbonate (22 mg, 0.20 mmol, 1.0 equiv) and Pd(dppf)Cl$_2$ (7 mg, 10 µmol, 5 mol%) were then added, the mixture was sparged again with nitrogen for 10 min, the flask was sealed and stirring was continued at 100°C for 2 h. The reaction mixture was then allowed to cool to ambient temperature and partitioned between CH$_2$Cl$_2$ (20 mL) and 1 M NaOH (10 mL). The phases were separated and the aqueous phase was extracted with CH$_2$Cl$_2$ (2 x 20 mL). The combined organic phases were washed with NaCl solution (20 mL, sat. aqueous), dried over Na$_2$SO$_4$, filtered and concentrated under reduced pressure. Purification by column chromatography (EtOAc/hexane, 40:60) afforded the corresponding furyl-substituted α,β-unsaturated ketone (46 mg, d.r. = 2:1).

General Procedure F was followed starting from the above product (43 mg, 0.16 mmol). Purification by column chromatography (EtOAc/hexane, 50:50 to 75:25) afforded the *trans*-substituted chloroacetamide **HW-01-198A** (27 mg, 39% over three steps) as a yellowish oil. Further purification by pTLC (EtOAc/hexane, 80:20) afforded the *cis*-substituted chloroacetamide **HW-01-198B** (4 mg, 6% over three steps) as a colorless film.

HW-01-198A [trans]: ^{1}H NMR (300 MHz, CDCl$_3$): δ 8.56 (dd, J = 5.0, 1.8 Hz, 2H), 7.73 (dd, J = 8.1, 1.7 Hz, 2H), 7.53 (dt, J = 7.9, 2.0 Hz, 1H), 7.44–7.27 (m, 6H), 6.26 (dd, J = 1.9, 0.9 Hz, 1H), 5.40 (d, J = 3.6 Hz, 1H), 4.63 (s, 2H), 4.54 (d, J = 3.6 Hz, 1H); ^{13}**C NMR** (151 MHz, CDCl$_3$): δ 164.3, 156.3, 149.5, 147.3, 144.6, 139.5, 135.3, 133.3, 131.0, 129.6, 128.8, 127.4, 124.0, 122.9, 108.8, 67.3, 51.4, 41.8; **HRMS** (ESI): exact mass calculated for C$_{20}$H$_{17}$ClN$_3$O$_2$ [(M+MeCN+H)$^+$] 407.1269, found 407.1246.

HW-01-198B [cis]: ^{1}H NMR (600 MHz, CDCl$_3$): δ 8.39 (dd, J = 4.9, 1.6 Hz, 1H), 8.32 (d, J = 2.3 Hz, 1H), 7.70–7.66 (m, 2H), 7.42–7.38 (m, 1H), 7.37–7.32 (m, 2H), 7.30 (d, J = 8.0 Hz, 1H), 7.13 (dd, J = 7.9, 4.8 Hz, 1H), 7.03 (d, J = 1.5 Hz, 2H), 5.78 (d, J = 11.4 Hz, 1H), 5.59 (s, 1H), 5.19 (d, J = 11.4 Hz, 1H), 4.73 (d, J = 13.5 Hz, 1H), 4.57 (d, J = 13.4 Hz, 1H); ^{13}**C NMR** (151 MHz, CDCl$_3$): δ 165.0, 156.1, 148.0, 147.6, 143.7, 141.4, 135.1, 134.9, 130.8, 129.8, 128.7, 127.5, 123.2, 119.0, 110.5, 63.8, 47.9, 42.1; **HRMS** (ESI): exact mass calculated for C$_{20}$H$_{17}$ClN$_3$O$_2$ [(M+MeCN+H)$^+$] 407.1269, found 407.1242.

HW-01-176A   **HW-01-176B**
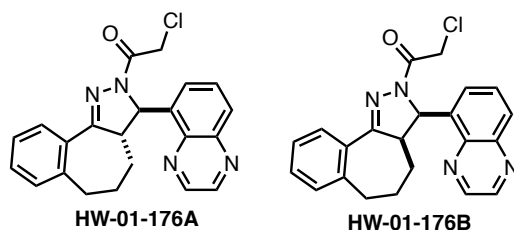
2-Chloro-1-(3-(quinoxalin-5-yl)-3a,4,5,6-tetrahydrobenzo[6,7]cyclohepta[1,2-c]pyrazol-2(3H)-yl)ethan-1-one. General Procedure A was followed starting from 1-benzosuberone (30 µL, 0.20 mmol) and quinoxaline-5-carbaldehyde (63 mg, 0.40 mmol). The crude α,β-unsaturated ketone (42 mg) was used in the following transformation without further purification.

General Procedure F was followed starting from the above product (41 mg, 0.14 mmol). Purification by column chromatography (EtOAc/hexane, 40:60) afforded the *trans*-substituted chloroacetamide **HW-01-176A** (9 mg, 17% over three steps) as a colorless film and the *cis*-substituted chloroacetamide **HW-01-176B** (5 mg, 9% over three steps) as a colorless film.

HW-01-176A [trans]: ^{1}H NMR ^{1}H NMR (600 MHz, CD$_2$Cl$_2$) δ 8.86 (m, 2H), 8.03 (dd, J = 8.5, 1.4 Hz, 1H), 7.82 – 7.71 (m, 2H), 7.58 – 7.49 (m, 1H), 7.28 (m, 2H), 7.17 (dd, J = 7.4, 1.4 Hz, 1H), 6.23 (d, J = 4.4 Hz, 1H), 4.74 (d, J = 13.6 Hz, 1H), 4.56 (d, J = 13.6 Hz, 1H), 3.21 (dt, J = 12.3, 5.0 Hz, 1H), 2.95 – 2.80 (m, 2H), 2.74 (m, 1H), 2.12 – 1.93 (m, 2H), 1.74 (m, 1H). ^{13}**C NMR** (151 MHz, CD$_2$Cl$_2$) δ 164.3, 162.5, 145.7, 144.5, 143.9, 142.7, 140.8, 138.8, 132.2, 130.7, 130.5, 130.1, 129.5, 129.0, 126.8, 125.9, 64.5, 57.9, 42.8, 36.7, 34.2, 26.2. **HRMS** (ESI): exact mass calculated for C$_{22}$H$_{20}$ClN$_4$O [(M+H)$^+$] 391.1320, found 391.1312.

HW-01-176B [cis]: ^{1}H NMR (600 MHz, CDCl$_3$): δ 8.88 (d, J = 6.7 Hz, 2H), 8.03 (td, J = 7.6, 6.9, 1.5 Hz, 2H), 7.71 (t, J = 7.8 Hz, 1H), 7.46 (d, J = 7.2 Hz, 1H), 7.33 (dtd, J = 18.5, 7.5, 1.6 Hz, 2H), 7.16–7.11 (m, 1H), 7.02 (d, J = 11.3 Hz, 1H), 4.73 (d, J = 13.0 Hz, 1H), 4.57 (d, J = 13.0 Hz, 1H), 4.03 (ddd, J = 13.0, 11.3, 3.5 Hz, 1H), 3.00 (ddd, J = 14.9, 10.6, 4.4 Hz, 1H), 2.65 (ddd, J = 14.7, 6.2, 3.9 Hz, 1H), 1.70 (ddp, J = 21.4, 10.7, 3.6 Hz, 2H), 1.32 (ddd, J = 13.5, 6.4, 3.3 Hz, 1H), 0.97 (ddt, J = 13.4, 9.6, 6.7 Hz, 1H); ^{13}**C NMR** (151 MHz, CDCl$_3$): δ 164.0, 162.0, 145.0, 144.2, 143.0, 141.4, 140.8, 135.0, 130.9, 130.8, 130.5, 129.8, 129.3, 128.9, 126.8, 126.7, 59.4, 50.0, 42.1, 34.2, 25.8, 24.7; **HRMS** (ESI): exact mass calculated for C$_{22}$H$_{20}$ClN$_4$O [(M+H)$^+$] 391.1320, found 391.1295.
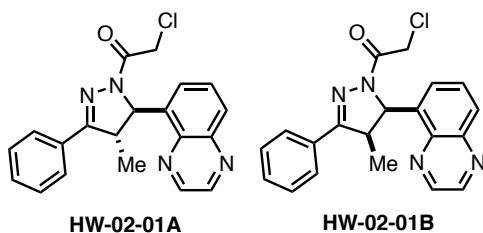
HW-02-01A   HW-02-01B

2-Chloro-1-(4-methyl-3-phenyl-5-(quinoxalin-5-yl)-4,5-dihydro-1*H*-pyrazol-1-yl)ethan-1-one. General Procedure D was followed starting from propiophenone (50 µL, 0.37 mmol) and quinoxaline-5-carbaldehyde (59 mg, 0.37 mmol). Purification by column chromatography (EtOAc/hexane, 25:75) afforded the corresponding α,β-unsaturated ketone (49 mg).

General Procedure F was followed starting from the above product (46 mg, 0.17 mmol). Purification by column chromatography (EtOAc/hexane, 35:65 to 40:60) afforded the *trans*-substituted chloroacetamide **HW-02-01A** (13 mg, 10% over three steps) as a white solid. Further purification by pTLC (EtOAc/hexane, 70:30) afforded the *cis*-substituted chloroacetamide **HW-02-01B** (2.5 mg, 2% over three steps, containing 9% of the *trans* product **xx**) as a white solid.

HW-02-01A [trans]: ^{1}H NMR (600 MHz, CDCl$_3$): δ 8.90 (d, *J* = 1.8 Hz, 1H), 8.88 (d, *J* = 1.8 Hz, 1H), 8.04 (dd, *J* = 8.4, 1.3 Hz, 1H), 7.75–7.71 (m, 2H), 7.69 (dd, *J* = 8.4, 7.2 Hz, 1H), 7.49–7.35 (m, 4H), 6.38 (d, *J* = 2.9 Hz, 1H), 4.78 (d, *J* = 13.2 Hz, 1H), 4.63 (d, *J* = 13.1 Hz, 1H), 3.55 (qd, *J* = 7.2, 3.0 Hz, 1H), 1.64 (d, *J* = 7.2 Hz, 3H); **^{13}C NMR** (151 MHz, CDCl$_3$): δ 164.3, 160.8, 144.9, 143.9, 143.4, 140.6, 137.5, 130.6, 130.0, 129.1, 128.8, 127.2, 125.1, 64.5, 50.0, 41.9, 18.9; **HRMS** (ESI): exact mass calculated for C$_{20}$H$_{18}$ClN$_4$O [(M+H)$^+$] 365.1164, found 365.1144.

HW-02-01B [cis]: ^{1}H NMR (500 MHz, CDCl$_3$): δ 8.91 (d, *J* = 1.8 Hz, 1H), 8.88 (d, *J* = 1.8 Hz, 1H), 8.07 (dd, *J* = 8.5, 1.4 Hz, 1H), 7.80–7.75 (m, 3H), 7.55 (dt, *J* = 7.2, 0.9 Hz, 1H), 7.45 (dd, *J* = 5.0, 1.9 Hz, 3H), 6.81 (d, *J* = 11.3 Hz, 1H), 4.81 (d, *J* = 13.4 Hz, 1H), 4.54 (d, *J* = 13.4 Hz, 1H), 4.38 (dq, *J* = 11.2, 7.5 Hz, 1H), 0.64 (d, *J* = 7.5 Hz, 3H); **HRMS** (ESI): exact mass calculated for C$_{20}$H$_{18}$ClN$_4$O [(M+H)$^+$] 365.1164, found 365.1140.
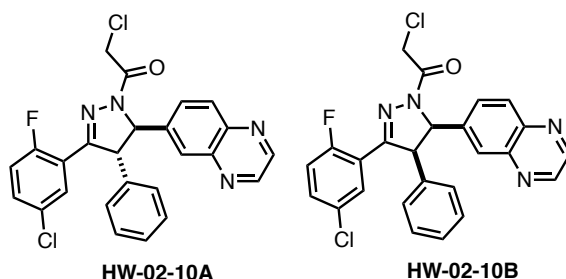
HW-02-10A   HW-02-10B

2-Chloro-1-(3-(5-chloro-2-fluorophenyl)-4-phenyl-5-(quinoxalin-6-yl)-4,5-dihydro-1*H*-pyrazol-1-yl)ethan-1-one. General procedure E was followed starting from 1-(5-chloro-2-fluorophenyl)-3-(quinoxalin-6-yl)prop-2-en-1-one (2.15g, 6.9 mmol, 1 equiv.). The intermediate product 2-bromo-1-(5-chloro-2-fluorophenyl)-3-(quinoxalin-6-yl)prop-2-en-1-one was obtained as a beige solid (2.66g, 99%). **^{1}H NMR** (300 MHz, CDCl$_3$) δ 8.90 (s, 2H), 8.63 (s, 1H), 8.18 (m, 2H), 7.96 (s, 1H), 7.64 – 7.45 (m, 2H), 7.17 (t, *J* = 8.8, 1H).
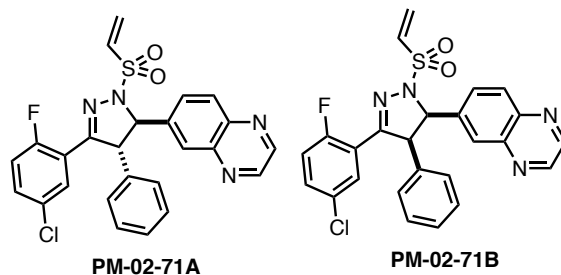
The vinyl bromide from above (2.66 g, 6.8 mmol, 1.0 equiv), phenylboronic acid (1.08 g, 8.8 mmol, 1.3 equiv), sodium carbonate (1.4 g, 0.14 mmol, 2.0 equiv) and Pd(dppf)Cl$_2$ (277 mg, 0.34 mmol, 5 mol%) was taken up in toluene/H$_2$O (4:1 v/v, 34 mL).

The resulting suspension was sparged with nitrogen for 10 min. The flask was sealed and the reaction mixture was stirred at 100 °C for 1.5 h. The reaction mixture was then allowed to cool to ambient temperature and partitioned between EtOAc (100 mL) and 1 M NaOH (30 mL). The phases were separated and the aqueous phase was extracted with EtOAc (3 x 70 mL). The combined organic phases were washed with NaCl solution (50 mL, sat. aqueous), dried over Na_2SO_4, filtered and concentrated under reduced pressure. Purification by column chromatography (EtOAc/hexane, 4:1 to 1:1 Hexane/EtOAc) afforded the corresponding phenyl-substituted α,β-unsaturated ketone (2.0 g, 76%) as a light yellow oil. **^{1}H NMR** (500 MHz, CDCl$_3$) *major isomer*, δ 8.82 – 8.77 (m, 2H), 7.90 (d, *J* = 1.9 Hz, 1H), 7.83 (d, *J* = 8.8 Hz, 1H), 7.59 (dd, *J* = 5.8, 2.7 Hz, 1H), 7.52 (s, 1H), 7.50 – 7.43 (m, 2H), 7.39 (dt, *J* = 4.9, 2.6 Hz, 3H), 7.34 (dd, *J* = 8.9, 2.1 Hz, 1H), 7.27 (d, *J* = 2.1 Hz, 1H), 7.07 (t, *J* = 8.9 Hz, 1H).

General Procedure F was followed starting from the corresponding chalcone (200 mg, 0.51 mmol). Purification by column chromatography (EtOAc/hexane, 50:50) afforded the *trans*-substituted chloroacetamide **HW-02-10A** (103 mg, 42% over two steps) as a yellow oil. Further purification by pTLC (EtOAc/hexane, 70:30) and column chromatography (MeOH/CH$_2$Cl$_2$, 1:99) afforded the *cis*-substituted chloroacetamide **HW-01-10B** (22 mg, 9% over three steps) as a colorless film.

HW-02-10A [trans]: **^{1}H NMR** (600 MHz, CDCl$_3$): δ 8.86 (s, 2H), 8.17 (d, *J* = 8.7 Hz, 1H), 7.96 (d, *J* = 2.0 Hz, 1H), 7.93 (dd, *J* = 6.2, 2.7 Hz, 1H), 7.67 (dd, *J* = 8.7, 2.1 Hz, 1H), 7.38–7.28 (m, 4H), 7.15–7.11 (m, 2H), 6.93 (dd, *J* = 10.6, 8.8 Hz, 1H), 5.63 (d, *J* = 4.0 Hz, 1H), 4.76 (dd, *J* = 4.0, 2.9 Hz, 1H), 4.74 (d, *J* = 13.4 Hz, 1H), 4.66 (d, *J* = 13.4 Hz, 1H); **^{13}C NMR** (151 MHz, CDCl$_3$): δ 164.5, 159.1 (d, *J* = 254.5 Hz), 153.1 (d, *J* = 3.9 Hz), 145.5, 145. 2, 143.1, 142.7, 141.9, 138.0, 132.2 (d, *J* = 8.9 Hz), 130.9, 129.9 (d, *J* = 3.3 Hz), 129.6, 129.1 (d, *J* = 3.2 Hz), 128.4, 127.7, 127.0, 125.8, 119.5 (d, *J* = 12.9 Hz), 118.1 (d, *J* = 24.3 Hz), 70.2, 62.6 (d, *J* = 6.1 Hz), 41.9; **HRMS** (ESI): exact mass calculated for C$_{25}$H$_{18}$Cl$_2$FN$_4$O [(M+MeCN+H)$^+$] 520.1101, found 520.1101.

HW-01-10B [cis]: **^{1}H NMR** (600 MHz, CDCl$_3$): δ 8.75 (d, *J* = 1.9 Hz, 1H), 8.73 (d, *J* = 1.8 Hz, 1H), 7.89 (dd, *J* = 6.1, 2.7 Hz, 1H), 7.73 (d, *J* = 8.7 Hz, 1H), 7.69 (d, *J* = 2.0 Hz, 1H), 7.29 (ddd, *J* = 8.8, 4.2, 2.7 Hz, 1H), 7.17 (dd, *J* = 8.7, 2.0 Hz, 1H), 6.90–6.82 (m, 4H), 6.76–6.65 (m, 2H), 6.09 (d, *J* = 12.0 Hz, 1H), 5.46 (dd, *J* = 12.0, 2.6 Hz, 1H), 4.78 (d, *J* = 13.5 Hz, 1H), 4.62 (d, *J* = 13.5 Hz, 1H); **^{19}F NMR** (376 MHz, CDCl$_3$): δ – 112.4; **^{13}C NMR** (151 MHz, CDCl$_3$): δ 165.2, 158.9 (d, *J* = 254.3 Hz), 153.5 (d, *J* = 3.4 Hz), 144.9, 144.7, 142.1, 141.9, 137.9, 133.2, 132.0 (d, *J* = 8.8 Hz), 129.9 (d, *J* = 3.0 Hz), 129.2, 129.1 (d, *J* = 3.3 Hz), 128.9, 128.2, 127.5, 126.9, 120.1 (d, *J* = 13.5 Hz), 118.0 (d, *J* = 23.9 Hz), 66.2, 58.6 (d, *J* = 5.3 Hz), 42.1; **HRMS** (ESI): exact mass calculated for C$_{25}$H$_{18}$Cl$_2$FN$_4$O [(M+MeCN+H)$^+$] 520.1101, found 520.1088.
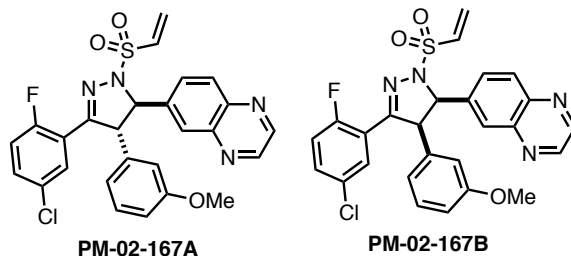

PM-02-71A   PM-02-71B

6-(3-(5-chloro-2-fluorophenyl)-4-phenyl-1-(vinylsulfonyl)-4,5-dihydro-1*H*-pyrazol-5-yl)quinoxaline. General procedure E was followed starting from 1-(5-chloro-2-fluorophenyl)-3-(quinoxalin-6-yl)prop-2-en-1-one (2.15g, 6.9 mmol, 1 equiv.). The intermediate product 2-bromo-1-(5-chloro-2-fluorophenyl)-3-(quinoxalin-6-yl)prop-2-en-1-one was obtained as a beige solid (2.66g, 99%). **¹H NMR** (300 MHz, CDCl₃) δ 8.90 (s, 2H), 8.63 (s, 1H), 8.18 (m, 2H), 7.96 (s, 1H), 7.64 – 7.45 (m, 2H), 7.17 (t, J = 8.8, 1H).

The vinyl bromide from above (2.66 g, 6.8 mmol, 1.0 equiv), phenylboronic acid (1.08 g, 8.8 mmol, 1.3 equiv), sodium carbonate (1.4 g, 0.14 mmol, 2.0 equiv) and Pd(dppf)Cl₂ (277 mg, 0.34 mmol, 5 mol%) was taken up in toluene/H₂O (4:1 v/v, 34 mL). The resulting suspension was sparged with nitrogen for 10 min. The flask was sealed and the reaction mixture was stirred at 100 °C for 1.5 h. The reaction mixture was then allowed to cool to ambient temperature and partitioned between EtOAc (100 mL) and 1 M NaOH (30 mL). The phases were separated and the aqueous phase was extracted with EtOAc (3 x 70 mL). The combined organic phases were washed with NaCl solution (50 mL, sat. aqueous), dried over Na₂SO₄, filtered and concentrated under reduced pressure. Purification by column chromatography (EtOAc/hexane, 4:1 to 1:1 Hexane/EtOAc) afforded the corresponding phenyl-substituted α,β-unsaturated ketone (2.0 g, 76%) as a light yellow oil. **¹H NMR** (500 MHz, CDCl₃) *major isomer*, δ 8.82 – 8.77 (m, 2H), 7.90 (d, J = 1.9 Hz, 1H), 7.83 (d, J = 8.8 Hz, 1H), 7.59 (dd, J = 5.8, 2.7 Hz, 1H), 7.52 (s, 1H), 7.50 – 7.43 (m, 2H), 7.39 (dt, J = 4.9, 2.6 Hz, 3H), 7.34 (dd, J = 8.9, 2.1 Hz, 1H), 7.27 (d, J = 2.1 Hz, 1H), 7.07 (t, J = 8.9 Hz, 1H).

General Procedure H was followed starting from the above product (267 mg, 0.69 mmol, 1.0 equiv.). Purification by column chromatography (EtOAc:hexane, 50:50 to 100:0) afforded the *trans*-substituted vinyl sulfonamide **PM-02-71A** (73 mg, 21%) as a white solid and the *cis*-substituted vinylsulfonamide **PM-02-71B** (68 mg, 20%) as a white solid.

PM-02-71A [trans] : ¹H NMR (600 MHz, CD₂Cl₂) δ 8.87 – 8.83 (m, 2H), 8.17 (d, J = 8.7 Hz, 1H), 7.94 (d, J = 2.1 Hz, 1H), 7.87 (dd, J = 6.1, 2.7 Hz, 1H), 7.80 (dd, J = 8.7, 2.1 Hz, 1H), 7.31 (m, 4H), 7.05 – 7.03 (m, 2H), 6.91 (dd, J = 10.4, 8.8 Hz, 1H), 6.77 (dd, J = 16.6, 10.0 Hz, 1H), 6.40 (d, J = 16.7 Hz, 1H), 6.25 (d, J = 10.0 Hz, 1H), 5.13 (d, J = 8.6 Hz, 1H), 4.83 (dd, J = 8.6, 3.1 Hz, 1H). **¹³C NMR** (151 MHz, CD₂Cl₂) δ 159.1 (d, J = 253.5 Hz), 154.5 (d, J = 3.6 Hz), 146.2, 146.0, 143.3, 142.3, 138.1, 132.8, 132.5 (d, J = 8.8 Hz), 131.7, 131.0, 130.2 (d, J = 3.1 Hz), 129.9 (d, J = 3.4 Hz), 129.8, 128.7, 128.5, 128.3, 127.8, 120.2 (d, J = 13.8 Hz), 118.3 (d, J = 24.2 Hz), 75.2, 64.6 (d, J = 5.0 Hz). **HRMS** (ESI): exact mass calculated for C₂₅H₁₈ClFN₄O₂S [(M+MeCN+H)⁺] 534.1161, found 534.1164.

PM-02-71B [cis] : ¹H NMR (600 MHz, CD₂Cl₂) δ 8.77 – 8.71 (m, 2H), 8.06 (dd, J = 6.3, 2.7 Hz, 1H), 7.88 (d, J = 2.0 Hz, 1H), 7.69 (d, J = 8.7 Hz, 1H), 7.40 (dd, J = 8.7, 2.0 Hz, 1H), 7.35 (ddd, J = 8.8, 4.3, 2.7 Hz, 1H), 7.01 – 6.93 (m, 4H), 6.86 – 6.78 (m, 2H), 6.74 (dd, J = 16.7, 10.0 Hz, 1H), 6.40 (d, J = 16.7 Hz, 1H), 6.30 (d, J = 9.9 Hz, 1H), 5.46 (d, J = 10.8 Hz, 1H), 5.18 (dd, J = 10.8, 2.5 Hz, 1H). **¹³C NMR** (151 MHz, CD₂Cl₂) δ 159.6 (d, J = 252.2 Hz), 156.0 (d, J = 3.5 Hz), 145.7 (d, J = 8.5 Hz), 142.7, 142.6, 138.1, 133.0, 132.8, 132.8, 132.5, 131.7, 130.3, 129.9, 129.7 (d, J = 3.3 Hz), 129.5, 128.9, 128.8, 128.7, 128.3, 120.1, 118.5 (d, J = 24.3 Hz), 71.0, 60.4 (d, J = 7.0 Hz). **HRMS** (ESI): exact mass calculated for C₂₅H₁₈ClFN₄O₂S [(M+MeCN+H)⁺] 534.1161, found 534.1159.

PM-02-167A   **PM-02-167B**

6-(3-(5-chloro-2-fluorophenyl)-4-(3-methoxyphenyl)-1-(vinylsulfonyl)-4,5-dihydro-1*H*-pyrazol-5-yl)quinoxaline. General procedure E was followed starting from 1-(5-chloro-2-fluorophenyl)-3-(quinoxalin-6-yl)prop-2-en-1-one (2.15g, 6.9 mmol, 1 equiv.). The intermediate product 2-bromo-1-(5-chloro-2-fluorophenyl)-3-(quinoxalin-6-yl)prop-2-en-1-one was obtained as a beige solid (2.66g, 99%).[1]**H NMR** (300 MHz, CDCl$_3$) δ 8.90 (s, 2H), 8.63 (s, 1H), 8.18 (m, 2H), 7.96 (s, 1H), 7.64 – 7.45 (m, 2H), 7.17 (t, *J* = 8.8, 1H).

The vinyl bromide from above (200 mg, 0.51 mmol, 1.0 equiv), 3-methoxyphenylboronic acid (58 mg, 0.61 mmol, 1.2 equiv), sodium carbonate (162 mg, 1.5 mmol, 2.0 equiv) and Pd(dppf)Cl$_2$ (19 mg, 0.026 mmol, 5 mol%) was taken up in toluene/H$_2$O (4:1 v/v, 2.5 mL). The resulting suspension was sparged with nitrogen for 10 min. The flask was sealed and the reaction mixture was stirred at 100 °C for 2 h. The reaction mixture was then allowed to cool to ambient temperature and partitioned between CH$_2$Cl$_2$ (20 mL) and 1 M NaOH (10 mL). The phases were separated and the aqueous phase was extracted with CH$_2$Cl$_2$ (2 x 20 mL). The combined organic phases were washed with NaCl solution (20 mL, sat. aqueous), dried over Na$_2$SO$_4$, filtered and concentrated under reduced pressure. Purification by column chromatography (EtOAc/hexane, 10:90 to 60:40) afforded the corresponding phenyl-substituted α,β-unsaturated ketone (174 mg, 81%). **^{1}H NMR** (300 MHz, CDCl$_3$) *major isomer* δ 8.75 (s, 2H), 7.89 (t, *J* = 2.0 Hz, 1H), 7.80 (d, *J* = 8.8 Hz, 1H), 7.54 (dd, *J* = 5.8, 2.7 Hz, 1H), 7.46 (s, 1H), 7.41 (ddd, *J* = 8.8, 4.4, 2.7 Hz, 1H), 7.33 (dd, *J* = 8.9, 2.0 Hz, 1H), 7.30 – 7.20 (m, 1H), 7.04 (t, *J* = 8.9 Hz, 1H), 6.92 – 6.87 (m, 1H), 6.84 – 6.73 (m, 2H), 3.70 (s, 3H). General Procedure H was followed starting from the above product (35 mg, 0.08 mmol, 1.0 equiv.). Purification by column chromatography (EtOAc:hexane, 30:70 to 100:0) afforded the *trans*-substituted vinyl sulfonamide **PM-02-167A** (22 mg, 54%) as a white solid and the *cis*-substituted vinylsulfonamide **PM-02-167B** (6 mg, 14%) as a white solid.

PM-02-167A [trans] : ^{1}H NMR (600 MHz, CD$_2$Cl$_2$) δ 8.86 (q, *J* = 1.9 Hz, 2H), 8.18 (d, *J* = 8.7 Hz, 1H), 7.97 (d, *J* = 2.0 Hz, 1H), 7.86 (dd, *J* = 6.2, 2.7 Hz, 1H), 7.81 (dd, *J* = 8.7, 2.1 Hz, 1H), 7.32 (ddd, *J* = 8.8, 4.3, 2.7 Hz, 1H), 7.24 (t, *J* = 7.9 Hz, 1H), 6.93 (dd, *J* = 10.4, 8.8 Hz, 1H), 6.83 (ddd, *J* = 8.3, 2.6, 0.9 Hz, 1H), 6.78 (dd, *J* = 16.7, 10.0 Hz, 1H), 6.63 (dt, *J* = 7.6, 1.2 Hz, 1H), 6.57 (t, *J* = 2.2 Hz, 1H), 6.41 (d, *J* = 16.6 Hz, 1H), 6.25 (d, *J* = 9.9 Hz, 1H), 5.17 (d, *J* = 8.5 Hz, 1H), 4.80 (dd, *J* = 8.5, 3.0 Hz, 1H), 3.71 (s, 3H). **^{13}C NMR** (151 MHz, CD$_2$Cl$_2$) δ 160.7, 159.2 (d, *J* = 253.4 Hz), 154.4 (d, *J* = 4.0 Hz), 146.1, 145.9, 143.3 (d, *J* = 5.4 Hz), 142.4, 139.6, 132.9, 132.5 (d, *J* = 9.0 Hz), 131.6, 131.0, 130.8, 130.2 (d, *J* = 3.6 Hz), 129.8 (d, *J* = 4.0 Hz), 128.6, 127.8, 120.4, 120.3 (d, *J* = 13.9 Hz), 118.3 (d, *J* = 24.0 Hz), 114.4, 113.6, 75.0, 64.5 (d, *J* = 5.6 Hz), 55.6. **HRMS** (ESI): exact mass calculated for C$_{26}$H$_{21}$ClFN$_4$O$_3$S [(M+MeCN+H)$^+$] 564.1267, found 564.1267.

PM-02-167B [cis] : ^{1}H NMR (400 MHz, CD2Cl2) δ 8.76 (d, *J* = 5.9 Hz, 2H), 8.04 (dd, *J* = 6.3, 2.7 Hz, 1H), 7.90 (s, 1H), 7.73 (d, *J* = 8.8 Hz, 1H), 7.45 (dd, *J* = 8.7, 2.0 Hz, 1H), 7.35 (dt, *J* = 7.3, 3.1 Hz, 1H), 7.03 – 6.94 (m, 1H), 6.90 (t, *J* = 8.0 Hz, 1H), 6.73 (dd, *J* = 16.6,

10.0 Hz, 1H), 6.54 – 6.23 (m, 5H), 5.45 (d, J = 10.8 Hz, 1H), 5.15 (dd, J = 10.9, 2.5 Hz, 1H), 3.48 (s, 3H). **^{13}C NMR** (151 MHz, CD$_2$Cl$_2$) δ 160.1, 159.6 (d, J = 254.2 Hz), 155.9 (d, J = 3.8 Hz), 145.7, 145.6, 142.7, 142.6, 138.1, 134.5, 132.8 (d, J = 8.9 Hz), 132.4, 131.7, 130.3 (d, J = 3.2 Hz), 129.9, 129.7 (d, J = 3.2 Hz), 128.8, 128.66, 121.8, 120.2 (d, J = 12.8 Hz), 118.5 (d, J = 24.3 Hz), 115.4, 113.6, 70.9, 60.4 (d, J = 6.9 Hz), 55.5. **HRMS** (ESI): exact mass calculated for C$_{26}$H$_{20}$ClFN$_4$NaO$_3$S [(M+MeCN+Na)$^+$] 586.1087, found 586.1109.

PM-2-162A   **PM-2-162B**
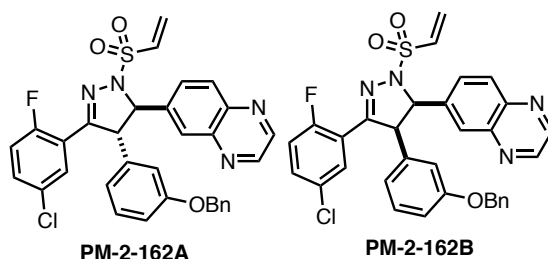
6-(4-(3-(benzyloxy)phenyl)-3-(5-chloro-2-fluorophenyl)-1-(vinylsulfonyl)-4,5-dihydro-1*H*-pyrazol-5-yl)quinoxaline. General procedure E was followed starting from 1-(5-chloro-2-fluorophenyl)-3-(quinoxalin-6-yl)prop-2-en-1-one (2.15g, 6.9 mmol, 1 equiv.). The intermediate product 2-bromo-1-(5-chloro-2-fluorophenyl)-3-(quinoxalin-6-yl)prop-2-en-1-one was obtained as a beige solid (2.66g, 99%). **^{1}H NMR** (300 MHz, CDCl$_3$) δ 8.90 (s, 2H), 8.63 (s, 1H), 8.18 (m, 2H), 7.96 (s, 1H), 7.64 – 7.45 (m, 2H), 7.17 (t, J = 8.8, 1H).

The vinyl bromide from above (200 mg, 0.51 mmol, 1.0 equiv), 3-benzyloxyphenylboronic acid (139 mg, 0.61 mmol, 1.2 equiv), sodium carbonate (162 mg, 1.5 mmol, 2.0 equiv) and Pd(dppf)Cl$_2$ (19 mg, 0.026 mmol, 5 mol%) was taken up in toluene/H$_2$O (4:1 v/v, 2.5 mL). The resulting suspension was sparged with nitrogen for 10 min. The flask was sealed and the reaction mixture was stirred at 100 °C for 2 h. The reaction mixture was then allowed to cool to ambient temperature and partitioned between CH$_2$Cl$_2$ (20 mL) and 1 M NaOH (10 mL). The phases were separated and the aqueous phase was extracted with CH$_2$Cl$_2$ (2 x 20 mL). The combined organic phases were washed with NaCl solution (20 mL, sat. aqueous), dried over Na$_2$SO$_4$, filtered and concentrated under reduced pressure. Purification by column chromatography (EtOAc/hexane, 10:90 to 60:40) afforded the corresponding phenyl-substituted α,β-unsaturated ketone (203 mg, 80%). **^{1}H NMR** (300 MHz, CDCl$_3$) δ 8.81 (s, 2H), 7.92 (d, J = 1.9 Hz, 1H), 7.82 (d, J = 8.8 Hz, 1H), 7.58 (dd, J = 5.8, 2.7 Hz, 1H), 7.49 (s, 1H), 7.40 – 7.27 (m, 8H), 7.09 (t, J = 8.9 Hz, 2H), 6.92 – 6.83 (m, 2H), 5.00 (s, 2H).

General Procedure H was followed starting from the above product (41 mg, 0.08 mmol, 1.0 equiv.). Purification by column chromatography (EtOAc:hexane, 20:80 to 100:0) afforded the *trans*-substituted vinyl sulfonamide **PM-02-162A** (28 mg, 59%) as a white solid and the *cis*-substituted vinylsulfonamide **PM-02-162B** (9 mg, 20%) as a white solid.

PM-02-162A [trans] : ^{1}H NMR (600 MHz, CD2Cl2) δ 8.85 (m, 2H), 8.17 (d, J = 8.7 Hz, 1H), 7.96 (d, J = 2.0 Hz, 1H), 7.85 (dd, J = 6.1, 2.7 Hz, 1H), 7.79 (dd, J = 8.7, 2.1 Hz, 1H), 7.38 – 7.35 (m, 4H), 7.34 – 7.29 (m, 2H), 7.27 – 7.21 (m, 1H), 6.95 – 6.89 (m, 2H), 6.75 (dd, J = 16.6, 9.9 Hz, 1H), 6.66 – 6.63 (m, 2H), 6.40 (d, J = 16.6 Hz, 1H), 6.22 (d, J = 9.9

Hz, 1H), 5.16 (d, J = 8.5 Hz, 1H), 4.98 (d, J = 1.6 Hz, 2H), 4.80 (dd, J = 8.5, 3.0 Hz, 1H). **13C NMR** (151 MHz, CD$_2$Cl$_2$) δ 159.8, 159.2 (d, J = 253.8 Hz), 154.3 (d, J = 3.9 Hz), 146.1, 145.9, 143.3 (d, J = 1.9 Hz), 142.3, 139.7, 137.1, 132.9, 132.5 (d, J = 9.4 Hz), 131.6, 131.0, 130.9, 130.2 (d, J = 3.8 Hz), 129.8 (d, J = 3.8 Hz), 128.9, 128.5, 128.5, 127.9, 127.8, 120.7, 120.2 (d, J = 14.0 Hz), 118.3 (d, J = 24.0 Hz), 115.1, 114.8, 75.0, 70.5, 64.5 (d, J = 5.5 Hz). **HRMS** (ESI): exact mass calculated for C$_{32}$H$_{24}$ClFN$_4$NaO$_3$S [(M+Na)$^+$] 621.1134, found 621.1110.

PM-02-162B [cis] : 1H NMR (600 MHz, CD$_2$Cl$_2$) δ 8.78 – 8.73 (m, 2H), 8.02 (dd, J = 6.3, 2.7 Hz, 1H), 7.90 (d, J = 2.0 Hz, 1H), 7.69 (d, J = 8.8 Hz, 1H), 7.38 – 7.27 (m, 6H), 7.23 (d, J = 7.4 Hz, 2H), 6.99 (dd, J = 10.7, 8.8 Hz, 1H), 6.73 (dd, J = 16.7, 10.0 Hz, 1H), 6.57 (dd, J = 8.4, 2.5 Hz, 1H), 6.45 – 6.37 (m, 3H), 6.29 (d, J = 10.0 Hz, 1H), 5.45 (d, J = 10.8 Hz, 1H), 5.13 (dd, J = 10.9, 2.4 Hz, 1H), 4.85 – 4.62 (m, 2H). **13C NMR** (151 MHz, CD$_2$Cl$_2$) δ 159.6 (d, J = 254.3 Hz), 159.2, 155.8 (d, J = 4.4 Hz), 145.7, 145.6, 142.7, 142.6, 138.1, 137.2, 134.5, 132.8 (d, J = 9.3 Hz), 132.4, 131.7, 130.3 (d, J = 3.5 Hz), 129.9, 129.8, 129.6 (d, J = 4.0 Hz), 128.9, 128.8, 128.6 (d, J = 3.3 Hz), 128.3, 127.7, 122.1 (d, J = 5.6 Hz), 120.1 (d, J = 13.1 Hz), 118.5 (d, J = 24.5 Hz), 114.8, 71.0, 70.3, 60.4 (d, J = 7.1 Hz). **HRMS** (ESI): exact mass calculated for C$_{32}$H$_{24}$ClFN$_4$NaO$_3$S [(M+Na)$^+$] 621.1134, found 621.1121.

PM-02-103A　　　　**PM-02-103B**
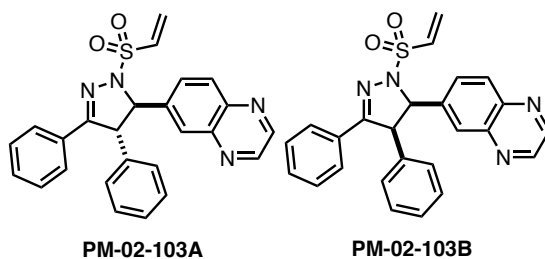
6-(3,4-diphenyl-1-(vinylsulfonyl)-4,5-dihydro-1*H*-pyrazol-5-yl)quinoxaline. General Procedure C was followed starting from deoxybenzoin (2.9 g, 15 mmol) and quinoxaline-6-carbaldehyde (790 mg, 5.0 mmol). Purification by column chromatography (EtOAc/hexane, 1:4 to 1:0) afforded the corresponding α,β-unsaturated ketone (1.5 g, 89%). **1H NMR** (300 MHz, CDCl$_3$) δ 8.83 – 8.71 (m, 2H), 8.02 (d, J = 7.5 Hz, 2H), 7.96 – 7.82 (m, 2H), 7.74 – 7.29 (m, 10H).

General Procedure H was followed starting from the above product (108 mg, 0.32 mmol, 1.0 equiv.). Purification by column chromatography (EtOAc:hexane, 40:60 to 100:0) afforded the *trans*-substituted vinyl sulfonamide **PM-02-103A** (70 mg, 49% over three steps) as a white solid and the *cis*-substituted vinylsulfonamide **PM-02-103B** (19 mg, 13% over three steps) as a white solid.

PM-02-103A [trans] : 1H NMR (600 MHz, CD$_2$Cl$_2$) δ 8.85 (d, J = 1.7 Hz, 2H), 8.16 (d, J = 8.7 Hz, 1H), 7.95 (d, J = 2.0 Hz, 1H), 7.80 (dd, J = 8.7, 2.0 Hz, 1H), 7.64 – 7.58 (m, 2H), 7.38 – 7.32 (m, 4H), 7.32 – 7.25 (m, 2H), 7.13 (dd, J = 8.0, 1.6 Hz, 2H), 6.76 (dd, J = 16.6, 10.0 Hz, 1H), 6.37 (d, J = 16.7 Hz, 1H), 6.20 (d, J = 9.9 Hz, 1H), 5.13 (d, J = 8.0 Hz, 1H), 4.76 (d, J = 8.0 Hz, 1H). **13C NMR** (151 MHz, CD$_2$Cl$_2$) δ 157.9, 146.1, 145.9, 143.3, 143.3, 142.7, 139.2, 133.0, 131.1, 131.0, 130.9, 130.3, 130.0, 128.9, 128.6, 128.6, 128.3, 128.1, 127.7, 74.9, 63.6. **HRMS** (ESI): exact mass calculated for C$_{25}$H$_{21}$N$_4$O$_2$S [(M+H)$^+$] 441.1380, found 441.1390.

PM-02-103B [cis] : 1H NMR (600 MHz, CD$_2$Cl$_2$) δ 8.75 (d, J = 9.1 Hz, 2H), 7.90 (d, J = 1.9 Hz, 1H), 7.77 – 7.67 (m, 3H), 7.44 (dd, J = 8.7, 2.0 Hz, 1H), 7.42 – 7.38 (m, 1H), 7.35 (t, J = 7.5 Hz, 2H), 7.05 – 6.94 (m, 3H), 6.89 (s, 2H), 6.77 (dd, J = 16.7, 10.0 Hz, 1H), 6.38 (d, J = 16.7 Hz, 1H), 6.27 (d, J = 10.0 Hz, 1H), 5.43 (d, J = 10.5 Hz, 1H), 5.07 (d, J = 10.6 Hz, 1H). **^{13}C NMR** (151 MHz, CD$_2$Cl$_2$) δ 159.9, 145.7, 145.6, 142.7, 142.6, 138.5, 133.7, 132.6, 132.2, 131.7, 131.2, 130.4, 130.0, 129.5, 129.1, 129.0, 128.7, 128.2, 128.0, 71.4, 59.2. **HRMS** (ESI): exact mass calculated for C25H21N4O2S [(M+H)$^+$] 441.1380, found 441.1400.

(R)-EN082:
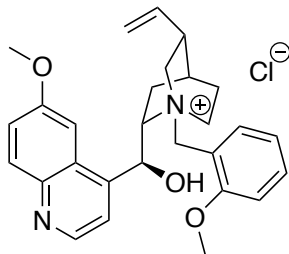
Catalyst A

Catalyst A (1S,2S,4S,5R)-2-((R)-hydroxy(6-methoxyquinolin-4-yl)methyl)-1-(2-methoxybenzyl)-5-vinylquinuclidin-1-ium chloride (for (R)-EN082): Thionyl chloride (1.0 mL, 14 mmol) was added dropwise to a solution of 2-methoxybenzyl alcohol (967 mg, 7.0 mmol) in DCM (20 mL) at 0 °C, and the solution was then stirred at rt for 4h. Volatiles were then evaporated to provide the benzyl chloride. Quinidine (324 mg, 1.0 mmol) was added to a solution of 2-methoxybenzyl chloride (313 mg, 2.0 mmol) in toluene (5 mL) and the mixture was stirred at 80 °C for 19h. After cooling to rt, the mixture was concentrated and and purified by silica gel chromatography (0-4% MeOH/DCM) to provide the title compound (150 mg, 0.31 mmol, 31%) as a maroon foam. **LC/MS** calc. 445.2, found 455.2. **^{1}H NMR** (400 MHz, DMSO-d_6) δ 8.82 (d, J = 4.6 Hz, 1H), 8.02 (d, J = 9.2 Hz, 1H), 7.77 (d, J = 4.6 Hz, 1H), 7.67 (d, J = 7.7 Hz, 1H), 7.58 (t, J = 7.9 Hz, 1H), 7.49 (d, J = 9.3 Hz, 1H), 7.39 (s, 1H), 7.25 (d, J = 8.3 Hz, 1H), 7.15 (t, J = 7.4 Hz, 1H), 6.98 (d, J = 3.6 Hz, 1H), 6.56 (s, 1H), 6.05 (ddd, J = 17.5, 10.7, 7.3 Hz, 1H), 5.77 (s, 1H), 5.29 – 5.17 (m, 2H), 5.06 (d, J = 12.6 Hz, 1H), 4.75 (d, J = 12.5 Hz, 1H), 4.21 (t, J = 10.5 Hz, 1H), 4.09 (s, 3H), 3.90 (s, 3H), 3.47 (t, J = 11.6 Hz, 1H), 2.95 (q, J = 10.1 Hz, 1H), 2.65 (d, J = 9.2 Hz, 1H), 2.38 (t, J = 11.6 Hz, 1H), 2.09 (s, 1H), 1.88 (s, 1H), 1.82 – 1.71 (m, 2H), 1.10 – 0.97 (m, 1H). Procedure followed from Mahé *et al.* Enantioselective Phase-Transfer Catalysis: Synthesis of Pyrazolines. *Angewandte Chemie International Edition* **2010**, *49* (39), 7072–7075. https://doi.org/10.1002/anie.201002485.
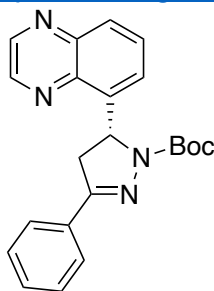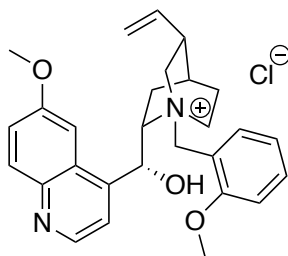
***tert*-butyl   (*R*)-3-phenyl-5-(quinoxalin-5-yl)-4,5-dihydro-1*H*-pyrazole-1-carboxylate**:
Following general procedure I and Catalyst A, (E)-1-phenyl-3-(quinoxalin-5-yl)prop-2-en-1-one (130 mg, 0.50 mmol) were combined in THF (1 mL) under nitrogen and stirred at 0 °C for 18 h. The mixture was diluted with EtOAc, filtered to remove salts, concentrated and purified by silica gel chromatography (0-35% EtOAc/Hex) to provide the pyrazoline (61 mg, 0.16 mmol, 31%) as a white solid. **LC/MS** calc. 375.15, found 375.2. **¹H NMR** (400 MHz, Chloroform-*d*) δ 8.97 – 8.91 (m, 2H), 8.09 (d, *J* = 8.4 Hz, 1H), 7.84 – 7.75 (m, 3H), 7.69 (d, *J* = 7.3 Hz, 1H), 7.44 – 7.39 (m, 3H), 6.65 (dd, *J* = 12.2, 5.4 Hz, 1H), 4.03 (dd, *J* = 17.3, 12.0 Hz, 1H), 3.17 (dd, *J* = 17.3, 5.4 Hz, 1H), 1.30 (s, 9H).
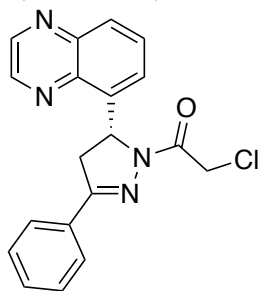
(*R*)-EN82

(R)-EN082 - (*R*)-2-chloro-1-(3-phenyl-5-(quinoxalin-5-yl)-4,5-dihydro-1*H*-pyrazol-1-yl)ethan-1-one - Following general procedure J, tert-butyl (R)-3-phenyl-5-(quinoxalin-5-yl)-4,5-dihydro-1H-pyrazole-1-carboxylate (40 mg, 0.11 mmol) was converted to **(R)-EN082** (22 mg, 0.064 mmol, 58%) as a white solid. **HRMS** calc. 351.1007, found 351.1007. **¹H NMR** (400 MHz, Chloroform-*d*) δ 8.92 (dd, *J* = 16.1, 1.7 Hz, 2H), 8.09 (d, *J* = 8.5 Hz, 1H), 7.84 – 7.71 (m, 3H), 7.59 (d, *J* = 7.2 Hz, 1H), 7.52 – 7.42 (m, 3H), 6.72 (dd, *J* = 11.9, 5.1 Hz, 1H), 4.81 (d, *J* = 13.4 Hz, 1H), 4.64 (d, *J* = 13.5 Hz, 1H), 4.07 (dd, *J* = 17.9, 11.9 Hz, 1H), 3.25 (dd, *J* = 17.9, 5.1 Hz, 1H). **¹³C NMR** (151 MHz, DMSO) δ 163.8, 156.8, 146.3, 145.3, 143.1, 139.7, 139.5, 131.2, 131.2, 130.5, 129.2, 129.0, 127.4, 125.8, 56.6, 43.0, 42.3.
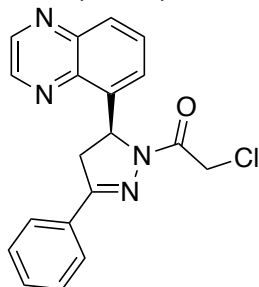
(S)-EN082:

Catalyst B

Catalyst   B   (1*S*,2*S*,4*S*,5*R*)-2-((*S*)-hydroxy(6-methoxyquinolin-4-yl)methyl)-1-(2-methoxybenzyl)-5-vinylquinuclidin-1-ium chloride (for *S*-EN082) was synthesized from quinine, otherwise identically to Catalyst A, according to Mahé *et al.* Enantioselective Phase-Transfer Catalysis: Synthesis of Pyrazolines. *Angewandte Chemie International Edition* **2010**, *49* (39), 7072–7075. https://doi.org/10.1002/anie.201002485.
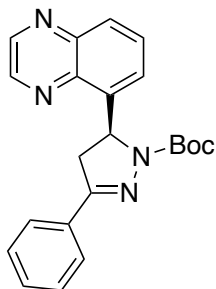
tert-butyl (*S*)-3-phenyl-5-(quinoxalin-5-yl)-4,5-dihydro-1*H*-pyrazole-1-carboxylate:
General Procedure I was followed from (E)-1-phenyl-3-(quinoxalin-5-yl)prop-2-en-1-one (130 mg, 0.50 mmol), using Catalyst B to provide the title compound (122 mg, 0.32 mmol, 65%) as a white solid. **LC/MS** calc. 375.17, found 375.2. **¹H NMR** (400 MHz, Chloroform-*d*) δ 8.94 (d, *J* = 10.0 Hz, 2H), 8.09 (d, *J* = 8.5 Hz, 1H), 7.84 – 7.76 (m, 3H), 7.69 (d, *J* = 7.3 Hz, 1H), 7.45 – 7.35 (m, 3H), 6.64 (dd, *J* = 12.2, 5.3 Hz, 1H), 4.02 (dd, *J* = 18.0, 12.7 Hz, 1H), 3.17 (d, *J* = 18.0 Hz, 1H), 1.30 (s, 9H).

(S)-EN82

(*S*)-EN082 - (*S*)-2-chloro-1-(3-phenyl-5-(quinoxalin-5-yl)-4,5-dihydro-1*H*-pyrazol-1-yl)ethan-1-one - Following general procedure J, tert-butyl (R)-3-phenyl-5-(quinoxalin-5-yl)-4,5-dihydro-1H-pyrazole-1-carboxylate (40 mg, 0.11 mmol) was converted to **(*S*)-EN082** (21.3 mg, 0.061 mmol, 47%) as a white solid. **HRMS** calc. 351.1007, found 351.1002. **¹H NMR** (400 MHz, DMSO-*d₆*) δ 9.04 (d, *J* = 3.9 Hz, 2H), 8.06 (d, *J* = 8.5 Hz, 1H), 7.85 – 7.78 (m, 3H), 7.56 (d, *J* = 7.2 Hz, 1H), 7.50 – 7.43 (m, 3H), 6.56 (dd, *J* = 11.9, 4.9 Hz, 1H), 4.92 (d, *J* = 13.9 Hz, 1H), 4.78 (d, *J* = 13.9 Hz, 1H), 4.08 (dd, *J* = 18.2, 12.0 Hz, 1H), 3.25 (dd, *J* = 18.1, 5.0 Hz, 1H). **¹³C NMR** (151 MHz, DMSO) δ 163.8, 156.8, 146.3, 145.3, 143.1, 139.7, 139.5, 131.2, 131.2, 130.6, 129.3, 129.0, 127.4, 125.8, 56.6, 43.0, 42.3.
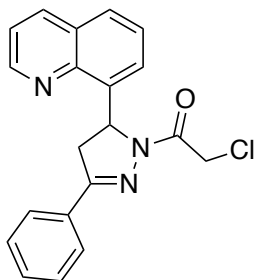
NJH-01-123:
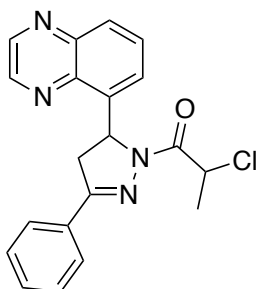
NJH-01-123

2-chloro-1-(3-phenyl-5-(quinoxalin-5-yl)-4,5-dihydro-1H-pyrazol-1-yl)propan-1-one:
(E)-1-phenyl-3-(quinoxalin-5-yl)prop-2-en-1-one (55mg, 0.20 mmol) was converted via General Procedure F and purified by silica gel chromatography (0-25% EtOAc/Hex) to give **NJH-01-123** (43 mg, 0.12 mmol, 59%) as a cream-colored solid. **HRMS** calc. 365.1164, found 365.1173. **^{1}H NMR** (400 MHz, Chloroform-*d*) δ 8.93 (dd, *J* = 11.0, 1.9 Hz, 2H), 8.09 (dd, *J* = 8.5, 1.4 Hz, 1H), 7.83 – 7.79 (m, 2H), 7.77 (d, *J* = 7.7 Hz, 1H), 7.65 (d, *J* = 7.1 Hz, 1H), 7.50 – 7.43 (m, 3H), 6.77 (dd, *J* = 11.9, 4.9 Hz, 1H), 5.60 (q, *J* = 6.8 Hz, 1H), 4.07 (dd, *J* = 17.9, 11.9 Hz, 1H), 3.22 (dd, *J* = 17.9, 4.9 Hz, 1H), 1.79 (d, *J* = 6.8 Hz, 3H).

NJH-01-124:
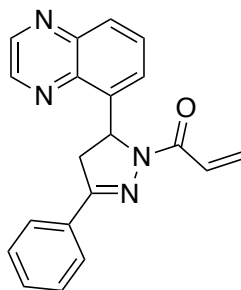
NJH-01-124

1-(3-phenyl-5-(quinoxalin-5-yl)-4,5-dihydro-1H-pyrazol-1-yl)prop-2-en-1-one (NJH-01-124): (E)-1-phenyl-3-(quinoxalin-5-yl)prop-2-en-1-one (55 mg, 0.20 mmol) was converted via General Procedure F and purified by silica gel chromatography (0-50% EtOAc/Hex) to give **NJH-01-124** (31 mg, 0.094 mmol, 47%) as a pale yellow solid. **HRMS** calc. 329.1397, found 329.1403. **^{1}H NMR** (400 MHz, Chloroform-*d*) δ 8.93 (d, *J* = 7.1 Hz, 2H), 8.07 (d, *J* = 8.6 Hz, 1H), 7.86 – 7.70 (m, 3H), 7.60 – 7.39 (m, 5H), 6.82 (dd, *J* = 11.8, 4.9 Hz, 1H), 6.51 (d, *J* = 17.2 Hz, 1H), 5.86 (d, *J* = 9.7 Hz, 1H), 4.06 (dd, *J* = 17.9, 12.0 Hz, 1H), 3.21 (dd, *J* = 17.8, 5.0 Hz, 1H). **^{13}C NMR** (151 MHz, DMSO) δ 162.5, 156.1, 146.3, 145.2, 143.1, 140.0, 139.7, 131.5, 131.0, 130.6, 129.2, 128.8, 128.5, 127.3, 125.7, 56.3, 42.1.
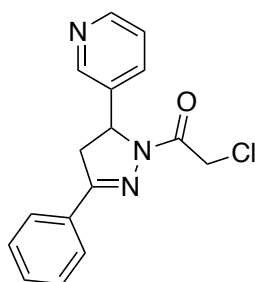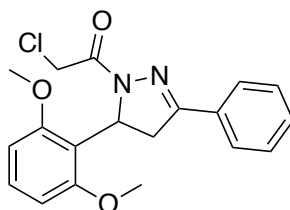
NJH-01-145:

NJH-01-145

2-chloro-1-(3-phenyl-5-(quinolin-8-yl)-4,5-dihydro-1H-pyrazol-1-yl)ethan-1-one (NJH-01-145): General Procedure A was followed starting from quinoline-8-carbaldehyde (157 mg, 1.0 mmol). After stirring at room temperature for 15 h, the solution was diluted with water and extracted with EtOAc (3x5mL). Extracts were combined, washed with brine, dried over Na$_2$SO$_4$, concentrated and purified by silica gel

chromatography (0-60% EtOAc/Hex) to obtain the chalcone (85 mg, 0.33 mmol, 33%) as an orange oil.

This chalcone ((*E*)-1-phenyl-3-(quinolin-8-yl)prop-2-en-1-one) (81 mg, 0.31 mmol) was converted via General Procedure F and purified by silica gel chromatography (0-50% EtOAc/Hex) to give **NJH-01-145** (35 mg, 0.10 mmol, 32%) as a white solid. **HRMS** calc. 350.1055, found 350.1057. **¹H NMR** (400 MHz, Chloroform-*d*) δ 8.98 (dd, *J* = 4.2, 1.8 Hz, 1H), 8.21 (dd, *J* = 8.3, 1.8 Hz, 1H), 7.79 (d, *J* = 8.2 Hz, 3H), 7.57 – 7.39 (m, 6H), 6.78 (dd, *J* = 11.7, 4.9 Hz, 1H), 4.75 (dd, *J* = 73.5, 13.2 Hz, 2H), 4.10 (dd, *J* = 18.0, 11.8 Hz, 1H), 3.26 (dd, *J* = 17.9, 4.9 Hz, 1H). **¹³C NMR** (151 MHz, DMSO) δ 163.7, 156.8, 150.4, 144.9, 138.7, 137.0, 131.3, 131.1, 129.2, 128.8, 128.1, 127.4, 126.8, 124.8, 122.1, 57.1, 43.0, 42.5.

NJH-01-147:

NJH-01-147

2-chloro-1-(3-phenyl-5-(pyridin-3-yl)-4,5-dihydro-1*H*-pyrazol-1-yl)ethan-1-one(NJH-01-147): General Procedure A was followed starting from pyridine-3-carbaldehyde (96 uL, 1.0 mmol). After stirring at room temperature for 15h, the solution was diluted with water and extracted with EtOAc (3x5mL). Extracts were combined, washed with brine, dried over Na$_2$SO$_4$, concentrated and purified by silica gel chromatography (0-70% EtOAc/Hex) to obtain the chalcone (50 mg, 0.24 mmol, 24%) as a clear colorless oil.

This chalcone (E)-1-phenyl-3-(pyridin-3-yl)prop-2-en-1-one (50 mg, 0.24 mmol) was converted via General Procedure F and purified by silica gel chromatography (0-80% EtOAc/Hex) to give **NJH-01-147** (21 mg, 0.070 mmol, 29%) as a white solid. **HRMS** calc. 300.0898, found 300.0917. **¹H NMR** (400 MHz, Chloroform-*d*) δ 8.62 (d, *J* = 2.4 Hz, 1H), 8.59 (d, *J* = 4.8 Hz, 1H), 7.80 (d, *J* = 7.7 Hz, 2H), 7.61 (d, *J* = 7.9 Hz, 1H), 7.56 – 7.47 (m, 3H), 7.32 (d, *J* = 4.9 Hz, 1H), 5.67 (dd, *J* = 11.9, 4.8 Hz, 1H), 4.63 (dd, *J* = 22.3, 13.8 Hz, 2H), 3.90 (dd, *J* = 17.9, 11.8 Hz, 1H), 3.29 (dd, *J* = 17.9, 4.9 Hz, 1H). **¹³C NMR** (151 MHz, DMSO) δ 163.9, 156.3, 149.2, 148.1, 137.3, 133.9, 131.3, 131.0, 129.3, 127.5, 124.3, 58.5, 42.9, 42.1.
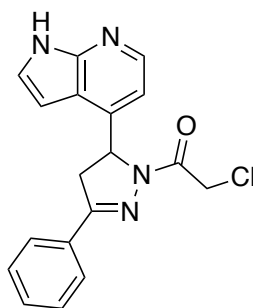
NJH-01-158:

NJH-01-158

2-chloro-1-(5-(2,6-dimethoxyphenyl)-3-phenyl-4,5-dihydro-1*H*-pyrazol-1-yl)ethan-1-one (NJH-01-158): General Procedure A was followed starting from 2,6-dimethoxybenzaldehyde (332mg, 2.0 mmol). After stirring at rt 15h, the mixture was diluted with water and extracted with EtOAc (3x5mL). Extracts were combined, washed with brine, dried over Na_2SO_4, concentrated and purified by silica gel chromatography (0-30% EtOAc/Hex) to obtain the chalcone (525 mg, 1.96 mmol, 98%) as a colorless oil. This chalcone (E)-3-(2,6-dimethoxyphenyl)-1-phenylprop-2-en-1-one (100 mg, 0.37 mmol) was converted via General Procedure F and purified by silica gel chromatography (0-50% EtOAc/Hex) to give **NJH-01-158** (89 mg, 0.25 mmol, 67%) as a white solid. **HRMS** calc. 359.1157, found 359.1139. **¹H NMR** (400 MHz, Chloroform-*d*) δ 7.85 – 7.73 (m, 2H), 7.54 – 7.42 (m, 3H), 7.23 (t, *J* = 8.3 Hz, 1H), 6.58 (d, *J* = 8.3 Hz, 2H), 6.21 (dd, *J* = 12.6, 6.2 Hz, 1H), 4.58 (d, *J* = 2.1 Hz, 2H), 3.80 (s, 6H), 3.60 (dd, *J* = 17.3, 12.6 Hz, 1H), 3.27 (dd, *J* = 17.3, 6.3 Hz, 1H). **¹³C NMR** (151 MHz, DMSO) δ 162.7, 158.4, 156.0, 131.8, 130.7, 129.4, 129.2, 127.1, 117.2, 105.2, 56.5, 51.7, 42.9.

NJH-01-159:

NJH-01-159

2-chloro-1-(3-phenyl-5-(1H-pyrrolo[2,3-b]pyridin-4-yl)-4,5-dihydro-1H-pyrazol-1-yl)ethan-1-one (NJH-01-159): 1*H*-pyrrolo[2,3-*b*]pyridine-4-carbaldehyde: n-BuLi (3.0 mL, 7.62 mmol, 2.5 M in hexanes) was added dropwise to a solution of 4-bromo-1H-pyrrolo[2,3-b]pyridine (500 mg, 2.54 mmol) in THF (20 mL) at -78 ºC and stirred at that temperature for 30 min. DMF (988 uL, 12.7 mmol) was added and the reaction was stirred at rt for 1h before being cooled to -78 ºC and quenched with sat. aq. NH_4Cl. The mixture was then warmed to rt, diluted with water and extracted with EtOAc (3x10 mL). Extracts were combined, washed with brine, dried over Na_2SO_4, concentrated and purified by silica gel chromatography (0-40% EtOAc/Hex) to obtain the aldehyde (178 mg, 1.22 mmol, 48%) as a yellow solid.

General Procedure A was followed starting from 1H-pyrrolo[2,3-b]pyridine-4-carbaldehyde (75 mg, 0.51 mmol). After stirring at rt 4h, water (15 mL) was added and the precipitate filtered to provide the chalcone (93 mg, 0.38 mmol, 74%) as a bright yellow solid. This chalcone (E)-1-phenyl-3-(1H-pyrrolo[2,3-b]pyridin-4-yl)prop-2-en-1-one was converted via General Procedure F and purified by silica gel chromatography (0-60% EtOAc/Hex) to give **NJH-01-159** (15 mg, 0.044 mmol, 22%) as a yellow solid. **LC/MS** calc. 339.1, found 339.1. **¹H NMR** (400 MHz, Chloroform-*d*) δ 9.55 (s, 1H), 8.31 (d, *J* = 4.9 Hz, 1H), 7.81 (d, *J* = 7.8 Hz, 2H), 7.55 – 7.46 (m, 3H), 7.35 (s, 1H), 7.04 (d, *J* = 5.0 Hz, 1H), 6.45 (d, *J* = 3.3 Hz, 1H), 5.94 (dd, *J* = 12.1, 5.4 Hz, 1H), 4.67 (s, 2H), 3.94 (dd, *J* = 17.8, 12.1 Hz, 1H), 3.39 (dd, *J* = 17.8, 5.4 Hz, 1H).
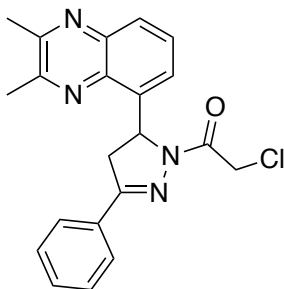
NJH-01-161:
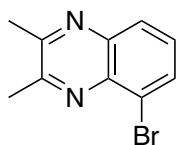
5-bromo-2,3-dimethylquinoxaline: 3-bromobenzene-1,2-diamine (1.0 g, 5.35 mmol) and diacetyl (517 mL, 5.89 mmol) were added to EtOH (20 mL), and the solution was stirred at reflux for 1h and cooled to rt. The mixture was then concentrated to dryness and the crude was redissolved in MeOH 95 mL. Water (90 mL) was then added and the precipitate filtered to provide the quinoxaline (1.17 g, 4.94 mmol, 92%) as a tan solid. **LC/MS calc.** 237.0, found 236.9. **^{1}H NMR** (400 MHz, Chloroform-*d*) δ 8.01 (t, *J* = 8.7 Hz, 2H), 7.57 (td, *J* = 7.9, 1.8 Hz, 1H), 2.85 (s, 3H), 2.81 (s, 3H).
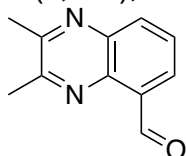
2,3-dimethylquinoxaline-5-carbaldehyde: 5-bromo-2,3-dimethylquinoxaline (474 mg, 2.0 mmol) was dissolved in THF (10 mL) and cooled to -78 ºC. n-BuLi in hexanes (960 mL, 2.4 mmol) was then added dropwise, and the mixture stirred at -78 ºC for 30 min. DMF (311 mL, 4.0 mmol) was then added at -78 ºC and the reaction stirred at rt for 1 hour. The reaction was then quenched with sat. aq. NH$_4$Cl at -78 ºC, warmed to rt, diluted with water and extracted with EtOAc (3x10mL). Extracts were combined, washed with brine, dried over Na$_2$SO$_4$, concentrated and purified by silica gel chromatography (0-50% EtOAc/Hex) to obtain the aldehyde (169 mg, 0.91 mmol, 45%). **LC/MS** calc. 187.1, found 187.1. **^{1}H NMR** (400 MHz, Chloroform-*d*) δ 11.41 (s, 1H), 8.04 (dd, *J* = 6.3, 3.5 Hz, 1H), 7.83 (t, *J* = 7.7 Hz, 1H), 7.72 (dd, *J* = 6.4, 3.4 Hz, 1H), 2.84 (s, 3H), 2.82 (s, 3H).
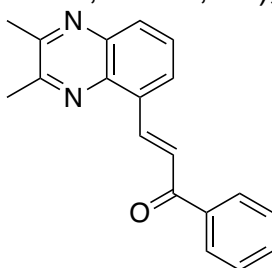

(E)-3-(2,3-dimethylquinoxalin-5-yl)-1-phenylprop-2-en-1-one: General Procedure A was followed starting from 2,3-dimethylquinoxaline-5-carbaldehyde (93 mg, 0.50 mmol). After stirring at room temperature for 5h, the mixture was diluted with water and extracted with EtOAc (3x5mL). Extracts were combined, washed with brine, dried over Na$_2$SO$_4$, concentrated and purified by silica gel chromatography (0-25% EtOAc/Hex) to obtain the chalcone (59 mg, 0.21 mmol, 41%). **LC/MS** calc. 289.1, found 289.1. **^{1}H NMR** (400 MHz, Chloroform-*d*) δ 8.96 (d, *J* = 16.0 Hz, 1H), 8.17 – 8.11 (m, 2H), 8.09 (d, *J* = 7.4 Hz, 2H), 8.04 (s, 1H), 7.76 (t, *J* = 7.9 Hz, 1H), 7.68 – 7.63 (m, 1H), 7.61 – 7.54 (m, 2H), 2.84 (s, 3H), 2.80 (s, 3H).

NJH-01-161

2-chloro-1-(5-(2,3-dimethylquinoxalin-5-yl)-3-phenyl-4,5-dihydro-1*H*-pyrazol-1-yl)ethan-1-one (NJH-01-161): (E)-3-(2,3-dimethylquinoxalin-5-yl)-1-phenylprop-2-en-1-one (30 mg, 0.10 mmol) was converted via General Procedure F and purified by silica gel chromatography (0-45% EtOAc/Hex) to give **NJH-01-161** (30 mg, 0.080 mmol, 80%) as a white solid. HRMS calc. 379.1320, found 379.1342. **¹H NMR** (400 MHz, Chloroform-*d*) δ 7.85 (d, *J* = 8.3 Hz, 1H), 7.71 (s, 2H), 7.54 (t, *J* = 7.7 Hz, 1H), 7.39 (s, 4H), 6.55 (d, *J* = 11.8 Hz, 1H), 4.62 (dd, *J* = 42.9, 13.4 Hz, 2H), 3.92 (dd, *J* = 17.9, 12.7 Hz, 1H), 3.18 (dd, *J* = 17.4, 4.2 Hz, 1H), 2.67 (s, 3H), 2.61 (s, 3H). **¹³C NMR** (151 MHz, DMSO) δ 163.7, 156.8, 154.5, 153.6, 141.2, 138.5, 137.8, 131.4, 131.1, 129.2, 129.0, 127.9, 127.4, 57.0, 42.9, 42.3, 23.6, 23.2.
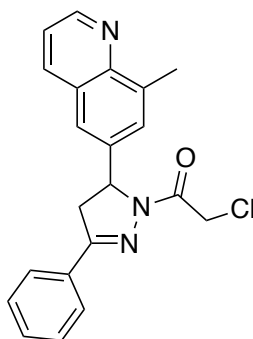
NJH-01-166:
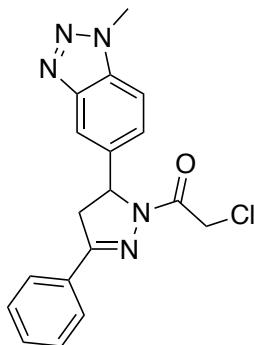
(1-methyl-1*H*-benzo[*d*][1,2,3]triazol-5-yl)methanol: LiAlH₄ (5.64 mmol, 1M in THF) was added dropwise to a solution of 1-methylbenzotriazole-5-carboxylic acid (500 mg, 2.52 mmol) in THF (10 mL) at 0 °C. The mixture was allowed to warm to rt and stirred for 5 h. The mixture was then diluted with Et₂O (40mL), and 0.2 mL water was added at 0 °C, followed by 0.6 mL 1M NaOH aq., 0.2 mL water, and finally Na₂SO₄ after 15 min at rt. The mixture was filtered, concentrated and purified by silica gel chromatography (0-80% EtOAc/Hex) to obtain the alcohol (308 mg, 1.89 mmol, 67%). **LC/MS** calc. 164.1, found 164.1.

1-methyl-1*H*-benzo[*d*][1,2,3]triazole-5-carbaldehyde: (1-methyl-1*H*-benzo[*d*][1,2,3]triazol-5-yl)methanol (200 mg, 1.22 mmol) and 4-methylmorpholine N-oxide (500 mg, 4.27 mmol) were combined in DCM (5 mL) with 4Å MS. TPAP (42 mg, 0.12 mmol) was then added and the mixture stirred as 2 hours before the alcohol was consumed. The mixture was diluted with Et₂O and filtered to remove NMO, filtrate

concentrated and purified by silica gel chromatography (0-30% EtOAc/Hex) to obtain the aldehyde (138 mg, 0.86 mmol, 70%). **LC/MS** calc. 162.1, found 162.0.

2-chloro-1-(5-(1-methyl-1H-benzo[d][1,2,3]triazol-5-yl)-3-phenyl-4,5-dihydro-1H-pyrazol-1-yl)ethan-1-one (NJH-01-166): General Procedure A was followed starting from 1-methyl-1H-benzo[d][1,2,3]triazole-5-carbaldehyde (80 mg, 0.50 mmol). After 16 h., water was added and the precipitate filtered to obtain the chalcone (117 mg, 0.44 mmol, 88%) as a tan powder. This chalcone (*E*)-3-(1-methyl-1*H*-benzo[*d*][1,2,3]triazol-5-yl)-1-phenylprop-2-en-1-one (40 mg, 0.15 mmol) was converted via General Procedure F and purified by silica gel chromatography (0-60% EtOAc/Hex) to give **NJH-01-166** (16 mg, 0.046 mmol, 31%) as a light yellow foam. **HRMS** calc. 354.1116, found 354.1093. ^{1}**H NMR** (400 MHz, Chloroform-*d*) δ 7.99 (s, 1H), 7.82 (d, *J* = 7.8 Hz, 2H), 7.59 – 7.43 (m, 5H), 5.85 – 5.76 (m, 1H), 4.64 (d, *J* = 4.8 Hz, 2H), 4.32 (s, 3H), 3.93 (dd, *J* = 18.0, 11.2 Hz, 1H), 3.34 (dd, *J* = 17.9, 5.0 Hz, 1H). ^{13}**C NMR** (151 MHz, DMSO) δ 163.8, 156.2, 145.7, 138.0, 133.3, 131.2, 131.1, 129.3, 127.4, 125.8, 116.2, 111.7, 60.5, 43.0, 42.6, 34.7.
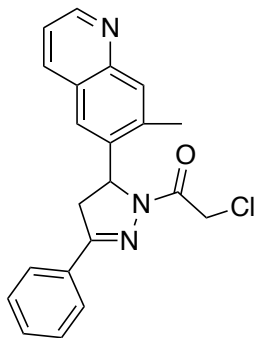
NJH-01-181:

NJH-01-181

2-chloro-1-(5-(8-methylquinolin-6-yl)-3-phenyl-4,5-dihydro-1H-pyrazol-1-yl)ethan-1-one (NJH-01-181): 6-bromo-8-methylquinoline (500 mg, 2.25 mmol) was converted to 8-methylquinoline-6-carbaldehyde via General Procedure K and purified by silica gel chromatography (0-40% EtOAc/Hex) to provide the aldehyde (184 mg, 1.08 mmol, 48%) as a pale orange solid.

Then, General Procedure A was followed starting from 8-methylquinoline-6-carbaldehyde (100mg, 0.58 mmol). After stirring overnight water (15 mL) was added, and the solids filtered to provide the chalcone (134 mg, 0.49 mmol, 85%) as a tan solid. (E)-3-(8-methylquinolin-6-yl)-1-phenylprop-2-en-1-one (75 mg, 0.27 mmol) was converted via General Procedure F and purified by silica gel chromatography (0-45% EtOAc/Hex) to give **NJH-01-181** (49 mg, 0.13 mmol, 49%) as a white powder. **HRMS** calc. 364.1211, found 364.1219. ^{1}**H NMR** (400 MHz, DMSO-d_6) δ 8.94 – 8.85 (m, 1H), 8.33 (d, *J* = 8.4 Hz, 1H), 7.90 – 7.81 (m, 2H), 7.67 (s, 1H), 7.56 – 7.47 (m, 5H), 5.74 (dd, *J* = 11.9, 5.0 Hz, 1H), 4.81 (dd, *J* = 32.2, 13.6 Hz, 2H), 3.99 (dd, *J* = 17.9, 11.4 Hz, 1H), 3.34 (dd, *J* = 17.9, 5.4 Hz, 1H), 2.71 (s, 3H). ^{13}**C NMR** (151 MHz, DMSO) δ 163.9, 156.2, 150.0, 146.6, 139.6, 137.8, 136.8, 131.2, 131.1, 129.3, 128.2, 127.7, 127.5, 122.8, 122.1, 60.5, 43.0, 42.5, 18.3.

NJH-01-182:

NJH-01-182

2-chloro-1-(5-(7-methylquinolin-6-yl)-3-phenyl-4,5-dihydro-1H-pyrazol-1-yl)ethan-1-one **(NJH-01-182):** 7-methylquinoline-6-carbaldehyde:6-bromo-8-methylquinoline (500 mg, 2.25 mmol) was converted to 7-methylquinoline-6-carbaldehyde via general procedure K and purified by silica gel chromatography (0-50% EtOAc/Hex) to provide the aldehyde (275 mg, 1.61 mmol, 71%) as a pale orange solid. LC/MS calc. 172.1, found 172.1.
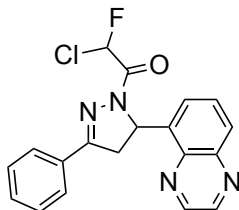
General Procedure A was followed starting from 7-methylquinoline-6-carbaldehyde (100 mg, 0.58 mmol). The reaction mixture was stirred for 16 hours at rt and an immiscible orange oil formed. Water was added and the mixture extracted with EtOAc (3x5mL). Extracts were combined, washed with brine, dried over Na_2SO_4, concentrated, and purified by silica gel chromatography (0 to 50% EtOAc/Hex.) to obtain the chalcone (151 mg, 0.55 mmol, 95%) as a yellow gummy solid. This chalcone (E)-3-(7-methylquinolin-6-yl)-1-phenylprop-2-en-1-one (75 mg, 0.27 mmol) was converted via General Procedure F and purified by silica gel chromatography (0-65% EtOAc/Hex) to give **NJH-01-182** (25 mg, 0.069 mmol, 25%) as a white solid. **HRMS** calc. 364.1211, found 364.1222. **¹H NMR** (400 MHz, DMSO-d_6) δ 8.83 (dd, J = 4.2, 1.7 Hz, 1H), 8.26 (dd, J = 8.2, 1.8 Hz, 1H), 7.91 (s, 1H), 7.87 – 7.82 (m, 2H), 7.57 (s, 1H), 7.51 – 7.41 (m, 4H), 5.87 (dd, J = 11.7, 4.9 Hz, 1H), 4.87 (dd, J = 37.1, 13.8 Hz, 2H), 4.05 (dd, J = 18.1, 11.9 Hz, 1H), 3.24 (dd, J = 18.1, 4.9 Hz, 1H), 2.62 (s, 3H). **¹³C NMR** (151 MHz, DMSO) δ 163.8, 156.3, 150.9, 147.5, 139.3, 137.4, 136.3, 131.2, 131.1, 130.0, 129.3, 127.4, 126.8, 123.2, 121.4, 58.0, 43.0, 41.8, 20.1.
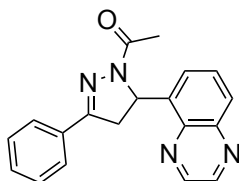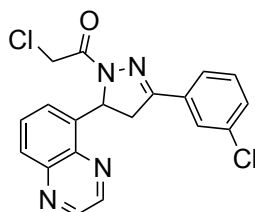

LEB-02-150

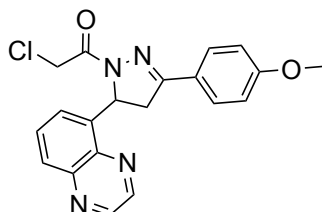**1-(3-phenyl-5-(quinoxalin-5-yl)-4,5-dihydro-1H-pyrazol-1-yl)ethan-1-one** **(LEB-02-150).** General Procedure A was followed starting from acetophenone (0.40 mmol) and quinoxaline-5-carbaldehyde (0.40 mmol). The corresponding chalcone precipitated out during the reaction and was filtered by gravity filtration to yield product (0.20 mmol) as a light yellow solid. General Procedure F was followed starting from the above product (1.0 equiv, 0.20 mmol). Purification by flash column chromatography (EtOAc/hexane 50:50) yielded the chloroacetamide **LEB-02-150** (0.08 mmol, 22.1% yield across all steps). **¹H NMR** (400 MHz, Chloroform-d) δ 8.97 – 8.89 (m, 2H), 8.07 (d, J = 8.4 Hz, 1H), 7.82 –

7.71 (m, 3H), 7.56 – 7.50 (m, 1H), 7.48 – 7.40 (m, 3H), 7.30 (s, 3H), 6.73 (dd, J = 11.9, 4.8 Hz, 1H), 4.05 (dd, J = 17.9, 12.1 Hz, 1H), 3.18 (dd, J = 17.5, 4.9 Hz, 1H). ^{13}**C NMR** (151 MHz, DMSO) δ 168.0, 155.2, 146.2, 145.2, 143.1, 140.3, 139.7, 131.6, 130.8, 130.6, 129.2, 128.7, 127.1, 125.5, 56.0, 42.4, 22.2. **HRMS** (ESI): exact mass calculated for $C_{19}H_{16}N_4O$ [(M+H)$^+$] 317.1397, found 317.1405.

LEB-02-157

2-chloro-2-fluoro-1-(3-phenyl-5-(quinoxalin-5-yl)-4,5-dihydro-1*H*-pyrazol-1-yl)ethan-1-one (LEB-02-157). General Procedure A was followed starting from acetophenone (0.40 mmol) and quinoxaline-5-carbaldehyde (0.40 mmol). The corresponding chalcone precipitated out during the reaction and was filtered by gravity filtration to yield product (0.38 mmol) as a yellow solid. Hydrazine monohydrate (2.0 equiv) was added to a suspension of the above product (1.0 equiv, 0.38 mmol) in EtOH (0.3 M). The resulting reaction mixture was stirred at reflux temperature for 4 h before it was concentrated under reduced pressure. The crude pyrazoline (1.0 equiv, 0.36 mmol) was added to a screw-cap oven-dried vial charged with a stir-bar, chlorofluoroacetate (1.2 equiv, 0.44 mmol), EDC hydrochloride (1.2 equiv, 0.44 mmol), HOBt (1.2 equiv, 0.44 mmol), DIEA (2.5 equiv, 0.92 mmol), and 2mL DMF. Reaction proceeded overnight, and was extracted in EtOAc, washed 3X with brine, and purified via flash column chromatography (EtOAc/hexane 50:50), yielding the corresponding chlorofluoroacetamide **LEB-02-157** (0.026 mmol, 6.4% yield across all steps). ^{1}**H NMR** (400 MHz, Chloroform-*d*) δ 8.97 – 8.84 (m, 2H), 8.13 – 8.08 (m, 1H), 8.06 – 7.95 (m, 1H), 7.83 – 7.75 (m, 3H), 7.63 – 7.57 (m, 1H), 7.54 – 7.44 (m, 3H), 6.70 (dd, J = 11.7, 5.1 Hz, 1H), 4.16 – 4.04 (m, 1H), 3.36 – 3.22 (m, 1H). **HRMS** (ESI): exact mass calculated for $C_{19}H_{14}ClFN_4O$ [(M+H)$^+$] 369.0913, found 369.0914.
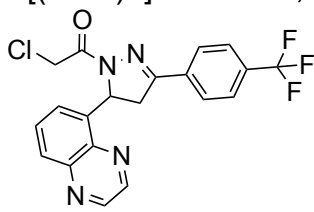

LEB-02-172

2-chloro-1-(3-(3-chlorophenyl)-5-(quinoxalin-5-yl)-4,5-dihydro-1*H*-pyrazol-1-yl)ethan-1-one (LEB-02-172). General Procedure A was followed starting from 3-chloroacetophenone (1.2 equiv, 0.76 mmol) and quinoxaline-5-carbaldehyde (1.0 equiv, 0.63 mmol). The corresponding chalcone precipitated out during the reaction and was filtered by gravity filtration to yield product (0.50 mmol) as a yellow solid. General Procedure F was followed starting from the above product (1.0 equiv, 0.50 mmol). Purification by flash column chromatography (EtOAc/hexane 50:50) yielded the chloroacetamide **LEB-02-172** (0.058 mmol, 9.2% yield across all steps). ^{1}**H NMR** (400 MHz, Chloroform-*d*) δ 8.92 (dt, J = 21.3, 1.8 Hz, 2H), 8.10 (dd, J = 8.5, 1.7 Hz, 1H), 7.81 – 7.74 (m, 2H), 7.68 – 7.62 (m, 1H), 7.58 (d, J = 7.3 Hz, 1H), 7.49 – 7.43 (m, 1H), 7.43 –

7.37 (m, 1H), 6.74 – 6.66 (m, 1H), 4.79 (dd, J = 13.5, 1.6 Hz, 1H), 4.63 (dd, J = 13.7, 1.4 Hz, 1H), 4.10 – 3.99 (m, 1H), 3.28 – 3.19 (m, 1H). **^{13}C NMR** (151 MHz, DMSO) δ 164.0, 155.6, 146.3, 145.3, 143.1, 139.7, 139.3, 134.1, 133.3, 131.2, 130.8, 130.5, 129.0, 126.9, 126.1, 56.9, 43.0, 42.2. **HRMS** (ESI): exact mass calculated for $C_{19}H_{14}Cl_2N_4O$ [(M+H) $^+$] 385.0617, found 385.063.
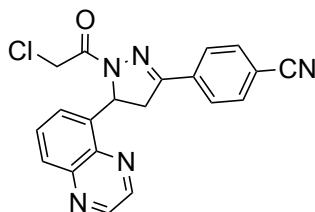

LEB-02-173

2-chloro-1-(3-(4-methoxyphenyl)-5-(quinoxalin-5-yl)-4,5-dihydro-1*H*-pyrazol-1-yl)ethan-1-one (LEB-02-173). General Procedure A was followed starting from 4-methoxyacetophenone (1.2 equiv, 0.76 mmol) and quinoxaline-5-carbaldehyde (1.0 equiv, 0.63 mmol). The corresponding chalcone precipitated out during the reaction and was filtered by gravity filtration to yield product (0.47 mmol) as a light yellow solid. General Procedure F was followed starting from the above product (1.0 equiv, 0.47 mmol). Purification by flash column chromatography (EtOAc/hexane 50:50) yielded the chloroacetamide **LEB-02-173** (0.025 mmol, 4.0% yield across all steps). **^{1}H NMR** (400 MHz, DMSO-d_6) δ 9.04 (q, J = 1.8 Hz, 2H), 8.05 (dd, J = 8.3, 1.4 Hz, 1H), 7.82 (dd, J = 8.5, 7.3 Hz, 1H), 7.77 – 7.70 (m, 2H), 7.53 (d, J = 7.2 Hz, 1H), 7.04 – 6.98 (m, 2H), 6.54 (dd, J = 11.9, 4.7 Hz, 1H), 4.90 (d, J = 13.8 Hz, 1H), 4.76 (d, J = 13.8 Hz, 1H), 4.04 (dd, J = 18.0, 11.9 Hz, 1H), 3.80 (s, 3H), 3.21 (dd, J = 18.0, 4.8 Hz, 1H). **HRMS** (ESI): exact mass calculated for $C_{20}H_{17}ClN_4O_2$ [(M+H) $^+$] 381.1113, found 381.1088.
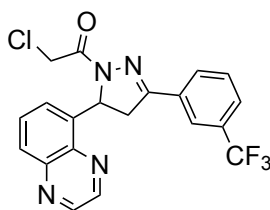

LEB-02-174

2-chloro-1-(5-(quinoxalin-5-yl)-3-(4-(trifluoromethyl)phenyl)-4,5-dihydro-1*H*-pyrazol-1-yl)ethan-1-one (LEB-02-174). General Procedure A was followed starting from 4-(trifluoromethyl)acetophenone (1.2 equiv, 0.76 mmol) and quinoxaline-5-carbaldehyde (1.0 equiv, 0.63 mmol). The corresponding chalcone precipitated out during the reaction and was filtered by gravity filtration to yield product (0.55 mmol) as a yellow solid. General Procedure F was followed starting from the above product (1.0 equiv, 0.55 mmol). Purification by flash column chromatography (EtOAc/hexane 50:50) yielded the chloroacetamide **LEB-02-174** (0.11 mmol, 18.9% yield across all steps). **^{1}H NMR** (400 MHz, DMSO-d_6) δ 9.05 – 9.00 (m, 2H), 8.00 (d, J = 8.2 Hz, 2H), 7.85 – 7.79 (m, 3H), 7.49 – 7.43 (m, 2H), 4.97 – 4.77 (m, 1H), 4.17 – 3.99 (m, 1H), 3.40 (s, 2H), 3.31 (dd, J = 18.2, 5.1 Hz, 1H). **HRMS** (ESI): exact mass calculated for $C_{20}H_{14}ClF_3N_4O$ [(M+H) $^+$] 419.0881, found 419.0865.
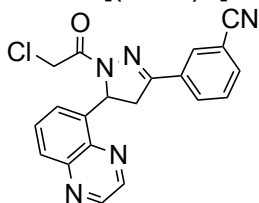
LEB-02-175

4-(1-(2-chloroacetyl)-5-(quinoxalin-5-yl)-4,5-dihydro-1H-pyrazol-3-yl)benzonitrile (LEB-02-175). General Procedure A was followed starting from 4-acetylbenzonitrile (1.2 equiv, 0.76 mmol) and quinoxaline-5-carbaldehyde (1.0 equiv, 0.63 mmol). The corresponding chalcone precipitated out during the reaction and was filtered by gravity filtration to yield product (0.57 mmol) as a yellow solid. General Procedure F was followed starting from the above product (1.0 equiv, 0.57 mmol). Purification by flash column chromatography (EtOAc/hexane 50:50) yielded the chloroacetamide **LEB-02-175** (0.050 mmol, 7.9% yield across all steps). **¹H NMR** (400 MHz, DMSO-d_6) δ 9.06 – 9.00 (m, 2H), 8.06 (dd, J = 8.4, 1.4 Hz, 1H), 8.00 – 7.91 (m, 4H), 7.83 (dd, J = 8.5, 7.3 Hz, 1H), 7.58 (dd, J = 7.3, 1.4 Hz, 1H), 4.15 – 3.99 (m, 2H), 3.39 (s, 2H), 3.31 (dd, J = 18.2, 5.2 Hz, 1H). **HRMS** (ESI): exact mass calculated for $C_{20}H_{14}ClN_5O$ [(M+H)$^+$] 376.096, found 376.0977.
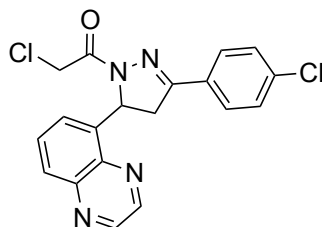

LEB-02-176

2-chloro-1-(5-(quinoxalin-5-yl)-3-(3-(trifluoromethyl)phenyl)-4,5-dihydro-1H-pyrazol-1-yl)ethan-1-one (LEB-02-176). General Procedure A was followed starting from 3-(trifluoromethyl)acetophenone (1.2 equiv, 0.76 mmol) and quinoxaline-5-carbaldehyde (1.0 equiv, 0.63 mmol). The corresponding chalcone precipitated out during the reaction and was filtered by gravity filtration to yield product (0.57 mmol) as a yellow solid. General Procedure F was followed starting from the above product (1.0 equiv, 0.57 mmol). Purification by flash column chromatography (EtOAc/hexane 50:50) yielded the chloroacetamide **LEB-02-176** (0.22 mmol, 35.3% yield across all steps). **¹H NMR** (400 MHz, DMSO-d_6) δ 9.06 – 9.03 (m, 2H), 8.12 – 8.04 (m, 3H), 7.84 (dt, J = 8.5, 6.7 Hz, 2H), 7.71 (t, J = 7.8 Hz, 1H), 7.57 (dd, J = 7.2, 1.4 Hz, 1H), 6.58 (dd, J = 12.0, 5.0 Hz, 1H), 4.97 (d, J = 14.1 Hz, 1H), 4.84 (d, J = 14.1 Hz, 1H), 4.12 (dd, J = 18.3, 12.1 Hz, 1H), 3.37 – 3.34 (m, 1H). **¹³C NMR** (151 MHz, DMSO) δ 164.1, 155.7, 146.3, 145.3, 143.1, 139.7, 139.3, 132.3, 131.3, 130.5, 130.5, 130.4, 130.2, 130.0, 129.8, 129.0, 127.5, 127.4, 127.4, 127.1, 125.9, 125.3, 123.8, 123.8, 123.7, 123.5, 121.7, 57.0, 43.0, 42.1. **HRMS** (ESI): exact mass calculated for $C_{20}H_{14}ClF_3N_4O$ [(M+H)$^+$] 419.0881, found 419.0857.
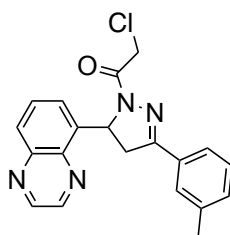
3-(1-(2-chloroacetyl)-5-(quinoxalin-5-yl)-4,5-dihydro-1H-pyrazol-3-yl)benzonitrile (LEB-02-182). General Procedure A was followed starting from 3-acetylbenzonitrile (1.2 equiv, 0.76 mmol) and quinoxaline-5-carbaldehyde (1.0 equiv, 0.63 mmol). The corresponding chalcone precipitated out during the reaction and was filtered by gravity filtration to yield product (0.46 mmol) as a light yellow solid. General Procedure F was followed starting from the above product (1.0 equiv, 0.46 mmol). Purification by flash column chromatography (EtOAc/hexane 50:50) yielded the chloroacetamide **LEB-02-182** (0.025 mmol, 4.0% yield across all steps). **^{1}H NMR** (400 MHz, DMSO-d_6) δ 9.09 – 9.00 (m, 2H), 8.28 – 8.23 (m, 1H), 8.14 (dt, J = 8.0, 1.4 Hz, 1H), 8.07 (dd, J = 8.4, 1.4 Hz, 1H), 7.96 (dt, J = 7.8, 1.4 Hz, 1H), 7.83 (dd, J = 8.4, 7.2 Hz, 1H), 7.68 (t, J = 7.9 Hz, 1H), 7.58 – 7.55 (m, 1H), 6.57 (dd, J = 11.9, 5.0 Hz, 1H), 4.96 (d, J = 14.1 Hz, 1H), 4.83 (d, J = 14.1 Hz, 1H), 4.14 – 4.01 (m, 1H), 3.34 – 3.27 (m, 1H). **HRMS** (ESI): exact mass calculated for $C_{20}H_{14}ClN_5O$ [(M+H)$^+$] 376.096, found 376.097.
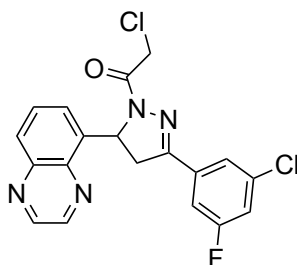

LEB-02-187

2-chloro-1-(3-(4-chlorophenyl)-5-(quinoxalin-5-yl)-4,5-dihydro-1*H*-pyrazol-1-yl)ethan-1-one (LEB-02-187). General Procedure A was followed starting from 4-chloroacetophenone (1.2 equiv, 0.76 mmol) and quinoxaline-5-carbaldehyde (1.0 equiv, 0.63 mmol). The corresponding chalcone precipitated out during the reaction and was filtered by gravity filtration to yield product (0.63 mmol) as a light yellow solid. General Procedure F was followed starting from the above crude product (1.0 equiv, 0.63 mmol). Purification by flash column chromatography (EtOAc/hexane 50:50) yielded the chloroacetamide **LEB-02-187** (0.12 mmol, 19.2% yield across all steps). **^{1}H NMR** (400 MHz, DMSO-d_6) δ 9.08 – 8.98 (m, 2H), 8.06 (dd, J = 8.4, 1.4 Hz, 1H), 7.87 – 7.77 (m, 3H), 7.58 – 7.49 (m, 3H), 6.55 (dd, J = 11.9, 5.0 Hz, 1H), 4.91 (d, J = 13.9 Hz, 1H), 4.78 (d, J = 13.9 Hz, 1H), 4.07 (dd, J = 18.2, 12.0 Hz, 1H), 3.26 (dd, J = 18.1, 5.0 Hz, 1H). **HRMS** (ESI): exact mass calculated for $C_{19}H_{14}Cl_2N_4O$ [(M+H)$^+$] 385.0617, found 385.0628.
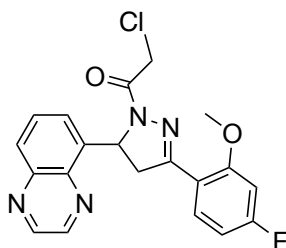

LEB-03-001c

2-chloro-1-(5-(quinoxalin-5-yl)-3-(*m*-tolyl)-4,5-dihydro-1*H*-pyrazol-1-yl)ethan-1-one (LEB-03-001c). General Procedure A was followed starting from 3-methylacetophenone (1.2 equiv, 0.76 mmol) and quinoxaline-5-carbaldehyde (1.0 equiv, 0.63 mmol). The corresponding chalcone precipitated out during the reaction and was filtered by gravity filtration to yield product (0.53 mmol) as a yellow solid. General Procedure F was followed

starting from the above crude product (1.0 equiv, 0.53 mmol). Purification by flash column chromatography (EtOAc/hexane 50:50) yielded the chloroacetamide **LEB-03-001c** (0.29 mmol, 46.7% yield across all steps). **¹H NMR** (400 MHz, DMSO-d_6) δ 9.28 – 8.93 (m, 2H), 8.17 – 7.87 (m, 2H), 7.85 – 7.79 (m, 1H), 7.69 – 7.49 (m, 1H), 7.40 – 7.13 (m, 2H), 5.01 – 4.71 (m, 2H), 3.27 – 3.04 (m, 1H), 2.51 (s, 3H), 2.35 (d, J = 14.1 Hz, 3H). **HRMS** (ESI): exact mass calculated for $C_{20}H_{17}ClN_4O$ [(M+H)$^+$] 365.1164, found 365.1185.
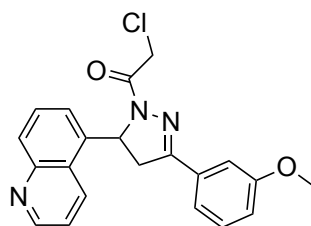
LEB-03-004c

2-chloro-1-(3-(4-fluoro-2-methoxyphenyl)-5-(quinoxalin-5-yl)-4,5-dihydro-1*H*-pyrazol-1-yl)ethan-1-one (LEB-03-004c). General Procedure A was followed starting from 3-chloro-5-fluoroacetophenone (1.2 equiv, 0.76 mmol) and quinoxaline-5-carbaldehyde (1.0 equiv, 0.63 mmol). The corresponding chalcone precipitated out during the reaction and was filtered by gravity filtration to yield product (0.51 mmol) as a light yellow solid. General Procedure F was followed starting from the above crude product (1.0 equiv, 0.51 mmol). Purification by flash column chromatography (EtOAc/hexane 50:50) yielded the chloroacetamide **LEB-03-004c** (0.23 mmol, 37.2% yield across all steps). **¹H NMR** (400 MHz, DMSO-d_6) δ 9.04 (dd, J = 4.3, 1.8 Hz, 2H), 8.08 – 7.91 (m, 2H), 7.85 (dt, J = 15.5, 7.9 Hz, 1H), 7.54 (d, J = 7.2 Hz, 1H), 6.89 (qd, J = 8.7, 2.4 Hz, 1H), 6.50 (dd, J = 11.9, 4.8 Hz, 1H), 4.91 – 4.71 (m, 1H), 4.15 – 4.00 (m, 1H), 3.72 (s, 2H), 3.18 (dd, J = 18.6, 4.9 Hz, 1H), 2.51 (dt, J = 3.7, 1.9 Hz, 3H). **¹³C NMR** (151 MHz, DMSO) δ 164.2, 163.5, 161.8, 154.8, 154.8, 146.3, 145.3, 143.1, 139.7, 139.2, 135.1, 135.0, 134.9, 134.8, 130.5, 129.1, 126.0, 123.5, 123.5, 118.4, 118.2, 113.3, 113.1, 57.2, 51.8, 43.0, 42.1, 25.0, 16.7. **HRMS** (ESI): exact mass calculated for $C_{20}H_{16}ClFN_4O$ [(M+H)$^+$] 403.0523, found 403.0546.

LEB-03-005c

2-chloro-1-(3-(4-fluoro-2-methoxyphenyl)-5-(quinoxalin-5-yl)-4,5-dihydro-1*H*-pyrazol-1-yl)ethan-1-one (LEB-03-005c). General Procedure A was followed starting from 4-fluoro-2-methoxyacetophenone (1.2 equiv, 0.76 mmol) and quinoxaline-5-carbaldehyde (1.0 equiv, 0.63 mmol). The corresponding chalcone precipitated out during the reaction and was filtered by gravity filtration to yield product (0.51 mmol) as a white solid. General Procedure F was followed starting from the above crude product (1.0 equiv,

0.51 mmol). Purification by flash column chromatography (EtOAc/hexane 50:50) yielded the chloroacetamide **LEB-03-005c** (0.13 mmol, 20.0% yield across all steps). **¹H NMR** (400 MHz, DMSO-d_6) δ 9.04 (dd, J = 4.3, 1.8 Hz, 2H), 8.08 – 7.91 (m, 2H), 7.85 (dt, J = 15.5, 7.9 Hz, 1H), 7.54 (d, J = 7.2 Hz, 1H), 6.89 (qd, J = 8.7, 2.4 Hz, 1H), 6.50 (dd, J = 11.9, 4.8 Hz, 1H), 4.91 – 4.71 (m, 1H), 4.15 – 4.00 (m, 1H), 3.72 (s, 2H), 3.18 (dd, J = 18.6, 4.9 Hz, 1H), 2.51 (dt, J = 3.7, 1.9 Hz, 3H). **¹³C NMR** (151 MHz, DMSO) δ 165.8, 164.1, 163.7, 160.3, 160.2, 155.1, 146.3, 145.3, 143.1, 139.6, 131.2, 131.1, 130.6, 128.9, 125.7, 116.7, 116.7, 108.1, 108.0, 101.1, 101.0, 56.8, 56.3, 45.3, 43.0. **HRMS** (ESI): exact mass calculated for $C_{20}H_{16}ClFN_4O$ [(M+H)$^+$] 399.1019, found 399.1042

.

LEB-03-008c

2-chloro-1-(3-(3-methoxyphenyl)-5-(quinolin-5-yl)-4,5-dihydro-1H-pyrazol-1-yl)ethan-1-one (LEB-03-008c). General Procedure A was followed starting from 3-methoxyacetophenone (1.2 equiv, 1.14 mmol) and quinoline-5-carbaldehyde (1.0 equiv, 0.95 mmol). The reaction was run for 15 minutes at 0°C. The corresponding chalcone was purified via flash chromatography (EtOAc/Hexane 50:50) to yield a light yellow solid (0.69 mmol). General Procedure F was followed starting from the above product (1.0 equiv, 0.69 mmol). Purification by flash column chromatography (EtOAc/hexane 50:50) yielded the chloroacetamide **LEB-03-008c** (0.29 mmol, 30.3% yield across all steps). **¹H NMR** (400 MHz, DMSO-d6) δ 8.99 (dd, J = 4.2, 1.6 Hz, 1H), 8.67 (d, J = 8.6 Hz, 1H), 7.98 (d, J = 8.5 Hz, 1H), 7.75 – 7.61 (m, 2H), 7.44 – 7.27 (m, 4H), 4.89 (d, J = 30.0 Hz, 1H), 4.11 (dd, J = 18.2, 11.9 Hz, 1H), 3.79 (s, 3H), 3.36 (s, 2H), 3.26 (d, J = 4.9 Hz, 1H). **¹³C NMR** (151 MHz, DMSO) δ 167.9, 164.3, 164.0, 162.4, 160.0, 159.9, 157.8, 156.5, 156.4, 151.5, 151.2, 150.8, 148.6, 148.6, 148.0, 144.8, 143.9, 140.8, 140.7, 139.7, 139.6, 137.9, 137.6, 137.5, 135.9, 133.3, 132.5, 132.4, 132.2, 132.1, 132.0, 131.7, 130.6, 130.4, 129.7, 129.6, 129.3, 129.1, 128.7, 127.0, 125.8, 125.7, 125.1, 122.8, 122.6, 122.2, 122.0, 120.1, 119.9, 117.4, 117.2, 112.8, 112.6, 112.4, 59.9, 57.4, 56.9, 55.9, 55.8, 55.5, 43.0, 42.7, 42.6, 42.5, 42.3, 24.8. **HRMS** (ESI): exact mass calculated for $C_{21}H_{18}ClN_3O_2$ [(M+H)$^+$] 380.116, found 380.1185.

1-(3-Phenyl-5-(quinoxalin-5-yl)-4,5-dihydro-1*H*-pyrazol-1-yl)but-2-yn-1-one (CMZ 07)
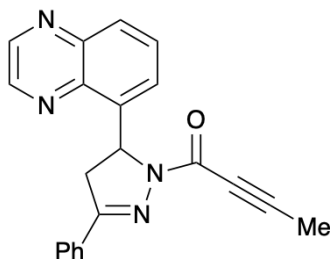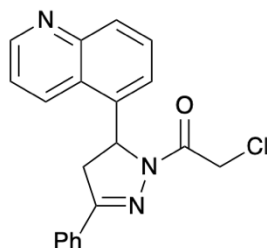
Step 1: Following General Procedure A, the chalcone was prepared from quinoxaline-5-carbaldehyde (500 mg, 3.16 mmol), acetophenone (443 μL, 3.79 mmol) and 5% (w/w) aq NaOH (3.8 mL, 4.74 mmol) in EtOH (10 mL). Filtration under reduced pressure gave the chalcone as a pale yellow solid (823 mg, quant) which was used without purification.

Step 2: Hydrazine hydrate (136 μL, 1.54 mmol, 50–60% wt solution) was added to a solution of the chalcone (200 mg, 0.77 mmol) in EtOH (2 mL) at rt and the resultant mixture was heated at reflux for 4 h before being cooled to rt. One half of the reaction mixture was then concentrated *in vacuo* and the crude pyrazoline was used immediately without purification.

Step 3: A solution of tetrolic acid (32 mg, 0.38 mmol) in DMF (0.5 mL) was added to a solution of the crude pyrazoline (0.38 mmol) in DMF (0.5 mL) at 0 °C. The reaction mixture was then treated sequentially with NMM (422 μL, 3.84 mmol) and T3P (642 μL, 1.08 mmol, 50 wt% in EtOAc) and allowed to warm to rt and stirred at rt for 16 h. Water (2 mL) and EtOAc (2 mL) were then added and the aqueous layer was extracted with EtOAc (3 × 2 mL). The combined organic extracts were washed sequentially with satd aq NaHCO$_3$ (6 mL) and brine (6 mL), then dried and concentrated *in vacuo*. Purification *via* flash column chromatography (**Sfär Silica HC D**, 0% grading to 100% EtOAc in hexane, product eluted at 55%) gave **CM 7** as a white solid (47 mg, 36% over 2 steps from the respective chalcone); **^{1}H NMR** (400 MHz, CDCl$_3$) δ$_H$ 2.08 (s, 3H), 3.11 (dd, *J* = 17.8, 4.8 Hz, 1H), 3.98 (dd, *J* = 17.8, 11.8 Hz, 1H), 6.62 (dd, *J* = 11.8, 4.8 Hz, 1H), 7.25 – 7.40 (m, 3H), 7.46 (d, *J* = 7.2 Hz, 1H), 7.59 – 7.75 (m, 3H), 7.92 – 7.99 (m, 1H), 8.77 – 8.83 (m, 2H). **^{13}C NMR** (151 MHz, CDCl$_3$) δ$_C$ 4.5, 42.5, 56.7, 73.9, 90.3, 125.6, 126.9, 128.7, 129.0, 130.1, 130.7, 131.1, 138.3, 140.2, 143.2, 143.9, 144.7, 151.3, 156.8. **HRMS (ESI):** exact mass calculated for C$_{21}$H$_{16}$N$_4$O [(M+H)$^+$] 341.1397, found 341.1376.

2-Chloro-1-(3-phenyl-5-(quinolin-5-yl)-4,5-dihydro-1*H*-pyrazol-1-yl)ethan-1-one (CMZ 13)

Step 1: Following General Procedure A, the chalcone was prepared from quinoline-5-carbaldehyde (55 mg, 0.35 mmol), acetophenone (49 μL, 0.42 mmol) and 5% (w/w) aq NaOH (0.4 mL, 0.52 mmol) in EtOH (1 mL). Filtration under reduced pressure gave the chalcone as a brown solid (58 mg, 65%).

Step 2: Following General Procedure F, the pure title compound was prepared from chalcone (58 mg, 0.22 mmol) and hydrazine hydrate (40 μL, 0.45 mmol, 50–60% wt solution) in EtOH (0.9 mL); then chloroacetyl chloride (27 μL, 0.34 mmol) and triethylamine (94 μL, 0.67 mmol) in CH_2Cl_2 (0.9 mL). Purification *via* flash column chromatography (**Sfär Silica HC D**, 0% grading to 100% EtOAc in hexane, product eluted at 61%) gave **CMZ 13** as a white solid (35 mg, 44% over 2 steps from the respective chalcone). **^{1}H NMR** (400 MHz, $CDCl_3$) $δ_H$ 3.13 (dd, *J* = 17.6, 4.9 Hz, 1H), 3.90 (dd, *J* = 17.6, 11.9 Hz, 1H), 4.55 (d, *J* = 13.4 Hz, 1H), 4.65 (d, *J* = 13.4 Hz, 1H), 6.21 (dd, *J* = 11.9, 4.9 Hz, 1H), 7.27 (d, *J* = 7.2 Hz, 1H), 7.31 – 7.44 (m, 4H), 7.57 (dd, *J* = 8.6, 7.2 Hz, 1H), 7.63 – 7.71 (m, 2H), 7.98 (d, *J* = 8.6 Hz, 1H), 8.29 (d, *J* = 8.6 Hz, 1H), 8.89 (dd, *J* = 4.3, 1.6 Hz, 1H). **^{13}C NMR** (151 MHz, $CDCl_3$) $δ_C$ 42.1, 42.4, 57.1, 121.4, 123.3, 125.2, 127.0, 129.0, 129.2, 130.0, 130.6, 131.2, 132.3, 136.6, 147.9, 149.6, 155.9, 164.5. **HRMS (ESI):** exact mass calculated for $C_{20}H_{16}ClN_3O$ [(M+H)$^+$] 350.1055, found 350.1029.

2-Chloro-1-(3-phenyl-5-(quinoxalin-6-yl)-4,5-dihydro-1*H*-pyrazol-1-yl)ethan-1-one (CMZ 15)
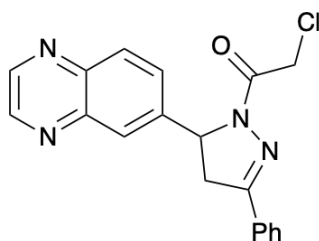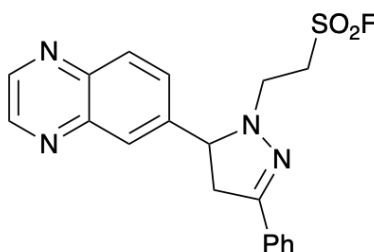

Step 1: Following General Procedure A, the chalcone was prepared from quinoxaline-6-carbaldehyde (301 mg, 1.90 mmol), acetophenone (267 μL, 2.28 mmol) and 5% (w/w) aq NaOH (2.28 mL, 2.85 mmol) in EtOH (9 mL). Filtration under reduced pressure gave the chalcone as a pale brown solid (445 mg, 90%).

Step 2: Following General Procedure F, the pure title compound was prepared from chalcone (100 mg, 0.38 mmol) and hydrazine hydrate (68 μL, 0.77 mmol, 50–60% wt solution) in EtOH (1.6 mL); then chloroacetyl chloride (46 μL, 0.58 mmol) and triethylamine (161 μL, 1.15 mmol) in CH_2Cl_2 (1.5 mL). Purification *via* flash column chromatography (**Sfär Silica HC D**, 0% grading to 100% EtOAc in hexane, product eluted at 59%) gave **CMZ 15** as a white solid (50 mg, 37% over 2 steps from the respective chalcone); **^{1}H NMR** (400 MHz, $CDCl_3$) $δ_H$ 3.23 (dd, *J* = 17.9, 4.9 Hz, 1H), 3.84 (dd, *J* =

17.9, 11.8 Hz, 1H), 4.49 – 4.61 (m, 2H), 5.74 (dd, J = 11.8, 4.9 Hz, 1H), 7.32 – 7.44 (m, 3H), 7.60 (dd, J = 8.7, 2.1 Hz, 1H), 7.61 – 7.72 (m, 2H), 7.91 (d, J = 2.1 Hz, 1H), 8.02 (d, J = 8.7 Hz, 1H), 8.73 (app s, 2H). **¹³C NMR** (151 MHz, CDCl₃) δ_C 42.1, 42.1, 60.2, 126.0, 126.8, 128.0, 128.8, 130.4, 130.5, 131.0, 142.4, 142.8, 142.9, 145.0, 145.2, 155.3, 164.2. **HRMS (ESI):** exact mass calculated for $C_{19}H_{15}ClN_4O$ [(M+MeCN+H)⁺] 392.1272, found 392.1243.

**2-(3-Phenyl-5-(227uinoxaline-6-yl)-4,5-dihydro-1*H*-pyrazol-1-yl)ethane-1-sulfonyl fluoride (CMZ 17)**

Step 1: Following General Procedure A, the chalcone was prepared from quinoxaline-6-carbaldehyde (301 mg, 1.90 mmol), acetophenone (267 μL, 2.28 mmol) and 5% (w/w) aq NaOH (2.3 mL, 2.85 mmol) in EtOH (9 mL). Filtration under reduced pressure gave the chalcone as a pale brown solid (495 mg, 90%) which was used without purification.

Step 2: Hydrazine hydrate (48 μL, 0.54 mmol, 50–60% wt solution) was added to a solution of the chalcone (71 mg, 0.27 mmol) in EtOH (1 mL) at rt and the resultant mixture was heated at reflux for 1.5 h before being cooled to rt. One third of the reaction mixture was then concentrated *in vacuo* and the crude pyrazoline was used immediately without purification.

Step 3: Ethene sulfonyl fluoride (25 μL, 0.30 mmol) was added to a solution of the crude pyrazoline (0.27 mmol) in THF (0.6 mL) at rt and stirred at 80°C for 4 h, then concentrated *in vacuo*. Purification *via* flash column chromatography (**Sfär Silica HC D**, 0% grading to 100% EtOAc in hexane, product eluted at 43%) gave **CMZ 17** as a pale yellow oil (63 mg, 60% over 2 steps from the respective chalcone); **¹H NMR** (400 MHz, CDCl₃) δ_H 3.06 (dd, J = 16.3, 13.8 Hz, 1H), 3.22 – 3.33 (m, 1H), 3.39 (app dt, J = 12.6, 7.7 Hz, 1H), 3.54 (dd, J = 16.3, 10.0 Hz, 1H), 3.84 – 3.99 (m, 2H), 4.45 (dd, J = 13.8, 10.0 Hz, 1H), 7.26 – 7.42 (m, 3H), 7.55 – 7.63 (m, 2H), 7.89 (dd, J = 8.7, 2.0 Hz, 1H), 8.05 – 8.13 (m, 2H), 8.80 (app s, 2H). **¹³C NMR** (151 MHz, CDCl₃) δ_C 43.2, 47.7, 49.5, 49.6, 71.2, 126.1, 128.2, 128.6, 129.0, 129.5, 130.3, 131.8, 141.6, 142.7, 142.9, 145.1, 145.2, 151.6. **HRMS (ESI)**: exact mass calculated for $C_{19}H_{17}FN_4O_2S$ [(M+H)⁺] 385.1129, found 385.1111.

3-Oxo-3-(3-phenyl-5-(quinoxaline-5-yl)-4,5-dihydro-1*H*-pyrazol-1-yl)propanenitrile (CMZ 22)
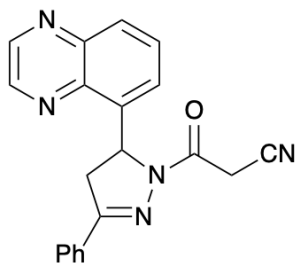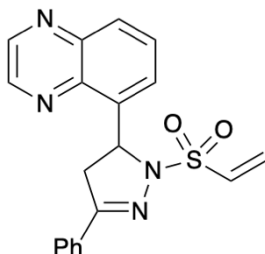
Step 1: Following General Procedure A, the chalcone was prepared from quinoxaline-5-carbaldehyde (500 mg, 3.16 mmol), acetophenone (443 μL, 3.79 mmol) and 5% (w/w) aq NaOH (3.8 mL, 4.74 mmol) in EtOH (10 mL). Filtration under reduced pressure gave the chalcone as a pale yellow solid (823 mg, quant) which was used without purification.

Step 2: Hydrazine hydrate (68 μL, 0.77 mmol, 50–60% wt solution) was added to a solution of the chalcone (100 mg, 0.38 mmol) in EtOH (2 mL) at rt and the resultant mixture was heated at reflux for 2 h before being cooled to rt. The reaction mixture was then concentrated *in vacuo* and the crude pyrazoline was used immediately without purification.

Step 3: A solution of cyanoacetic acid (33 mg, 0.38 mmol) in DMF (0.5 mL) was added to a solution of the crude pyrazoline (0.38 mmol) in DMF (0.5 mL) at 0 °C. The reaction mixture was then treated sequentially with NMM (422 μL, 3.84 mmol) and T3P (643 μL, 1.08 mmol, 50 wt% in EtOAc) and allowed to warm to rt and stirred at rt for 16 h. Water (2 mL) and EtOAc (2 mL) were then added and the aqueous layer was extracted with EtOAc (3 × 2 mL). The combined organic extracts were washed sequentially with satd aq NaHCO$_3$ (6 mL) and brine (6 mL), then dried and concentrated *in vacuo*. Purification *via* flash column chromatography (**Sfär Silica HC D**, 0% grading to 100% EtOAc in hexane, product eluted at 48%) gave **CMZ 22** as a white solid (11 mg, 8% over 2 steps from the respective chalcone); **^{1}H NMR** (600 MHz, DMSO-d_6) δ$_H$ 3.27 (dd, *J* = 18.2, 5.0 Hz, 1H), 4.10 (dd, *J* = 18.2, 11.9 Hz, 1H), 4.36 (d, *J* = 19.2 Hz, 1H), 4.48 (d, *J* = 19.1 Hz, 1H), 6.55 (dd, *J* = 11.9, 5.0 Hz, 1H), 7.43 – 7.53 (m, 3H), 7.59 (dd, *J* = 7.4, 1.3 Hz, 1H), 7.78 – 7.82 (m, 2H), 7.82 – 7.86 (m, 1H), 8.06 (dd, *J* = 8.4, 1.3 Hz, 1H), 9.04 (dd, *J* = 10.5, 1.8 Hz, 2H). **^{13}C NMR** (151 MHz, CDCl$_3$) δ$_C$ 25.5, 40.1, 42.3, 56.3, 116.0, 125.5, 127.0, 128.7, 128.9, 130.1, 130.7, 130.9, 138.9, 139.3, 142.7, 144.9, 145.9, 156.7, 160.5. **HRMS (ESI)**: exact mass calculated for C$_{20}$H$_{15}$N$_5$O [(M+H)$^+$] 342.135, found 342.1336.

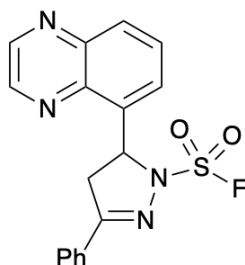**5-(3-Phenyl-1-(vinylsulfonyl)-4,5-dihydro-1*H*-pyrazol-5-yl)quinoxaline (CMZ 23)**

Step 1: Following General Procedure A, the chalcone was prepared from quinoxaline-5-carbaldehyde (500 mg, 3.16 mmol), acetophenone (443 μL, 3.79 mmol) and 5% (w/w) aq NaOH (3.8 mL, 4.74 mmol) in EtOH (10 mL). Filtration under reduced pressure gave the chalcone as a pale yellow solid (823 mg, quant) which was used without purification.

Step 2: Hydrazine hydrate (204 µL, 2.31 mmol, 50–60% wt solution) was added to a solution of the chalcone (300 mg, 1.15 mmol) in EtOH (4.5 mL) at rt and the resultant mixture was heated at reflux for 2 h before being cooled to rt. The reaction mixture was then concentrated *in vacuo* and the crude pyrazoline was used immediately without purification.

Step 3: Following General Procedure G, the pure title compound was prepared from crude pyrazoline (1.15 mmol), triphenylphosphine oxide (712 mg, 2.56 mmol), trifluoromethanesulfonic anhydride (194 µL, 1.15 mmol), vinyl sulfonic acid (125 mg, 1.15 mmol), pyridine (93 µL, 1.15 mmol) and triethylamine (321 µL, 2.31 mmol) in CH_2Cl_2 (17 mL). Purification *via* flash column chromatography (**Sfär Silica HC D**, 0% grading to 100% EtOAc in hexane, product eluted at 53%; then SNAP Ultra C18, 20% grading to 100% MeCN in water, product eluted at 43%) gave **CMZ 23** as a white solid (33 mg, 24% over 2 steps from the respective chalcone); [1]**H NMR** (400 MHz, DMSO-d_6) δ_H 3.29 (dd, J = 17.9, 9.0 Hz, 1H), 4.14 (dd, J = 17.9, 11.9 Hz, 1H), 6.18 (dd, J = 11.9, 9.0 Hz, 1H), 6.26 – 6.40 (m, 2H), 7.02 (dd, J = 16.5, 10.0 Hz, 1H), 7.42 – 7.54 (m, 3H), 7.73 – 7.79 (m, 2H), 7.90 – 7.97 (m, 1H), 7.98 – 8.02 (m, 1H), 8.10 (dd, J = 8.4, 1.7 Hz, 1H), 8.95 – 9.08 (m, 2H). **HRMS (ESI)**: exact mass calculated for $C_{19}H_{16}N_4O_2S$ [(M+H)$^+$] 365.1067, found 365.1061.

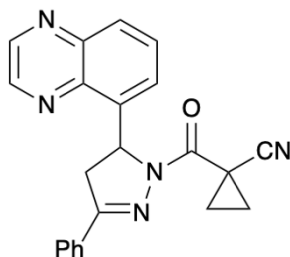## 3-Phenyl-5-(quinoxalin-5-yl)-4,5-dihydro-1*H*-pyrazole-1-sulfonyl fluoride (CMZ 24)

Step 1: Following General Procedure A, the chalcone was prepared from quinoxaline-5-carbaldehyde (500 mg, 3.16 mmol), acetophenone (443 µL, 3.79 mmol) and 5% (w/w) aq NaOH (3.8 mL, 4.74 mmol) in EtOH (10 mL). Filtration under reduced pressure gave the chalcone as a pale yellow solid (823 mg, quant) which was used without purification.

Step 2: Hydrazine hydrate (204 µL, 2.31 mmol, 50–60% wt solution) was added to a solution of the chalcone (300 mg, 1.15 mmol) in EtOH (4.5 mL) at rt and the resultant mixture was heated at reflux for 4 h before being cooled to rt. One third of the reaction mixture was then concentrated *in vacuo* and the crude pyrazoline was used immediately without purification.

Step 3: 1-(Fluorosulfuryl)-2,3-dimethyl-1H-imidazol-3-ium trifluoromethanesulfonate (126 mg, 0.38 mmol) was added to a solution of the crude pyrazoline (0.38 mmol) in MeCN (0.7 mL) at rt and stirred at this temperature for 16 h. Water (2 mL) was then added and the aqueous layer was extracted with EtOAc (3 × 2 mL). The combined organic extracts were washed sequentially with brine (2 × 2 mL), then dried and concentrated *in vacuo*. Purification *via* flash column chromatography (**Sfär Silica HC D**, 0% grading to 100% EtOAc in hexane, product eluted at 25%) gave **CMZ 24** as a white solid (34 mg, 25% over

2 steps from the respective chalcone); **^{1}H NMR** (400 MHz, CDCl$_3$) δ$_H$ 3.24 (dd, J = 17.7, 8.2 Hz, 1H), 4.18 (dd, J = 17.7, 11.4 Hz, 1H), 6.50 (dd, J = 11.4, 8.2 Hz, 1H), 7.30 – 7.46 (m, 3H), 7.68 – 7.74 (m, 2H), 7.74 – 7.78 (m, 1H), 7.84 – 7.92 (m, 1H), 8.04 (dd, J = 8.5, 1.6 Hz, 1H), 8.73 – 8.88 (m, 2H). **^{13}C NMR** (151 MHz, CDCl$_3$) δ$_C$ 44.3, 61.4, 127.2, 127.6, 129.0, 129.8, 130.0, 130.3, 131.7, 138.0, 140.3, 143.2, 144.3, 145.4, 160.2. **HRMS (ESI)**: exact mass calculated for C$_{17}$H$_{13}$FN$_4$O$_2$S [(M+MeCN+H)$^+$] 398.1081, found 398.1097.

1-(3-Phenyl-5-(quinoxalin-5-yl)-4,5-dihydro-1*H*-pyrazole-1-carbonyl)cyclopropane-1-carbonitrile (CMZ 29)
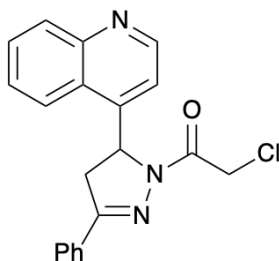

Step 1: Following General Procedure A, the chalcone was prepared from quinoxaline-5-carbaldehyde (500 mg, 3.16 mmol), acetophenone (443 μL, 3.79 mmol) and 5% (w/w) aq NaOH (3.8 mL, 4.74 mmol) in EtOH (10 mL). Filtration under reduced pressure gave the chalcone as a pale yellow solid (823 mg, quant) which was used without purification.

Step 2: Hydrazine hydrate (204 μL, 2.31 mmol, 50–60% wt solution) was added to a solution of the chalcone (300 mg, 1.15 mmol) in EtOH (4.5 mL) at rt and the resultant mixture was heated at reflux for 4 h before being cooled to rt. One third of the reaction mixture was then concentrated *in vacuo* and the crude pyrazoline was used immediately without purification.

Step 3: A solution of 1-cyano-1-cyclopropane carboxylic acid (85 mg, 0.77 mmol) in DMF (1 mL) was added to a solution of the crude pyrazoline (0.77 mmol) in DMF (1 mL) at 0 °C. The reaction mixture was then treated sequentially with NMM (845 μL, 7.68 mmol) and T3P (1.3 mL, 2.15 mmol, 50 wt% in EtOAc) and allowed to warm to rt and stirred at rt for 16 h. Water (5 mL) and EtOAc (5 mL) were then added and the aqueous layer was extracted with EtOAc (3 × 5 mL). The combined organic extracts were washed sequentially with satd aq NaHCO$_3$ (15 mL) and brine (15 mL), then dried and concentrated *in vacuo*. Purification *via* flash column chromatography (**Sfär Silica HC D**, 0% grading to 100% EtOAc in hexane, product eluted at 39%) gave **CMZ 29** as a white solid (41 mg, 15% over 2 steps from the respective chalcone); **^{1}H NMR** (400 MHz, CDCl$_3$) δ$_H$ 1.57 – 1.66 (m, 3H), 1.72 (ddd, J = 9.2, 4.7, 3.2 Hz, 1H), 3.13 (dd, J = 17.9, 5.4 Hz, 1H), 3.95 (dd, J = 17.9, 11.8 Hz, 1H), 6.63 (dd, J = 11.8, 5.4 Hz, 1H), 7.27 – 7.42 (m, 3H), 7.48 (d, J = 7.2 Hz, 1H), 7.67 (app t, J = 8.0 Hz, 1H), 7.74 – 7.87 (m, 2H), 7.93 – 8.04 (m, 1H), 8.60 – 8.95 (m, 2H). **^{13}C NMR** (151 MHz, CDCl$_3$) δ$_C$ 14.2, 17.9, 18.6, 42.1, 57.4, 120.9, 125.7, 127.3, 129.0, 129.4, 130.3, 131.0, 131.1, 138.9, 140.2, 143.2, 144.3, 145.1, 156.4, 162.5. **HRMS (ESI)**: exact mass calculated for C$_{22}$H$_{17}$N$_5$O [(M+H)$^+$] 368.1506, found 368.1524.

2-Chloro-1-(3-phenyl-5-(quinolin-4-yl)-4,5-dihydro-1*H*-pyrazol-1-yl)ethan-1-one (CMZ 35)

Step 1: Following General Procedure A, the chalcone was prepared from quinoline-4-carbaldehyde (137 mg, 0.87 mmol), acetophenone (204 μL, 1.74 mmol) and 5% (w/w) aq NaOH (0.3 mL, 0.38 mmol) in EtOH (5 mL). Extraction with EtOAc and purification *via* flash column chromatography (**Sfär Silica HC D**, 0% grading to 100% EtOAc in hexane, product eluted at 42%) gave the chalcone as a yellow solid (39 mg, 17%).

Step 2: Following General Procedure F, the pure title compound was prepared from chalcone (39 mg, 0.15 mmol) and hydrazine hydrate (27 μL, 0.30 mmol, 50–60% wt solution) in EtOH (1.5 mL); then chloroacetyl chloride (18 μL, 0.23 mmol) and triethylamine (63 μL, 0.45 mmol) in CH_2Cl_2 (1.5 mL). Purification *via* flash column chromatography (**Sfär Silica HC D**, 0% grading to 100% EtOAc in hexane, product eluted at 46%) gave **CMZ 35** as a white solid (31 mg, 58% over 2 steps from the respective chalcone); **¹H NMR** (400 MHz, CDCl₃) δ_H 3.12 (dd, *J* = 17.6, 5.1 Hz, 1H), 3.95 (dd, *J* = 17.6, 12.0 Hz, 1H), 4.53 (d, *J* = 13.2 Hz, 1H), 4.69 (d, *J* = 13.2 Hz, 1H), 6.23 (dd, *J* = 12.0, 5.1 Hz, 1H), 7.09 (d, *J* = 4.5 Hz, 1H), 7.28 – 7.41 (m, 4H), 7.52 – 7.59 (m, 1H), 7.61 – 7.67 (m, 2H), 7.67 – 7.71 (m, 1H), 7.88 – 7.93 (m, 1H), 8.07 – 8.12 (m, 1H), 8.77 (d, *J* = 4.5 Hz, 1H). **¹³C NMR** (151 MHz, CDCl₃) δ_C 41.9, 42.0, 57.1, 116.5, 122.9, 125.1, 127.0, 127.8, 129.1, 129.9, 130.3, 131.4, 146.6, 147.5, 149.5, 156.0, 164.7. **HRMS (ESI)**: exact mass calculated for $C_{20}H_{16}ClN_3O$ [(M+H)⁺] 350.1055, found 350.1066.

2-Fluoro-1-(3-phenyl-5-(quinoxalin-5-yl)-4,5-dihydro-1*H*-pyrazol-1-yl)ethan-1-one (CMZ 38)
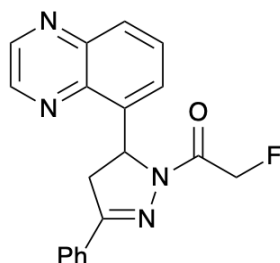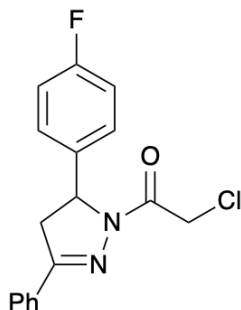

Step 1: Following General Procedure A, the chalcone was prepared from quinoxaline-5-carbaldehyde (500 mg, 3.16 mmol), acetophenone (443 μL, 3.79 mmol) and 5% (w/w) aq NaOH (3.8 mL, 4.74 mmol) in EtOH (10 mL). Filtration under reduced pressure gave the chalcone as a pale yellow solid (823 mg, quant) which was used without purification.

Step 2: Hydrazine hydrate (94 μL, 1.06 mmol, 50–60% wt solution) was added to a solution of the chalcone (138 mg, 0.53 mmol) in EtOH (2.2 mL) at rt and the resultant mixture was heated at reflux for 2 h before being cooled to rt. The reaction mixture was

then concentrated *in vacuo* and the crude pyrazoline was used immediately without purification.

Step 3: A solution of fluoroacetic acid (41 mg, 0.53 mmol) in DMF (0.7 mL) was added to a solution of the crude pyrazoline (0.53 mmol) in DMF (0.7 mL) at 0 °C. The reaction mixture was then treated sequentially with NMM (583 μL, 5.30 mmol) and T3P (887 μL, 1.48 mmol, 50 wt% in EtOAc) and allowed to warm to rt and stirred at rt for 16 h. Water (2 mL) and EtOAc (2 mL) were then added and the aqueous layer was extracted with EtOAc (3 × 2 mL). The combined organic extracts were washed sequentially with satd aq NaHCO$_3$ (6 mL) and brine (6 mL), then dried and concentrated *in vacuo*. Purification *via* flash column chromatography (**Sfär Silica HC D**, 0% grading to 100% EtOAc in hexane, product eluted at 46%) gave **CMZ 38** as a white solid (20 mg, 11% over 2 steps from the respective chalcone); **^{1}H NMR** (400 MHz, CDCl$_3$) δ$_H$ 3.12 (dd, *J* = 17.9, 5.3 Hz, 1H), 3.94 (dd, *J* = 17.9, 11.9 Hz, 1H), 5.21 – 5.63 (m, 2H), 6.59 (dd, *J* = 11.9, 5.3 Hz, 1H), 7.28 – 7.41 (m, 3H), 7.42 – 7.50 (m, 1H), 7.58 – 7.69 (m, 3H), 7.98 (dd, *J* = 8.4, 1.4 Hz, 1H), 8.69 – 8.89 (m, 2H). **^{13}C NMR** (151 MHz, CDCl$_3$) δ$_C$ 42.1, 56.9, 78.7, 79.8, 126.1, 126.9, 129.0, 129.2, 130.3, 130.9, 131.0, 138.6, 140.4, 143.1, 144.1, 144.7, 156.7, 165.2, 165.3. **HRMS (ESI):** exact mass calculated for C$_{19}$H$_{15}$FN$_4$O [(M+H)$^+$] 335.1303, found 335.1304.

2-Chloro-1-(5-(4-fluorophenyl)-3-phenyl-4,5-dihydro-1*H*-pyrazol-1-yl)ethan-1-one (CMZ 47)

Step 1: Following General Procedure A, the chalcone was prepared from 4-fluorobenzaldehyde (259 μL, 2.42 mmol), acetophenone (339 μL, 2.90 mmol) and 5% (w/w) aq NaOH (2.9 mL, 3.63 mmol) in EtOH (3 mL). Filtration under reduced pressure gave the chalcone as a pale yellow solid (547 mg, quant).

Step 2: Following General Procedure F, the pure title compound was prepared from chalcone (100 mg, 0.44 mmol) and hydrazine hydrate (78 μL, 0.88 mmol, 50–60% wt solution) in EtOH (3 mL); then chloroacetyl chloride (53 μL, 0.66 mmol) and triethylamine (185 μL, 1.33 mmol) in CH$_2$Cl$_2$ (1.5 mL). Purification *via* flash column chromatography (**Sfär Silica HC D**, 0% grading to 100% EtOAc in hexane, product eluted at 16%) gave **CMZ 47** as a white solid (44 mg, 31% over 2 steps from the respective chalcone); **^{1}H NMR** (400 MHz, CDCl$_3$) δ$_H$ 3.15 (dd, *J* = 17.9, 4.7 Hz, 1H), 3.73 (dd, *J* = 17.9, 11.8 Hz, 1H), 4.44 – 4.57 (m, 2H), 5.51 (dd, *J* = 11.8, 4.7 Hz, 1H), 6.90 – 7.00 (m, 2H), 7.11 – 7.23 (m, 2H), 7.33 – 7.45 (m, 3H), 7.65 – 7.72 (m, 2H). **^{13}C NMR** (151 MHz, CDCl$_3$) δ$_C$ 42.3, 42.3, 60.0, 115.9, 116.1, 127.0, 127.0, 127.8, 129.0, 129.0, 130.8, 131.1, 136.8, 136.8, 155.5, 161.6, 163.3, 164.1. **HRMS (ESI):** exact mass calculated for C$_{17}$H$_{14}$ClFN$_2$O [(M+H)$^+$] 317.0852, found 317.0845.
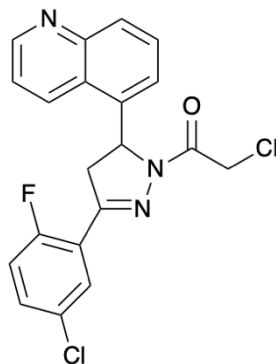
2-Chloro-1-(3-(2,5-dichlorophenyl)-5-(quinolin-5-yl)-4,5-dihydro-1*H*-pyrazol-1-yl)ethan-1-one (CMZ 51)
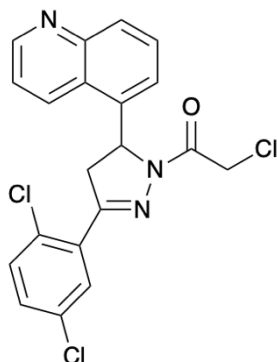
Step 1: Following General Procedure A, the chalcone was prepared from quinoline-5-carbaldehyde (200 mg, 1.27 mmol), 2′5′-dichloroacetophenone (367 μL, 2.55 mmol) and 5% (w/w) aq NaOH (438 μL, 0.55 mmol) in EtOH (4 mL). Filtration under reduced pressure and purification *via* flash column chromatography (**Sfär Silica HC D**, 0% grading to 100% EtOAc in hexane, product eluted at 32%) gave the chalcone as a yellow oil (168 mg, 40%).

Step 2: Following General Procedure F, the pure title compound was prepared from chalcone (168 mg, 0.51 mmol) and hydrazine hydrate (91 μL, 1.03 mmol, 50–60% wt solution) in EtOH (4 mL); then chloroacetyl chloride (61 μL, 0.77 mmol) and triethylamine (214 μL, 1.54 mmol) in CH_2Cl_2 (1.5 mL). Purification *via* flash column chromatography (**Sfär Silica HC D**, 0% grading to 100% EtOAc in hexane, product eluted at 45%) gave **CMZ 51** as a white solid (53 mg, 25% over 2 steps from the respective chalcone); **^{1}H NMR** (400 MHz, CDCl$_3$) δ$_H$ 3.28 (dd, *J* = 18.1, 4.9 Hz, 1H), 4.10 (dd, *J* = 18.1, 12.0 Hz, 1H), 4.51 (d, *J* = 13.5 Hz, 1H), 4.62 (d, *J* = 13.5 Hz, 1H), 6.23 (dd, *J* = 12.0, 4.9 Hz, 1H), 7.23 – 7.34 (m, 3H), 7.43 (dd, *J* = 8.6, 4.2 Hz, 1H), 7.61 (dd, *J* = 8.6, 7.3 Hz, 1H), 7.69 (d, *J* = 2.3 Hz, 1H), 8.01 (d, *J* = 8.6 Hz, 1H), 8.29 (d, *J* = 8.6 Hz, 1H), 8.90 (dd, *J* = 4.2, 1.6 Hz, 1H). **^{13}C NMR** (151 MHz, CDCl$_3$) δ$_C$ 42.1, 44.9, 57.6, 121.5, 122.8, 125.0, 129.6, 129.8, 130.2, 131.2, 131.4, 131.5, 131.6, 132.4, 133.3, 136.0, 148.6, 150.1, 154.1, 164.7. **HRMS (ESI):** exact mass calculated for $C_{20}H_{14}Cl_3N_3O$ [(M+H)$^+$] 418.0275, found 418.029.

2-Chloro-1-(3-(5-chloro-2-fluorophenyl)-5-(quinolin-5-yl)-4,5-dihydro-1*H*-pyrazol-1-yl)ethan-1-one (CMZ 53)

Step 1: Following General Procedure A, the chalcone was prepared from quinoline-5-carbaldehyde (207 mg, 1.31 mmol), 5′-chloro-2′-fluoroacetophenone (352 μL, 2.63 mmol) and 5% (w/w) aq NaOH (452 μL, 0.57 mmol) in EtOH (4 mL). Filtration under reduced pressure and purification *via* flash column chromatography (**Sfär Silica HC D**, 0% grading to 100% EtOAc in hexane, product eluted at 31%) gave the chalcone as a yellow solid (56 mg, 14%).

Step 2: Following General Procedure F, the pure title compound was prepared from chalcone (54 mg, 0.17 mmol) and hydrazine hydrate (31 μL, 0.35 mmol, 50–60% wt solution) in EtOH (4 mL); then chloroacetyl chloride (21 μL, 0.26 mmol) and triethylamine (72 μL, 0.52 mmol) in CH_2Cl_2 (1.5 mL). Purification *via* flash column chromatography (**Sfär Silica HC D**, 0% grading to 100% EtOAc in hexane, product eluted at 52%) gave **CMZ 53** as a white solid (31 mg, 44% over 2 steps from the respective chalcone); **^{1}H NMR** (400 MHz, CDCl$_3$) δ$_H$ 3.09 – 3.31 (m, 1H), 3.88 – 4.04 (m, 1H), 4.52 (app dd, *J* = 13.4, 1.8 Hz, 1H), 4.63 (app dd, *J* = 13.4, 1.8 Hz, 1H), 6.22 (dd, *J* = 12.2, 5.0 Hz, 1H), 6.99 (ddd, *J* = 10.7, 8.7, 1.9 Hz, 1H), 7.24 (d, *J* = 7.3 Hz, 1H), 7.28 – 7.36 (m, 1H), 7.43 (ddd, *J* = 8.7, 4.1, 1.9 Hz, 1H), 7.52 – 7.66 (m, 1H), 7.86 – 7.95 (m, 1H), 8.00 (d, *J* = 8.7 Hz, 1H), 8.28 (d, *J* = 8.7 Hz, 1H), 8.90 (dt, *J* = 4.1, 1.9 Hz, 1H). **^{13}C NMR** (151 MHz, CDCl$_3$) δ$_C$ 42.0, 44.4, 44.5, 57.3, 118.2, 118.4, 120.2, 120.3, 121.5, 122.9, 125.1, 128.5, 128.5, 129.6, 129.8, 130.2, 130.2, 131.9, 132.4, 132.5, 136.2, 148.3, 149.9, 151.5, 151.5, 159.0, 160.7, 164.7. **HRMS (ESI):** exact mass calculated for $C_{20}H_{14}Cl_2FN_3O$ [(M+H)$^+$] 402.0571, found 402.0560.
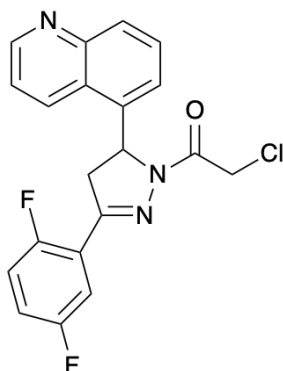
2-Chloro-1-(3-(2,3-dichlorophenyl)-5-(quinolin-5-yl)-4,5-dihydro-1*H*-pyrazol-1-yl)ethan-1-one (CMZ 56)
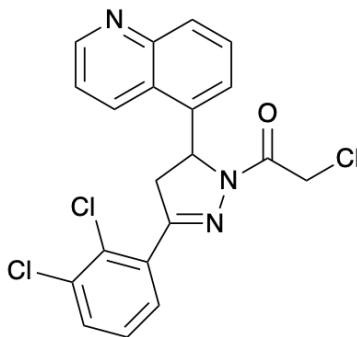
Step 1: Following General Procedure A, the chalcone was prepared from quinoline-5-carbaldehyde (213 mg, 1.36 mmol), 2′3′-dichloroacetophenone (396 μL, 2.71 mmol) and 5% (w/w) aq NaOH (466 μL, 0.58 mmol) in EtOH (4 mL). Filtration under reduced pressure and purification gave the chalcone as a pale brown solid (445 mg, quant).

Step 2: Following General Procedure F, the pure title compound was prepared from chalcone (306 mg, 0.93 mmol) and hydrazine hydrate (165 μL, 1.87 mmol, 50–60% wt solution) in EtOH (4 mL); then chloroacetyl chloride (111 μL, 1.40 mmol) and triethylamine (390 μL, 2.80 mmol) in CH_2Cl_2 (4.7 mL). Purification *via* flash column chromatography (**Sfär Silica HC D**, 0% grading to 100% EtOAc in hexane, product eluted at 40%; then SNAP Ultra C18, 20% grading to 100% MeCN in water, product eluted at 63%) gave **CMZ 56** as a white solid (9 mg, 2.4% over 2 steps from the respective chalcone); **^{1}H NMR** (400 MHz, CDCl$_3$) δ$_H$ 3.26 (dd, *J* = 17.7, 5.1 Hz, 1H), 4.09 (dd, *J* = 17.7, 11.9 Hz, 1H), 4.49 (d, *J* = 12.8 Hz, 1H), 4.65 (d, *J* = 12.8 Hz, 1H), 5.89 (dd, *J* = 11.9, 5.1 Hz, 1H), 7.03 (dd, *J* = 8.0, 1.6 Hz, 1H), 7.14 (t, *J* = 8.0 Hz, 1H), 7.36 (dd, *J* = 8.0, 1.6 Hz, 1H), 7.53 (dd, *J* = 8.7, 4.2 Hz, 1H), 7.58 (dd, *J* = 7.3, 1.5 Hz, 1H), 7.65 (dd, *J* = 8.7, 7.3 Hz, 1H), 8.14 (app dt, *J* = 8.4, 1.1 Hz, 1H), 8.95 (dd, *J* = 4.2, 1.5 Hz, 1H), 9.49 - 9.59 (m, 1H). **^{13}C NMR** (151 MHz, CDCl$_3$) δ$_C$ 41.9, 43.5, 57.6, 122.6, 124.0, 126.2, 127.4, 128.0, 129.5, 129.6, 130.1, 130.2, 131.6, 134.1, 137.2, 129.5, 146.8, 149.2, 155.1, 164.3**. HRMS (ESI):** exact mass calculated for $C_{20}H_{14}Cl_3N_3O$ [(M+H)$^+$] 418.0275, found 418.0287.

2-Chloro-1-(3-(2,5-difluorophenyl)-5-(quinolin-5-yl)-4,5-dihydro-1*H*-pyrazol-1-yl)ethan-1-one (CMZ 63)

Step 1: Following General Procedure A, the chalcone was prepared from quinoline-5-carbaldehyde (200 mg, 1.27 mmol), 2′5′-difluoroacetophenone (161 μL, 1.27 mmol) and 5% (w/w) aq NaOH (438 μL, 0.55 mmol) in EtOH (4 mL). Filtration under reduced pressure and purification *via* flash column chromatography (**Sfär Silica HC D**, 0% grading to 100% EtOAc in hexane, product eluted at 44%) gave the chalcone as a yellow solid (59 mg, 16%).

Step 2: Following General Procedure F, the pure title compound was prepared from chalcone (59 mg, 0.20 mmol), hydrazine hydrate (35 μL, 0.40 mmol, 50–60% wt solution) in EtOH (4 mL); then chloroacetyl chloride (24 μL, 0.30 mmol) and triethylamine (84 μL, 0.60 mmol) in CH$_2$Cl$_2$ (1.5 mL). Purification *via* flash column chromatography (**Sfär Silica HC D**, 0% grading to 100% EtOAc in hexane, product eluted at 56%) gave **CMZ 63** as a white solid (30 mg, 38% over 2 steps from the respective chalcone); **^{1}H NMR** (400 MHz, CDCl$_3$) δ$_H$ 3.23 (ddd, *J* = 18.5, 5.1, 3.0 Hz, 1H), 4.00 (ddd, *J* = 18.5, 12.0, 3.0 Hz, 1H), 4.51 (d, *J* = 13.4 Hz, 1H), 4.62 (d, *J* = 13.4 Hz, 1H), 6.23 (dd, *J* = 12.0, 5.1 Hz, 1H), 6.94 – 7.12 (m, 2H), 7.26 (d, *J* = 7.2 Hz, 1H), 7.45 (dd, *J* = 8.6, 4.3 Hz, 1H), 7.58 – 7.69 (m, 2H), 8.03 (d, *J* = 8.6 Hz, 1H), 8.31 (d, *J* = 8.6 Hz, 1H), 8.91 (dd, *J* = 4.3, 1.6 Hz, 1H). **HRMS (ESI)**: exact mass calculated for C$_{20}$H$_{14}$ClF$_2$N$_3$O [(M+H)$^+$] 386.0866, found 386.0881.